Investigating Co-crystallisation of Primary Amides and Carboxylic acids

Comparative Analysis of Benzamide, Isonicotinamide and Nicotinamide co-crystal growth with Carboxylic Acids

Hafsa Shamim JAVED BSc, MSc

Submitted for the degree of

Doctor of Philosophy

Postgraduate Studies in Pharmaceutics

School of Pharmacy

UNIVERSITY OF

BRADFORD

2010

Investigating Co-crystallisation of Primary Amides and Carboxylic acids

Keywords

Co-crystals, Crystallisation, Hotstage microscopy, X-ray diffraction, Thermal Analysis, polySNAP, dSNAP, Phase diagram

Abstract

Crystal Engineering is the design of crystalline material using non-covalent synthesis. Co-crystals are multi-component crystals which are constructed from complementary intermolecular interactions, they are also known as supramolecular complexes. Design of such materials utilises the synthon approach, this involves the understanding of common intermolecular interactions which occur in the crystal packing and is used to design new solids with desired physical properties and chemical properties. Primary amides form supramolecular heterosynthons, these synthons represent an opportunity for a design of multi-component crystals in which one molecule contains a primary amide and a second molecule which is complimentary to the primary amide, usually carboxylic acids. The progress with regards to the screening process for the determination of co-crystals is evident in the literature, In particular, high throughput solution growth methods and solvent drop grinding.
The comparison of Isonicotinamide and Benzamide as a co-crystal component has been presented. This study was motivated by the observation that the CSD contains 24 Isonicotinamide and 1 Benzamide co-crystal. The interaction with carboxylic acids is the focus of the work, in particular those which form Isonicotinamide co-crystal are being screened with Benzamide.
Our work utilises a ReactArray Microvate to carry out the low throughput solution growth on a matrix of carboxylic acid with Benzamide, this study has been coupled with the Kofler hot stage microscope method which visually aids to screen and view co-crystal phase formation. Crystallisation screens have resulted in the identification of known co-crystal phases of Isonicotinamide and Benzamide, additionally new co-crystal phases have also been identified with Fumaric, 3-hydroxybenzoic acid, Mandelic Acid, 4-Nitrobenzoic Acid and Tartaric Acid. Single crystal structures of the Fumaric and 4-Nitrobenzoic acid have been obtained.

In order to develop an understanding of co-crystal formation in Isonicotinamide and Benzamide with our supramolecular library, packing landscape analysis is being undertaken using both the CSD and crystal structures we have obtained. This is undertaken as collaboration with Dr Andy Parkin and Professor Gilmore (University of Glasgow), we have identified that the dSNAP analysis is a way forward for the analysis of how co-crystals pack. The analysis highlighted the subtleties that were present in the packing motifs of the Isonicotinamide co-crystals. In particular the cis and trans orientation of the amide and acid carbonyl to each other and the planar and off planar layer assemblies. All of which are required to maximise the hydrogen bond usage of the components comprising the co-crystals.

Further investigations have led to the collaborative project with Syngenta Ltd in the design of a co-crystal screen using a high through-put robot, Crissy® -Automation Platform by Zinsser Analytical, using an extended screen of 16 acid coformers with Isonicotinamide, Benzamide and Nicotinamide the sample have been characterised using a reflectance diffraction method, GADDS. Further analysis of this data involves the use of polySNAP, which has led to further collaboration with Professor Gilmore's group.

Another method of screening includes thermal microscopy, which involves the Kofler contact method. This procedure is simple and quick to identify new phases, and can be verified with DSC thermal analysis ensuring correlation of new phase melting points.

This work also presents an attempt in mapping ternary phase diagrams to understand phase behaviour of the three model AI's with Succinic Acid. The choice of approach through the construction of a phase diagram of a two-component system was undertaken as these phase diagrams can give a practical insight for preparing co-crystals. Previously it has been discussed how similar solubility determines the straight forward phase diagram of a 1:1 mixture where all the regions are well defined, however, components with a less comparable solubility tend to map a phase diagram skewed like the one shown in the study by Chiarella et al, 2007, thus narrowing the region where co-crystal growth is possible.

Structure determination is the most desirable confirmation method of co-crystal formation, although other methods are superior in identifying a new phase, but to grow a crystal requires a skill in fine tuning solvent evaporation techniques. This study has revealed the limitations of these simple techniques and attempted to apply low through-put and high through-put methods to maximise co-crystal output. Thermal techniques, Kofler contact and DSC have also been studied as screening methods which show positive results as compared to solution growth. It has also been shown that identifying solubility of components is important as the differences alter the location and size of the phase regions of where the co-crystal is thermodynamically stable.

Publications and Presentations

Sections of this work have previously been presented in the following forms:

Peer Reviewed Articles

Blagden, N; Berry, D; Parkin, A; Javed, H; Ibrahim, A; Gavin, P.T; De Matos, L.L; Seaton, C.C. (2008), Current Direction of Co-crystal Growth. Submitted to the New Journal of Chemistry: An International Journal of the Chemical Sciences Vol 32, Issue 10, pages 1645-1808

Abstracts / Posters

BACG 2006 Herriot Watt
'A comparative study of co-crystal formation between amides and carboxylic acid'

Erice 2007, BCA 2008 York,
'A comparative study of co-crystal formation between amides and carboxylic acid II'

BACG 2008
'A comparative study of co-crystal formation between amides and carboxylic acid II. Screening with a Reactarray Microvate and Kofler contact method.'

Podium Presentations

Syngenta 2007
'A comparative study of co-crystal formation between amides and carboxylic acid '

Acknowledgements

بِسْمِ اللهِ الرَّحْمٰنِ الرَّحِيْمِ

Greatest thanks to my supervisor, Dr Nick Blagden, I really appreciate all the support, guidance and encouragement as well as his patience and empathetic nature. You are a great supervisor!!

I also thank Syngenta for financial support, and Dr Neil George and Dr James Forrest for suggestions and guidance on the development of this work. Thank you James for helping me with the screening and showing me how to use the high through-put robot and Raman.

I Thank Professor Gilmore of The University of Glasgow and his group, especially the Late Dr Andrew Parkin, for all his invaluable help with the dSNAP, you will be missed. Also, Dr Gordon Barr, thank you for helping with all the polySNAP work and extending my polySNAP license month after month after month after month!!! Thanks

I thank the following people from the IPI and University of Bradford.

Firstly, thank you Dr Colin Seaton, for invaluable help and advice along the way. Also, everyone from the office for keeping me smiling, laughing and motivated when I would feel down especially, Ajay, Dave, Kat, Mohammad Isreb, Stephen and Aldi. Dr Ian Scowen and Dr Tas Munshi, for the crystal structure determination, and general x-ray analysis. Professor Anant Paradkar for his all help and perspective with phase diagrams and my random questions which always began with... ‘‘Prof you know with my phase diagram.....’’

I am grateful for the support from my family, especially my sister’s Sadia and Saira, who have always brightened my day when I felt I was at a dead end and made sure I don’t go crazy. Thanks to my mum peering her head as she opened my door everyday and in the middle of the night and saying ‘‘....do you want some food?? ....you still up??’’

Special thanks to my friend Amna, with her help and motivation I would not have got this far.

This thesis is dedicated to my Grandad, Muhammad Hussain,

Miss you lots Daddy

Contents

List of symbols and Abbreviation

AI	Active ingredient
API	Active pharmaceutical ingredient
CBZ	Carbamazepine
CCD	Charged-coupled device
CCDC	Cambridge Crystallographic Data Centre
cqs	ConQuest file
CSD	Cambridge structural database
DSC	Differential Scanning Calorimetry
GADDS	General Area Detector Diffraction System
HTP	High-through put
ICTA	International Confederation for Thermal Analysis
ICTAC	International Confederation for Thermal Analysis and Calorimetry
INA	Isonicotinamide
MDS	Multidimensional Scaling
MMDS	3D Metric Multidimensional scaling
PXRD	Powder X-ray diffraction
SR	Supramolecular reagent
TG	Thermogravimetry
TGA	Thermogravimetric Analysis
UV	Ultraviolet

List of Figures

List of Tables

List of Schemes

List of Appendices

Chapter One: Introduction

1.1General Introduction

Crystal engineering is the design and targeted synthesis of a crystal with specified desirable physicochemical properties (these may include electrical, magnetic, optical, etc). The basis of crystal engineering is to employ an understanding of intermolecular interactions present in the crystal packing (Desiraju, 2003), to target specific assemblies which optimise the desired physicochemical properties. This is achieved by employing molecular building blocks which generate specific assemblies via targeted intermolecular interactions to generate the desired functionality within the solid. The selectivity inherent to the building blocks or synthons are molecules or ions which interact with one another by exploiting non-covalent interactions. (Desiraju, 2003) Crystal engineering stems from a branch of chemistry known as supramolecular chemistry, this is chemistry beyond the molecule.

1.2 Crystal Engineering

Crystal engineering requires a link to be made between molecular structures and the occurrence of classes of intermolecular interactions which consistently lead to specific crystal packing features. To highlight this ethos the following definition from the literature and work of Gautum Desiraju has led to a clear definition and recognition of Crystal Engineering:

'...defined as the understanding of intermolecular interaction in the context of crystal packing and in the utilisation of such an understanding in the design of new solids with desired physical and chemical properties.' (Desiraju, 1989)

Crystal engineering is a branch of supramolecular chemistry (Steed & Atwood, 2006) where the ambition is to generate crystal structures from first principals using intermolecular non-covalent interactions (Steed & Atwood, 2006, Aakeröy & Beatty, 2001), and as such is chemistry beyond the molecule. It is an approach, which employs molecular building blocks, which are assembled via intermolecular forces to produce functional solid materials. The building blocks/synthons are molecules or ions which interact with one another exploiting non-covalent interactions. (Desiraju, 1989, Steed & Atwood, 2006) These non-covalent interactions define the self assembly process in crystallisation, the behaviour of the molecular components involved, and their tendency to associate or isolate themselves, i.e. the chemical selectivity in solution. (Lehn, 1994)

The fundamentals of crystal engineering were described in 1962 by Von Hippel as 'molecular engineering'. Modern crystal engineering can be traced to studies by Schmidt, where his studies on light-induced or photochemical reactions of molecules complexes in the solid state pioneered this branch of supramolecular chemistry. Schmidt for instance reports the targeted photodimerization through specific packing

arrangements of Cinnamic acids, the reversible photochromy of the anils of salicylaldehyde, fulgides, and tetrachloronaphthoquinone, and all were well established by the early 20th century (Corey, 1967). However, the relationship between the photochemistry of organic compounds and the resulting molecular stereochemistry was poorly understood. This problem prompted the use of the term "crystal engineering", which was first introduced by Schmidt and co-workers at the Weizmann Institute in 1964 (Desiraju, 1989, Corey, 1967).

Since Schmidt, modern crystal engineering has developed quickly with the arrival of modern crystallographic techniques such as the use of four-circle diffractometers and charged-coupled device (CCD) instruments. As a result, modern crystal engineering has expanded to study intermolecular forces in the solid state, as well as structure prediction, control and rationalisation. In addition, it incorporates the synthesis of crystalline materials and novel molecular building blocks for applications in the pharmaceutical and petrochemical industries. Crystal engineering as it is practised now can be broken down in the components of analysis and synthesis (Steed & Atwood, 2006).

This concept of analysis and synthesis has been ascribed by Dario Braga as a 'bottom-up' approach involving supramolecular entity from the convolution of physical and chemical properties of the individual building blocks with the periodicity of symmetry operators of the crystals (Braga, 2002, Braga, et al 2002, Vishweshwar, 2006).

1.3 Intermolecular Interactions

Intermolecular bonding describes the intermolecular forces between stable molecules or between functional groups. Most intermolecular interactions are electrostatic in nature, and can be classified according to their distance dependency and directionality for crystal engineering purposes (Desiraju, 1995, 2003). These intermolecular forces comprise hydrogen bonds and van der Waals forces (dipole-dipole, dipole-induced dipole, induced dipole-induced dipole, and $\pi\cdots\pi$ interactions).

Van der Waals interactions are medium range forces, these are isotropic in character and define molecular shape, size, and they contribute to the overall crystal stability, providing a driving force for close packing of the molecules. Longer range forces such as hydrogen bonds are much more highly directional than van der Waals forces and also exhibit some covalent character. Very long range ionic forces exert very specific controls and constraints on crystal structure (Desiraju, 1995, 2003).

1.3.1 Hydrogen Bonding

Hydrogen bonding is an important concept in supramolecular chemistry and molecular biology (Jeffery, 1997).

The concept has stemmed from the hydrogen bond chapter in Pauling's (1940 2nd edt) Nature of the Chemical Bond.

'...Under certain conditions an atom of hydrogen is attracted by rather strong forces to two atoms, instead of only one, so that it may be considered to be acting as a bond between them. This is called the hydrogen bond.'

He also has stated '...the hydrogen atom with one stable orbital (1s orbital) can only form one covalent bond, and that the hydrogen bond is largely ionic in character and is formed only between the most electronegative atoms..' (Pauling, 1940)

Research shows that hydrogen bonding is frequently encountered and the most important interaction in crystals. The frequency with which the elements nitrogen and oxygen occur in organic compounds, coupled with the strength and directionality of the hydrogen bond as compared to other forces account for its significance (Desiraju, 1989). Hence, the hydrogen bond possesses the most reliable directional dependence, and can be considered as the "master key'' for molecular recognition (Desiraju, 1995, Steed & Atwood, 2005).

Hydrogen bonding has been defined as a donor acceptor interaction specifically involving hydrogen atoms. Hydrogen bonds may be simple, with one donor and one acceptor, bifurcated (three-centre), or trifurcated (four centred) (Aakeröy, 1993).

The simplest and most common arrangement shows a donor and acceptor interaction can be defined as D−H···A where D and A are atoms that have electro negativities higher than hydrogen, these are presented in the table 1.1 below.

Table 1.1: Typical hydrogen bond donors and acceptors commonly seen in the literature in multicomponent systems such as co-crystals.

Donors	Acceptors
C—H	C═C, C≡C, arenes
N—H	N, O
P—H	P
O—H	O, N

S —H	S
F —H	F
Cl —H	Cl
Br —H	Br
I —H	I

The hydrogen bond is mainly electrostatic in nature, where the hydrogen atom has a partial positive charge, δ_+, while the more electronegative atoms each have a partial negative charge, δ_-, Figure 1.1

Figure 1.1: Partial positive and negative charges associated with the hydrogen atom (H), the donor atom (D), and the acceptor atom (A) in a hydrogen bond.

$$\begin{array}{ccccc} \delta^- & & \delta^+ & & \delta^- \\ D & \text{———} & H & \text{------} & A \end{array}$$

The bond is formed when the electronegativity of the donor atom, D, relative to the hydrogen in the covalent D —H is such that the effect is the removal of electrons from the hydrogen atom leaving it with a partial positive charge (partially unshielded). The hydrogen bond acceptor, A, must have a lone pair electrons or polarisable π electrons to interact with the D—H bond, typically H (σ*) to A(nπ) orbital interactions are involved. The strength of hydrogen bonds lie between covalent bonds (200 - 400 kJ mol^{-1}) and weak Van der Waals interactions (≤ 5 kJ mol^{-1}), depending on the electro negativity of the donor and acceptor atoms participating in the interaction. Hydrogen bonds can be classified as strong, moderate or weak hydrogen bond interactions (Aakeröy, 1993, Jeffery, 1997) discussed further in section 1.3.1.1.

In order for an interaction to be considered a hydrogen bond, certain geometric criteria need to be met. The characteristic hydrogen bond geometry D —H---A —X, is given

by the covalent bond length D —H, the H ---A hydrogen bond length, and the D to A separation distance. These three quantities define the hydrogen bond angle θ, this angle is useful in determining whether or not a certain interaction is a hydrogen bond as is the H--- A —X angle and the planarity of the DHAX system are valuable indicators, particularly for strong hydrogen bonds (Desiraju, 1995).

Figure 1.2: Hydrogen bonds have an angular dependence, θ and φ.

The net effect in the system D— H--- A is to weaken the D— H bond compared to the same bond being in an isolated system. Therefore, hydrogen bonding can be observed by a wide range of spectroscopic analysis, i.e. vibrational shift of the bonds in IR and Raman spectroscopy, NMR observes the chemical shift caused by the change in the electronic environment around the proton, and characteristic bond lengths and angles associated with the hydrogen bonding by X-ray diffraction (Jeffery, 1997).

1.3.1.1 Strong, Medium and Weak Hydrogen Bonding

As mentioned earlier, hydrogen bonding can be classified as (i) strong, (ii) medium and (iii) weak hydrogen bonds. The classification of hydrogen bonds varies according to authors, Jeffery (1997) describes as:

(i) Strong hydrogen bonds are formed by groups in which there is a deficiency of electron density in the donor group, i.e., —$\overset{+}{O}$— H, $\diagup\!\!\diagup$ $\overset{+}{N}$— H, or an excess of electron density in the acceptor group, i.e., F^-, O —H, $\overline{O}$ —C, O —P, N < or involve D-A pairs as ionic bonds. This is typically expected as a deficiency of electron of the donors

group further de-shields the proton and increases the positive charge, while an electron excess on the acceptor group increases its negative charge and the interaction with the de-shielded proton, these are sometimes referred to as ionic hydrogen bonds. Hydrogen bond can also be forced; this is when configuration and conformation of the molecule forces the neutral donor and acceptor groups into a closer hydrogen bond contact than normal hydrogen bonding contact.

(ii) Moderate hydrogen bonds are generally formed by neutral donor and acceptor groups, i.e., O—H, >N—H, N(H) — H, and O < , O =C, N <, whereby the donor atoms are electronegative relative to hydrogen and the acceptor atoms have lone pair unshared electrons. This type of bonding is regarded as normal hydrogen bonds with the other two categories being the minority exceptions. Moderate bonds are the most common hydrogen bonds in chemistry and nature, they are important and essential components of the structure and function of biological molecules.

(iii) Weak hydrogen bonds are formed when the hydrogen atom is covalently bonded to a slightly more elector-neutral atom relative to hydrogen, for example, C —H or Si — H, or when the acceptor group has no lone pairs but has π electrons, as in C ≡C or an aromatic ring. Table 1.2 describes the properties of these three categories.

Table 1.2: Properties of strong, moderate and weak hydrogen bonds (Jeffery, 1997 where A-H···B is replaced by D-H···A)

	Strong	Moderate	Weak
D-H···A interaction	Mainly covalent	Mainly electrostatic	Electrostatic
Bond energy ($kjmol^{-1}$)	60-120	16-60	12
Bond lengths (Å)			
H···D	~1.2-1.5	~1.5-2.2	~2.2-3.2
A···D	2.2-2.5	2.5-3.2	3.2-4.0
Bond angles (°)	175-180	130-180	90-150

Relative IR vibration shift (symmetrical stretching mode, cm^{-1})	25%	10-25%	<10%
^{1}H NMR chemical shift downfield (ppm)	14-22	<14	-----
Examples	Gas phase dimers with strong acids/bases Proton sponges HF complexes	Acids Alcohols Phenols Hydrates Biological molecules	Gas phase dimers with weak acids/bases Minor components of 3- centre bonds C-H hydrogen bonds O-H π hydrogen bonds

The strength of hydrogen bonds is governed by the electronegativities of both the donor and acceptor atoms participating in the interaction. For example, the energies for O−H···O and N−H···O hydrogen bonds, range from 20 to 40 kJ mol^{-1} (Desiraju 1995). Generally, when the donor and acceptor atoms are neutral, hydrogen-bond strength corresponds to energies between 20 - 65 kJ mol^{-1} (Steiner, 2002). This range is typical of medium strength hydrogen bonds, while for weaker hydrogen bonds such as C−H···O interactions the energies are between 2 - 20 kJ mol^{-1}(Desiraju, 1995). When the donor and acceptor atoms in a hydrogen bond are ionic (i.e. as a result of proton transfer), hydrogen-bond strength can increase to 40 - 190 kJ mol^{-1}, and is thus defined as a strong hydrogen bond. Covalent bonds are usually stronger than hydrogen bonds, with energies between 100 - 400 kJ mol^{-1}, although the strongest of hydrogen bonds can be greater than the weakest of covalent bonds (Steiner, 2002).

1.4 Introduction to Co-crystals

The broad scope of crystal engineering and design ethos will now be outlined. In order to understand the activity of crystal engineering as applied to co-crystallisation, the fundamentals of the crystalline state need to be summarised. In particular, this section reviews the definition of a crystal in the solid state and what constitutes as a co-crystal.

1.4.1 What is a Crystal?

The key concept of crystal engineering is the deliberate construction of crystalline materials from molecules or ions using selected non-covalent interactions. As mentioned in previous sections, the goal in this area is to synthesize functional materials, which have specific tuneable properties (Aakeröy, 2001).

There are two classes of solid, (i) crystalline and (ii) amorphous, both of which differ from one another in how the constituent molecules are arranged. Mullin, defines (Mullin, 2004) crystals in his book as *'...a regular arrangement of constituent molecules, atoms or ions, into a fixed and regular repeating pattern known as a lattice..'*

Hence, crystals are solids that have a regular arrangement, leading to a fixed geometry or lattice, e.g. diamonds, whereas amorphous solids have a more random arrangement e.g. glass (Mullin, 2004) with local but no long range order.

1.4.2 What is a Co-crystal?

The term 'Co-crystal' was thought to have been introduced by Etter and Panunto in 1988 (Etter & Panunto, 1988), however, a definition of the term is again of debate and is discussed by Desiraju in his 2003 paper (Desiraju, 2003) and Dunitz answer to Desiraju's paper (Duntz, 2003). Aakeröy, in his 2005 paper *'...building co-crystals with molecular sense and supramolecular sensibility...'* (Aakeröy, 2005), suggests that co-crystals are *'...made from reactants that are solids at ambient temperature and that a co-crystal is structurally homogeneous crystalline material that contains two or more neutral building blocks...'* (Aakeröy, 2005). The definition which clarifies the basis of what a co-crystal is that *'...A co-crystal is multi-component crystal in which two or more molecules that are solid at ambient conditions and are constructed from complementary intermolecular interactions (hydrogen bond)...'* (Almarsson & Zaworotko, 2004, (Aakeröy, 2005). In the broadest sense Co-crystals may also include molecular complexes, solvates, inclusion compounds and many other multi-component crystal systems (Almarsson & Zaworotko, 2004). More recently co-crystals may be referred to as supramolecular complexes (Almarsson & Zaworotko, 2004).

There is still considerable debate on whether to include solvates in the set of co-crystals. Morrisette et al. (2004) claim that co-crystals (of drugs and drug candidates) are part of the broader family of multi-component crystal systems that includes salts, solvates, clatherates, inclusion crystals and hydrates, and that the primary difference between solvates and co-crystals is the physical state of the single components. If at room temperature one component is liquid, then the crystals are designated solvates, however if both components are solids at room temp then the crystals are designated co-crystals. Solvate are commonplace as they often occur as a serendipitous result of crystallisation from solution (Almarsson & Zaworotko, 2004), these may be unstable as dehydration /

desolvation may be observed; depending on storage conditions. Solvent loss may lead to an amorphous phase which are usually less chemically stable and can crystallise into less soluble forms. Co-crystals can be rationally designed to achieve the stable phase because they are unlikely to separate from solid dosage forms, especially when the co-crystallising agents are solid at room temperature (Almarsson & Zaworotko, 2004).

1.4.2.1 Co-crystals: Commercial value and beneficial use in industry in the context of active pharmaceutical ingredient, (API).

We have discussed that crystal engineering is the design of crystalline materials, and that these materials can be fine tuned to produce desirable physical properties e.g. solubility, crystal morphology, mechanical stability etc whilst retaining its biophysical or molecular activity is of great interest to industry. The classical method used in industry to improve the solubility and the bioavailability involves the pharmacologically active molecule to be processed as solvates (hydrates) or to convert an API into one of its salts; typically either chloride or nitrate salt (Aakeröy, 2003). Although these routes can lead to materials that eventually become commercially viable, there is a potential chance of potentially useful drugs that may never reach this point due to stringent requirements of processing, storage or bioavailability.

Co-crystallisation is becoming a steadfast approach to modifying an API's properties, and the increased interest in this subset of solid state crystal engineering has arisen, as the approach is able to simultaneously address a mode of crystal form which is able to utilise multiple functional groups present in a single active pharmaceutical ingredient. Consequently, pharmaceutical co-crystals are an attractive alternative to polymorphs,

salts and solvates a route to the modification of an active pharmaceutical ingredient (API) during dosage form. If a crystalline material contains both a pharmaceutically relevant molecule and a structure-directing (but biologically/environmentally passive) component which can be rationally assembled through intermolecular synthesis, then the inherent activity of the drug molecule remains intact while the physical properties of the bulk material are modified (Aakeröy, 2003).

Co-crystal formers which are suitable for pharmaceutical applications remain to be enumerated fully, however, there are over a hundred solid materials which have "Generally Regarded As Safe" ("GRAS") status, this includes food additives and other accepted substances. It may also be considered to make use of sub therapeutic amounts of eminently safe drug substances.

Carbamazepine (CBZ) is well studied API for co-crystallisation. Oral administration of CBZ holds challenges such as low water solubility with high dosage requirement for therapeutic effect, dissolution limited bioavailability and auto induction for metabolism. It has complex crystal forms which have been identified as four anhydrous polymorphs, a dehydrate, an acetone solvate, and two ammonium salts. These are all self-complementary. Carbamazepine is therefore, ideal to demonstrate how APIs can be converted to pharmaceutical co-crystals and how they optimise physicochemical properties over existing forms. A study of CBZ : Saccharin co-crystal appears to be superior to the existing crystal forms of CBZ in terms of stability relative to the anhydrous polymorph of CBZ, it posses more favourable dissolution and suspension stability and favourable oral absorption profile in dogs (Hickey, 2007**,** Shan & Zaworotko, 2007).

The dissolution study of Itraconazole-dicarboxylic acid co-crystals compared the pure crystalline and amorphous drug. The co-crystals were found to have better solubility and bioavailability as compared to the pure crystalline drug (Remenar et, al, 2003). Thus, the space of pharmaceutical co-crystals would therefore be on a much larger scale with thousands of possibilities for any given drug when at least two synthons are present in the API. A combinatorial approach such as high-throughput crystallisation is the most probable way to screen such volumes, however, this could be time consuming and expensive in industry and therefore the challenge for researches in both industry and academia lies with identifying those combinations without carrying out endless crystallisation experiments.

1.5 Design Strategies of Co-crystallisation

Crystal engineering has matured into a paradigm for the preparation of new crystalline materials. The initial approach prior to experimental work involves systematic searches using the Cambridge structural database (CSD) to gain a detailed understanding of the supramolecular chemistry of the functional groups present in a given molecule. This is a precondition for designing co-crystals, and this process aids the selection of appropriate co-crystal formers (Desiraju, 1995). Many authors (Aakeröy, 2005, Braga 2005, Fleishman 2003), have highlighted the hierarchical approach using supramolecular synthons that are present for a range of functional groups in order to design and build new co-crystals.

1.5.1 Hydrogen bond rules

It is useful to have a set of guidelines when predicting hydrogen bond patterns in the solid state. Systematic searching of the CSD to identify preferential hydrogen-bond patterns in organic crystals and co-crystals was initiated by Etter, (Etter, 1991), and has led to the formulation of three rules for hydrogen bond utilisation. (Etter, 1991, Aakeroy, 2001, Donohue, 1952) The first rule was developed by work done by Donohue in 1952: *'...all acidic hydrogen available in a molecule will be used in hydrogen bonding in the crystal structure of that compound…'* (Donohue, 1952). The second and third rules were formulated by Etter's studies on organic co-crystals: '*…all good acceptors will be used in hydrogen bonding when there are available hydrogen-bond donors, and the best hydrogen-bond donor and the best hydrogen-bond acceptor will preferentially form hydrogen bonds to one another*…' (Etter, 1990,1991).

In short :

1) All good proton donors and acceptors are used in hydrogen bonding

2) Six-membered ring intramolecular hydrogen bonds form in preference to intermolecular hydrogen bonds

3) The best proton donor and acceptor remaining after intramolecular hydrogen bond formation will form intermolecular hydrogen bonds to one another (but all acceptors may not necessarily interact with donors).

These rules are based upon energetically favourable types of hydrogen-bond patterns, geometries and functional groups. With the knowledge of known hydrogen bond lengths crystal engineers are able to apply these rules and predict hydrogen bond motifs.

1.5.2 Synthon approach

Design of such materials utilises the synthon approach that involves the understanding of common intermolecular interactions, which occur in the crystal packing and using this to design new solids with desired physical properties and chemical properties. The term "synthon" was first introduced by Corey in 1967 (Corey, 1967) in his article 'General Methods for the Construction of Complex Molecules'. The molecular synthons possess complementary functional groups of a molecule, which can engage in molecular association (Desiraju, 1995, 2003, Vishweshwar, 2006). Desiraju in 1995 (Desiraju, 1995) defined these supramolecular synthons as *'...structural units within supermolecules which can be formed and/or assembled by known or conceivable synthetic operations involving intermolecular interactions…'.* The synthons are spatial arrangements of intermolecular interaction, a desirable attribute of a supramolecular synthon is the property of robustness. Identification of robust synthons greatly facilitates the synthetic aspects of crystal engineering (Desiraju, 2003).

The relationship between functional groups in molecules and derived supramolecular synthon is illustrated in Scheme 1.1 (Desiraju, 2003).

Scheme 1.1: Common motifs observed in Crystal Engineering, Type 1 & 3 show a dimer, Type 2 & 4 show a catemer. Adapted from Supramolecular Synthons in Crystal Engineering-A New Organic Synthesis (Desiraju, 1995)

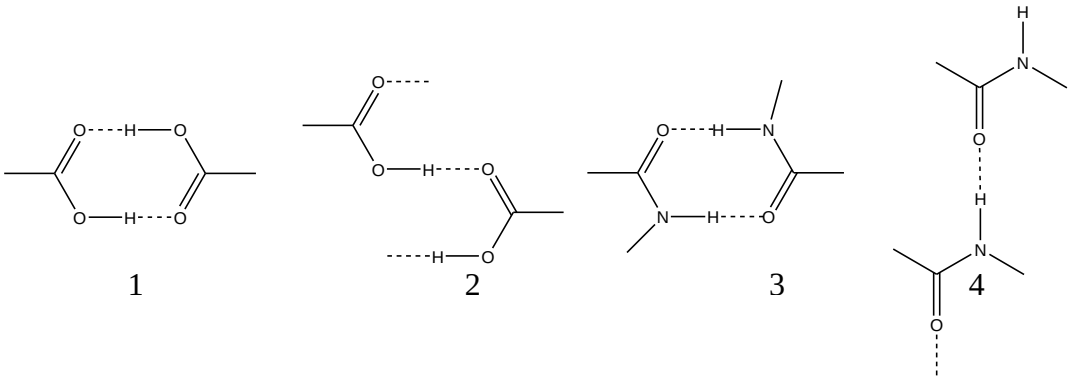

Generally, carboxylic acids and amides contain functional groups are self-complementary and thus are capable of forming supramolecular homosynthons. Scheme 1.1 presents the most common hydrogen bonding of the conventional OH···N and NH···O variety (Desiraju, 1995), the hydrogen bonds have identical centrosymmetrically related hydrogen bonds. Clearly two different types of synthons are being formed, type **1** carboxylic acid dimer and **3** shows carboxamide dimer, whereas type **2** and **4** show catemer.

Scheme 1.1 and 1.2 show how the carboxylic acid and amide groups are self-complementary and capable in forming homo synthons (type 1, 3 from scheme 1.1 and Scheme 1.2a). It is observed that acid and amide homodimers can be formed a two-point donor-acceptor molecular recognition path, this is shows in Scheme 1.2a**.** There is also possible interaction with functional groups that are different but complementary, Scheme 1.2b shows that carboxylic acids and amides are complementary to each other and can interact to form a supramolecular heterosynthon (Etter, 1991, Almarsson, 2004).

Scheme 1.2: The formation of supramolecular synthons between acids and amides: a) Supramolecular homosynthons exhibited by acid-acid and amide-amide dimers; b) Supramolecular heterosynthon exhibited by acid-amide dimers (Almarsson & Zaworotko, 2004).

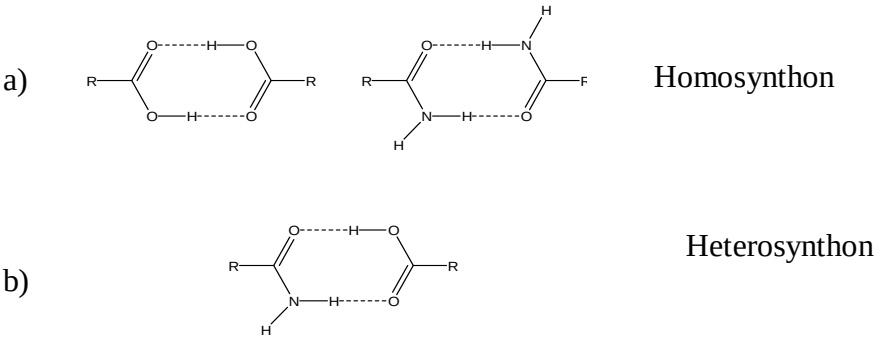

Figure 1.3 presents benzoic acid, a classic example to illustrate hierarchical self organisation of the carboxylic dimer (Desiraju, 2003).

Figure 1.3: Self assembly of a crystal structure, showing the functional group involved in the synthon.,(Adapted from Desiraju, 2003)

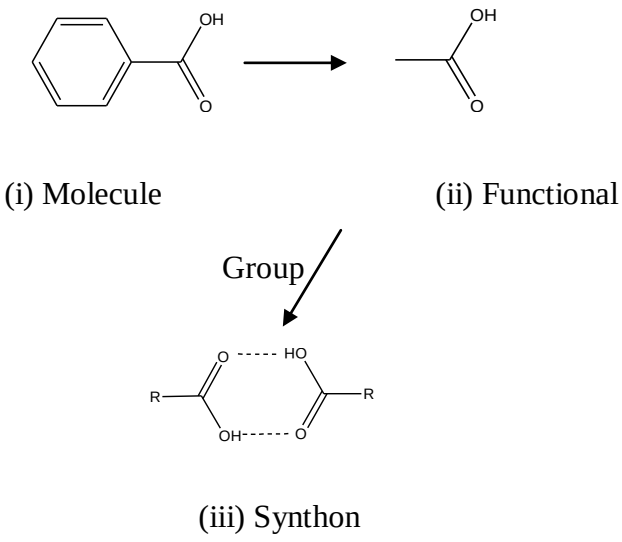

These highlighted synthons are typical examples of a library of synthons that can be employed in crystal engineering to construct / predict zero, one-, two- and three-dimensional supramolecular networks.

1.5.2.1 Zero-dimensional structures

The benzoic acid dimer is zero dimensional structure, the simplest level of supramolecular architecture. Figure 1.4 (a) (Desiraju, 1995).

Figure 1.4: Zero-dimensional structures in the (a) benzoic acid dimer and (b) benzoic acid···pyridine hetero system.

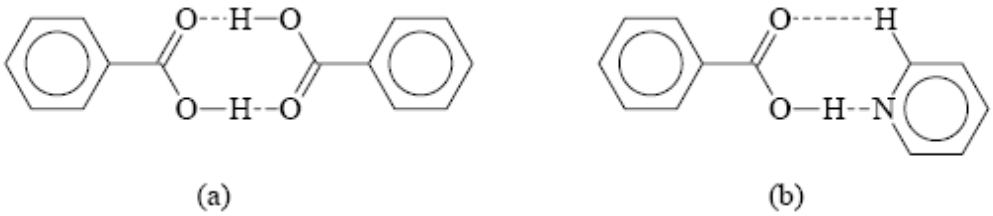

(a) (b)

Hetero synthons such as carboxylic acid···pyridine are also involved in zero dimensional structures, this is shown in the benzoic acid···pyridine hetero system, Figure 1.4 (b).

1.5.2.2 One-dimensional architectures

Extending from zero-dimensional structures into infinite one-dimensional chains, ribbons, and ladders requires at least two recognition sites are required by the molecule for the extension to increased dimensionality to be accomplished. Critical is the angle between the recognition sites decides the shape of the one-dimensional chains. This can be seen in the example of terephathalic acid, where there are two carboxylic acid moieties separated by 180° with respect to each other, and a linear chain is formed of these molecules, Figure 1.5.(Desiraju 1995).

Figure 1.5: An infinite, linear chain formed upon the assembly of terephthalic acid molecules via a homomeric acid synthon.

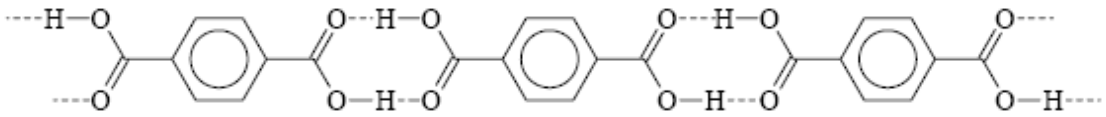

An infinite one-dimensional chain is also formed by isophthalic acid; though the angle between the two carboxylic acid groups is 120°, the consequential chain adopts a zigzag pattern or a crinkled ribbon Figure 1.6.(Desiraju 1995)

Figure 1.6: An infinite zigzag chain formed by the assembly of isophthalic acid molecules via a homomeric acid synthon..

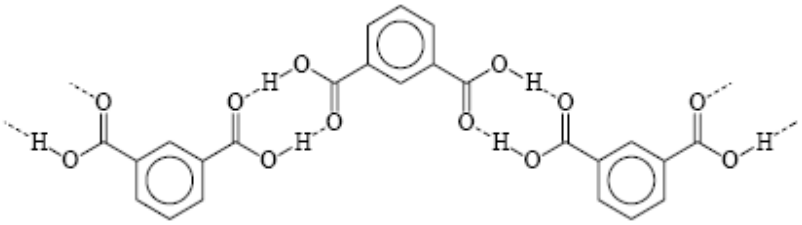

1.5.2.3 Two-dimensional sheets

When molecules possess at least one more recognition site, a two-dimensional architecture develops, hence a one-dimensional system interlinks and expands into a two-dimensional entity (Desiraju 1995). For example, trimesic acid contains one more carboxylic acid moiety than isophthalic acid, upon extension the cross-linking of chains formed by isophthalic acid fragments yields an infinite two-dimensional honeycomb sheet, Figure 1.7.

Figure 1.7: An infinite two-dimensional honeycomb sheet formed from the assembly of trimesic acid molecules.

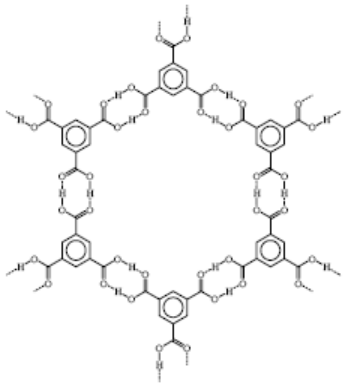

1.5.2.4 Three-dimensional architectures

The most primitive of supramolecular systems are the three-dimensional architectures when it comes to crystal engineering since they require extensions of building blocks in all three spatial coordinates and create open ended architectures, with void or channel features

Infinite three-dimensional architectures can also be composed from organic building blocks *via* hydrogen bonding (Desiraju 1995, Aakeröy, 1994). A three-dimensional diamondoid structure is formed in the crystal structure of adamantane-1, 3, 5, 7-tetracarboxylic acid, where carboxylic acid moieties are arranged tetrahedrally about the adamantyl center, Figure 1.8 (Desiraju, 1995).

Figure 1.8: Three-dimensional diamondoid framework

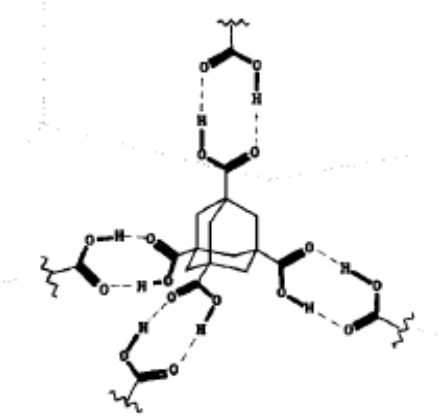

1.5.3 Graph set notation: Hydrogen bonding networks

Etter reports that graph set were first employed by Kuleshova and Zorkii (Etter, 1990-1991) on organic crystal structures. Etter presents a description of how hydrogen bond motifs can be described by assigning a graph set notation to the motif. Figure 8 highlights the basic motifs observed in a range of molecular solids. Motifs are described by the nature of the hydrogen bond, i.e. hydrogen donor or acceptor, in the hydrogen-bonded molecules of interest. These hydrogen bonds configure to form dimers and chains. The molecules that are hydrogen bonded together by repetition are then designated by descriptors, which describe whether the motif is infinite or finite and whether it is cyclic or not. The designators are **C** (chain), **D** (dimer or other finite set) **R** (rings) and **S** (intramolecular hydrogen bond). The numbers of donors **(d)** in each motif are assigned subscript whereas acceptors **(a)** are assigned superscripts. The size of the motif corresponds to the number of atoms in the repeat unit (**n)** (Etter, 1990).

Figure 1.9: Graph set Notation showing the common examples where intermolecular interaction may occur in a multicomponent system; I: shows a head to tail chain formation via the - - - H----N--C==O- - - where there is one donor atom and one acceptor atom and four atoms in the unit, II: shows the common homo synthon exhibited by amide and carboxylic acids dimers, III: shows the typical discrete hydrogen bonding, IV: less commonly seen self intramolecular hydrogen bond between an C==O- - -H----O.

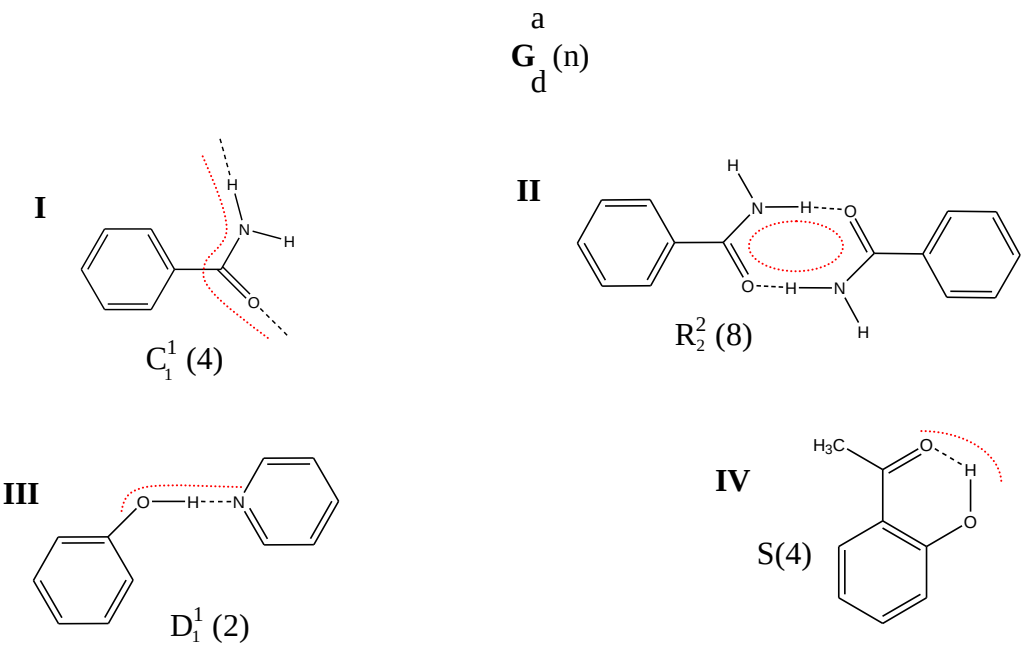

1.5.4 Phase Equilibria

Phase equilibria is one of the foundations of crystal engineering, as it defines the thermodynamic picture of phase formation. This section will discuss a few basic definitions and examine the phase rule and how understanding of the phase transitions and the nature of crystalline material under a given set of conditions is important with respect to solubility and phase diagrams.

1.5.4.1 Phase Rule

A *phase* is defined to be the homogeneous portion of a system (Mullin, 2004), which is physically distinct, and mechanically separable (Davey &Garside, 2000), these would be gases, pure liquids (melts), solids and solutions. Therefore a heterogeneous system comprises of two or more phases, e.g. gases or vapours are one-phase systems as are mixtures of two or more completely miscible liquids or solids, but mixtures which consist of two partially miscible liquids or a heterogeneous mixture of two solids are two-phase systems.

Equilibrium is a state of rest of a system, where at constant temperature *T*, pressure *P*, and composition *x*, the phases remain constant for infinite time. A change in any of these will alter the equilibrium state. It is important to understand that every system has a number of degrees of freedom, which is the number of variables that can be changed without altering the number of phases present (Mullin, 2004). In 1876, J. Willard Gibbs, introduced the phase rule which explains this relationship of number of components, phases and degrees of freedom of a system by means of the equation

Equation 1.5 the phase rule

$$P + F = C + 2 \qquad \text{(Eq.1.5)}$$

Where:

P is the number of phases in the system. Phase is homogeneous, physically distinct and mechanically separable component of a mixture.

C is the minimum number of chemical components required to compromise all the phases in the system

F is the number of degrees of freedom in a system. The number of variables (e.g. pressure composition and temperature) that are independently changed without affecting the number of phases

Phase diagrams can be used map out the behaviour and relation between *T, P* and *x*, along with the crystal structure of solid phases. The data generated, graphically map out the equilibria between phases of a system in two or three dimensions (Mullin, 2004, Davey & Garside, 2000).

1.5.4.2 Phase diagrams

Here we will focus on two types of phase diagrams, the binary phase diagram and ternary phase diagrams.

1.5.4.2.1 Binary systems and Eutectics

The three variables that affect the phase equilibria of a binary system are temperature, pressure and concentration. The behaviour of this type of system can be represented by a space model of three mutually perpendicular axes of pressure, temperature and concentration or three diagrams with pressure-temperature, pressure-concentration and temperature-concentration axes. However, in the case of crystallisation process the

focus is on the liquid and solid phases of a system. Therefore, phase diagrams are constructed using a temperature - concentration profile to map phase stability zones. Co-crystal phase formation and eutectic behaviour are identifiable from a two-component mixture, A and B, by measuring either their melt temperatures or just the temperatures at which B just dissolves or at which A crystallises. Diagram 1.1 depicts a typical single eutectic diagram for component A and B.

Diagram 1.1: Simple eutectic phase diagram for a two component system. Highlighting the liquidus line and the point at which when a eutectic is reached upon temperature increase. Also highlighting the melt zones, solid zones.

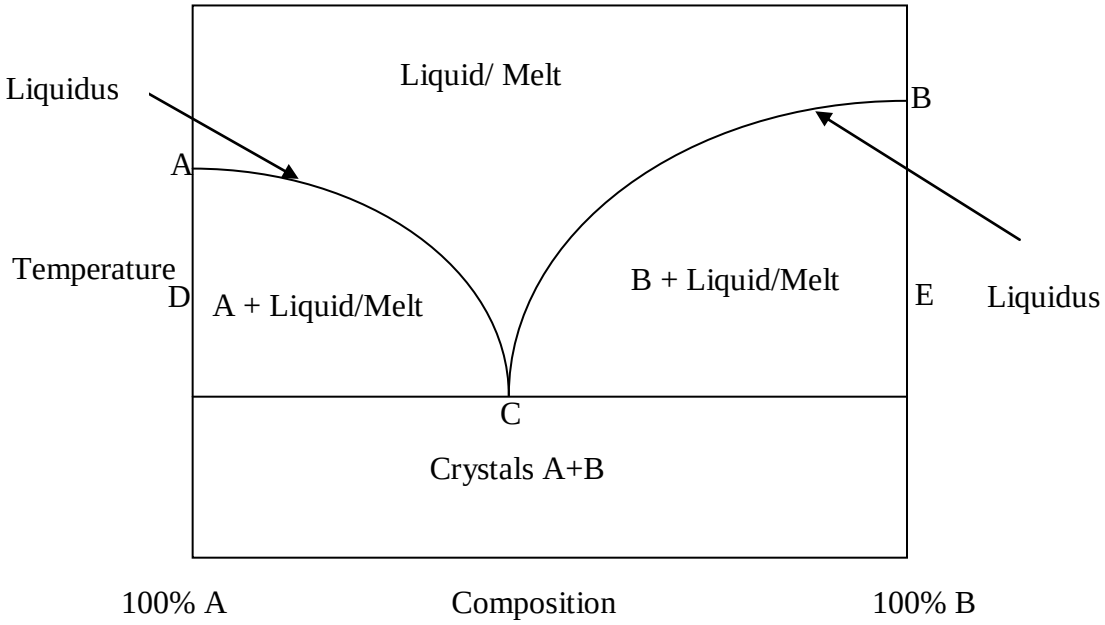

Lines ACB is referred to as the liquidus line, it gives the equilibrium composition of the liquid phase. The point where the line intersects, point C, is the eutectic point. Line BC correspond to the solution of B and AC corresponds to the solutions of A and B, along this line pure A is in equilibrium with A/B liquid, whilst at point C solid A, B and liquid composition C and vapour are at equilibrium. Therefore, at point C there are no degrees of freedom and thus, the eutectic temperature and concentration are fixed. In a three component system the eutectic temperature varies with composition.

1.5.4.2.2 Ternary systems

For a co-crystal in equilibrium with solvent, the phase diagram required is that of a ternary system consists of three components and can be presented as an equilateral triangle. Each apex represents the pure components A, B and C. The points on the side of the triangle stand for the binary system, AB, BC or AC; points within a system represent a ternary system ABC.

Figure 1.10: A schematic of a typical ternary phase diagram where each apex/axis highlights either solid phases or liquid phase.

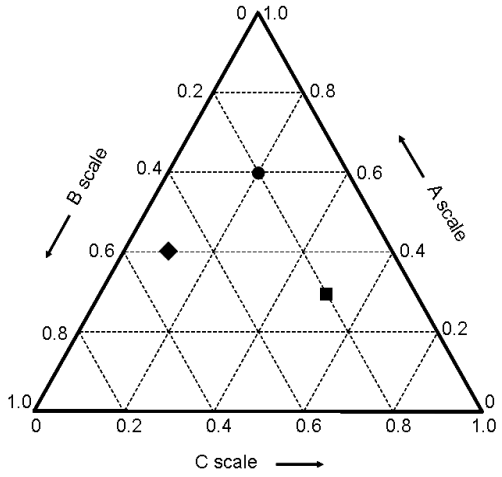

1.5.4.2.3 Phase diagrams in Co-crystal systems

The route to co-crystal growth is solvent evaporation, phase diagrams can be used to locate the co-crystal zone in the phase diagram. A typical phase diagram expected from a 1:1 mixture is shown in Figure 1.11a, where components have similar solubility, the region are well defined and it is easy to locate the co-crystal region. Figure 1.11 b shows a much different picture, components which have dissimilar solubility produce a more skewed phase diagram, and the region where a co-crystal maybe located is reduced to a much narrower region.

Figure 1.11: Typical Phase diagram where a) solubility of component 1 and 2 are similar, b) difference in solubility in system b causing a skew in the plot

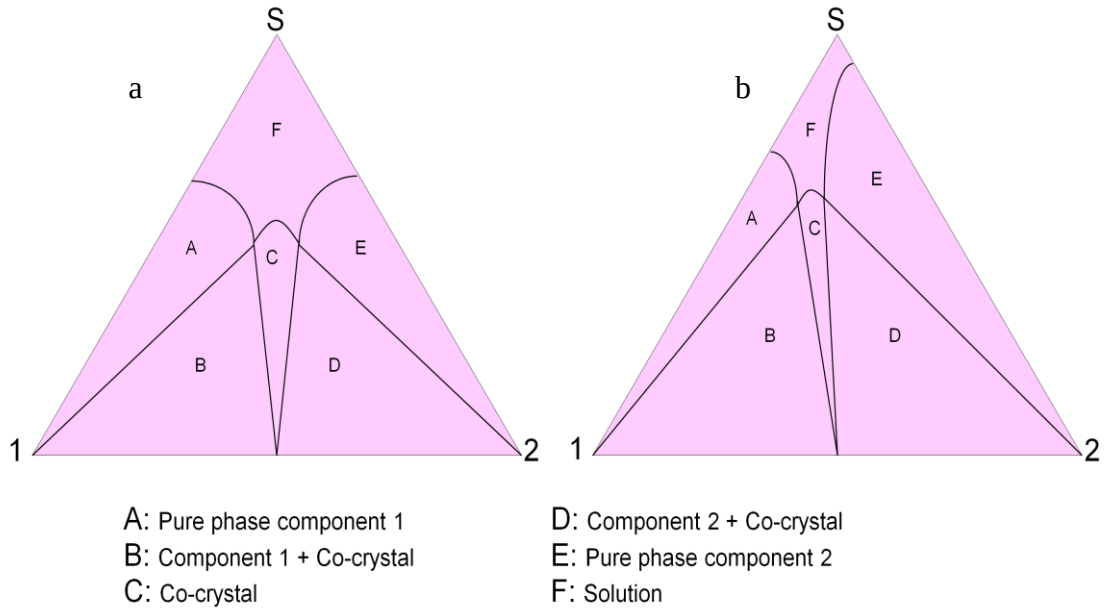

A worked example, (Chiarella, 2007), presents trans-Cinnamic and Nicotinamide system. They employed a solubility test and found that trans-Cinnamic acid and Nicotinamide have similar solubility in Nicotinamide, however in water Nicotinamide is much more soluble. The phase diagrams produced show that in a 1:1 mixture of the two components in methanol yield co-crystals Figure 1.12, and the water systems is much more skewed toward the Nicotinamide therefore a co-crystal may not be formed from the 1:1 mixture from water Figure 1.13.

Figure 1.12: Ternary phase diagram of methanol, Cinnamic acid and Nicotinamide (Chiarella, 2007)

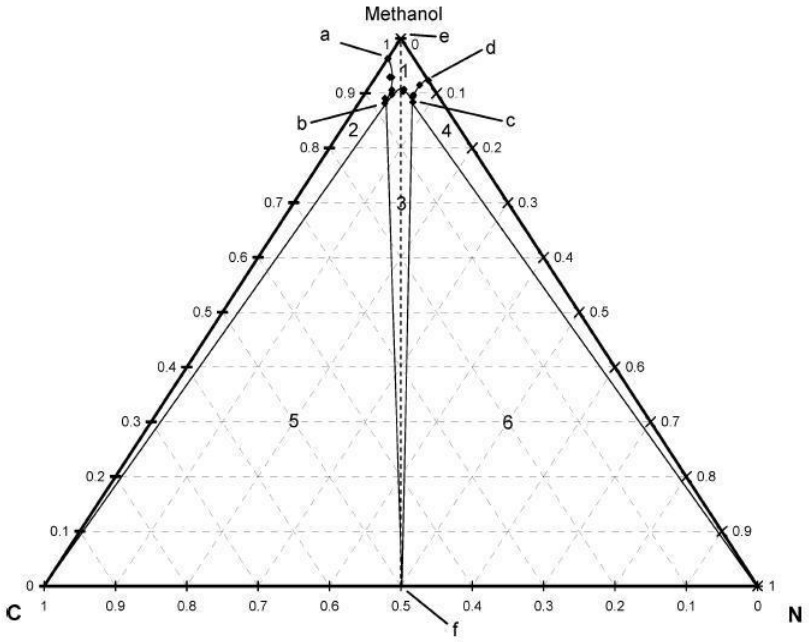

Figure 1.13: Ternary phase diagram of water, Cinnamic acid and Nicotinamide (Chiarella, 2007)

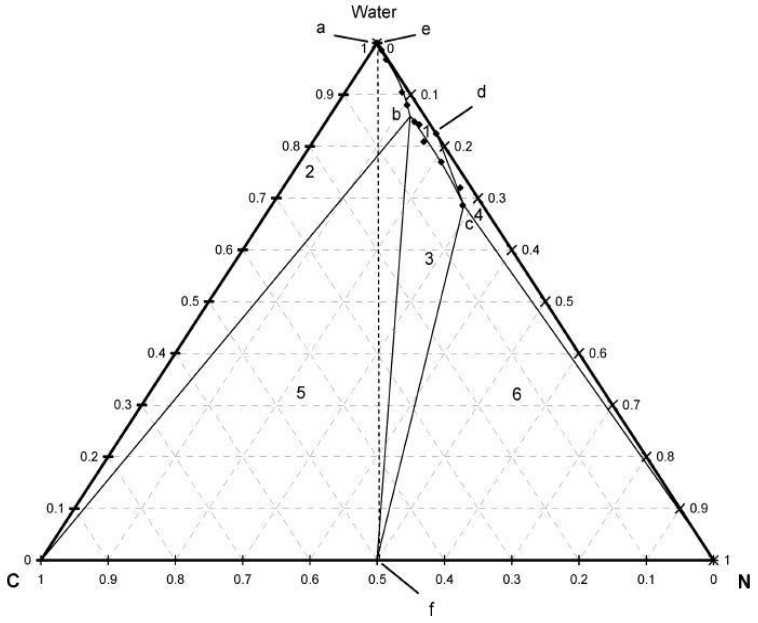

Phase diagrams highlight subtle difference in solubilities between target compounds and the co-crystallising agent, and the effect this has on the location of the co-crystal.

1.6 Crystal Growth and Nucleation

Crystallisation is a supramolecular process which by definition is a self-assembly process where component molecules find and recognise one another in solution and form an ordered solid crystalline solid. For crystallisation to occur, the solution must undergo three steps, supersaturation, nucleation and crystal growth (Mullin, 2004, Davey & Garside, 2000).

1.6.1 Supersaturation

Supersaturation refers to a solution which contains a higher concentration of the dissolved material (solute) than it would be expected in the same solution at equilibrium at a specific temperature. The degree of supersaturation is the primary driving force for the crystallisation process (Davey & Garside, 2000).

Figure 1.14 represents a hypothetical solubility curve, the blue curve is the solubility curve, the composition of a solution below this curve is undersaturated and existing crystals will be dissolved. The region above this solubility curve is supersaturated. The red line illustrates the composition of a solution above which spontaneous crystallisation occurs. The space between the two curves is the metastable zone; here crystallisation is not probable, but maybe induced by seeding (Mullin, 2004).

Figure 1.14: Diagram showing the solubility-supersolubiltiy diagram, the favourable metastable zone where crystallisation is prominent is highlighted to be between the red and blue lines.

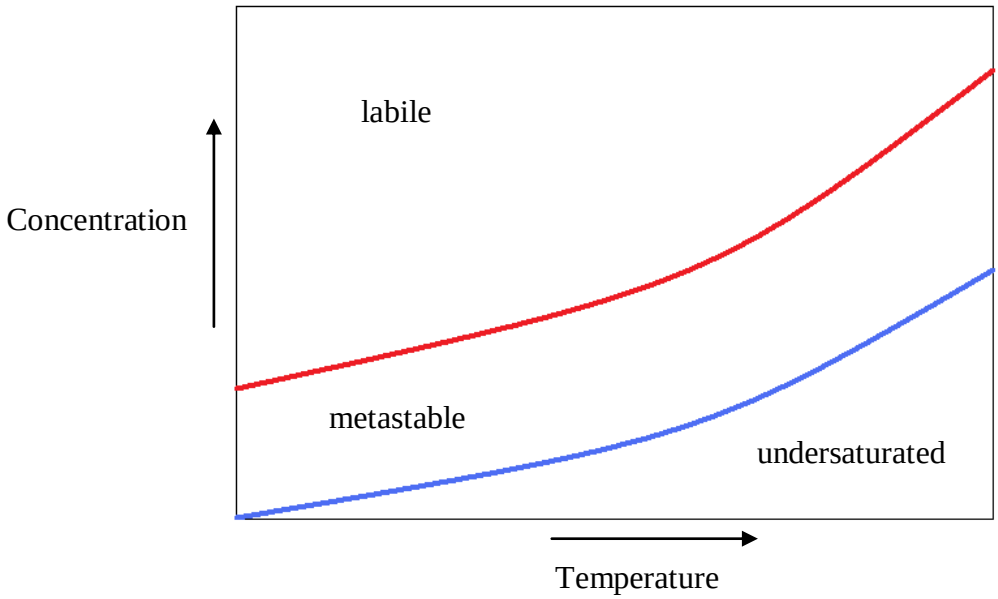

1.6.2 Nucleation

Creating new crystalline solid phases from a supersaturated solution is central to all types of crystallisation; however, supersaturation alone is not sufficient to initialise crystal growth. Before crystals can develop the solution must have building blocks, nuclei or seeds that act as central crystallisation sites. Nucleation may occur spontaneously or it may be induced artificially by a variety of methods such as mechanical shock, ultrasound, UV light and magnetic fields. Nucleation has been subdivided into primary and secondary nucleation. Primary is when a nucleus spontaneously forms, and secondary when a solution is seeded, these can either occur as heterogeneous or homogeneous processes (Figure 1.15)

Figure 1.15: Subdivisions of nucleation routes primary and secondary (Mullin, 2004)

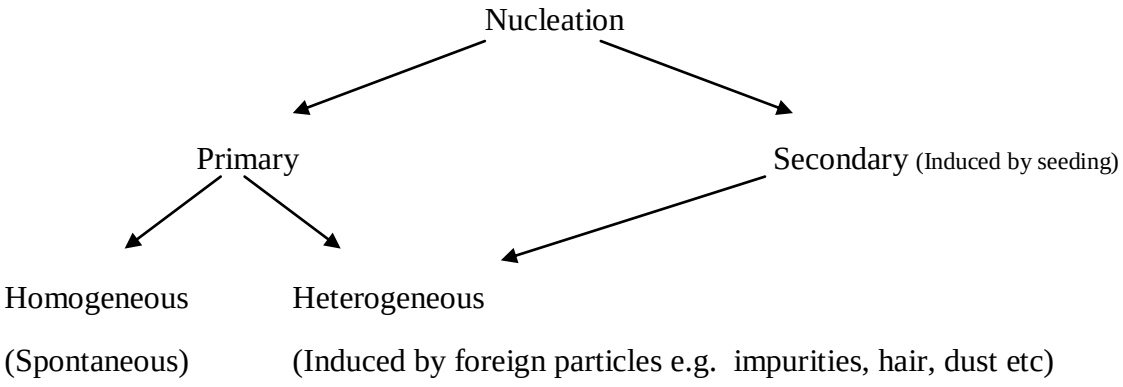

1.7 Co-crystal preparation methods

There are a number of procedures which can be used for co-crystal synthesis. Co-crystals are usually prepared by slow evaporation or solutions containing stoichiometric mole ratios of two or more components. They can also be prepared using the grinding method where two components are ground together, a co-crystal phase is formed from the ground mixture (Etter, 1991). Examples of acid-amide co-crystals i) Hex-2-enoic Acid: Isonicotinamide. (Aakeroy, 2003), ii) Piracetam and Gentistic acid (Vishweshwar, 2005).

Figure 1.16: Packing arrangements of i) Hex-2-enoic Acid: Isonicotinamide ii) Piracetam and Gentistic acid

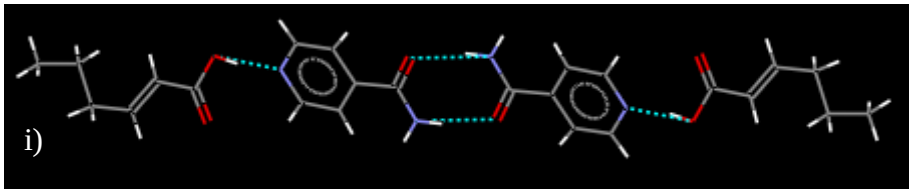

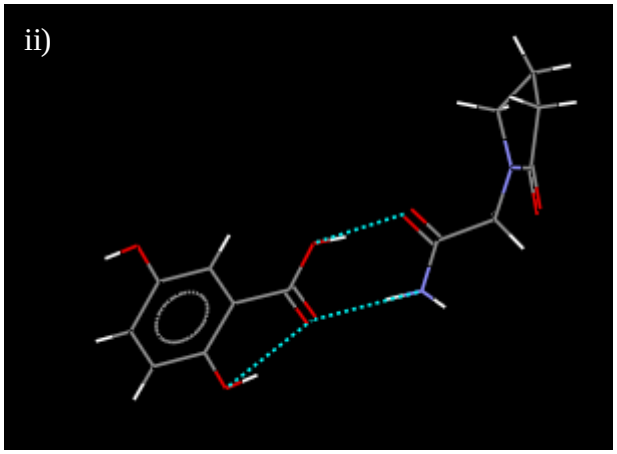

Figures 16(i) and 16(ii) show co-crystals with the anticipated hydrogen bond patterns of the acid to amide dimer, Figure 1.16(ii) and amide-to-amide dimer Figure 1.16(i). The hex-2-enoic acid: Isonicotinamide co-crystal also exhibits a pyridine and carboxylic acid moiety.

Solvent drop grinding has led to increased interest of solid-state grinding as a method which may help to control (Shan et al, 2002, Trask, 2004 a, b, c, d) polymorphs and also enhance kinetics and co-crystal formation. Additionally to this, sublimation and growth from the melt are also suitable methodologies for co-crystal growth.

1.8 Polymorphism and Polymorphism in Co-crystals

McCrone defined polymorphism as "…a solid crystalline phase of a given compound resulting from the possibility of at least two different arrangements of the molecules of that compound in the solid state…" (McCrone, 1965). In the 1999 Joel Bernstein and Roger Davey paper, (Bernstein & Davey, 1999) the authors comment on how different polymorphs have different structures and therefore each molecule has its own chemical and physical properties. The definition above is appropriate when speaking in the context of active pharmaceutical drugs (API's). These are highly functional and conformationally flexible molecules, this situation manifests itself when API's associate in the form of diverse set of multiple modes of self-organisation or self-assembly with other molecules. Hence crystal nucleation and growth is governed by a combination of thermodynamic and kinetic factors. Attaining a desired polymorph is of the utmost importance in drugs, agrochemicals, explosives, dyes, pigments flavours and confectionary products (Vishweshwar, 2006).

Awareness of polymorphs has grown, there has been a huge increase in the effort by crystal engineers to understand the phenomenon and to gain control over crystallisation process in order to selectively obtain a desired polymorph or suppress the growth of an undesired one. (Vishweshwar, 2006, Bernstein & Davey, 1999) It is important for

pharmaceuticals in the context of intellectual property (IP) rights to make sure that that they have control over polymorphism in the development and marketing of drugs.

The Cambridge Structural Database is helpful in the study of polymorphism, both in crystals and co-crystals. An analysis on polymorphism using the CSD is presented in *'Pharmaceutical Co-crystals- Review'* by Vishwesherwar et, al 2005 (Vishweshwar, 2005). The results are presented in Table 1.3.

Table 1.3: CSD search statistics shown (Aug'05 update) for all polymorphic systems. (Vishweshwar, 2006)

	No. Of entries in CSD	% Of organic structures
Organic crystal structures	130448	100[c]
Single component molecular organic structures	9621	7.3[c]
Single component polymorphic structures	94900	72.7[c]
Hydrates	1600[a]	1.7[d]
Co-crystals	1487[b]	1.1[e]
Polymorphic co-crystals	21[a]	1.5[d]

The CSD searches were conducted with only organic crystal structures. A CSD with 'only organics' as a parameter also retrieves structures containing metals like Na, K, Ca etc. Such entries were excluded from the statistics shown in the table above.

[a] Only one ref code was counted for each polymorphic compound.
[b] Co-crystals sustained by strong hydrogen bonds.
[c] Percentage with respect to organic systems only.
[d] Percentages with respect to 94, 900 and 1, 487 sub-totals respectively.

From Table 1.3 it is evident that 21 hydrogen-bonded co-crystals were identified in the CSD that exhibit polymorphism. As time progresses and research in this field continues we are likely to see an increase in the number of co-crystal reported in the CSD. The CSD supports both the archiving of crystal structures and software to search these archives. The specific features in the CSD relevant to the research in this project are as follows.

1.9 The Cambridge Structural Database (CSD)

The Cambridge Crystallographic Data Centre (CCDC) is the centre of the Cambridge Structural Database (CSD). The CCDC manages and maintains the CSD and all other components available for structural analysis. The CSD is an invaluable tool for the organisation and statistical analysis of experimental structure data for crystal engineers. It was initiated in 1965 by Dame Cathy Lonsdale, with almost 2000 entries initially, however today it carries accurate X-ray crystal structures of over a quarter of a million compounds (Nangia, 2002). The article by McMahon, Vishweshwar et al (McMahon, 2005), illustrates the apparent simplicity in data mining and structural analysis for today's crystal engineer. McMahon and colleagues carried out a CSD analysis of primary amides. The results show that Primary amides are very diverse in their ability to form hydrogen bonds with the two hydrogen bond donors (NH_2) and an acceptor (CO).

Figure 1.17: Extracted from (McMahon et al., 2005) A Histogram of N-H···O hydrogen bond lengths in primary amide dimers retrieved from the CSD

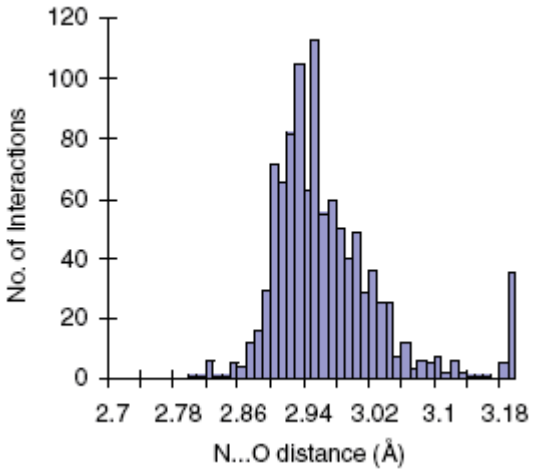

The histogram above has been extracted from McMahon, it illustrates the N-H···O hydrogen bond formation in Primary amide dimers. The CSD survey carried out also

took the formation of heterosynthons into consideration. Table 1.4 lists key contact data for amides, and has been extracted from the paper presented by McMahon, 2005.

Table 1.4: Primary amide general acceptor-donor table

Pro-Synthon	Total Groups (i)	Total Hetero (%) (ii)	Total Amide Homo (%) (iii)	Total Pro-syn Homo (%) (iv)	Hetero exclusive of Homos(%) (v)	Range (Å) (vi)	Mean (Å) σ (vii)
Dimer	1231	–	428(34.8)	–	–	2.75–3.15	2.95(5)
Catemer	1231	–	227(18.4)	–	–	2.75–3.20	2.96(8)
Acid CO 2pt	148	69(46.6)	65(43.9)	9(6.1)	40(27.0)	2.80–3.25	2.96(8)
Acid OH 2pt	148	69(46.6)	65(43.9)	9(6.1)	40(27.0)	2.40–2.80	2.56(6)
Alcohol CO	255	110(43.1)	78(30.6)	60(23.5)	41(16.1)	2.60–3.00	2.75(8)
Alcohol NH2	255	112(43.9)	78(30.6)	60(23.5)	43(16.9)	2.73–3.20	3.00(9)
Cyano	62	33(53.2)	42(67.7)	–	12(19.4)	3.00–3.30	3.15(9)
Cl^-	56	41(73.2)	8(14.3)	–	34(60.7)	3.10–3.60	3.34(8)

The trends in the analysis indicate that there are 80 primary amide structures in which competing hydrogen bond donor and/or acceptor groups are absent. The percentage or occurrence for the dimer is seen to be 84% with 14% for catemer. Focussing on Acid-Amide interactions, McMahon et al's results show that there are 148 crystal structures where both the acid and amide moiety is present, 69 of these structures hold the acid-amide heterosynthon, whereas only 9 hold the acid-amide homosynthon and 65 exhibit the amide homosynthon (McMahon, 2005).

1.10 Characterisation techniques

1.10.1 Thermal analysis

Thermal analysis is the ideal tool to examine the variation of one or more properties of a sample with increase of temperature. It is a powerful tool which provides valuable information for chemists on a multitude of thermodynamic events such as melting points and crystal phase transitions.

1.10.1.1 Differential Scanning Calorimetry (DSC)

The International Confederation for Thermal Analysis (ICTA) nomenclature committee has defined DSC to be "a technique for recording the energy necessary to establish a zero temperature difference between a substance and a reference material against either time or temperature, as the two specimens are subjected to identical temperature regimes in an environment heated or cooled at a controlled rate' (Pope & Judd, 1977).

In some differential scanning calorimeters, separate heat source and temperature detecting devices are applied to the sample and reference materials. Most differential scanning calorimeters fall into two categories:

1. Power compensation: The DSC cell is designed to have the provision of separate temperature sensors and heaters for the sample and the reference. During a thermal process, any temperature difference between the sample and reference materials will be resigned by differential thermal power supplied to the heaters to eliminate the difference. The differential thermal power is recorded as instrument signal, and therefore, this type of calorimeters belongs to "power-compensation" calorimeter (Wilson & Haines, 2002).

2. Heat-flux: Another type of calorimeter is “heat-flux” type where the sample and reference materials share the same furnace. The instrumental signal is derived from the temperature difference between the sample and reference whilst heating. Additional software is incorporated in the instrument to convert the temperature difference into differential thermal power (Wilson & Haines, 2002).

DSC is a universal and versatile technique for the characterisation of pharmaceutical solids because it gives useful insights on thermal reaction of the sample. The technique can be used to measure the glass transitions, ‘cold’ crystallisation, phase changes, melting points, crystallisation, product stability and the decomposition of the material. In addition to this mixture analysis of polymorphs can also be performed as well as establishing a relationship between DSC profile and two-component phase diagram, so that it may provide some clues of the formation of co-crystal (Pope & Judd, 1977).

1.10.1.2 Thermogravimetric Analysis (TGA)

TGA is the evaluation and the interpretation of the results from an experimental technique called thermogravimetry (TG). This technique has been defined by the International Confederation for Thermal Analysis and Calorimetry (ICTAC), as *“a technique in which the mass change of a substance is measured as a function of temperature whilst the substance is subjected to a controlled temperature programme”* (Wilson & Haines, 2002).

The instrument consists of several essential components, such as the microbalance, furnace, and thermocouples. Modern microbalance design incorporates an electronic

zero detection device, with an electromagnetic system to restore the balance. This new design allows users to reduce the amount of sample loaded from one gram or more to 10-100 mg, so that a more uniform temperature can be accomplished throughout the sample. The temperatures generated by the furnace are dependent on the type of alloy wire or ribbon wound on the ceramic or silica tube in the furnace. More commercial systems can cool samples using liquid nitrogen, they can be programmed to control sample temperature from -160°c to 1600°c. During heating, an inert purge gas such as nitrogen or argon is used to prevent air-mediated oxidation or combustion. To measure the temperature of the sample and to maintain a linear heating rate of the furnace, the TGA houses two separate sets of thermocouples. One is used for the measurement of sample temperature; this has to be located very close to the sample, usually underneath the sample but not quite touching. The other couple is to measure the furnace temperature in order to obtain a steady and linear heating rate (Wilson & Haines, 2002).

TGA is an ideal technique to determine thermal properties of pharmaceutical solids. It is highly sensitive as it can detect many thermal events such as decomposition, sublimation, reduction, desorption, absorption and vaporization, based by weight changes in a material as a function of temperature under controlled atmosphere (Hatakeyama & Zhenhai, 1998). In case a solvate crystal is obtained from solvent co-crystallization. TG can be used to detect any lose of a volatile component from the sample. Such a reaction can be picked by an allied technique like Differential Scanning Calorimetry (DSC).

1.10.1.3 Hotstage microscopy, the Kofler approach

Thermomicroscopy provides a simple and quick screening method which helps determine chemical and physical properties of compounds. The hot stage contact method is based on the work carried out by Lehmann, where he developed hot stages to elucidate co-crystal formation in 1877 (Davis, 2004). These mixed fusion methods have been further refined by Kofler and Kofler (Davis, 2004). Kofler and Kofler developed the Kofler Hot Stage which allows controlled heating under the microscope. A mixed fusion sample is prepared by melting the component with the highest melting point (A) first on one edge of a cover slip on a microscope slide, once cooled then the other component (B) is melted on another edge of the coverslip. (Figure 1.18). The two components will meet as component B melt is drawn under the coverslip and mixes with the solid of the component A. The point at which the two components meet is the mixing zone. Both ends of the slide contain 100% of either component where the area between forms a concentration gradient. When the slide is reheated and observed under the microscope, any new phase formed can be observed.

This region is then placed under a microscope and heated on a hot stage, Observations of this region are done using cross polarised filters, anisotropic crystals possess certain optical properties such as interference or polarisation (McCrone, 1957).

Figure 1.18: A schematic representation of the regions when preparing a Kofler slide: region A represents the highest melting component, region B represents the lowest melting zone and the region in-between is the mixing zone where any potential new phases may appear upon heating under polarised light.

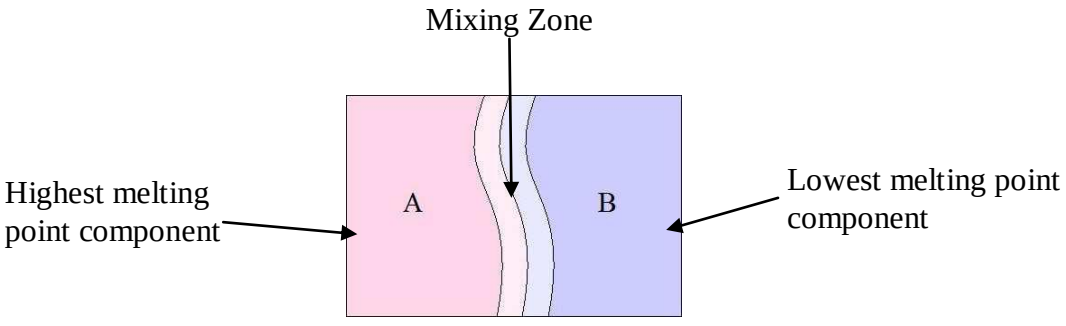

1.10.2 X-ray Powder Diffraction

In X-ray diffraction the data collected from the scattering of the radiation beam provides necessary information on the atomic arrangements and structure of crystalline materials. A pattern is produced from which the positions of the atoms and the structure can be determined. The pattern is produced by the scattering of the waves spread out spherically from all the atoms in the sample. There is some interference caused in the radiation beam by the atoms, this affects the intensity of the scattered radiation, which can be positive or negative. Negative interference reduces the strength of the signal, therefore only the positive interference is recorded, thus giving a pattern full of peaks. The peaks in an X-ray diffraction pattern are directly related to the atomic spacing of the material that is being irradiated. X-ray diffraction is one of the most important tools of solid-state chemistry. It is key to the determination of atomic arrangements, geometry and crystal structures.

W. L. Bragg showed that every beam that is diffracted from a crystal can be regarded geometrically as if it were a reflection from sets of parallel planes passing through lattice points.

This is very similar to light being reflected on a mirror, where the angle of incidence and reflection are equal. Thus suggesting the incoming and outgoing beams lie on one plane as do the normal and reflecting planes, Figure 1.19.

In order to define a plane three integers are necessary. These correspond to the three unit-cell edges, *hkl*. The spacing between successive planes is determined by lattice geometry, which is a function of the unit cell parameters. Thus allowing each observed diffracted beam/reflection to be labelled with its three indices and the net scattering angle, (2θ from the direct beam direction) to be calculated from the unit cell geometry.

This is well described by the Bragg equation (equation 1.10), this equation has become universally used as the basis for X-ray diffraction geometry (Clegg, 1998).

Figure 1.19: The Bragg's law, for diffraction by a 3D crystal structure; one set of parallel lines is seen edge-on. Adapted from (Clegg, 1998)

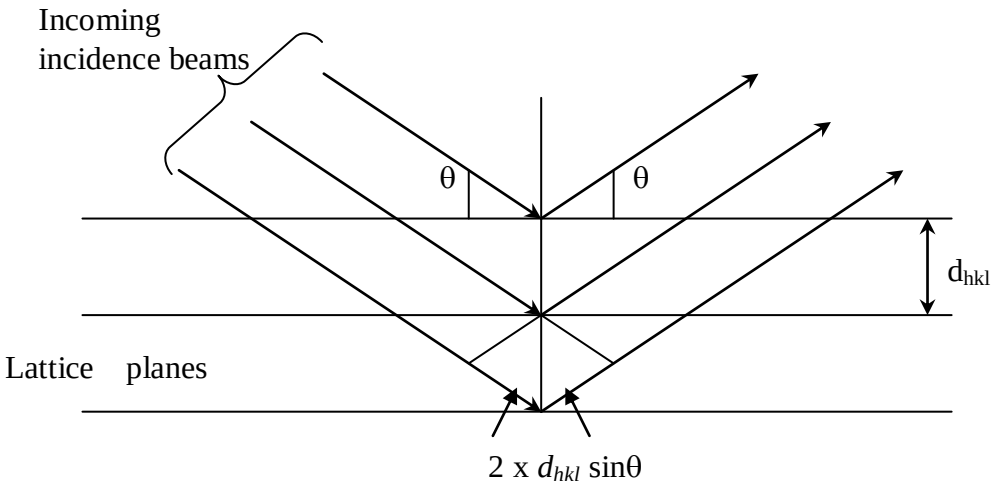

Equation 1.10 Braggs Law

$$n\lambda = 2d_{hkl} \sin\theta \qquad (1.10)$$

Where:

d_{hkl} = inter-planar cross sectional space

λ = Wavelength of X-ray

θ = Scattering angle

1.10.2.1 X-ray diffraction methodology

X-ray powder diffraction was the principal technique used in determining co-crystal formation. A Bruker AXS D8 Advance powder X-ray diffractometer was used, it has a copper K_α radiation source and scintillation counter detector. The software used to collect the data is the DIFFRAC^{plus}, files were converted and read into EVA, which is a qualitative and Semi-quantitative phase analysis package. Samples are in the form of a microcrystalline powder, this should present all possible crystal faces. Once irradiated, each of them gives its own diffraction pattern.

Samples are prepared by grinding larger crystals into a crystalline powder. This was then presented on a Perspex disc and placed perpendicular to the incident beam in the Bruker D8 machine. The powder patterns collected where then compared against the patterns of the starting materials to determine whether co-crystal is present. These powder patterns were taken from published structures in the CSD using the Mercury program.

1.10.2.2 Single crystal X-ray diffraction

Single-crystal X-ray diffraction is a non-destructive analytical technique which provides detailed information of the three-dimensional arrangement of atoms in a crystal by examining the diffraction of X-rays from an ordered array of many molecules (Bernstein, 2002). The fundamental principles of single crystal X-ray diffraction is the same as PXRD, however the analysis is much more challenging.

This technique is mostly used for precise determination of a unit cell, including cell dimensions and positions of atoms within a lattice. Bond lengths and angles are directly related to the atomic positions in the crystal lattice. Applications of single-crystal diffraction include:

- New mineral identification, crystal solution and refinement
- Determination of unit cell, bond-lengths, bond-angles and site-ordering
- Characterization of cation-anion coordination
- Variations in crystal lattice with chemistry
- With specialized chambers, structures of high pressure and/or temperature phases can be determined
- Determination of crystal-chemical vs. environmental control on mineral chemistry
- Powder patterns can also be derived from single-crystals

Chapter Two: Design Strategy for co-crystallisation

2.1 Introduction

The previous chapter introduced the concepts of crystal engineering and co-crystallisation. This chapter explains the rationale behind the strategy that has been employed to initiate co-crystal growth. The techniques used to screen, the primary amides and co-crystallising agents and the thesis aims and objectives.

2.2 Thesis aims and objectives

2.2.1 Project Aims

The project aims to understand contrast the formation of carboxylic acid co-crystal with two amides by probing the packing arrangement similarities and subtleties in structural conformation in order to design co-crystals by use of structural features which are desirable to the pharmaceutical, fine chemicals and agrochemical industry. Isonicotinamide and Benzamide were selected for this work, as the former is a well documented and used co-crystal former whilst the latter has only two reported compounds. The approach adopted was to examine the crystal growth of these systems in a limited screen, along with concurrent work on developing a database search of co-crystal packing. To this end collaboration with the developer of dSNAP, Dr Gordon Barr of The University of Glasgow, was undertaken. This code integrates the output from the Cambridge Structural Database for key molecular packing features within a series of crystal structures. The limited crystal screen protocols were developed and implemented on a series of target systems. The focus was to setup a generic route to molecular solid formation which could be assessed for robustness. This screen was then extended to a low through-put device and then further extended to the high through-put with the addition of a structurally similar active ingredient Nicotinamide, the screen for which was designed and developed on site at Syngenta, the data from this screen will be

analysed by the use of polySNAP, further extending collaborative work with Professor Gilmores group at The University of Glasgow. Simultaneous work also involves the Kofler contact method which allows visual inspection of potential co-crystal phases, this work will be validated with extended thermal experiments using DSC.

To further understand phase behaviour during co-crystallisation, phase diagrams have been investigated with co-crystals formed with the three active ingredients and Succinic Acid.

2.2.2 Objectives

The objectives of the work is outlined by four key issues which will be addressed

1. Synthon and Motif strategies within the literature, by identification of known co-crystals of the target formers. Solution screen development using basic slow evaporation methods, low through put and high through put. (chapters 3, &5)
2. Understanding of the packing arrangements of the comparison model by implementation of dSNAP for co-crystal systems (chapter 4)
3. How does the analysis of PXRD patterns from a High through-put screen compare to results from thermal techniques of the binary systems. (chapter 5 & 6)
4. Understanding phase behaviour by plotting Phase diagrams of three models in methanol system and a water system (chapter 7)

2.3 Compound Selection

The main concept to consider when selecting compounds for co-crystallisation is whether they hold functional characteristics to act as hydrogen bond donors and acceptors as well as the general rules for hydrogen bonding in the design of hydrogen bonded solids as outlined in section 1.3.1. Also, compounds that are polymorphic display structural flexibility, which can therefore increase the chances of co-crystallisation as mentioned in section 1.8. For the initial work the co-crystal examples given below will be the basis of the work presented in later chapters, with the introduction of programs such as dSNAP and polySNAP, screening methods using Hotstage microscopy and a High through-put robot.

2.3.1 Isonicotinamide

Extensive research carried out by Christer Aakeröy and his group (Aakeröy et, al, 2002-2006) include the co-crystallisation of Isonicotinamide (INA) and shows that this amide has demonstrated to be a reliable supramolecular reagent (SR) when combined with carboxylic acids. Additionally a review of the Cambridge Structural database (CSD) revealed that INA co-crystallises with a series of carboxylic acid. The search shows that there are over 25 co-crystal structures reported in the CSD, 20% of which exhibit the acid-pyridine hydrogen bond motif. As discussed in the previous chapter pyridines and primary amides can hydrogen bond to carboxylic acids forming robust synthons. The co-crystals from this review are presented in Table 2.1, consist of the following co-formers.

Table 2.1: Co-crystal structures viewed in the literature and corresponding Reference codes from CSD deposits. All structures have been labelled 1-13 and have been referred to accordingly through this chapter.

	Acids	Isonicotinamide	Benzamide
1	Acetic Acid	JAWWAG	N/A
2	Tartaric Acid	Private communication	N/A
3	Succinic Acid	LUNNUD LUNNUD01	BZASUC
4	Fumaric Acid	LUNNOX	N/A
5	Glutaric Acid	ULAWOT ULAXAG	N/A
6	Adipic Acid	ULAWUZ ULAXAG	N/A
7	Benzoic Acid	BUDWEC	N/A
8	2-Hydroxybenzoic Acid	XAQQEM	N/A
9	3-Hydroxybenzoic Acid	LUNMEM	N/A
10	4-Hydroxybenzoic Acid	VAKTOR	N/A
11	Cinnamic Acid	LUNMAI	N/A
12	d, l-Mandelic Acid	LUNPAL	N/A
13	4-Nitrobenzoic Acid	AJAKEB	N/A

A description of the crystal packing seen in the amide co-crystals present in the CSD will be covered, the aim is to present a view of the types of motifs present.

2.3.1.1 Acid - Amide packing of Isonicotinamide co-crystal review:

In this section the packing arrangements of Isonicotinamide – Carboxylic Acid co-crystal is discussed and examples using Mercury outputs are provided, the numbers correspond to the numbers associated to the co-crystal phase listed in Table 2.1.

Mono Carboxylic Acids/Benzoic Acid Derivatives: 1:1 ratio.

Isonicotinamide with carboxylic acid 1, 7-13, supramolecules are formed with 4 components (2 INA, 2 Acid), these are assembled via acid-pyridine and exhibit complementary amide-amide Hydrogen interactions.

Co-crystal **1** is extended into a 2-D sheet, formed via N-H---O and C-H---O H-Bonds between supermolecules, whereas for **7, 9, 12, 13,** components are assembled via acid-pyridine H-bond interactions and self complementary amide-amide interactions, which when extended gives a 2-D cross linked laddered network. **8, 11** form an infinite tape, while **10** forms an infinite zig zag chain.

Figure 2.1: a) showing packing for co-crystal 8 and b) co-crystal system 10

a) b)

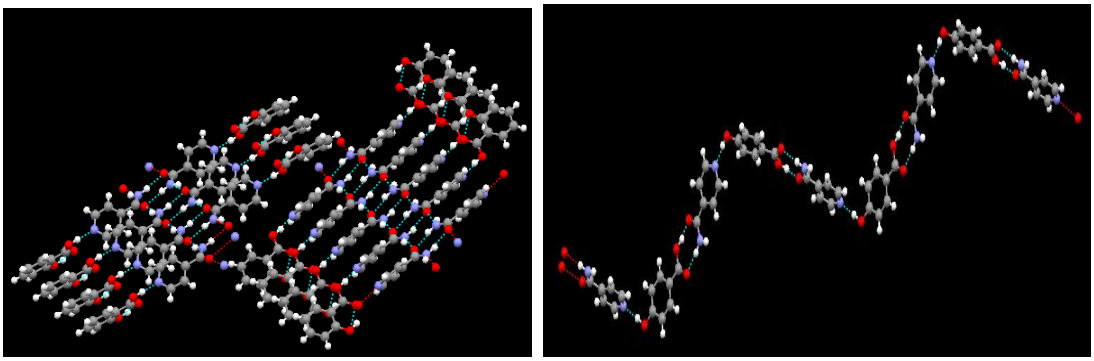

Di-Carboxylic Acids: 1:1 ratio. Co-crystals 5, 6. Hydrogen bonded tapes assembled via acid-pyridine and acid-amide hydrogen interactions. The N-H---O and C-H---O interactions between the tapes extend to form an extended tape/ribbon.

Figure 2.2: showing packing for co-crystal system 5

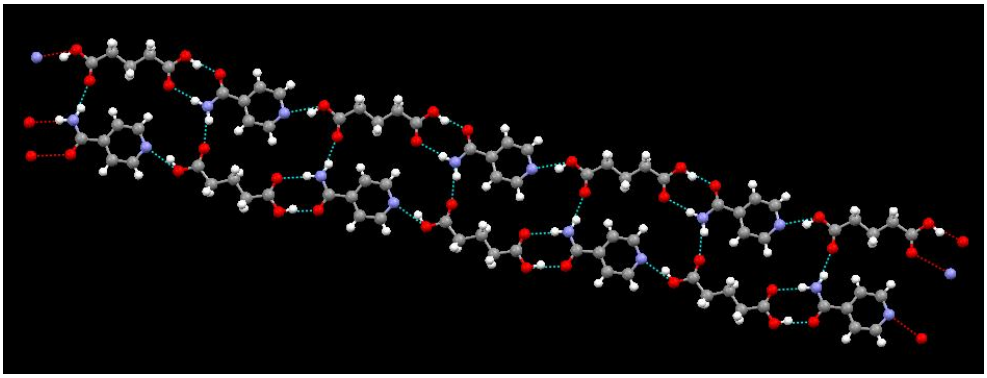

Di-Carboxylic Acids: 2:1 ratio. Co-crystals **3, 4.** 4 component supermolecule via acid-pyridine H-bond interactions and self complementary amide-amide interactions forms 1-D chain when extended, between the chain interaction between N-H---O gives a 2-D sheet.

5, 6. Tapes assembled via acid-pyridine H-bond interactions. A sheet is formed via N-H---O and C-H----O interactions between the tapes.

The packing reveals that the primary intermolecular interaction is the O-H---N hydrogen bond between the acid and the N-heterocyclic nitrogen atom as well as the amide-amide dimer.

For this project we have selected Isonicotinamide as a model active ingredient (AI) because it has robust acceptor and donor sites allowing co-crystallisation with small simple carboxylic acids, which range as mono-carboxylic acids, di-carboxylic acids and benzoic acid derivatives. These are to be compared with another 1° amide, Benzamide. The rationale behind this was to switch off/ neutralise one end of the ditopic Isonicotinamide. Since the pyridine is the best hydrogen bond acceptor and donor,

taking away this site will leave a monotopic structure. A CSD search was once again established and only one co-crystal with the selected carboxylic acid has been reported, Table 2.1 also displays the results from this search.

2.3.2 Benzamide

A literature review and structure search of the database has revealed that this primary amide has a low success rate in the formation of co-crystals with small carboxylic acids. The CSD search showed 7 structures which contain Benzamide, only one of which has the acid-amide hydrogen bond motif. Because of this low rate of co-crystals present in the CSD for Benzamide, and the literature indicating a number of carboxylic acids which co-crystallise with Isonicotinamide; also highlighted in Table 2.1, these acids shall be investigated as co-crystallisers with Benzamide. Consequently, any successful single crystals would be analysed and the structures obtained with Benzamide and the respective Isonicotinamide co-crystals shall be reviewed for structural similarities.

2.3.2.1 Acid - Amide packing of Benzamide co-crystal review:1:1 ratio

Co-crystal **3.** Components are assembled via acid-amide interactions, which when extended gives a tape formed via C-H---O interactions.

Figure 2.3: showing packing for co-crystal system 3

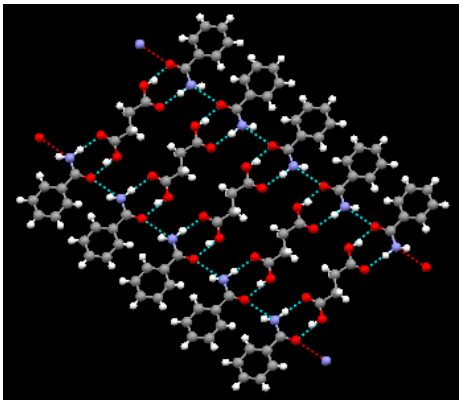

On the basis of the success rate and the compatibility of Isonicotinamide and the carboxylic acids presented here it would be interesting to compare the success of co-crystal formation with Benzamide.

2.3.3 Nicotinamide

For the studies presented later, Nicotinamide has been employed in the high through-put screen and phase diagram determination.

Nicotinamide, also known as niacinamide and nicotinic acid amide, is a water-soluble vitamin and is part of the vitamin B group (B3). It has been reported that Nicotinamide possesses six polymorphs (Kofler & Kofler, 1943), however only form I of the polymorphs can be obtained from solution, the others being meta-stable (Hino et al, 2001, Berry et al, 2008). Nicotinamide structurally possess potential synthons which are compatible for intermolecular interaction with carboxylic acids. Searches of the literature and the CSD identified that there are 23 structures which contain Nicotinamide, only 8 of these structures were molecular adducts whilst the remaining were redeterminations of Nicotinamide form I, salts and have no coordinates. This search shows that this AI is a promising contender for co-crystal formation with the carboxylic acids selected for the high through-put screen.

2.4 Experimental Design

Co-crystals have been prepared from solution and by solid-state/solvent mediated grinding as discussed in section 1.7. The examples of the Isonicotinamide carboxylic acids discussed in section 2.3.1 and have been prepared with following stoichiometric amounts. With one Isonicotinamide per mono-carboxylic acids, with two Isonicotinamide per di-carboxylic acid, and all of these were dissolved in warm ethanol and then cooled to room temperature, crystals were formed upon slow evaporation of the solvents, and this could take from hours to days for any crystals to nucleate (Aakeröy et al., 2002).

2.4.1 Slow Evaporation

The work undertaken for this study includes crystallisation using the slow evaporation method, as this is the simplest way to grow crystals. Solutions must be prepared in a suitable solvent and it must be saturated or nearly saturated. For this the solubility of the two must have similar solubility in the solvent otherwise the least soluble component will crystallise out exclusively.

This evaporation method has been established in this work as a preliminary technique to reiterate the Isonicotinamide work established by Aakeröy et al., 2002, and additionally to form a comparison with a structurally similar amide, Benzamide. This bench method will then be modified to be implemented on a low through-put device, ReactARRAY (chapter 3). This will allow slow-evaporation in a temperature controlled environment. The results from these screens will be further analysed to identify the structural similarities and behaviour of successful co-crystals from the least competitive amide using dSNAP.

2.5 dSNAP

The Cambridge Structural Database (CSD) is forever growing, with this and the large number of datasets retrieved whilst searching, it can be sometimes difficult to classify chemical information. However, although there are various algorithms and data mining strategies in the literature, (Orpen 2002, Allen & Motherwell 2002), there is however a niche for a freely available program which classifies results from database searches (Aakeröy & Beatty, 2001). In 2005 Barr et al indicated detail in flexibility and presented a new approach encoded in the dSNAP program which is designed to assist structural chemist in classifying information extracted from CSD searches.

dSNAP is a computer program which classifies and clusters structural fragments extracted from the Cambridge Structural Database. The methodology is based on cluster analysis and multivariate data processing of distance matrix information describing the extracted fragments.

For this program, it is essential to have single crystal data from the CSD or experimental single crystals from the screens carried out in this work.

2.6 High through-put

The concepts of high through-put (HTP) screening have been well established and applied across the entire pharmaceutical value chain, including the screening of active molecules in discovery, form selection for preclinical candidates, final form optimisation, and process chemistry development of crystallisation processes for bulk drug and intermediates as well as identification of new solid forms for product life cycle management. High through-put form screening is available and has been described in the literature, indicating that this new methodology is just at beginning to make a platform for itself (Morissette el al., 2004).

A contribution to this work involves the use of a high through-put robot as a method to screen for co-crystals with the above mentioned active ingredients, Isonicotinamide, Benzamide and Nicotinamide, along with the following coformers and solvents.

Figure 2.4: Benzoic acid derivatives used for the High through-put screen and Hotstage microscopy.

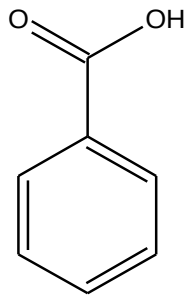

Benzoic Acid

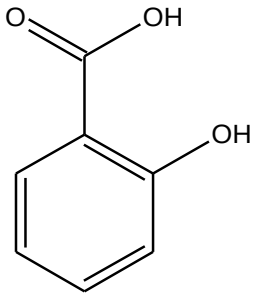

2 Hydroxybenzoic Acid

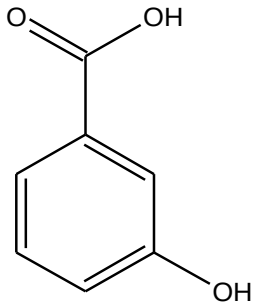

3 Hydroxybenzoic Acid

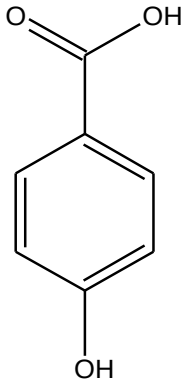

4 Hydroxybenzoic Acid

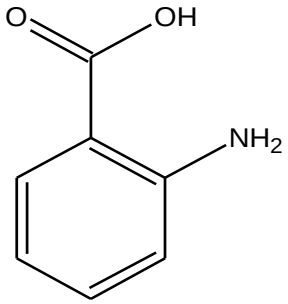

2 Aminobenzoic Acid

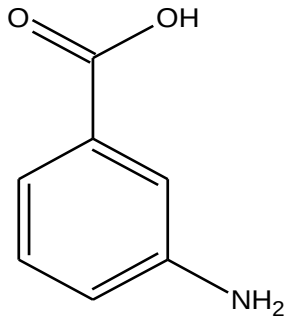

3 Aminobenzoic Acid

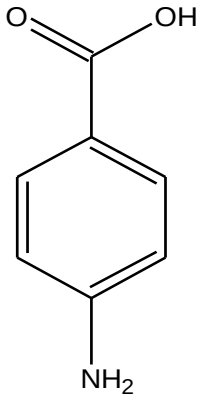

4 Aminobenzoic Acid

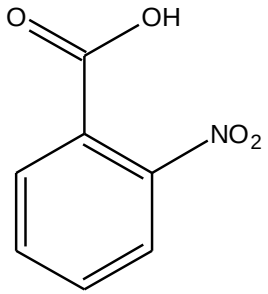

2 Nitrobenzoic Acid

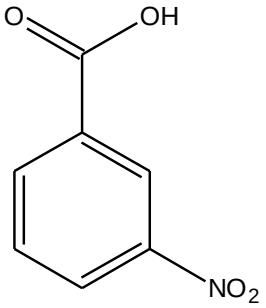

3 Nitrobenzoic Acid

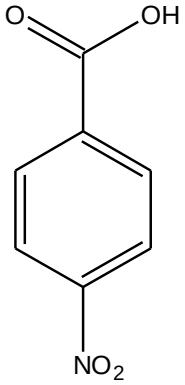

4 Nitrobenzoic Aci

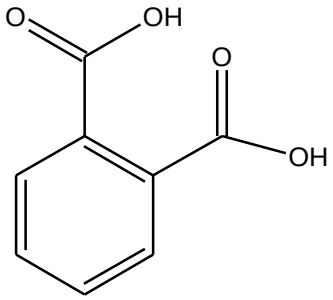

Phthalic Acid

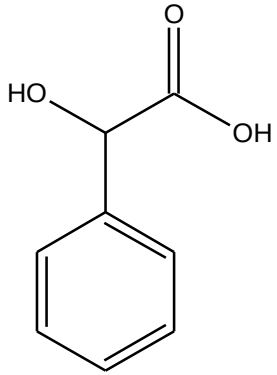

Mandelic Acid

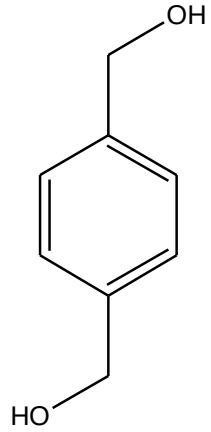

1,4 Benzene dimethanol

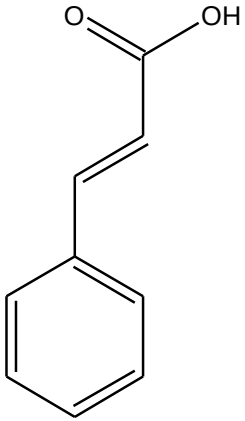

Cinnamic Acid

Figure 2.5: di-carboxylic acids used for High through-put screen and Hotstage microscopy.

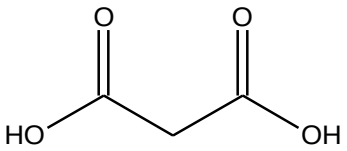

Malonic Acid

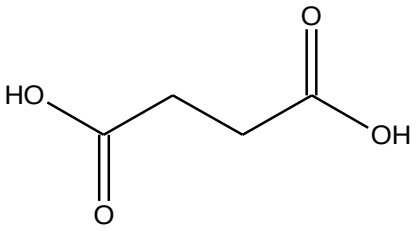

Succinic Acid

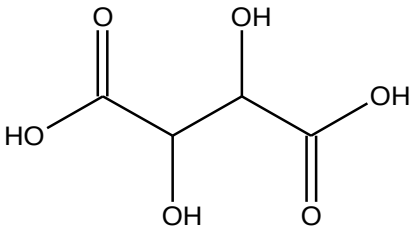

Tartaric Acid

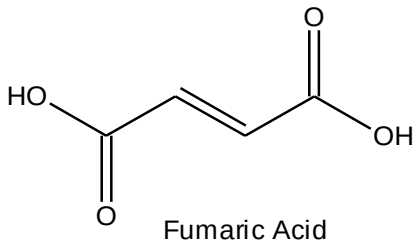

Fumaric Acid

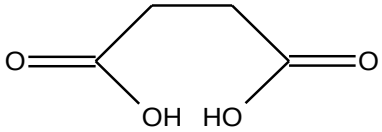

Malic Acid

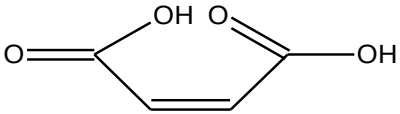

Maleic Acid

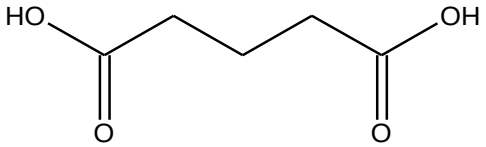

Glutaric Acid

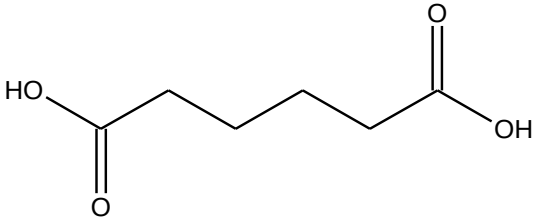

Adipic Acid

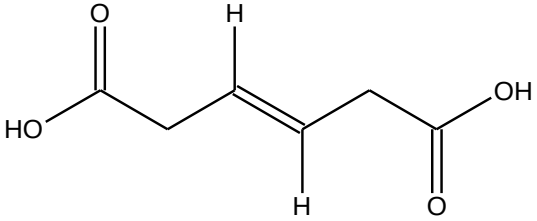

Trans β hydromuconic Acid

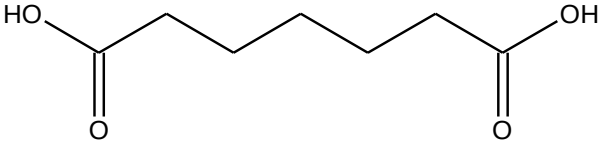

Pimelic Acid

Table 2.2: Active ingredients and coformers used in High through-put screen with corresponding solubilites and respective solvents. Solubility measure are according to 0.1g/ ml

Active Ingredient	RMM (g)	Solubility (%)	Solvent
Benzamide	121.14	10	Methanol
Isonicotinamide	122.12	10	Methanol
Nicotinamide	122.12	10	Methanol
Coformer	**RMM (g)**	**Solubility (%)**	**Solvent**
1, 4 Benzene dimethanol	138.16	5	Propanol
2 Nitrobenzoic acid	167.12	10	Methanol
3 Aminobenzoic acid	137.14	3	Methanol
3 Nitrobenzoic acid	167.12	10	Acetone
4 Aminobenzoic acid	137.14	10	Methanol
4 Nitrobenzoic acid	167.12	3	Acetone
Adipic acid	146.14	10	Methanol
Butanoic acid	88.1	10	Methanol
Fumaric acid	116.07	5	Methanol
Maleic acid	116.1	10	Methanol
Malic acid	134.09	10	Methanol
Phthalic acid	166.14	5	Ethanol
Pimelic acid	160.17	10	Methanol
Succinic acid	118.09	10	Methanol
Tartaric acid	150.09	10	Methanol
Trans β hydromuconic acid	144.13	3	Methanol

The preparation of co-crystals from solution requires the two components to have similar solubility in the solvent used otherwise the least soluble component will tend to crystallise out. One of the key points in co-crystallisation of an AI is to modify its physicochemical properties such as poor solubility. It is therefore a necessary condition for successful co-crystallisation to occur that the coformer is mutually soluble. All solvents selected have been approved by the FDA guidelines and Syngenta health and safety policy.

2.7 Kofler Hotstage

Another method used to screen and identify co-crystal phases is the Kofler contact method (Kofler, 1941). This method is a quick and simple way, it involves the melting of the component with the highest melting point between a microscope slide and a cover slip, and allowing cooling and re-crystallising. The second component should have a lower melting point, this is added to a free edge of the cover slip and heated so that the melt seeps under the cover slip and makes contact with the higher melting component. Where these two phases meet is the mixing zone, here the determination of a eutectic, mixed phase, or molecular compound of the liquid phases can be observed when placed on a temperature controlled hot stage and microscope using polarised light. For this work many new phases have been observed, with only a small number of failed attempts due to decomposition of coformers/carboxylic acids upon heating.

2.8 Future Thought of Work

Further investigation and rationalisation of co-crystal formation have been attempted using dSNAP and working with the a limited dataset has certainly highlighted subtleties in the crystal packing, however, to develop a protocol/method to understand these subtleties, further understanding is required of the entities by which co-crystals form. In particular the link between the pair wise design strategies and the impact on overall success with minor structural modification. For this project was contrasting the co-crystal behaviour of Benzamide, Isonicotinamide and Nicotinamide with a series of carboxylic acid co-formers.

With this in mind, a preliminary study was undertaken and is presented here as an indication to highlight a possible way forward using a computational led approach. Historically the interaction between a solute and solvent and the co operative impact of the electronic densities was profiled using the induced dipole moment. Work by Le Fèvre (1948), discusses the induced moment in a solvent molecule collinear with the chief moment of the solute as shown in equation 2.8

Equation 2.8 Fèvre Induced Dipole:

$$\boldsymbol{\mu_{ind} = 2\mu\alpha(\varepsilon + 2)/3r^3\,\varepsilon} \qquad (2.8)$$

Where α is the polarizability of a solvent molecule and μ is the dipole moment, we have attempted to adopt this equation to accommodate pair-wise association of solutes undergoing molecular complex formation. The success for specific combination is experimentally verified by the outcome conditions of the Hotstage screen. For our purposes and to simplify the initial feasibility of this approach, the focus was upon calculating the product of dipole moment and polarizability of interacting pairs as being proportional to the overall induced moment.

Equation 2.8.1 Modified dipole equation:

$$\boldsymbol{\mu_{ind} \propto \mu\alpha} \qquad (2.8.1)$$

Using equation 2.8.1, we have attempted to calculate the group contribution to a specific mode of association, where the difference in the dipole (μ) define the dipole of the hydrogen bond donor or acceptor site, and polarizability (α) which defines the polarisability of the hydrogen bond donor or acceptor site, of the coformers used in the study. This requires computation of the co-former and their parent molecules (the co-former with the hydrogen bond moiety replaced by hydrogen) and then computing the differences in dipole and polarisability of the coformers from that of the parent. This generates an approximation of the group contribution these quantities. The chemical entities used match the AI models used during Hotstage analysis. The aim of this calculation is to evaluate an estimation of product bond differences calculated with parent molecule and compare with the AI models, this would highlight the extent of dipole moment and polarisability along the hydrogen bond fragment (amino, nitro, carbonyl acid).

For this approach the following annotation was assigned to the amides and acid employed for the co-crystal systems presented in Chapter 5. Three groupings are envisaged acid self association, amide self association and the association for the complex permutation of these quantities. For the complex an average was taken to reach the average figure of the induced dipole moment.

Where $\boldsymbol{\mu_{ind}} \propto \mu\boldsymbol{\alpha}$ and

$\alpha_1\,\mu_1$ is for acid coformer

$\alpha_2\,\mu_2$ is for acid parent

$\alpha_3\,\mu_3$ is for amide (AI)

$\alpha_4\,\mu_4$ is for amide parent

$$\boldsymbol{Acid\ Self\ association} = (\boldsymbol{\alpha_1} - \boldsymbol{\alpha_2})(\boldsymbol{\mu_1} - \boldsymbol{\mu_2})$$

$$\boldsymbol{Amide\ Self\ association} = (\boldsymbol{\alpha_3} - \boldsymbol{\alpha_4})(\boldsymbol{\mu_3} - \boldsymbol{\mu_4})$$

$$\boldsymbol{Induced\ dipole\ momonet} = \frac{[(\boldsymbol{\alpha_1} - \boldsymbol{\alpha_2})(\boldsymbol{\mu_3} - \boldsymbol{\mu_4}) + (\boldsymbol{\alpha_3} - \boldsymbol{\alpha_4})(\boldsymbol{\mu_1} - \boldsymbol{\mu_2})]}{\mathbf{2}}$$

For the initial step in this study MOPAC within Mercury has been used with Hamiltonian method, PM3, to calculate the dipole and polarizability, details of which are widely reported in the literature (Le Fèvre, 1948). We have only used the conformations as is from the crystal structures a full future study would have to examine conformation and minimisation.

Below in table 2.3- 2.4the total sum of the dipole (μ) and the polarisability (α) average in $Å^3$ for the acids are given, along with the appropriate parent compound. (i.e. removing acid group from aminbenzoic acid and replacing with hydrogen leads to aniline). Those values for the amides are given for comparison.

Table 2.3: Sum of calculated dipole and polarisation of coformer and parent molecule of coformer.

Coformers	Isotropic Average (α) ($Å^3$)	Dipole Total Sum (μ)	Parent	Isotropic Average (α) ($Å^3$)	Dipole Total Sum (μ)
2 Aminobenzoic Acid	14.26067	1.16	Analine	23.12611	2.806

3 Aminobenzoic acid	28.8063	0.603	Analine	23.12611	2.806
4 Aminobenzoic Acid	28.83104	0.553	Analine	23.12611	2.806
Benzoic Acid	12.74775	2.396	Benzene	10.18784	0
Phthalic Acid	15.41667	3.102	Benzene	10.18784	0
Malic Acid	9.02892	5.636	Butanoic Acid	8.85973	6.661
Succinic Acid	9.25186	0	Butanoic Acid	8.85973	6.661
Tartaric Acid	10.23043	3.834	Butanoic Acid	8.85973	6.661
Fumaric Acid	18.33078	0.127	Crotonic Acid	8.15323	2.151
Maleic Acid	9.7636	2.393	Crotonic Acid	8.15323	2.151
Pimelic Acid	14.76023	3.273	Heptanoic Acid	13.79883	1.955
Adipic Acid	25.66317	0.134	Hexanoic Acid	11.98047	2.006
Trans B Hydromuconic Acid	20.07063	0	Hexanoic Acid	11.98047	2.006
2 Nitrobenzoic Acid	14.82729	6.496	Nitrobenzene	12.17161	5.162
3 Nitrobenzoic Acid	29.85699	1.642	Nitrobenzene	12.17161	5.162
4 Nitrobenzoic Acid	14.90951	4.083	Nitrobenzene	12.17161	5.162
2 Hydroxybenzoic Acid	13.42965	2.346	Phenol	32.14642	3.56
3 Hydroxybenzoic Acid	13.43805	1.92	Phenol	32.14642	3.56
4 Hydroxybenzoic	13.35981	3.483	Phenol	32.14642	3.56

Acid					
Malonic Acid	8.6809	3.581	Propanoic Acid	6.66292	1.831
1, 4 Benzene dimethanol	14.91808	0.054	p-xylene	13.82214	0
Cinnamic Acid	16.60408	2.933	Styrene	13.63709	0.039
Mandelic Acid	15.6876	3.885	Toluene	23.74607	0.128
Glutaric Acid	11.01605	3.2	Valeric Acid	11.28113	9.999

Active Ingredient (AI)	Isotropic Average (α) ($Å^3$)	Dipole Total Sum (μ)
Benzamide	13.54311	3.73
Isonicotianmide	12.95283	3.67
Nicotinamide	12.95221	3.857

Table 2.4: The self association of the dipole and polarisability of the acid coformer and its parent molecule, amide and its parent molecule is also presented.

Coformers	α_1 ($Å^3$)	μ_1	Parent	α_2 ($Å^3$)	μ_2	Self association ($\alpha_1 - \alpha_2$)($\mu_1 - \mu_2$)
2 Aminobenzoic Acid	14.26	1.16	Analine	23.13	2.81	14.59
3 Aminobenzoic acid	28.81	0.60	Analine	23.13	2.81	-12.51
4 Aminobenzoic Acid	28.83	0.55	Analine	23.13	2.81	-12.85
Benzoic Acid	12.75	2.40	Benzene	10.19	0.00	6.13
Phthalic Acid	15.42	3.10	Benzene	10.19	0.00	16.22
Malic Acid	9.03	5.64	Butanoic Acid	8.86	6.66	-0.17
Succinic Acid	9.25	0.00	Butanoic Acid	8.86	6.66	-2.61
Tartaric Acid	10.23	3.83	Butanoic Acid	8.86	6.66	-3.87
Fumaric Acid	18.33	0.13	Crotonic Acid	8.15	2.15	-20.60
Maleic Acid	9.76	2.39	Crotonic Acid	8.15	2.15	0.39

Pimelic Acid	14.76	3.27	Heptanoic Acid	13.80	1.96	1.27
Adipic Acid	25.66	0.13	Hexanoic Acid	11.98	2.01	-25.61
Trans B Hydromuconic Acid	20.07	0.00	Hexanoic Acid	11.98	2.01	-16.23
2 Nitrobenzoic Acid	14.83	6.50	Nitrobenzene	12.17	5.16	3.54
3 Nitrobenzoic Acid	29.86	1.64	Nitrobenzene	12.17	5.16	-62.25
4 Nitrobenzoic Acid	14.91	4.08	Nitrobenzene	12.17	5.16	-2.95
2 Hydroxybenzoic Acid	13.43	2.35	Phenol	32.15	3.56	22.72
3 Hydroxybenzoic Acid	13.44	1.92	Phenol	32.15	3.56	30.68
4 Hydroxybenzoic Acid	13.36	3.48	Phenol	32.15	3.56	1.45
1, 4 Benzene dimethanol	14.92	0.05	p-xylene	13.82	0.00	0.06
Cinnamic Acid	16.60	2.93	Styrene	13.64	0.04	8.59
Mandelic Acid	15.69	3.89	Toluene	23.75	0.13	-30.28
Glutaric Acid	11.02	3.20	Valeric Acid	11.28	10.00	1.80

Active ingredient	A_3 ($Å^3$)	μ_3	Parent molecule	α_4 ($Å^3$)	μ_4	Self Association ($\alpha_3 - \alpha_4$)($\mu_3 - \mu_4$)
Benzamide	13.54	3.73	Benzene	10.19	0.00	12.52
Isonicotianmide	13.54	3.67	Pyridine	0.31	37.72	-450.72
Nicotinamide	13.54	3.86	Pyridine	0.31	37.72	-448.24

The data set were then used to construct Table 2.5, which includes the outcomes from the melt screens, and these experimental outcomes are described in fully in chapter six,. Table 2.5 contrasts the computed average of the component models used for the Hotstage microscopy work with the parent components using equation 2.8.1.

Table 2.5: Average induced dipole moments calculated for component molecules used during Hotstage microscopy. Key below gives identification of results from Hotstage.

Key

Hotstage Hit

Hotstage Fail

Thermal Decomposition

Coformers	Benzamide [(α1 – α2)(μ3 - μ4) + (α3 - α4)(μ1 - μ2)]/2	Isonicotinamide [(α1 - α2)(μ3 - μ4) + (α3 - α4)(μ1 - μ2)]/2	Nicotinamide [(α1 - α2)(μ3 - μ4) + (α3 - α4)(μ1 - μ2)]/2
2 Aminobenzoic Acid	-19.30	140.05	139.22
3 Aminobenzoic acid	6.90	-111.29	-110.76
4 Aminobenzoic Acid	6.86	-112.04	-111.51
Benzoic Acid	8.79	-27.73	-27.49
Phthalic Acid	14.96	-68.50	-68.01
Malic Acid	-1.40	-9.66	-9.65
Succinic Acid	-10.44	-50.76	-50.72
Tartaric Acid	-2.19	-42.05	-41.92
Fumaric Acid	15.59	-186.68	-185.73
Maleic Acid	3.41	-25.82	-25.67
Pimelic Acid	4.00	-7.65	-7.56
Adipic Acid	22.38	-245.35	-244.07
Trans B Hydromuconic Acid	11.72	-151.02	-150.26
2 Nitrobenzoic Acid	7.19	-36.39	-36.14
3 Nitrobenzoic Acid	27.08	-324.41	-322.75
4 Nitrobenzoic Acid	3.30	-53.76	-53.50
2 Hydroxybenzoic Acid	-36.94	310.64	308.89
3 Hydroxybenzoic Acid	-37.64	307.68	305.93
4 Hydroxybenzoic Acid	-35.17	319.35	317.60
1, 4 Benzene dimethanol	2.13	-18.30	-18.20
Cinnamic Acid	10.39	-31.36	-31.09
Mandelic Acid	-8.73	162.07	161.31
Glutaric Acid	-11.90	-40.48	-40.51

Visual inspection Table 2.5 highlighted certain trends as follows. For the Isonicotinamide and Nicotinamide, where Hotstage showed a positive new phase, values calculated show a similarity in the computed dipole moment of the functional group taking part in the intermolecular interaction of a co-crystal. If we take the Succinic acid example, we already know from the structure determination and packing discussed with this work that the carbonyl acid group forms an acid-pyridine interaction and a homo amide-amide dimer for the Isonicotinamide and Nicotinamide system. However, for the Benzamide with Succinic acid system, we have found that a hetero dimer of acid-amide is formed. If we look at the values of these system from the table above (highlighted in red), we find that the Isonicotinamide and Nicotinamide have an average value of which are -50.76, -50.72 respectively, they are quite similar, but for Benzamide, a value of -10.44 is calculated, this suggest that in the absence of the pyridine ring the association of the dipole moment of the Benzamide Succinic acid system is much higher than its competitor amides, but lower than the self associated coformer and parent molecules, 12.52 (amide self association), -2.61 (coformer self association).

If we consider the benzoic acid example, we can highlight that with benzoic has a higher dipole with Benzamide, whereas a much lower negative dipole with Isonicotinamide and Nicotinamide. The Hotstage shows that benzoic acid shows a new phase with all three amides. However, if we introduce nitro, amino and hydroxyl groups, the dipole moments decreases with Benzamide, but increases with the Isonicotinamide and Nicotinamide. On addition of nitro and amino, the dipole decreases with Isonicotinamide and Nicotinamide, but increases with Benzamide.

Since Benzamide has only one donor/acceptor site, we assume that it can only form a hetero dimer, as literature shows and the examples shown here. However, to build a

hypothesis single crystal structures are required of the hits found during Hotstage. Similar trends are observed for the other systems suggesting this approach should be developed further.

We have attempted, to display a quick investigation of the induced dipole moment as an indication of the level of initial association viability of our model AI and the acid-coformers presented here. The data applied to the MOPAC software is from crystal structures that have been deposited into the CSD, the calculation involves a semi-empirical method, PM3, and due to time constraints, structure geometry has not been established.

To further investigate the effect of dipole moments using the PM3 method, each molecule taken from the CSD should be refined prior to running the semi-empirical formula to calculate the dipole and polarisability. The inclusion of popular API components such as Carbamazepine can be studied to build further understanding of the behaviour of the functional groups as a first principal method.

Chapter Three: Investigating and comparing co-crystallisation of 1° amides with carboxylic acids

3.1 Introduction

The literature revealed that Isonicotinamide (INA) successfully forms co-crystals with carboxylic acids whereas Benzamide has a lower success rate. An experimental matrix was set up using the reported Isonicotinamide-carboxylic acid co-crystals from the literature and compared with Benzamide using the same carboxylic acids. Two methods have been exploited here:

Slow evaporation: Quick and simple bench method of a super saturated solution where the samples are left to incubate at a set temperature of 20° C

Low through-put method: A streamline device called ReactArray Microvate, allows 48 samples to be simultaneously incubated at controlled temperatures.

3.2 Experimental

3.2.1 Bench slow evaporation

Crystal growth was undertaken from supersaturated solutions, typical quantities are given in Table 3.1, using the slow evaporation method. Crystallisation studies for each system were at 1:1 and 2:1 ratios for di-carboxylic acid to amide respectively. The compositions employed are given in Table 3.1, the ratio of acid: amides in grams is indicated, and for each sample, the specified mass components were dissolved in 50 ml of a series of selected solvents (Water, Methanol, Ethanol, and Tetrahydrofuran) and left in an incubator at 25° C. All materials, solvents and compounds were bought from Sigma-Aldrich.

3.2.2 Low through-put method using a ReactArray Microvate

The ReactArray device has 48 wells, set on a heating block which has 12 independent temperature zones. Each well has a depth of 3 cm. The sample vials used for this experiment were glass tubes, with a diameter of 1 cm and volume capacity of 5 ml if filled to the top. Magnetic beans which were 1.5 x 5mm where used to equilibrate samples. This device has been used to grow single crystals of Benzamide and 4-Nitrobenzoic Acid, Tartaric Acid and Fumaric Acid as discovered from the evaporation method above. Additionally the above mentioned matrix has been used with this device to further screen for co-crystals which may not have been successful using the simple bench evaporation technique. Experiments were set up using solvents; Hexane, Toluene, Ethyl Acetate, Tetrahydrofuran, Ethanol, Methanol and Water. Stoichiometric ratios of 1:1, 1:2 and 2:1 were used with 2 ml of solvent. The ReactArray was programmed to equilibrate sample at 25 °C for an hour, temperature was then ramped to 60 °C and held for 8 hours and then cooled to 25° C at a rate of 5° C/min. The previous matrix which gave a success rate of 5 co-crystals out of 11 have been reproduced. The weights are given in Table 3.2.

Figure 3.1: ReactARRAY Microvate showing the 48 wells and the 12 independent heating regions

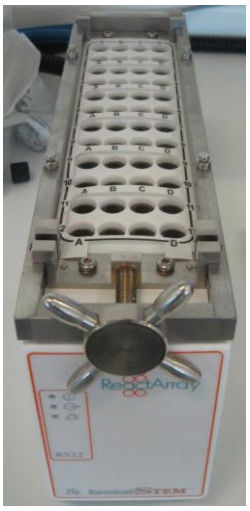

Table 3.1: Summary of the quantities of Acid: Amide in grams used in the bench solvent evaporation solution co-crystallisation.

	Isonicotinamide	Benzamide
	1:1 1g	1:1 1g
	2:1 2g	2:1 2g
Fumaric Acid	0.958g	0.950g
Succinic Acid	0.975g	0.970g
Tartaric acid	1.239g	1.230g
Glutaric Acid	1.091g	1.081g
Adipic Acid	1.206g	1.197g
Benzoic Acid	1.008g	1.00g
2-Hydroxybenzoic Acid	1.140g	1.131g
3-Hydroxybenzoic Acid	1.140g	1.131g
4-Hydroxybenzoic Acid	1.140g	1.131g
Mandelic Acid	1.256g	1.249g
Cinnamic Acid	1.223g	1.213g
4-Nitrobenzoic Acid	1.380g	1.370g

Table 3.2: Summary of the quantities and solvents used in grams for the co-crystallisation of acid: Amide using the ReactARRAY Microvate as a Low through-put method

	Isonicotinamide (g)			Benzamide (g)		
	1:1	1:2	2:1	1:1	1:2	2:1
	0.025g	0.025g	0.050g	0.025g	0.025g	0.050g
Fumaric Acid	0.024	0.048	0.024	0.024	0.048	0.024
Succinic Acid	0.024	0.048	0.024	0.024	0.049	0.024
Tartaric acid	0.03	0.061	0.03	0.031	0.062	0.031
Glutaric Acid	0.027	0.054	0.027	0.027	0.055	0.027
Adipic Acid	0.03	0.06	0.03	0.03	0.06	0.03
Benzoic Acid	0.025	0.05	0.025	0.025	0.05	0.025
2-Hydroxybenzoic Acid	0.028	0.057	0.028	0.029	.0.57	0.029
3-Hydroxybenzoic Acid	0.028	0.057	0.028	0.029	.0.57	0.029
4-Hydroxybenzoic Acid	0.028	0.057	0.028	0.029	.0.57	0.029
Mandelic Acid	0.031	0.062	0.031	0.031	0.063	0.031
Cinnamic Acid	0.03	0.06	0.03	0.031	0.061	0.031
4-Nitrobenzoic Acid	0.034	0.068	0.034	0.034	0.069	0.034

3.3 Results and Discussion

3.3.1 Bench method vs. Low through-put method

The summative results from the screen using quantities in Tables 3.1 and 3.2 are presented in Table 3.3. Table 3.3 is laid out to highlight the respective success and failures seen during the Co-crystallisation studies. The outcome with regards success or failure was determined using a combination of PXRD and Hotstage microscopy.

Table 3.3: Positive or negative result of experimental screen, where in the case of Isonicotinamide successful growth is identified as being previously published. A positive result is highlighted with a green box and a tick, a failure is highlighted with a cross in a red box

	Isonicotinamide		Benzamide	
	Co-crystallisation		Co-crystallisation	
Adipic Acid	✓	Published	×	
Glutaric Acid	✓	Published	×	
Fumaric Acid	✓	Published	✓	New Phase/Mixture
Succinic Acid	✓	Published	✓	Published
Tartaric Acid	✓	Published	✓	New Phase/Mixture
Benzoic Acid	✓	Published	×	
2-Hydroxybenzoic Acid	✓	Published	×	
3-Hydroxybenzoic Acid	✓	Published	✓	New Phase/Mixture
4-Hydroxybenzoic Acid	✓	Published	×	
Cinnamic Acid	✓	Published	×	

DL-Mandelic Acid	✓	Published	✓	New Phase/Mixture
4-Nitrobenzoic Acid	✓	Published	✓	New Phase/Mixture

Results from the slow evaporation have also been recreated using the low through-put screen, some single crystals have been grown which represent new co-crystal phases, and these will be discussed in the next section. However, as mentioned earlier the vial size used for the ReactARRAY experimental procedure had a diameter 1cm and volume of 5ml, these were made of glass which caused difficulty when extracting crystal samples from the bottom of the vial. In attempt to overcome this problem, experiments where repeated using polypropylene round bottomed centrifuge tube, however, these tubes also seemed to be difficult when extracting crystal sample.

3.3.2 Discussion solution growth

The experimental results obtained indicate that the examples of Isonicotinamide co-crystals reported in the literature were all successfully re-created using the following solvents (water, methanol, ethanol and THF). This highlights the robust nature of the associated synthons. However, a number of potentially new Benzamide co-crystals were also identified from the screens. Previously only the Benzamide: Succinic acid (Chiarella, Davey, & Peterson, 2007) system has been published. Currently further analysis is being undertaken to fully identify the new co-crystals phases of Benzamide.

Figures 3.2 - 3.6 presents a comparison of X-ray powder patterns where a new phase is indicated from mixture of Benzamide and Fumaric Acid, Tartaric Acid, 3-Hydroxy

benzoic Acid, DL-Mandelic Acid, 4-Nitrobenzoic Acid. These new phases have been indicated by an arrow. Details of the critical peaks are given in Appendix B.

Figure 3.2: Powder diffraction comparison of potential Benzamide with Fumaric acid grown from low through-put method

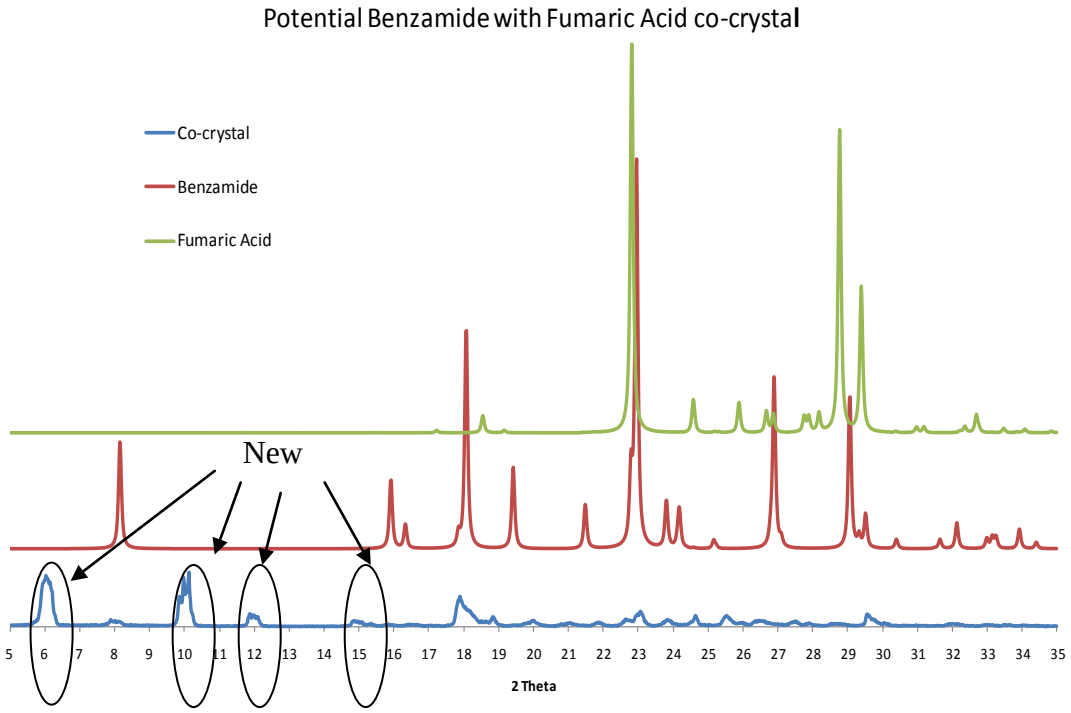

Figure 3.3: Powder diffraction comparison of potential Benzamide with Tartaric acid grown from low through-put method

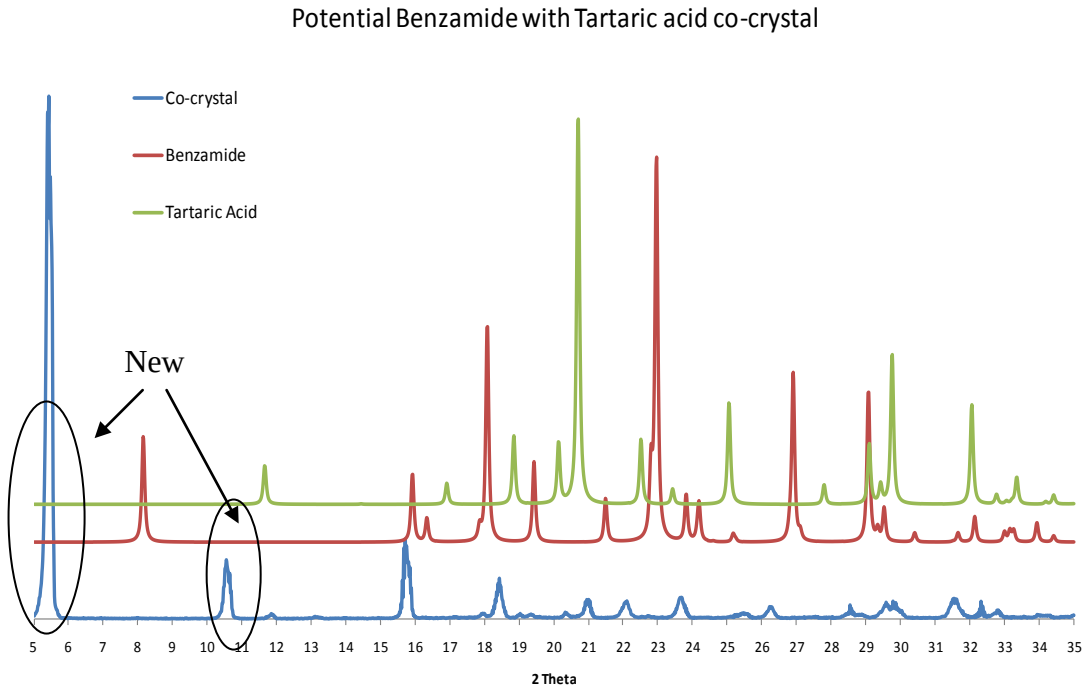

Figure 3.4: Powder diffraction comparison of potential Benzamide with 3-hydroxybenzoic acid grown from low through-put method

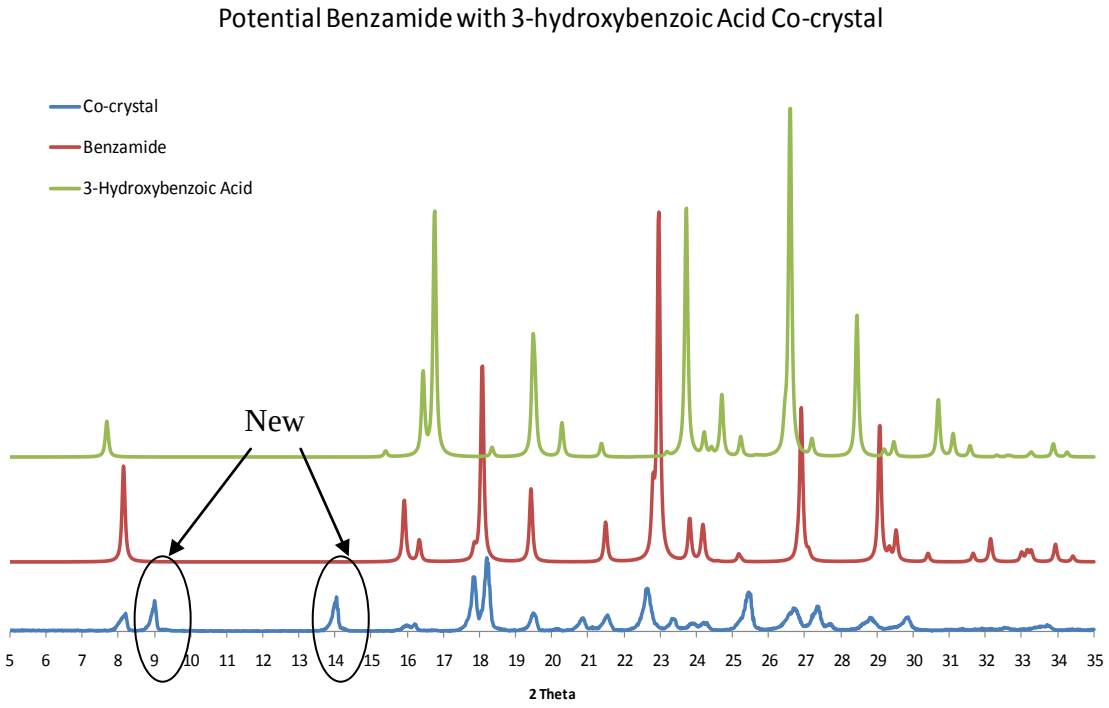

Figure 3.5: Powder diffraction comparison of potential Benzamide with Mandelic acid grown from low through-put method

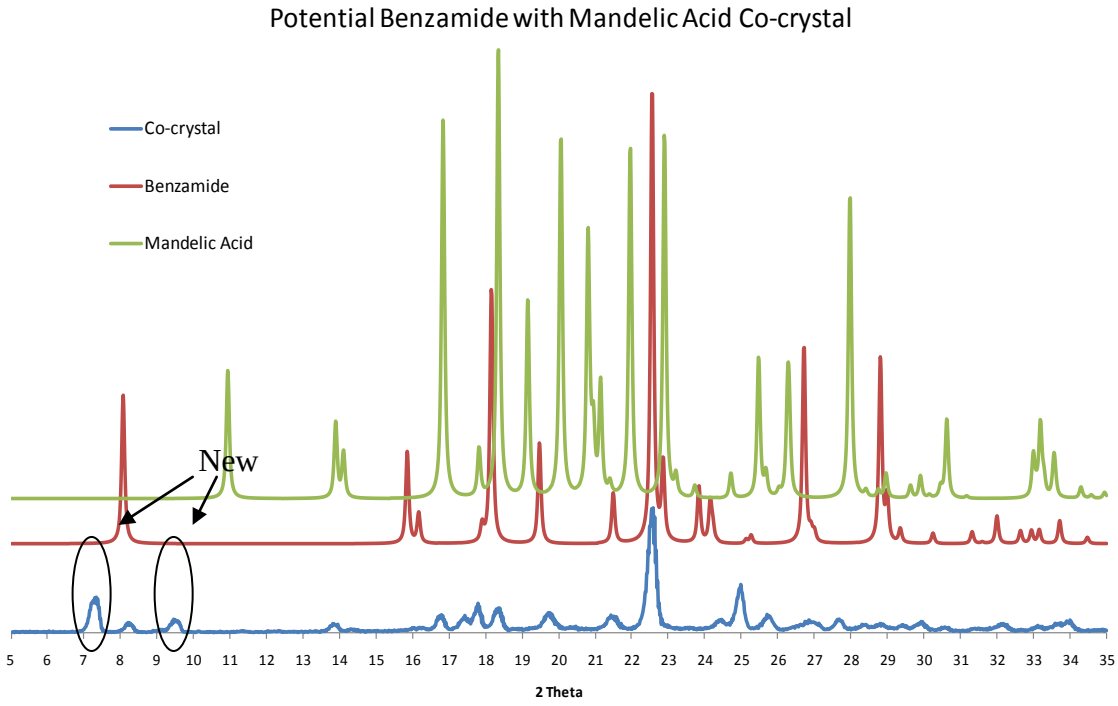

Figure 3.6: Powder diffraction comparison of potential Benzamide with Mandelic acid grown from low through-put method

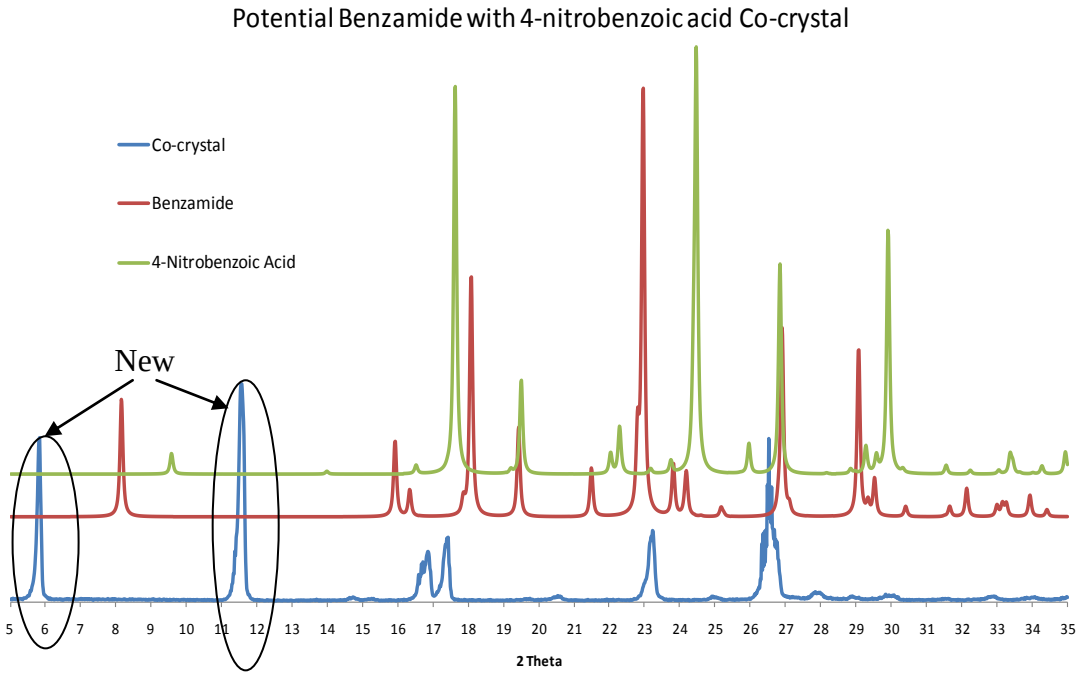

3.3.2.1 Discussion on X-ray results

From Figures 3.2 - 3.6 the trend which emerges is that the evaporation method, gives five possible new phases with Benzamide. The X-ray patterns show four new peaks with Fumaric Acid at 2θ angles (˚) (6.02, 10.052, 11.906 and 15.311), 2 new peaks with Tartaric Acid (5.424, 10.557), 2 new peaks 3-Hydroxybenzoic Acid (9.297, 14.015), 2 new peaks with Mandelic Acid (7.284, 9.10), and 2 new peaks with 4-Nitrobenzoic Acid (5.799, 11.544) which are not present in the parent structures. However, further determination and characterisation is required to fully justify a new phase being present. These methods will be Single crystal X-ray, hot stage microscopy and DSC.

3.3.2.2 Single Crystal analysis

From the X-ray powder diffraction new phases have been identified. Suitable material for single crystal structure determination has been grown. Single crystal determination was sent to University of Glasgow for Benzamide: Fumaric Acid sample, whilst the Benzamide: 4-Nitrobenzoic Acid was determined on the in-house system by Dr Ian Scowen. Experimental details for both structures are given below in Table 3.4

The literature review and CSD search shows there are far more co-crystal with Isonicotinamide than Benzamide, but here it has been observed that using the same carboxylic acids which successfully co-crystallise with Isonicotinamide, Benzamide co-crystallises with 5 of the acids out of the 13 acids investigated. ***(All the relevant CIF files are contained in a CD within Appendix H)***

Table 3.4: Crystallographic Data For Benzamide: Fumaric Acid and Benzamide : 4-Nitrobenzoic acid

Compound	Benzamide: Fumaric Acid	Compound	Benzamide:4-Nitrobenzoic Acid
Formula	$C_9H_9N_1O_3$	Formula	$C_{14}H_{12}N_2O_4$
Mass, M_r	179.18	Mass, M_r	272.26
Temp (K)	150 K	Temp (K)	296 (2) K
Cryst Syst	Monoclinic	Cryst Syst	
Space Group	$P2_1/n$	Space Group	P-1
Z	4	Z	2
a (Å)	5.318 (6) Å	*a* (Å)	6.3184 (4) Å
b (Å)	5.351 (6) Å	*b* (Å)	6.8802 (5) Å
c (Å)	29.64 (4) Å	*c* (Å)	15.6401 (11) Å
α (deg)	90°	α (deg)	95.749 (5)°
β (deg)	96.03 (5)°	β (deg)	98.806 (4)°
γ (deg)	90°	γ (deg)	106.239 (4)°
V (Å)	838.8 (18) $Å^3$	*V* (Å)	637.72 (8) $Å^3$
R-Factor %	5.69	R-Factor %	12.03

A full detail of refinement, atomic coordinates, isotropic displacement parameters ($Å^2$), atomic displacement parameters ($Å^2$), geometric parameters (Å), and hydrogen-bond geometry (Å) is given in Appendix D.

3.3.2.2.1 Analysis of Benzamide: Fumaric Acid:

This crystal is Monoclinic with a space group of $P2_1/n$. It has the unit cell dimensions of 5.318 5.351 29.64 Å, and β = 96.03 °. The crystal structure, forms dimerised hydrogen bonding, showing the common hetero-synthon (Figure 3.7).

Figure 3.7: Mercury analysis of Benzamide : Fumaric Acid crystal structure

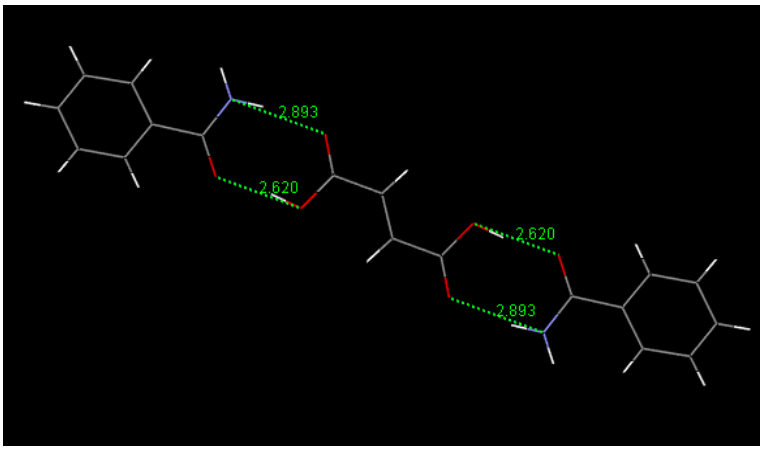

The bond types which are present are the N-H···O Benzamide to Fumaric acid and O-H···O Fumaric Acid to Benzamide leading to a ring ($R^2_2(8)$), i.e. hetero-dimer synthon. Closer inspection on the packing shows a herringbone ladder which is stacked, Figure 3.8 i-iii.

Figure 3.8: Herringbone stacking Packing i) down the a axis we see a stacking in the zigzag stack, ii) packing in a single unit cell, iii) shows the packing down the b axis

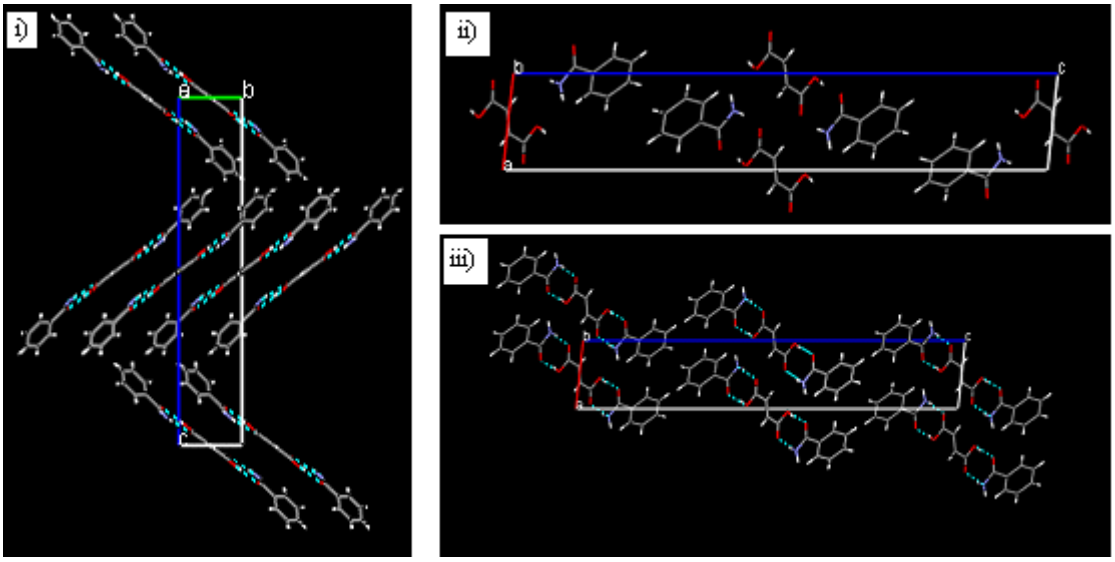

The Hydrogen bonding angles and distances for the dimer are shown in the Table 3.5 below

Table 3.5: Hydrogen-bond geometry lengths are give in Angstrom(Å), and bond angles are given in degrees (°)

D—H···*A*	*D*—H	H···*A*	*D*···*A*	*D*—H···*A*
N8—H81···O4	0.95	1.95	2.893 (2)	169
O3—H31···O7	0.96	1.67	2.620 (2)	171

3.3.2.2.2 Analysis of Benzamide: 4-NitrobenzoicAcid

This structure has a Z value of 2 in space group $P\bar{1}$ with angles 95.75, 98.81, 106.24° and unit cell dimensions of 6.318 6.88 15.64 Å. The Figure below depicts the hydrogen bonding to be a hetero dimer synthon i), by expanding the contact we can see that the packing is stacked forming 2D layers. We can see that the stacking is of π- π stacking, offset slightly over the nitro group of the acid Figure 3.9 iii).

Figure 3.9: Packing analysis of Benzamide and 4-Nitrobenzoic Acid i) Dimer hydrogen bonding, ii) view of the packing down a axis, iii) packing down b axis, we can see the offset stacking over the nitro group

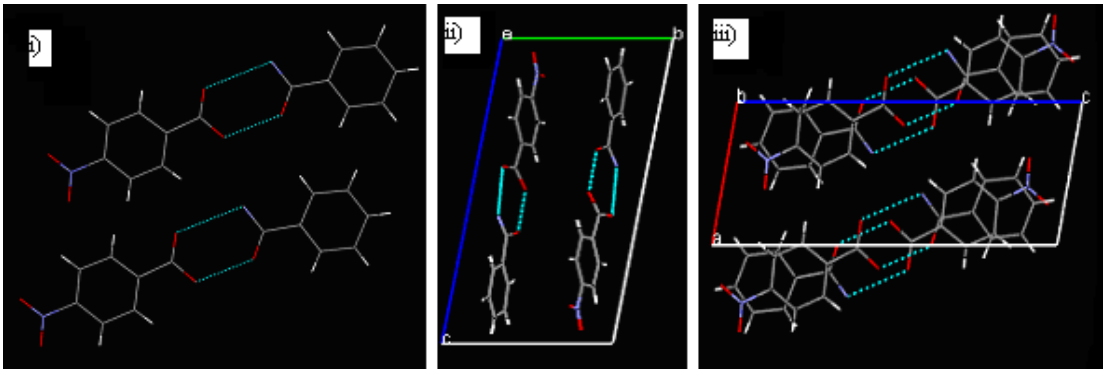

However, the 12.03 R % factor from the structures analysis for this new phase is slightly high, suggesting poor quality crystals. New crystals are in the process of being grown using different methods and solvents.

3.4 Thermal Analysis

Methods of analysis of the solid-state have been carefully reviewed in the study of polymorphic behaviour of crystals (Bernstein, 2002) as well as the solid-state chemistry of drugs (Byrn et al, 1999). For this study we have focussed on the thermal activity of the above mentioned screen using the Kofler contact method on a Hotstage microscope and Differential scanning calorimetry (DSC).

3.4.1 Hotstage Microscopy

In this study, the acid and amide was mixed using the Kofler contact method, where one end contains pure acid and the other pure amide. The region in between the pure phases, also referred to as the mixing zone, holds the presence of a new phase upon heating, this can be observed under a polarised light microscope. A detailed account of the preparation of the slides has been described in chapter 1 and 6.

The heating stage (Hotstage) was purchased from Linkam, and a Zeiss microscope was used which has the axioplan imaging software. A heating profile from room temperature to 260° C at a rate of 1° C per minute was employed. Images were captured at 5x's magnification at 60 second intervals.

3.4.2 Differential Scanning Calorimetry (DSC)

Differential scanning calorimetry (DSC) is one of the most widely used thermal analysis techniques for the characterization of pharmaceutical solids. It measures the temperature and heat flow associated with thermal transition in a material. Properties measured by DSC include glass transitions, 'cold' crystallisation, phase changes, melting, crystallization, product stability, and decomposition. For this study all experiments have been carried out for the successful Benzamide co-crystal phases for which powder X-ray diffraction has been discussed earlier. The DSC machine used is a TA instruments Q2000. The temperature axis and cell constant of the DSC cell were calibrated with indium (10 mg, 99.999% pure, melting point 156.60 ° C, the heat of fusion 28.40 J.g). A small sample of each co-crystal phase identified from the solution screen was weighed to 0.001 mg of quantities of 2-5 mg into aluminium pans, crimped with aluminium lids. All samples where heated from 25 ° C to the relevant temperature for each material (up to a maximum of 250 ° C) at 10° C min^{-1}.

3.4.3 Thermalgravimetric Analysis (TGA)

Thermogravimetric Analysis (TGA) measures weight changes in a material as a function of temperature under a controlled atmosphere. TGA is an ideal technique to determine the thermal properties of pharmaceutical material. The same samples were analysed using TA instruments Q5000 TGA machine, where quantities of 2-5 mg of crystals from solvent co-crystallisation were heated from 25° C to 400° C at 10° C min^{-1}.

3.4.4 Thermal analysis Results and Discussion

Thermal analysis has been used as a method to identify new phases in the solid state. The new co-crystal phases discovered by PXRD characterisation and single crystal where single crystals have grown from solution screen have been the subject of this analysis. Table 3.6 represents the results of the samples which hold new phases and the respective temperatures at which starting material melts and at which the new phases emerge and melt away. The same samples have been investigated using DSC and TGA to identify melting points and endothermic peaks which would highlight presence of crystallisation upon heating.

Table 3.6: A summary of the Hotstage microscopy results and DSC endothermic peaks of Benzamide co-crystal phases as identified from the solution screen. The results show the number of new phases and the respective temperatures and ratios

Benzamide Co-crystal phases	Hotstage °C	DSC endothermic peaks °C
Fumaric Acid	n/a	139.62
Tartaric Acid	n/a	120.74 141.21
3-Hydroxybenzoic Acid	n/a	93
Mandelic Acid	76	76.2
4-Nitrobenzoic Acid	180-185.6	123.47 180.5 184.13 239.81
Succinic Acid	117	117.07 128.48

The Hotstage experiment has deemed to be very informative as a visual aid of the emergence of new phases for Mandelic, 4-nitrobenzoic acid and the already reported Succinic acid co-crystal with Benzamide. However, it has not been possible to identify the co-crystal phases of the Benzamide with Fumaric and Tartaric acid, since both the pure acid components sublime during the preparation of the microscope slides, where as with Benzamide: 3-hydroxybenzoic acid, a microscope slide was prepared but upon

heating no new phases emerged. Below are the images taken during Hotstage for Benzamide and Mandelic acid, it is clear to see the new phases for each sample with the temperature highlighted in the top left corner.

Figure 3.10: Images highlighting the emergence of new phases of the Benzamide Mandelic acid system, using Hotstage microscopy with Linkam controlled heating stage mounted on a Zeiss Microscope using cross polarised light and axiocam camera at times 5 magnification lens.

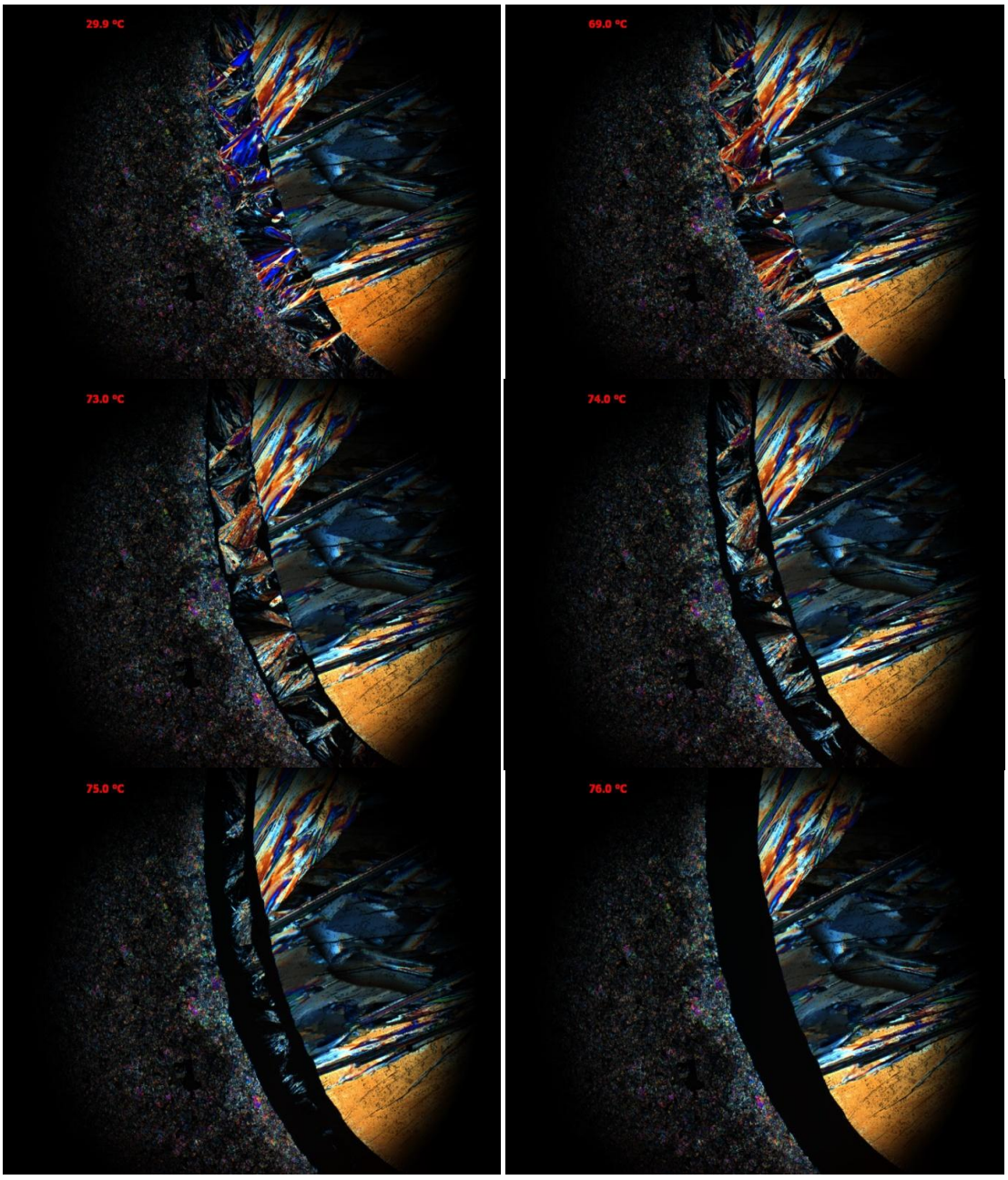

With the increase in the temperature, the remaining phases melt away at their respective melting points. The images for the whole Mandelic acid experiment and the remaining Fumaric and 4-Nitrobenzoic acid can be viewed from the compact disc attached in Appendix I.

DSC has been coupled with the Hotstage microscopy to view endothermic peaks at the temperatures as viewed from the Kofler contact method. These are also displayed in Table 3.2. The DSC traces are given below in Figure 3.11-16 for each sample taken from the solution screen. Each Figure highlights the onset temperature and average peak temperature and enthalpy of fusion, ΔH_f (J/g) of the samples.

Figure 3.11: DSC results for Benzamide Fumaric acid co-crystal sample from solution

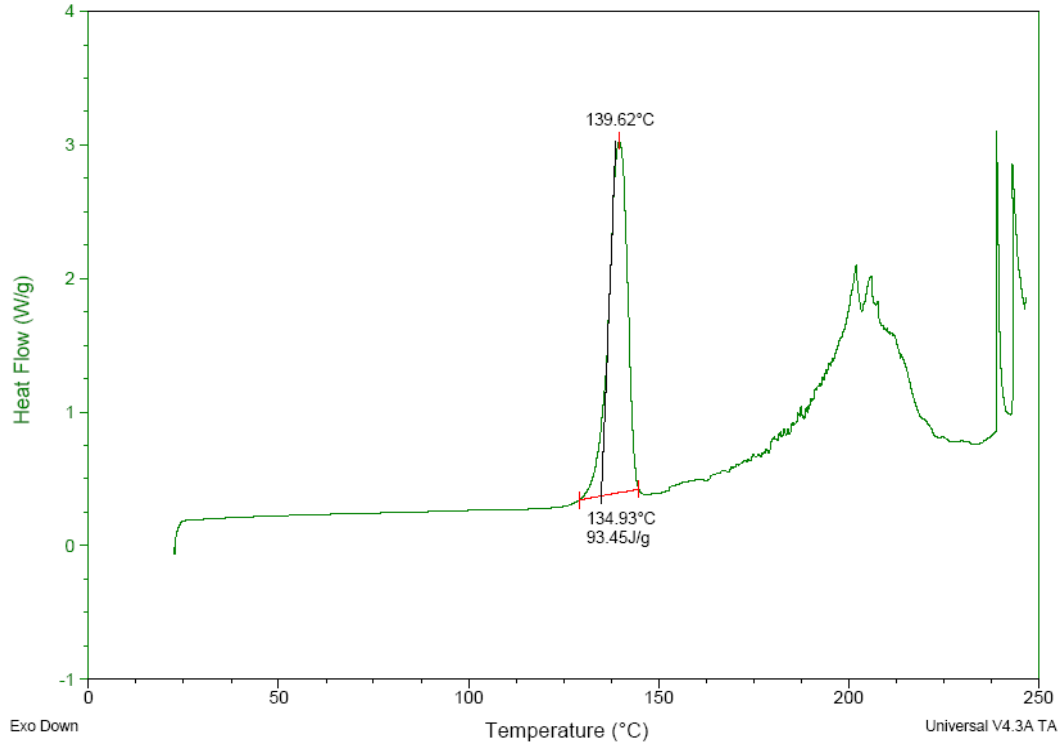

Figure 3.12: DSC results for Benzamide Tartaric acid co-crystal sample from solution

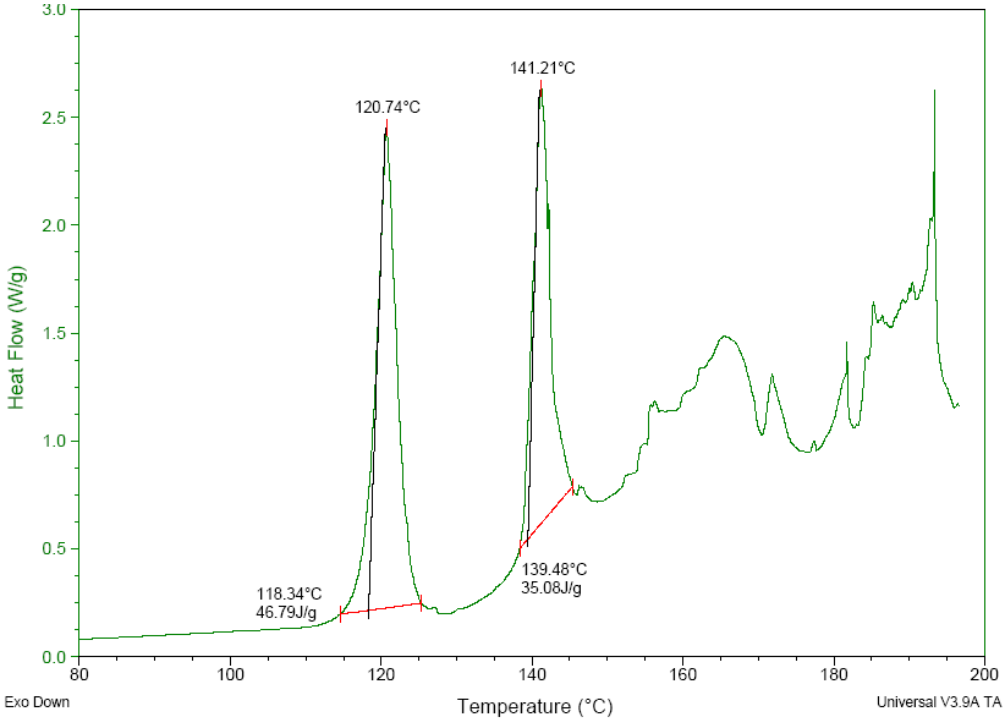

Figure 3.13: DSC results for Benzamide 3-Hydroxybenzoic acid co-crystal sample from solution

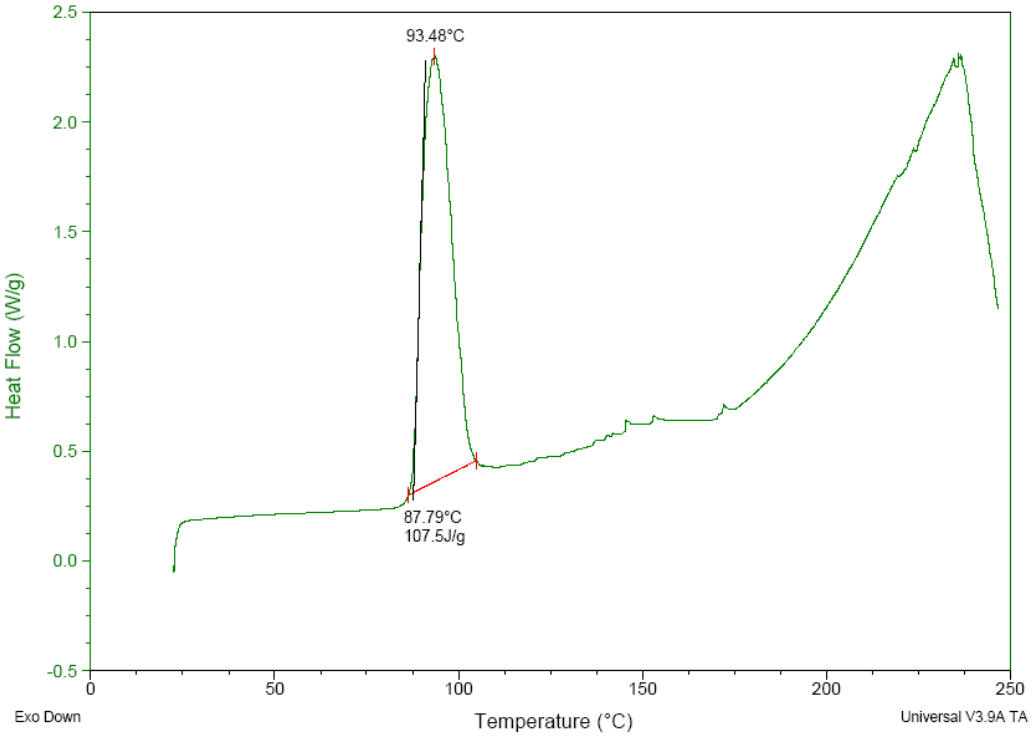

Figure 3.14: DSC results for Benzamide Mandelic acid co-crystal sample from solution

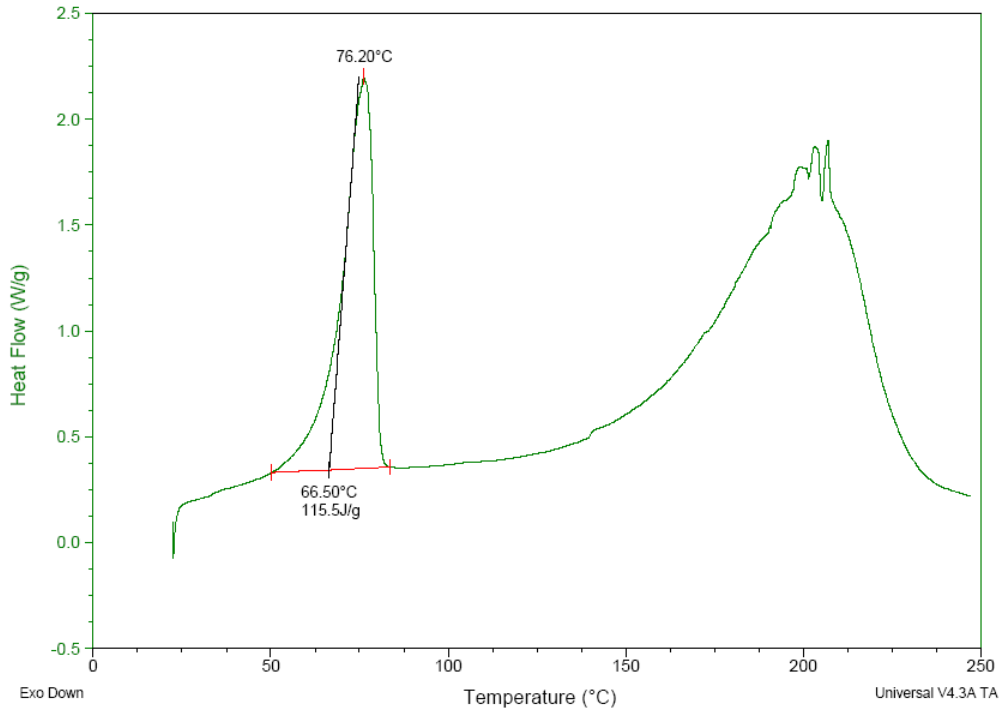

Figure 3.15: DSC results for Benzamide 4-nitrobenzoic acid co-crystal sample from solution

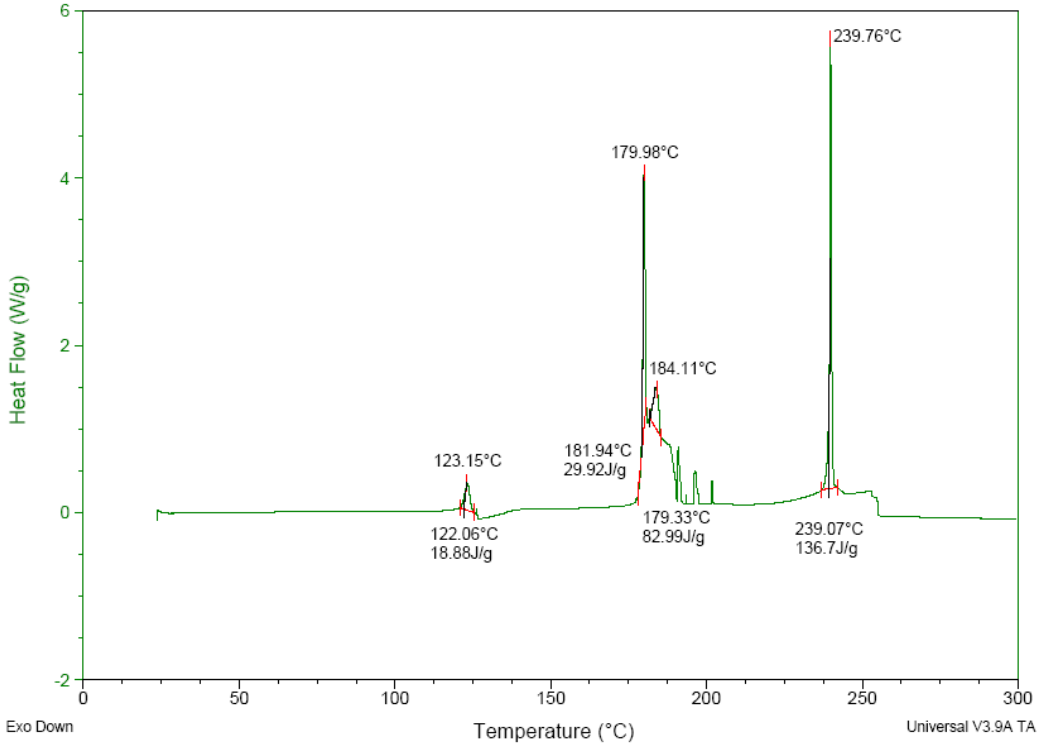

Figure 3.16: DSC results for Benzamide Succinic acid co-crystal sample from solution

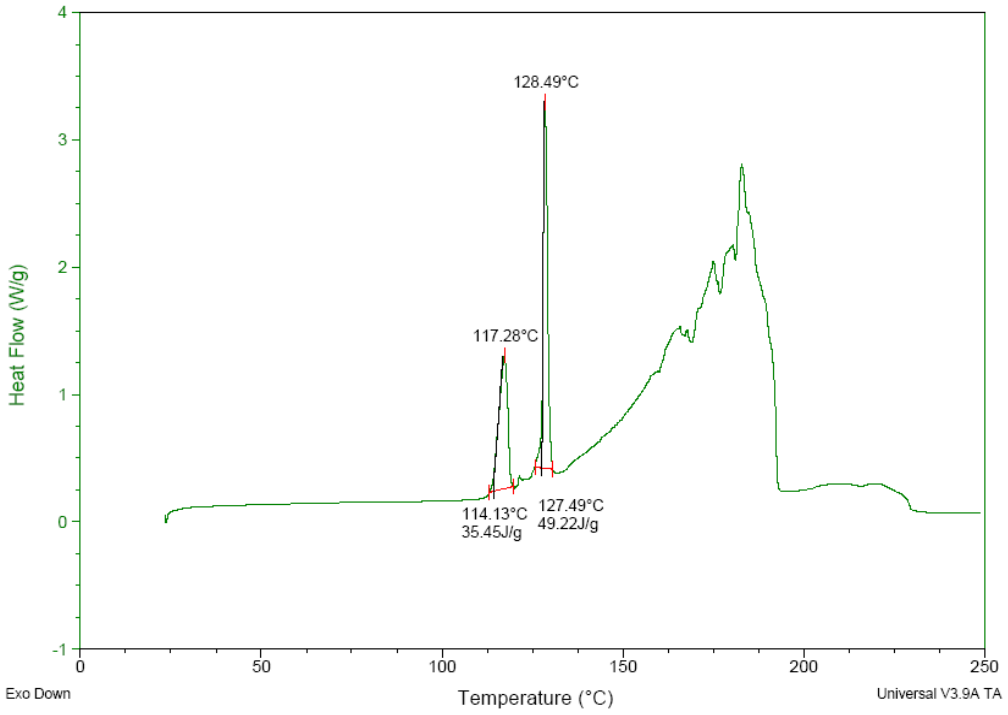

For the samples which sublime during the preparation of the microscope slide for Hotstage analysis, it is not possible to make a comparison to validate the findings of the Hotstage work, however with Mandelic, 4-Nitrobenzoic acid and Succinic acid, it is possible. The Hotstage for Mandelic shows the appearance of a new phase in the mixing zone which melts away at 76 ° C (Figure 3.10), the DSC data shown in Figure 3.14 is in agreement to the Hotstage result hosting an endothermic peak at 76.2° C. The same trend is displayed for each of the thermal experiments, giving a positive correlation of temperature. As well as the characteristic endothermic peaks for the new phases at 180-185.6 ° C (Hotstage) for 4-Nitrobenzoic acid the DSC shows an early peak at 123.47 ° C which is not viewed in the Hotstage, and two peaks at 180.5 and 184.13 ° C, this suggest that during Hotstage it could be possible that there is a conversion of the new phase we are seeing. Also, the DSC pattern for Succinic acid sample gives two endothermic peaks, but the Hotstage, only shows one phase present as the temperature is increased.

The Hotstage microscopy technique seems to be a quick and simple way to screen and identify phase changes of binary components. The DSC technique, also acts as a complementary method and can be useful in confirming transition changes which may be seen during Hotstage melting. Although these techniques show some degree of agreement with the findings, they have their limitations with respect to these samples. To further investigate the work presented here later chapters discuss this initial co-crystal screen and an expanded screen which utilises the Hotstage microscopy method as one route to identify co-crystal phases.

3.5 Summary

To summarise, this chapter discusses the techniques used to grow co-crystals and the atypical model compound Isonicotinamide was selected, which according to the literature tends to be a high yielding supramolecular building block (Aakeroy et, al. 2002). In contrast forming co-crystals with the less reported Benzamide as the active ingredient was undertaken; which to date has only one reported co-crystal, with the co-formers which have formed co-crystals with Isonicotinamide . The methods discussed here have been challenging in the approach of yielding nice crystalline material which can further be investigated by single crystal, however, we have present two cases where structure determination has confirmed two new co-crystals of Benzamide with Fumaric acid and Benzamide with 4-nitrobenzoic acid. To further understand the behaviour and nature of why one compound is more robust than another all reported co-crystals mentioned from the CSD in this section have been the subject of a closer look at the crystal structure and the fragments present that build the crystal. A collaborative project with the University of Glasgow using dSNAP software developed by them is the subject of the next chapter.

Chapter Four: Investigating and comparing structural difference using the structural comparison software dSNAP

4.1 Introduction

4.1.1 dSNAP

The Cambridge Structural Database (CSD) is forever growing, with this and the large number of datasets retrieved whilst searching, it can be sometimes difficult to classify chemical information. However, although there are various algorithms and data mining strategies in the literature, (Orpen 2002, Allen & Motherwell 2002), there is however a niche for a freely available program which classifies results from database searches (Aakeroy, Beatty, 2001). In 2005 Barr et al indicating detail in flexibility presented a new developed a new approach encoded in the dSNAP program which is designed to assist structural chemist in classifying information extracted from CSD searches.

4.1.2 What is dSNAP?

dSNAP is a computer program which classifies and clusters structural fragments extracted from the Cambridge Structural Database. The methodology is based on cluster analysis and multivariate data processing of distance matrix information describing the extracted fragments.

Previous papers by Barr et, al (Barr et al, 2004-2007) have shown how pattern matching coupled with cluster analysis and multivariate statistical methods can be used to classify large numbers of powder patterns (PolySNAP) (Krzanowski, 2000).

In this section the term ‘structure’ and ‘hit’ refers to individual crystal structure determination mined from the CSD, these ‘structures’ or ‘hits’ contain the defined search query and are labelled by an individual CSD reference code, whilst the term

'fragment' refers to the part of the structure matching the search query. It is possible for a structure to contain one or more fragments, these fragments lie in chemically distinct environments and thus may exhibit significantly different geometries, these are therefore treated independently (Krzanowski, 2000). In these circumstances, the software will suffix individual reference codes with a number consistent with the order in which the fragment is outputted, this then allows users to simply reference back to the fragments when studying structures within the ConQuest search program (Clegg, 1998)

4.1.2.1 Algorithms

All the theory for dSNAP has been published by the authors of the programme. For this work the approach will be briefly summarised to underline why the approach was adopted for studies in this thesis. As mentioned above dSNAP uses Multivariate statistical analysis, this is described as a collection of procedures that involve observations and analysis of more than one statistical variable at a time. dSNAP also uses clustering analysis which is a multivariate technique. This section discusses Clustering analysis and the hierarchical approach used by dSNAP, and Multidimensional Scaling (MDS), (Barr, 2005, 2007, Krzanowski, 2000, Parkin, 2006).

Clustering is the classification of objects into partitioning of a dataset into subsets (clusters), this is so that each subset shares some common trait, and this is often proximity according to some defined distance measure. Clustering is a common technique for statistical data analysis.

Data clustering algorithms can be hierarchical or partitional. Hierarchical algorithms locate successive clusters by using clusters which have previously established, where as a partitional algorithm will determine all the clusters at once. Hierarchical algorithms can be agglomerative ('bottom-up'), which begin with each element as a separate cluster and then merges them into successively larger clusters, or divisive ('top-down') algorithms, these begin with the whole set and proceed to divide into successively smaller clusters, (Barr, 2006, Parkin, 2006, Krzanowski, 2000).

dSNAP uses agglomerative algorithms to build up a hierarchy of clusters. This hierarchy is presented as a tree diagram (Dendrogram), where at one end of the tree are the individual fragments and the other end is a single cluster containing every fragment.

The tree can be cut by a tie bar at different heights, this gives clustering at a selected precision of similarity.

dSNAP uses 3D Metric Multidimensional scaling (MMDS) as a visualisation of similarities or dissimilarities in data. Multidimensional scaling uses an algorithm that starts with a matrix of item-item similarities, a location is assigned to each item in low-dimensional space, thus making this method suitable for 3D visualisation.

Metric Multidimensional scaling is a superset of MDS, it generalises the optimisation procedure to a variety of loss functions and input matrices of known distances with

weights, (Barr, 2005, 2006). For this reason, the co-crystal system packing subtleties would be with prudent use of the code be extracted and analysed. The authors for dSNAP were keen for end users to test their scaling approach to this problem. In order to undertake this analysis the user needs to aware of the variable and data space implementation.

4.1.2.2 Variable space

We have outlined how dSNAP investigates the data space using MMDS algorithms. dSNAP also allow users to explore variable space. This section explains how variable space is used in dSNAP.

Variable space is the underlying geometries that are stored in the data matrix *x*, this can be used to create a new distance matrix. A single fragment will have many variables and the complete list of distances and angles completely defines a fragment (Barr, 2005, Krzanowski, 2000, Parkin, 2006).

Each column of *x* contains a distance or an angle, there are *m* such columns, each of these are subjected to linear regression every other column in turn to generate an (*m* x *m*) symmetric correlation matrix ρ^{v} and the corresponding distance matrix d^{v} using Equation 4.1, (Barr, 2005).

Equation 4.1 Distance correlation matrix

$$\boldsymbol{p^s = 2d^s - I} \tag{4.1}$$

Where

I = identity matrix

$\boldsymbol{\rho^s}$ = correlation matrix corresponding to d^s

The ρ^v and d^v matrices can be used to generate a Dendrogram, an MMDS plot etc in the same way as d^s. These can be viewed by accessing the 'Variables' tab which is found on the left hand side of the main dSNAP window. The results are interpreted differently, the spheres in the MMDS plot represent features such as a distance or angle, and variables that are-clustered tightly together have a high correlation. This feature can also be shown in a Dendrogram (Barr, 2005, 2006).

4.1.2.3 Data and Variable Space

We have discussed how dSNAP allows separate analysis on the fragments and their underlying structural variables. In dSNAP these are shown as data space and variables space.

The calculations carried out in the Data Space section of dSNAP are concerned with the fragment structures. This operates by collating all of the geometric data for a single fragment and treating it as a single entity to compare against the other fragments in the dataset. This allows the program to calculate similarities between fragments.

The calculations carried out in the Variables Space section are concerned with the geometric variables. This groups every instance of each variable in all of the fragments

available and treating these as a single variables. This allows trends and clustering of geometric variables to be established (Barr, 2005, 2006).

4.2 Running dSNAP

4.2.1 Limitations

Currently dSNAP is limited to approximately 4000 fragments (*n*) and 4000 structural parameters (*m*) per fragment. For each fragment only 3-10 atoms of any fragment can be used in the analysis.

4.2.1.1 Program Requirements

The software is a highly modified and extended version of the computer program *PolySNAP* (Barr, 2004). The software requires a PC with windows 2000 or *XP*. The program is written in a variety of languages: the user interface is written in Visual Basic, the underlying code is in C++, the graphics is also in C++ and OpenGL, whereas the cluster analysis code is written in FORTRAN 95, (Barr, 2006). For this project, the authors of dSNAP; wanted to work in a collaborative contribution with an end user to gage the code operation in a new application area of co-crystals, and act on any critical issues that arise.

4.2.1.2 Standard Run

This section gives an outline of the main stages involved in a standard run and a diagram to show the process involved, Figure 4.1, (Barr, 2006). All of which was modified to the needs of co-crystal systems which pertains to the work in this thesis.

The main stages involved in a standard run are:

1) In ConQuest, define search fragment of interest.
2) In ConQuest, define a geometric variable in the fragment.

3) In Conquest, perform search.

4) Export relevant files from ConQuest.

5) Import and processing of data files into dSNAP.

6) Perform cluster analysis.

7) Output results to file and graphically to screen to allow interpretation

8) Reclassification of results where necessary

Figure 4.1: The process involved in a standard run of *dSNAP* (Barr, 2006)

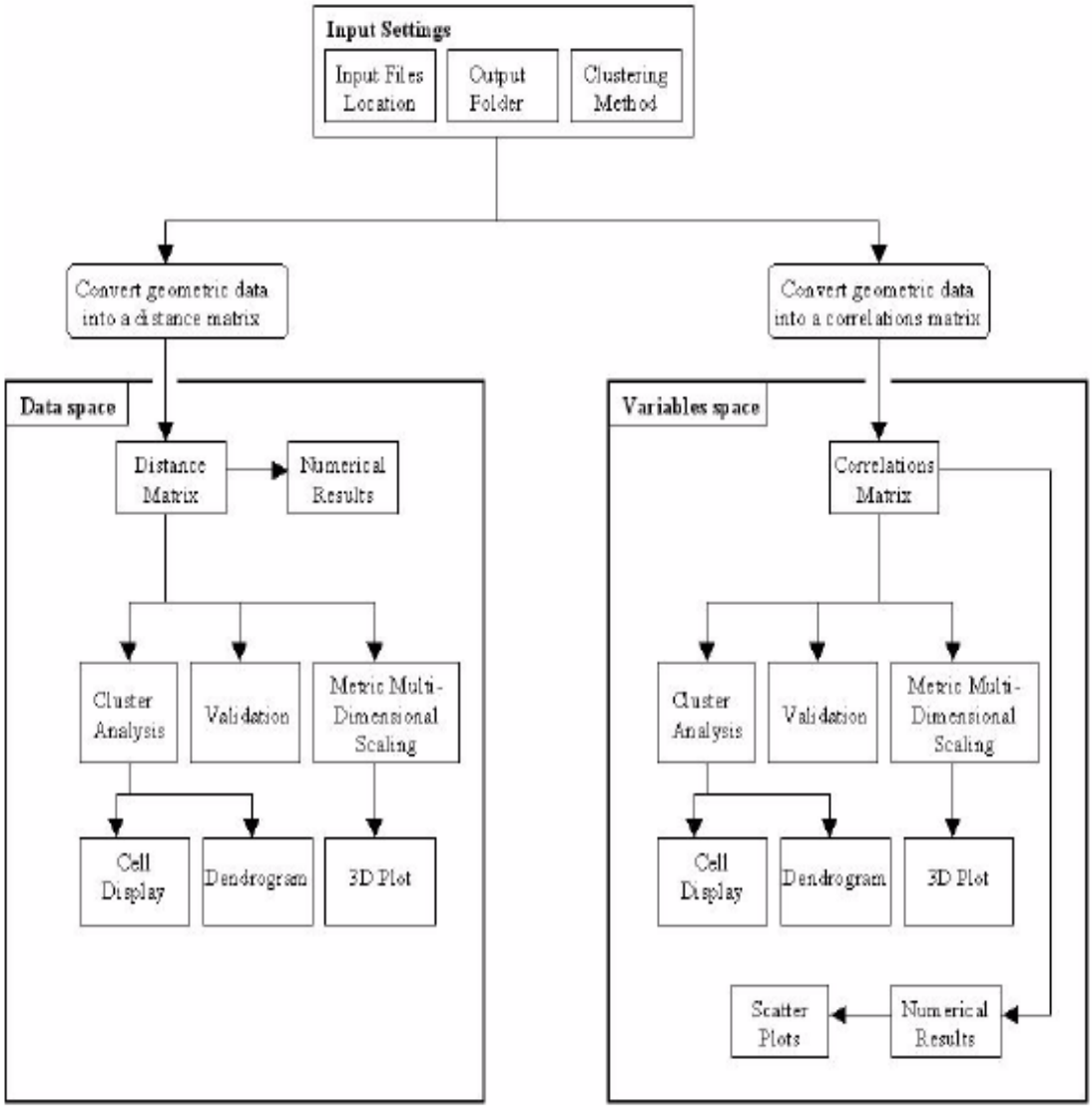

4.2.2 dSNAP Features

dSNAP presents results in Data space and Variables Space, this section discusses the key features of dSNAP. The Cell Display, Dendrogram, 3D Metric Multidimensional Scaling, and Numerical Results are discussed when presented in the Data space, for the Variables space results, the Cell Display, Dendrogram, 3D Metric Multidimensional Scaling, and Numerical Results and Variable space plots will be discussed. *(This information has been taken from the online manual which can be accessed via the website, http://www.chem.gla.ac.uk/snap/dSNAP_beta.html)*

4.2.2.1 Data space results display

Cell Display

This screen is the default graphics pane, see Figure 4.2, all nodes are arranged as fragments alphabetically in Refcode order. It displays the results by colour coding groups of fragments belonging to the same cluster group. This colour labelling is derived from the Dendrogram. The cell display is useful for easily identifying the number and variety of fragments in a single hit by displaying all the fragments in a hit as well as assigning them to the same or different clusters. The display window also presents a key on the left-hand side with a legend to represent each cluster. By clicking on one of the groups the user can highlight every cell in that cluster, this can be a useful feature when dealing with large data sets, (Barr, 2006).

Figure 4.2: A typical cell display from the dSNAP output. The different colours represent the different groups that the data has been clustered into. Each group has a specific feature.

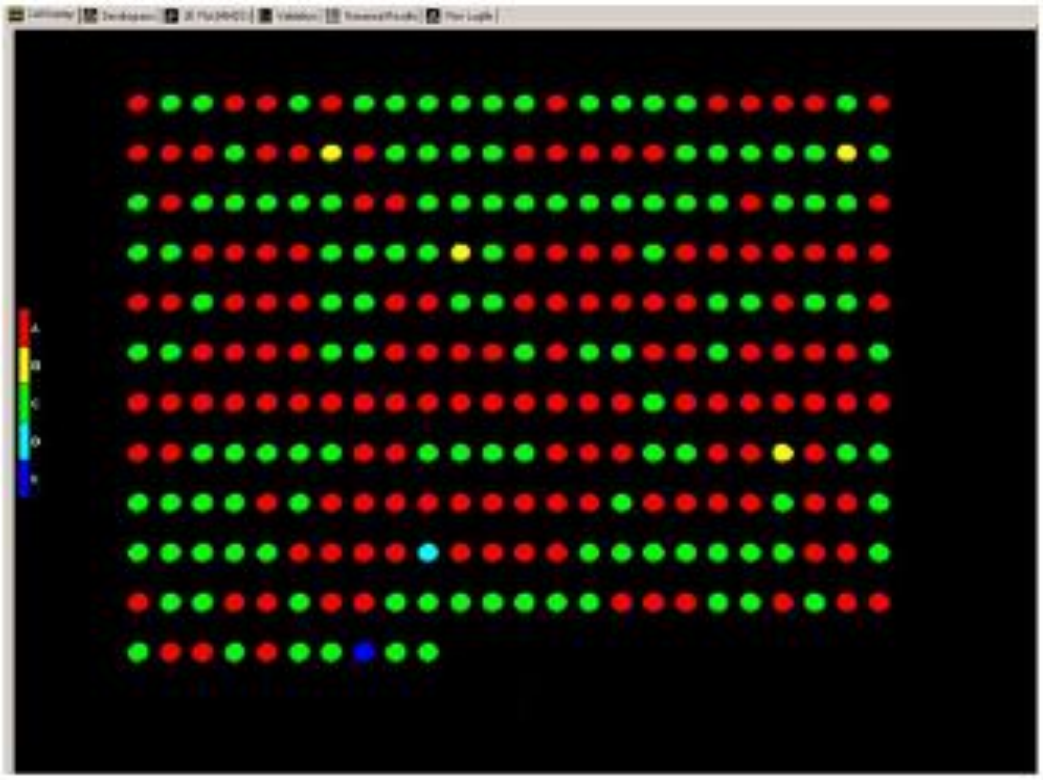

4.2.2.2 Dendrogram

The Dendogram, see Figure 4.3, displays the results from the cluster analysis and is the most important display in dSNAP as it visually presents the results is a hierarchical method of classification. As mention is previously, the Dendogram is like a tree diagram, each fragment is represented by one a box at the bottom of the screen. Figure 4.3

Figure 4.3: Dendrogram presented by dSNAP in the data space results. This display is a much aesthetically pleasing way to view data as compared to the cell display. Each sample is paired/grouped to a conformational/geometrically similar sample.

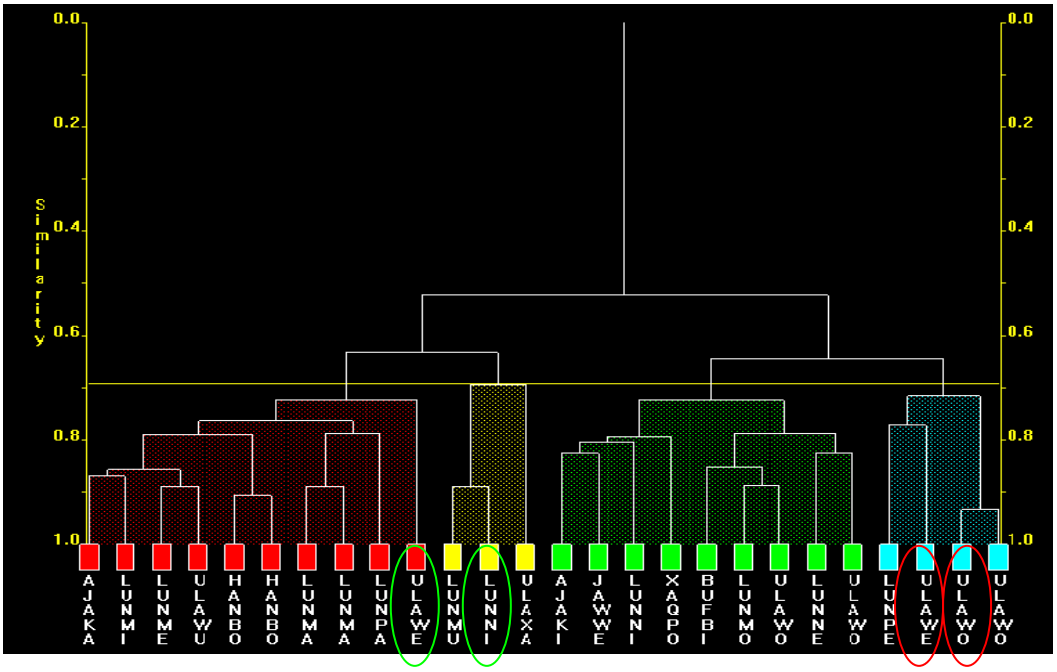

Figure 4.3 shows a typical output, and we can see that the Dendogram shows a scale on the vertical axis which is an index of similarity. The Dendrogram tree branches out according to the calculated similarity between the fragments that each branch connects to. A horizontal bar (tie-bar) connects two branches according to the similarity, (Barr, 2006). For example the pale blue cluster from Figure 4.3 shows there are two groups labelled ULAWO, these are connected nearer the bottom of the Dendogram, this means that these two fragments are highly similar and can be justified in being grouped together. On the other hand, two branches that do not meet until nearer the top of the Dendogram then the fragments associated are considered to be less similar and more loosely related to each other. In Figure 4.3 this has been highlighted with rings, red for similar fragments, and green for less similar.

A manually adjustable yellow cut-level is also present on the Dendogram, this decides how the Dendogram is split into separate clusters, (Barr, 2006).

4.2.2.3 3D MMDS Plot

A multidimensional scaling upon the distance matrix is plotted and shown as a series of spheres arranged in 3D space. Similarity is represented by the spatial distance between the spheres in the plot. Hence, the closer the spheres are the more similar the fragments are. Fragments that are strongly related will group together in the 3D plot and form a cluster, (Barr, 2006).

This 3D screen is the second important visual feature of dSNAP, this allows users to interpret the level of similarity between fragments both within a cluster and within the whole dataset. The colour coding for each fragment outlined in the Dendogram applies to the 3D sphere as it did in the cell display. The colour coding connection between the two features allows easy comparison of the two methods. If the cut-level in the Dendogram is adjusted, subsequently the colour in the 3D plot is also updated.

The goodness of fit of the results is indicated in the top-left corner of the display. This is computed as a correlation coefficient between the observed distance matrix and the derived calculated one. The closer the number is to 1.0, suggests a good fit. Low numbers suggest the program may have had trouble adequately partitioning the data, (Barr, 2006).

4.2.2.4 Numerical Results

This tab displays the correlation matrix generated from the raw numeric data that is used as the basis for the cluster analysis.

The screen will display the refcodes of the fragments and values which tell users how well fragments are correlated. A value of 1.0 signifies a perfect 100% correlation, whereas a value of 0.0 signifies a 0% correlation. Thus, a value closer to 1.0 the better correlation between two fragments, the more similar they are. It is also possible to have negative values. This suggests anticorrelation, (Barr, 2006).

4.2.2.5 Variable space results display

The Variables tab on the left-hand tab bar allows users to view the results in variables space (Barr, 2006).

Figure 4.4: Tabs available in the dSNAP screen

4.2.2.6 Cell Display

This display is different to the one discussed earlier. The cell display presents a display with a different number of cells as it is now showing the number of independent variables (angles and distances) instead of the number of fragments, (Barr, 2006).

Figure 4.5: Cell display in the variables space, each node represented a structural variable in the fragment of the structure being probed.

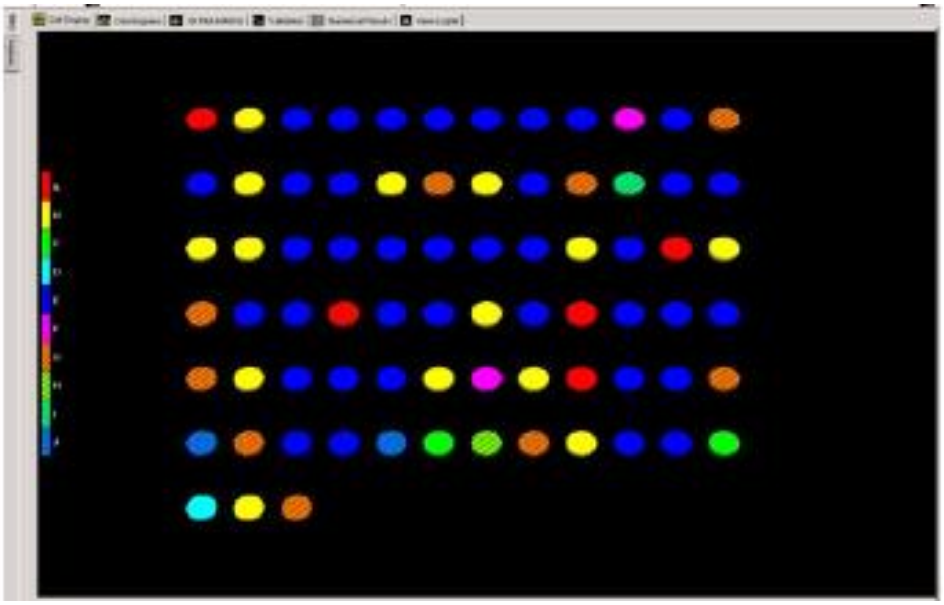

In data space, cells represent single fragments, where as in variables space each cell represents a single structural variable in the fragment that was defined in the original search query. Clustering of the variables is according to how well they have correlated to each other. It should be expected that the clusters in variables space will be more diffuse than in data space, (Barr, 2006).

4.2.2.7 Dendrogram

The Dendogram shows individual defined variables in the fragment. The tie bars indicate the level of correlation between the variables it joins. Variables that have been joined by a low tie bar are highly correlated, in turn, variables joined by high tie bars have low correlation. Variables space can be a useful tool for accessing and interpreting the important factors that give rise to the clustering in data space, (Barr, 2006).

4.2.2.8 3D MMDS Plot

In data space, each sphere is a representation of individual fragments, whilst in variable space each sphere represents a structural variable in the fragment.

Spheres that are plotted close to each other are variables that are considered to be highly correlated, (Barr, 2006).

4.2.2.9 Variable Space Scatter Plots

A scatter plot is opened in a new window by clicking on a cell in the Numerical Results pane. Each of the plotted points represents a fragment, the colours used in the scatter plot are taken from the data space Dendogram. This allows users to analyse any possible relationship between trends in particular variable values and the resulting fragment clusters, (Barr, 2006).

A scatter plot can only be created for two different variables. There will be entries in the numerical display where the variable has been correlated to itself and has a correlation of 100%, a scatter plot for this is not possible to obtain. However, for two variables with 100% correlation a scatter plot is possible, however this is rare, (Barr, 2006).

Figure 4.6: Typical scatter plot viewed from a set of data which give a) scatter plot with poor correlation and b) scatter plot of good correlation

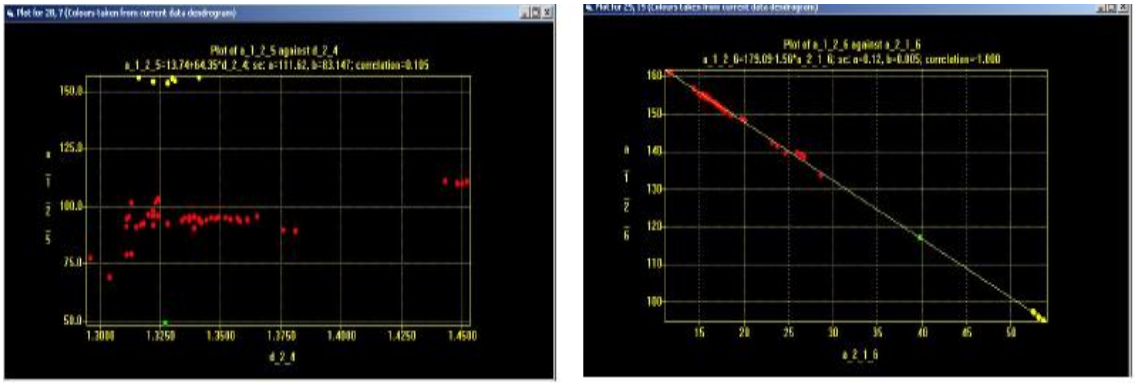

4.3 Worked example dSNAP

Central to the work on the pair wise contacts present in a co-crystal based on amides is the intermolecular contacts found in amides and carboxylic acids. For this reason a re-run of the example involving primary amides-carboxylic acid interactions and

carboxylic acid-carboxylic-acid motifs of Parkin et al 2006 was undertaken (section 4.4). This was also undertaken to ensure the current version of dSNAP available for this work was generating outputs consistent with previous studies. The results presented are based on the fragments shown in Figure 4.7. The fragments had defined contacts 1-8 for bond length, angle and torsions and were used to search the CSD, (Parkin, 2006). The results below are taken from Parkin et al 2006, and give an idea of the expected output from such fragments.

Figure 4.7: The two search fragments used. Contact was defined between any of the atoms 2, 3 or 4 and any of atoms 6, 7 or 8. The atom numbering is shown in blue extracted from (Parkin, 2006)

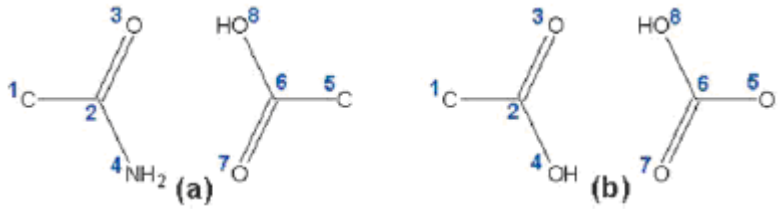

A cluster analysis using dSNAP of these fragments gives the following results, (Parkin, 2006), see Figure 4.8.

Figure 4.8: Dendrogram and MMDS plot of carboxylic acid-amide interaction, (Parkin, 2006)

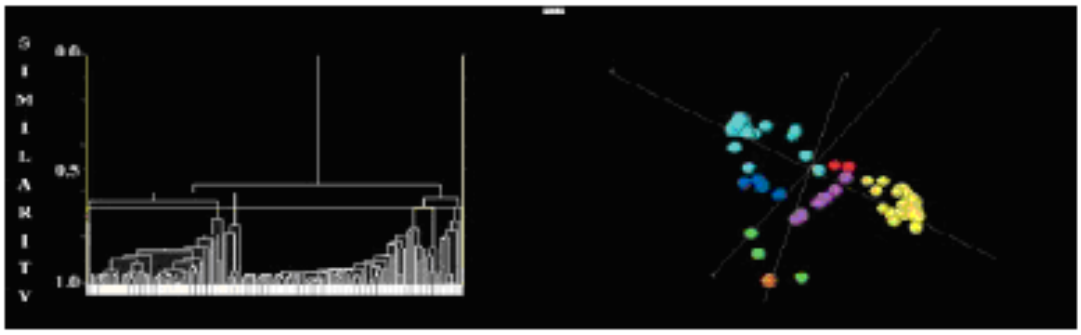

dSNAP is able to represent data in several forms, Figure 4.8 shows the results in both a Dendogram format and a Metric multidimensional scaling (MMDS) plot, which is a three-dimensional Euclidean space in which one point or sphere represents one fragment in the data set.

The Dendogram is cut at the 68% similarity level, each cluster is shaded in a different colour. The MMDS clearly shows that there are seven distinct clusters. Another way dSNAP presents its results is through a scatter plot, the results are presented in Parkin et al Figure 4.9, (Parkin, 2006).

Figure 4.9: (a) Scatter plot of the N4…O7 distance (Dist5) against the O3…O8 distance (Dist10)

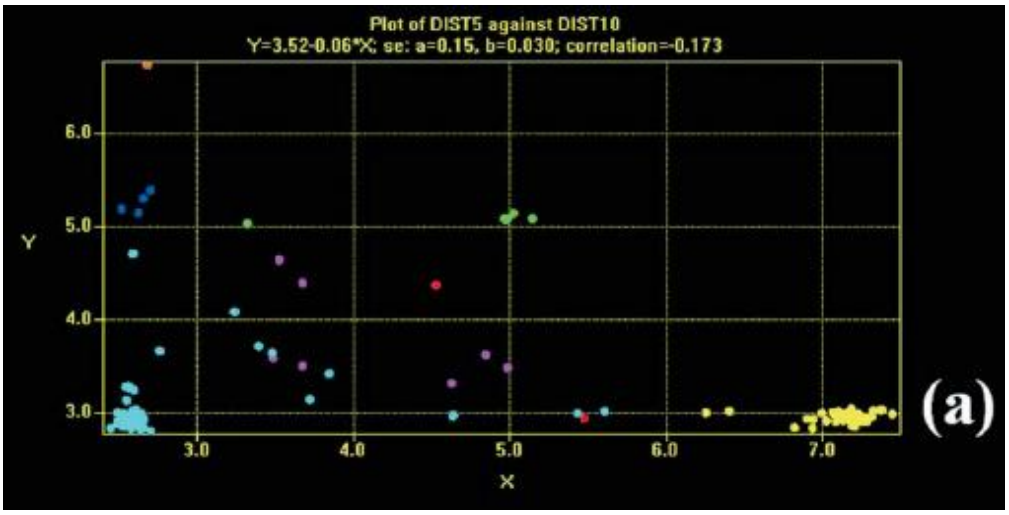

As a result there are seven different clusters, however there are two distinct clusters that have been identified; other clusters are not clearly defined. It is therefore wise to view these 2D scatter plots using two different contacts, Figure 4.10, (Parkin, 2006).

Figure 4.10: (b) the C1…C6 distance (Dist23) against the C2…C5 distance (Dist8), for the acid…amide fragment.

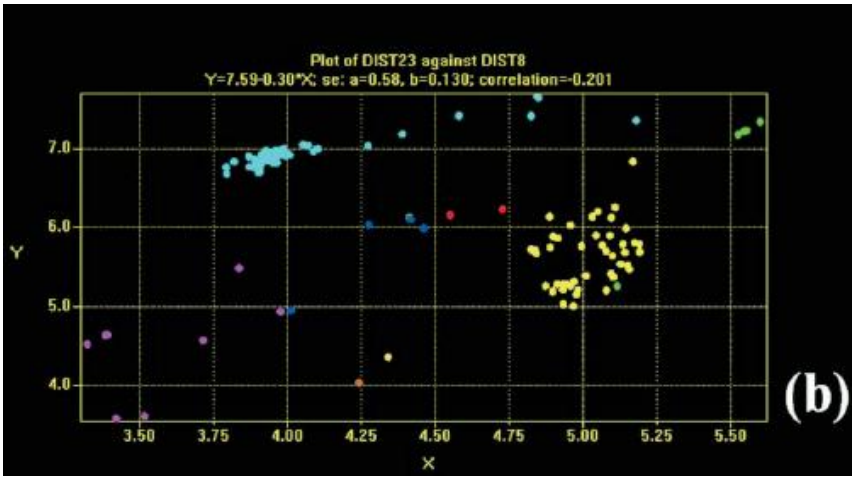

The scatter plot (Figure 4.10) shows a much more clear distinction of groups, and therefore suggests that a single parameter or a single pair of parameters is not enough to describe all the differences between the individual clusters, and illustrating the advantages of including the full geometric description of the search fragment. The full cluster analysis consolidates all these geometric differences, and the structural scientist can use the convenient parameter plots to determine the important underlying drivers for the geometries obtained, (Parkin, 2006).

With large datasets, dSNAP allows further classification by re-clustering larger groups to reveal sub clusters each of which are chemically and structurally distinct.

This example was reworked initially to gain a benchmark for running the search in the Cambridge Structural Database (CSD).

4.4 dSNAP results and discussion

The work presented in this section is in collaboration with Dr Andy Parkin and Professor Chris Gilmore of The University of Glasgow. dSNAP was used to analyse acid-amide interactions. Initially the same acid-amide search done by Parkin et al 2006 was undertaken using dSNAP version 0.9.5. The raw files used by Parkin et al 2006 were requested to see how they carried out the search. Initially the fragment shown in Figure 4.11 were drawn in CSD and used, this was the same fragment presented in Parkin et al. When searching the CSD, the same search restrictions were employed as reported in Parkin et al, this gave 101 hits, this was then put into dSNAP giving the following results shown below in Figure 4.13

Figure 4.11: Search fragment employed by Parkin et al

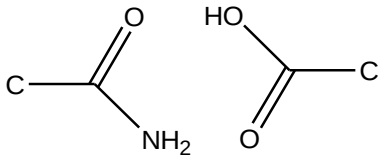

Figure 4.12: Search fragment as it would be drawn in ConQuest, 3D parameters have been selected and a contact has been outlined which is less than the sum of the van der Waals radii of the two closest atoms (highlighted in pink)

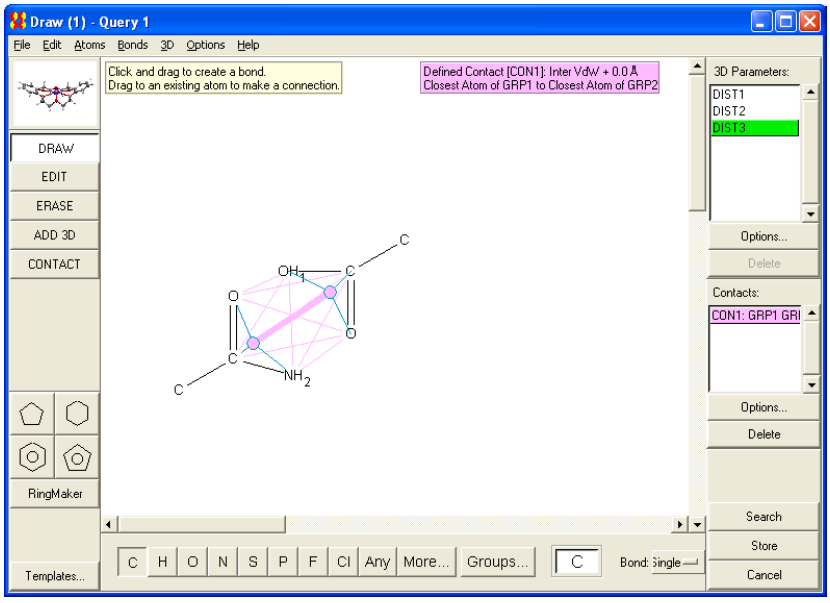

Figure 4.13: Dendrogram showing the results from the search presented in Parkin et al (Parkin, 2006).

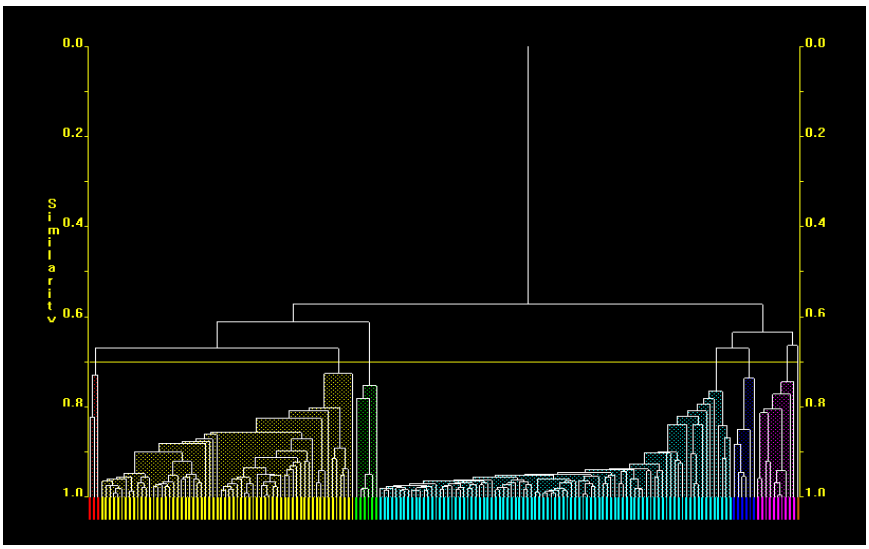

The Dendogram shows that from the 101 hits, 179 fragments have been derived to have the carboxylic acid- primary amide interactions. As expected the results are the same as those reported in Parkin et al 2006 paper, (Parkin, 2006).

Figure 4.14: 3D MMDS plot of the results from the acid – amide fragment researched by Parkin et al (2006).

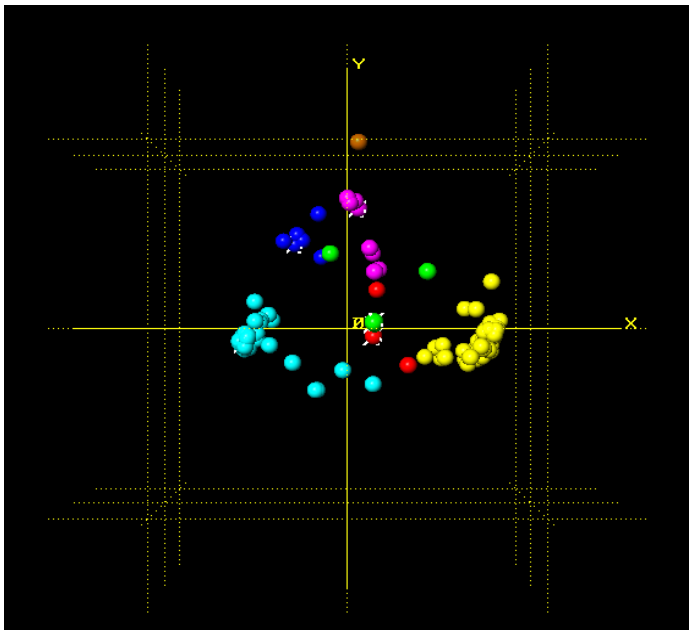

The Dendogram in Figure 4.13 gives the seven clusters presented in the Dendogram and the MMDS plot in Parkin, (2006). However, the research for this project consists of looking at carboxylic acid- primary amide interactions of Isonicotinamide and Benzamide and a series of carboxylic acid selected from a literature review. However the contacts specified were modified to make them relevant to the features in these co-crystal systems. Therefore, the search fragment used in the CSD search concentrates around the benzene ring where position 4 on the ring is labelled as 'X' allowing for searches to include any substitute for the carbon being replaced as 'N' nitrogen with an amide feature, this is shown in Figure 4.15:

Figure 4.15: Acid - Amide fragment used for the work in this project by searching the Cambridge structural database

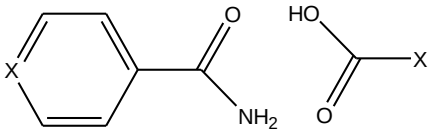

The ConQuest (.cqs) file used by Parkin **(**2006) was adapted to show the fragment of interest to this research, Figure 4.16. This was done so that dSNAP is able to calculate and cluster the similarities between two atoms using a larger peripheral. An interaction was defined as a contact that is less than the sum of the Van der Waals radii of the two closet atoms. Geometric parameters were identified and the CSD search was observed (Figure 4.16 below). The CSD produced 57 hits from which dSNAP successfully ran the file producing 108 fragments which contain the carboxylic acid – primary amide fragment shown in Figure 4.16.

Figure 4.16: CSD snap shot showing the fragment and all requested bond length and angles highlighted for the search.

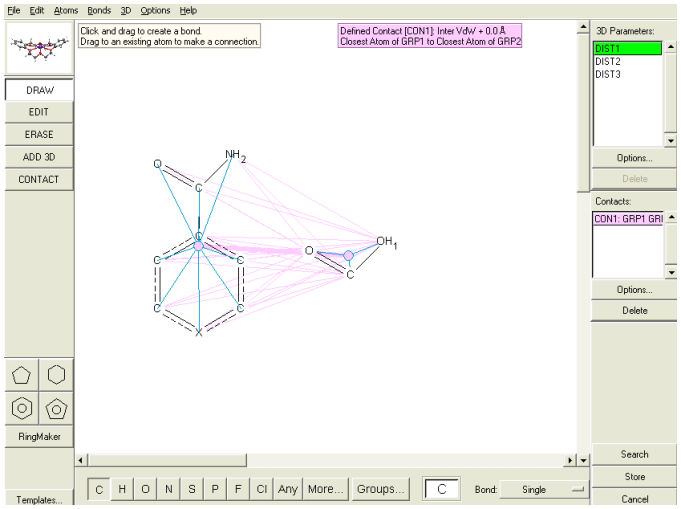

The dSNAP analysis shows a Dendogram very different to the ones shown earlier.

Figure 4.17: Dendrogram output of search results exported into dSNAP for this project. Nine distinct groups have formed from the clustering analysis.

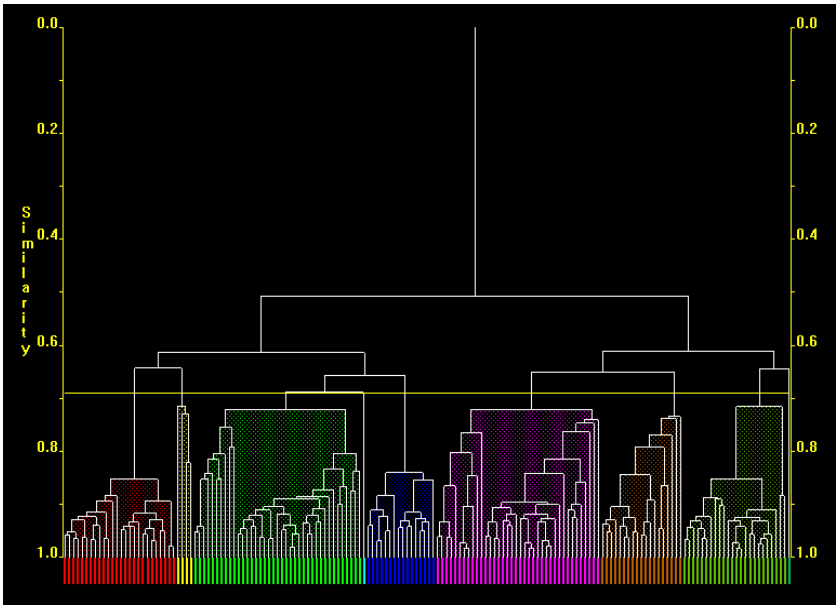

The similarity bar of the Dendogram was set to 68%, showing that there are 9 distinct clusters. The 3D MMDS plot shows an interesting image of clusters. It can be seen that there are two clustering groups opposite to each other which are then sub clustered with respect to what is shown in the Dendogram.

Figure 4.18: 3D MMDS plots showing the distribution of the fragments in 3D space, showing the 9 clusters and how they correlate

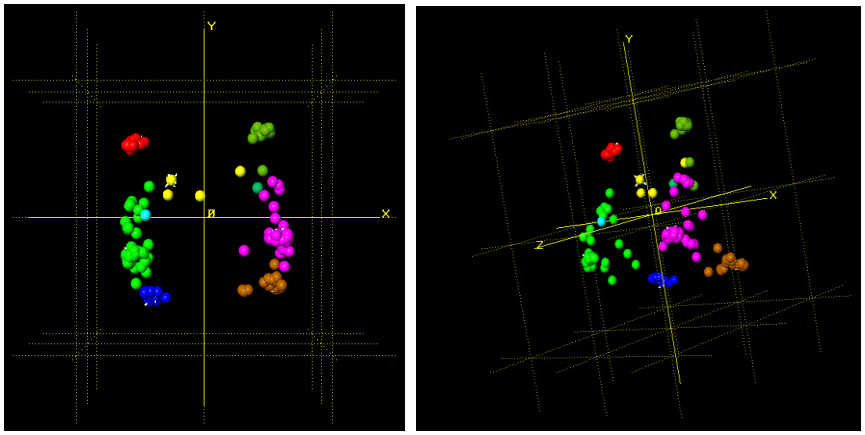

By selecting the 'Numerical results' tab, and then selecting the variables tab on the top left-hand side of the pane, angles and distances can be selected and compared by

plotting Variable scatter plots. The dSNAP program automatically highlights significant correlation in bold. However, in this instance the numerical result did not do this even when the cut-off value for the correlation was set higher/lower from the default of 0.8. However, the data in the Numerical results tab show Figures of above 0.8, but upon viewing the plot we see that the clusters identified in the Dendogram are scattered everywhere where as in the examples presented in Parkin (2006) we would expect individual groups to be clustered in a linear or a group orientation. Below we see a plot with a correlation of 0.922, Figure 4.19

Figure 4.19: Scatter plot of d_2_4 against d_1_4, a linear clustering is expected but not seen here.

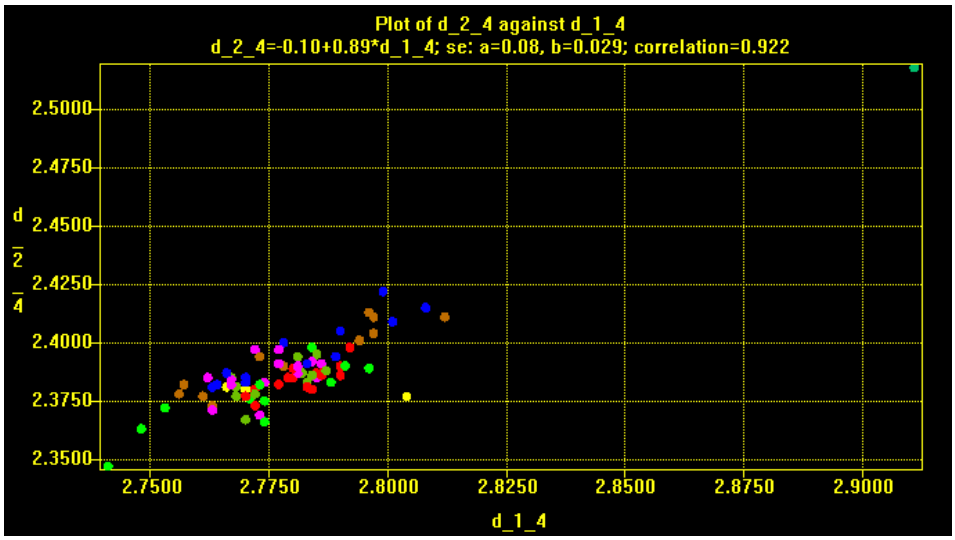

This has been communicated to the Glasgow group, suggestions have been made that this is due to symmetry of atoms outlined in the CSD search, this is especially in the case of the acid groups.

As mentioned previously, the Dendogram shows that there are 9 groups which can be viewed in the 3D feature of dSNAP. This allows us to see how the contacts have been distributed between a primary amide and Carboxylic acid groups. All observations are outlined in Table 4.1

Table 4.1: A summarised account of the observations of the clusters grouped in the Dendrogram

Group	
A	Acid-Pyridine Motif orientation, where O2 is orientated towards the N on Pyridine ring and O3 is away from it
B	Acid-Pyridine Motif slightly offset
C	Acid-Amide Motif slightly offset
D	Not clear-requires subclustering
E	Facing amide, showing the dimer interactions
F	Not clear-requires subclustering
G	Shows dimer and some deviations from it
H	Acid group facing pyridine ring
I	Acid group facing pyridine ring

The most common motifs observed are of hydrogen bonded dimer which involves 35 fragments and acid-pyridine motif involving 73 fragments. However, as reported in Parkin et al, these groups do not represent the limits of the classification process. Each of the larger groups can be re-clustered individually this should reveal further sub-clusters each of which are chemically and structurally distinct, these can then be further clustered if necessary. Appendix E presents the re-clustering of group, A, C, E, F, G and H.

Within the re-clustering, using its internal 3D viewer, dSNAP allows you to look at each node/group and the fragment(s) which is related to the node/group. However, this only shows one interaction which is exhibited by the molecules in the fragment.

4.4.1 Results of Re-clustering

Systems which were used in the experimental have been highlighted and analysed. A mono-carboxylic acid (Cinnamic acid, LUNMAI), di-carboxylic acid (Succinic acid, LUNNUD, LUNNUD01) and a benzoic acid derivative (3-Hydroxybenzoic acid, LUNMEM) have been selected and the analysis of which is reported here.

Figure 4.20: Fragment viewer of re-clustered group Aa. Fragment shows the pyridine ring pointing towards the acid group.

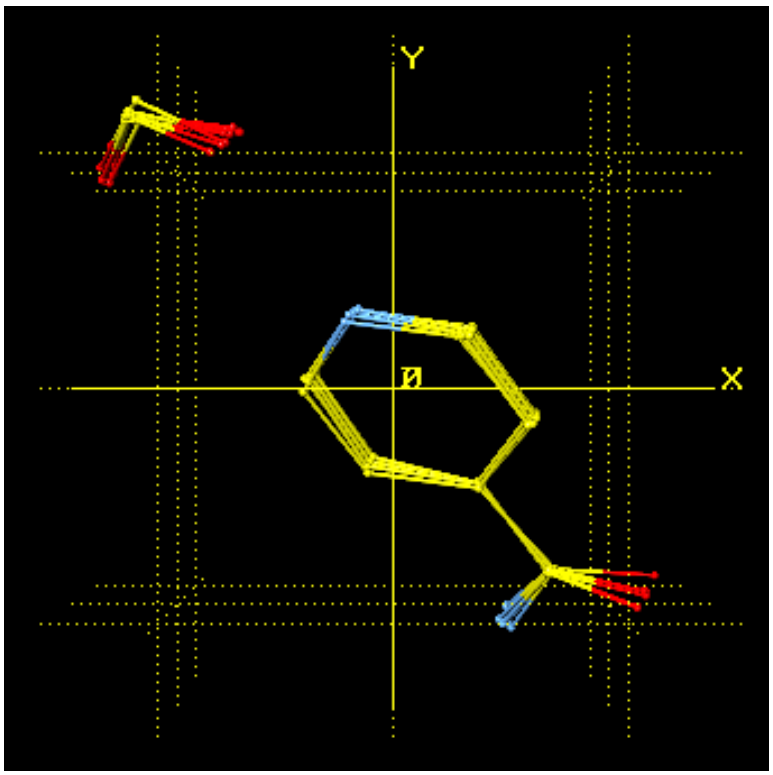

In order to get a broad perspective of other interactions involved, dSNAP integrates with Mercury which allows users to look at the fragments in a particular clustering

presented in dSNAP. This allows further analysis of packing patterns within a particular clustering.

With reference to the re-clustered groups presented in Appendix E it is observed that the re-clustering of Group A re-clusters to a further 4 different cluster which have the same acid-pyridine interaction shown in the fragment viewer (Figure 4.20).

4.4.2 Cinnamic Acid: Isonicotinamide Co-crystal

Cinnamic Acid is a monocarboxylic acid and it has been found to have 4 substructures according to the CSD hit list. These are read into dSNAP as LUNMAI_01, _02, _03, _04. From the analysis carried out we see that Group Aa clusters LUNMAI_02 and _03 to have some geometrical similarities, and Group Ce clusters LUNMAI_01 and _04 to have similarities.

Selecting fragments from Group Aa Dendogram and opening into the internal fragment viewer we see that dSNAP has clustered this structure according to an acid-pyridine interaction.

Figure 4.21: Typical Acid-Amide interaction observed in dSNAP

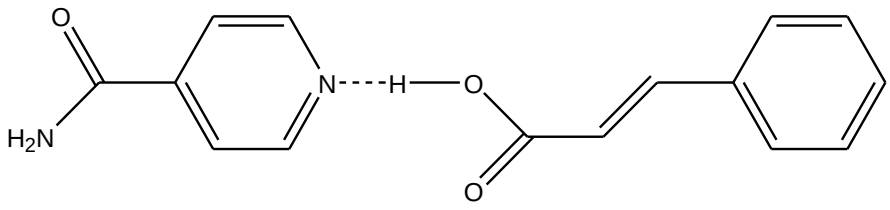

Viewing up the Y axis of the 3D plot we are able to see that the molecules are not entirely planar. There is some deviation from the acid-pyridine interaction presented even though both fragments are within the same crystal structure.

Figure 4.22: Fragment viewer of Cinnamic Acid : Isonicotinamide Co-crystal from dSNAP search. Highlighting the acid-pyridine interaction and a the conformation of the functional groups which make up the fragment of the Cinnamic acid : Isonicotinamide system

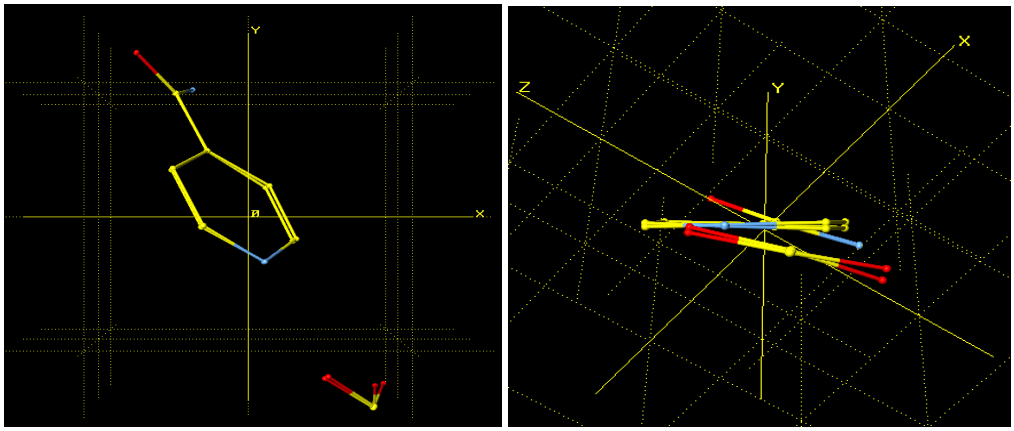

Selecting the Cinnamic fragments from Group Ce Dendogram (see Appendix E) and opening into the internal fragment viewer we see that dSNAP has clustered this structure according to an acid-amide interaction with neighbouring supermolecules (Figure 4.23-24).

Figure 4.23: Acid-Amide interaction of neighbouring molecules.

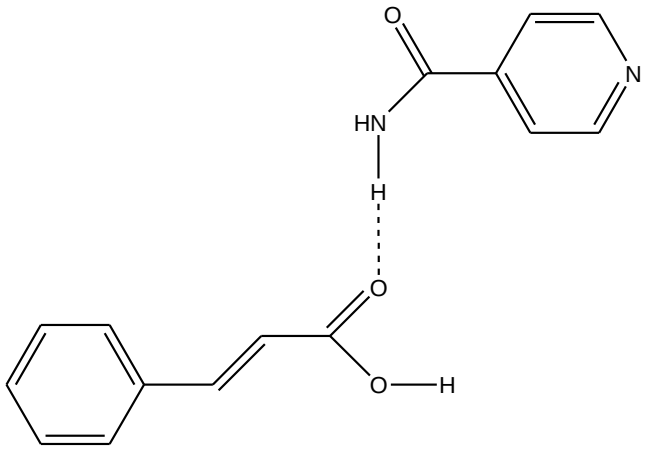

Figure 4.24: Fragment viewer showing the configuration of the Cinnamic fragments clustered in Group Ce

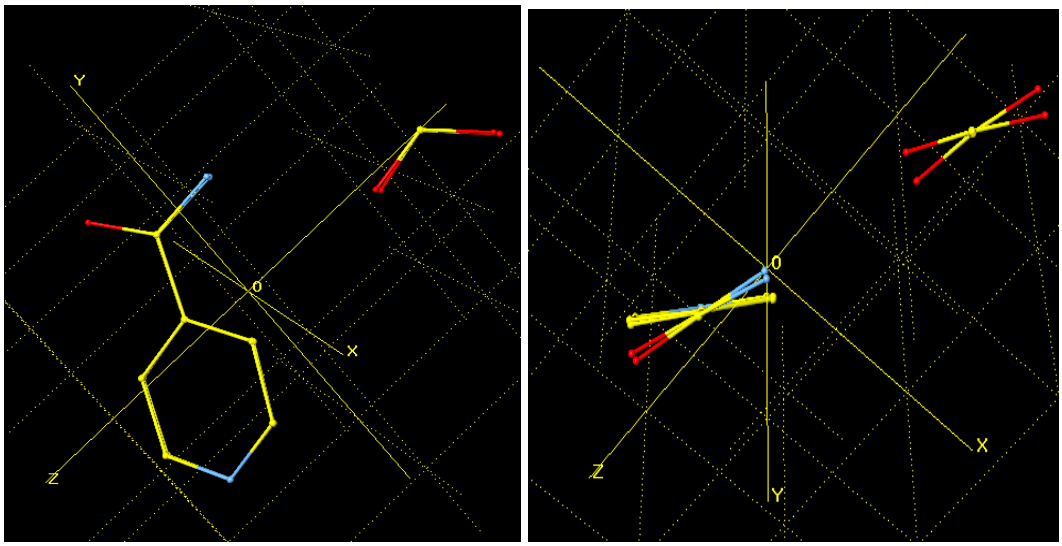

It is clear from the fragment viewer that these substructures are deviating from each other even though they present the same interactions with the same structure.

The distortion and how the substructures are interacting beyond the acid-pyridine interaction outlined by dSNAP can be further investigated by using Mercury.

4.4.2.1 Mercury analysis of LUNMAI

It is observed that this crystal structure is formed from 4 components. The primary interaction outlined is the acid-pyridine and the amide-amide homosynthons. At first glance it looks like both substructures _02 and _03 are identical, however on close inspection this is not the case.

Figure 4.25: (i) Presents the LUNMAI fragments viewed in Mercury. The conformation and distortion is shown in (ii) and (iii)

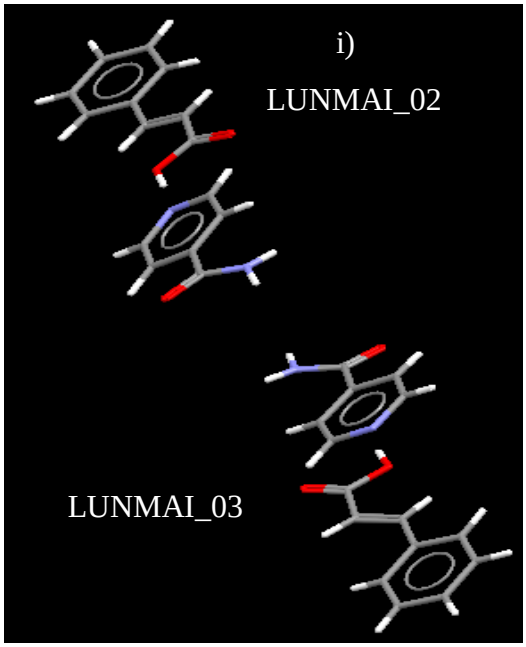

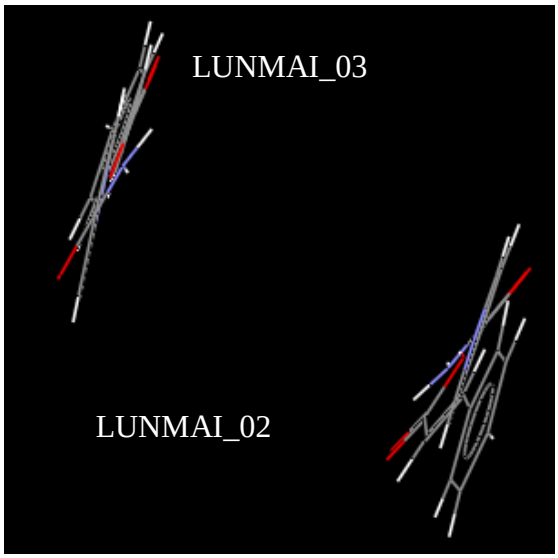

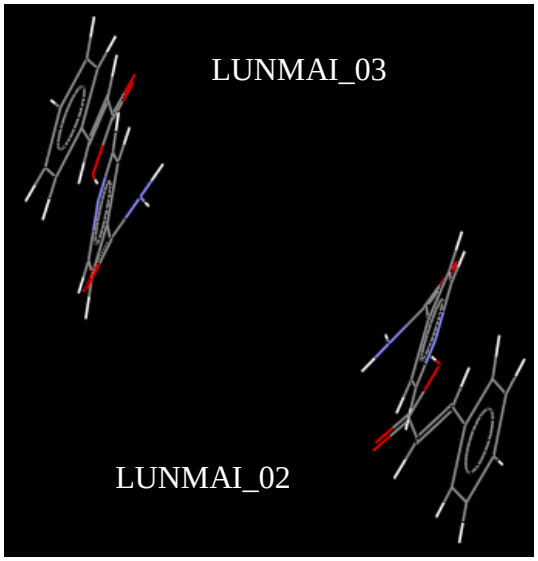

Figure 4.25 (i) shows that the substructures are orientated opposite to each other. In substructure _02, the carboxylic acid is orientated with the acid group facing the pyridine ring of the primary amide, Isonicotinamide, with a hydrogen bond forming from the nitrogen of the pyridine to the acid, N···O-H. Literature, (Aakeroy, 1997) suggests that there is flexibility in the geometry of the supermolecule due to rotation

around this N···O-H hydrogen bond. Such molecules can either be organised in a trans-trans-trans conformation or cis-trans-cis conformation.

Scheme 4.2.1: trans-trans-trans configuration

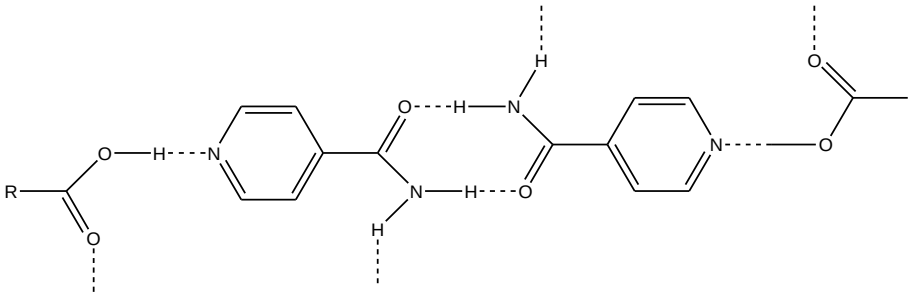

Scheme 4.2.2: cis-trans-cis configuration

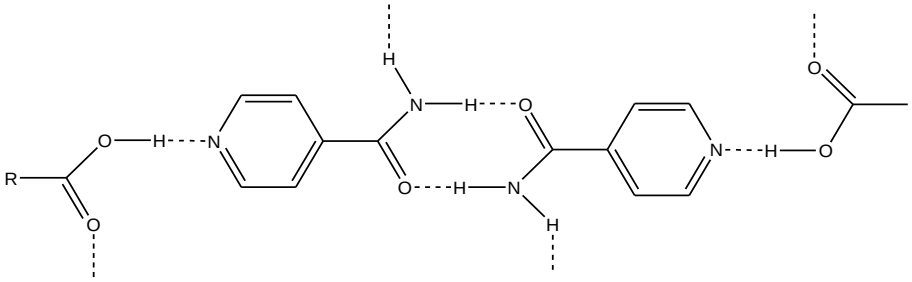

In the case of Cinnamic acid Isonicotinamide and as reported in (Aakeroy, 2002) these substructures are in the trans-trans-trans conformation, with respect to its near planar geometry, the carbonyls from the acid and the amide are organised in this fashion. Figure 4.26-28.

Figure 4.26: Mercury view of Cinnamic Acid : Isonicotinamide co-crystal, Amide-Amide interactions are highlighted, along with an Acid-pyridine interaction.

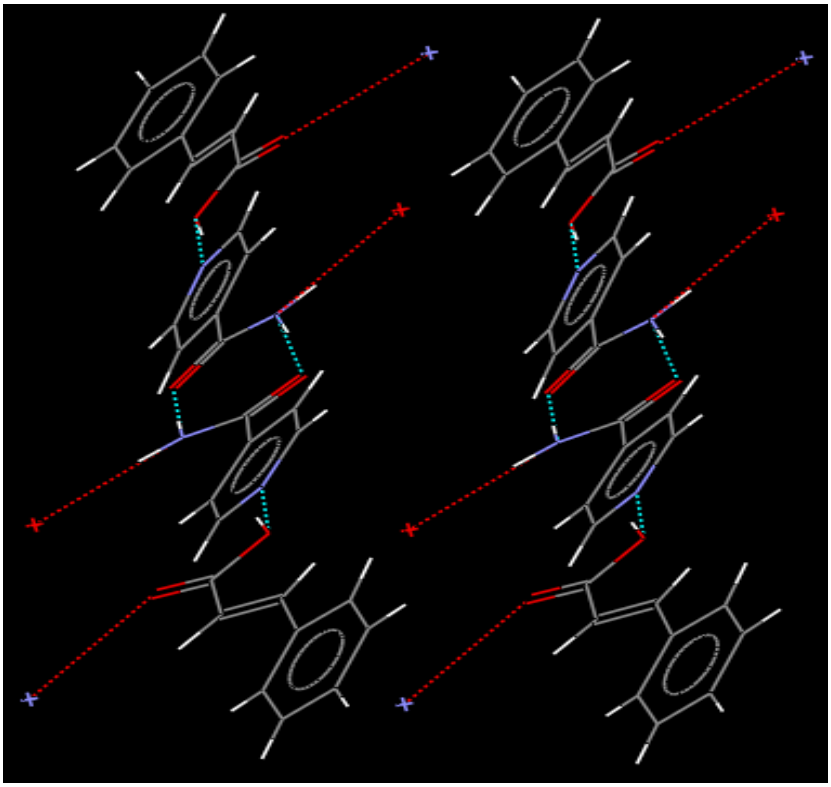

Figure 4.27: Trans-Trans-Trans conformation highlighted in Cinnamic Acid : Isonicotinamide co-crystal

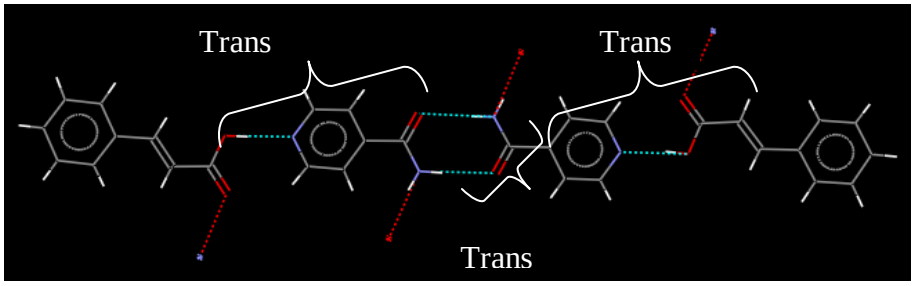

Extension along the secondary interaction of such trans-trans-trans supermolecules results in an interconnection via anti-amide proton and carbonyl oxygen, this produces an infinite 1D tape (Aakeroy, 2002) Figure 4.28 shows the graph set of the infinite tape.

Figure 4.28: The extended a infinite tape is formed, and a secondary ring, $R^4_4(22)$, via N-H···O and O-H···N hydrogen bonds between the supermolecules

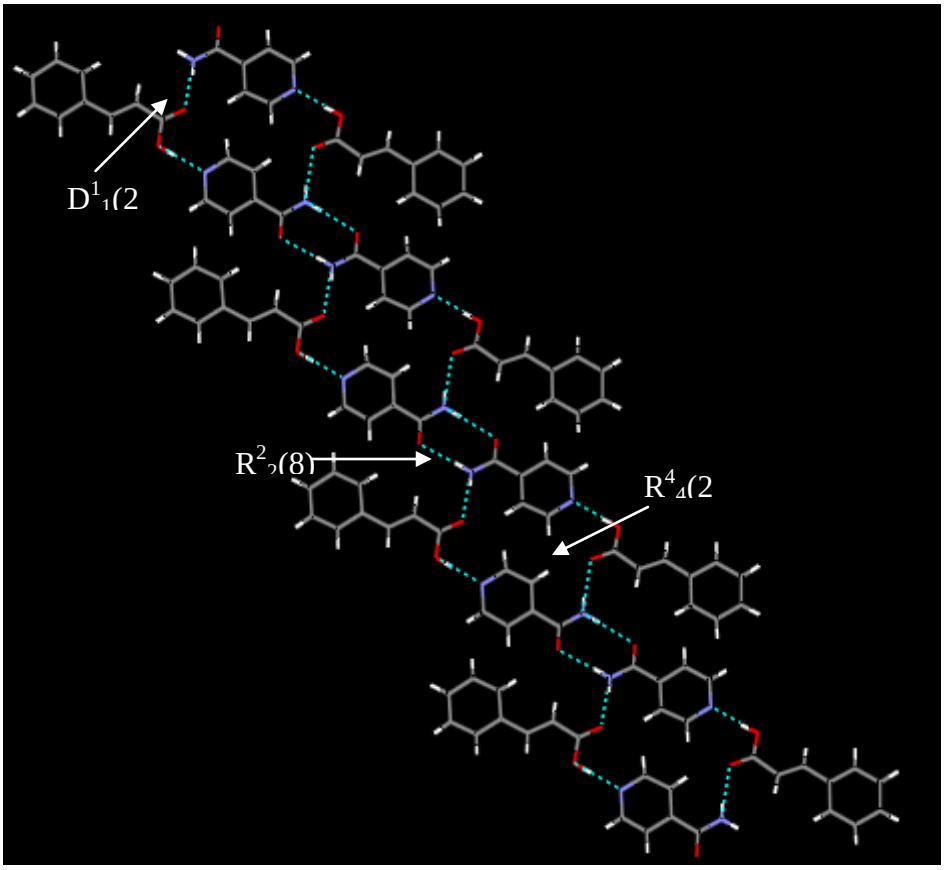

4.4.3 3-Hydroxybenzoic Acid: Isonicotinamide Co-crystal

The crystal structure of 3-Hydroxybenzoic Acid with Isonicotinamide, has three substructures. LUNMEM_01, _02, and_03. The dSNAP program has clustered all three of these substructures into three different groups.

LUNMEM_01 appears in group Aa, _02 in group Ca and _03 is found in group Ce.

Group Aa, is a cluster that consists of fragments with acid-pyridine interactions. Figure 4.29 shows the 3-hydroxybenzoic acid: Isonicotinamide fragment view in the fragment viewer.

Figure 4.29: 3-hydroybenzoic Acid: Isonicotinamide (LUNMEM) fragment from Group Aa

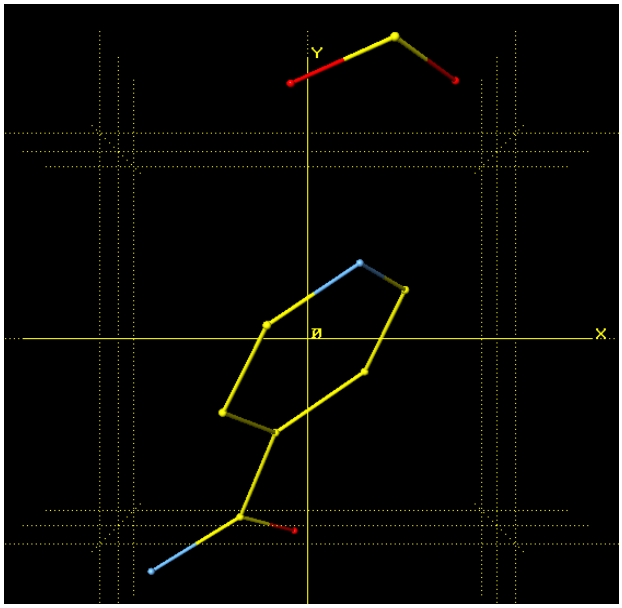

Group Ca is a clustering of fragments which have the O2 positioned towards N1 of the Pyridine ring, slightly offset in orientation to group A sub cluster. This is shown in Figure 4.30.

Figure 4.30: 3-hydroxybenzoic Acid fragment from Group Ca

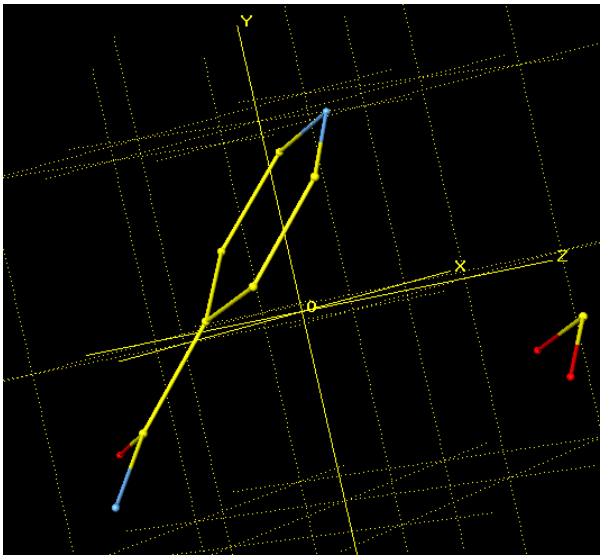

Group Ce is representing fragments with Orientation of acid group next to the amide group. LUNMEM_03.

Figure 4.31: 3-hydroxybenzoic acid : Isonicotinamide orientation view in the fragment viewer

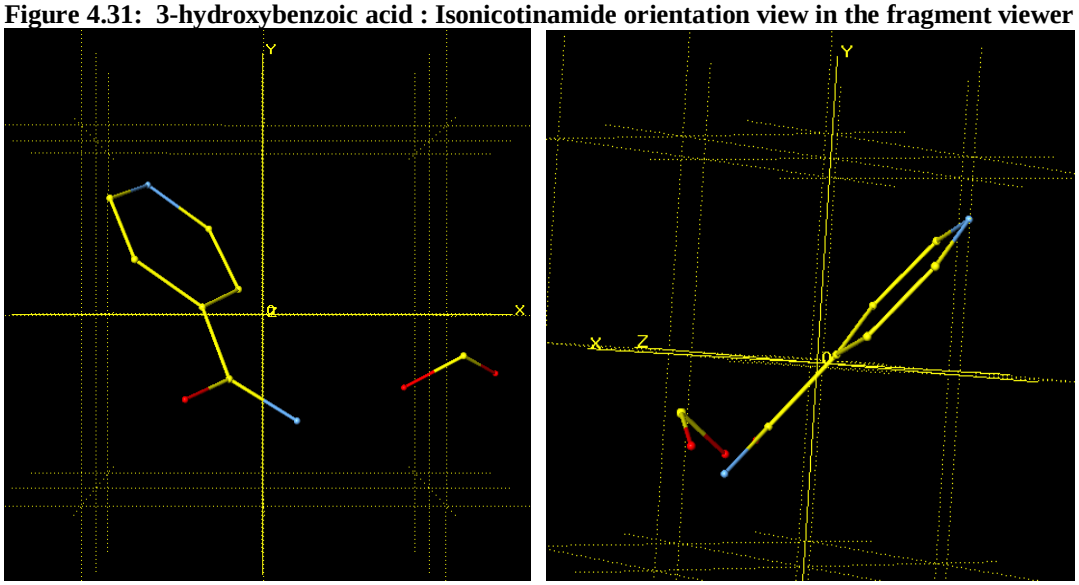

4.4.3.1 Mercury analysis of LUNMEM

The first interaction is the acid-pyridine as outlined in group Aa as substructure LUNMEM_01. Upon extension, we see a four component structure, where primary interactions are via acid-pyridine and a complementary homodimer is observed.

Isonicotinamide forms amide-amide homosynthon, $R^2_2(8)$ with another Isonicotinamide, the primary aromatic nitrogen forms acid-amide interactions $D^1_1(2)$,

Figure 4.32: Co-crystal for 3-hydroxybenzoic Acid: Isonicotinamide shown in Mercury, Interactions have been highlighted as amide-amide dimers and acid-pyridine interactions.

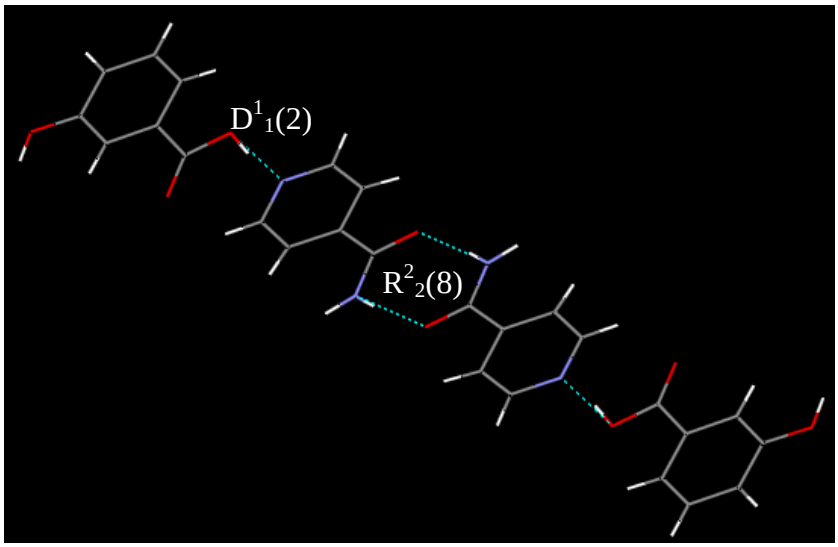

Adjusting the viewing of the supermolecule we can see a near planar geometry, Figure 4.33.

Figure 4.33: Near planar geometry of the co-crystal for 3-hydroxybenzoic Acid: Isonicotinamide shown in Mercury

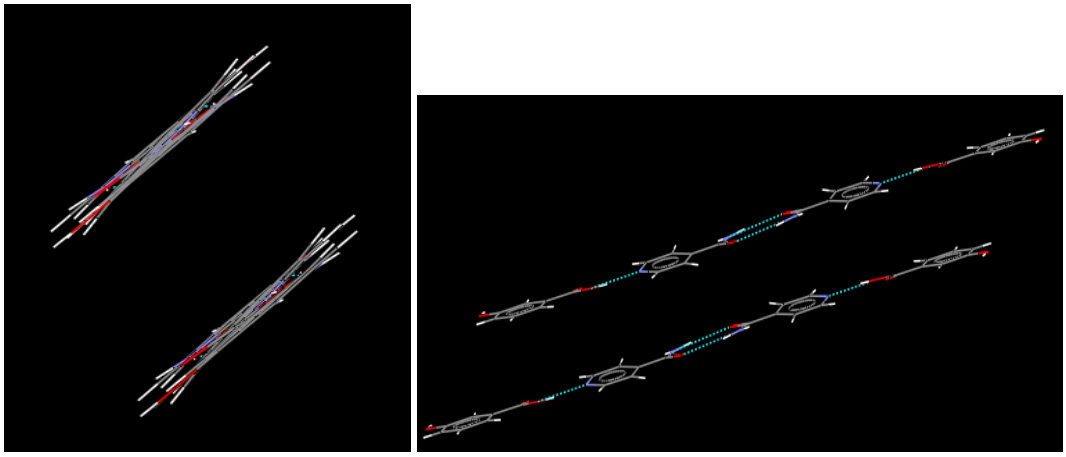

Again a trans-trans-trans conformation has resulted, see Figure 4.34.

Figure 4.34: Trans-Trans-Trans configuration of LUNMEM co-crystal.

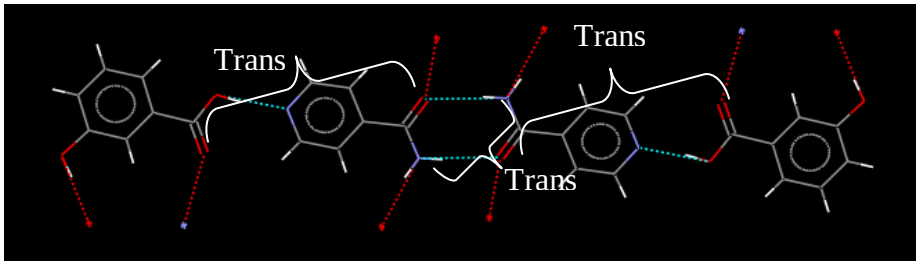

Group Ca observes the O2 positioned towards N1 of the Pyridine ring in the fragment but slightly offset. However, upon viewing this in Mercury there is actually a short weak contact between C1 of Isonicotinamide and C13 of the acid.

Figure 4.35: Mercury analysis of 3-hydroxybenzoic acid and Isonicotinamide, a discrete hydrogen bond has been picked up by dSNAP, this has been highlighted in Mercury to show there is some π-π stacking observed.

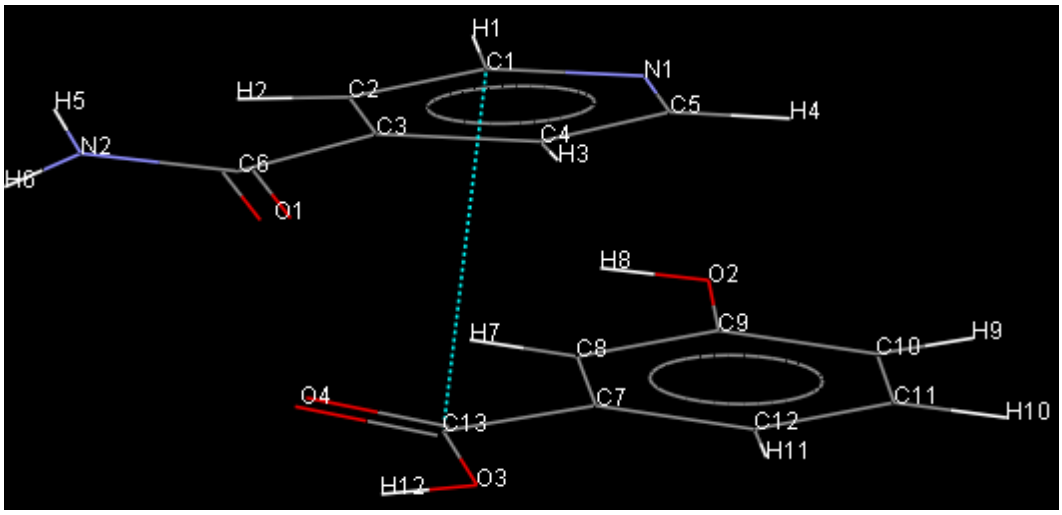

Fragment LUNMEM_03 is clustered in the Ce group, this group shows the acid group next to the amide group in a perpendicular manner. This is an N-H···O interaction, which connects two chains to form 2D cross-linked laddered network. Figure 4.36

Figure 4.36: i) Discrete interaction between N-H…O iii) Mercury analysis of the secondary ring formed via a N-H···O and O-H···O hydrogen bond interaction, giving $R^4_4(22)$ ring ii) Extension of the intermolecular interactions gives a laddered conformation

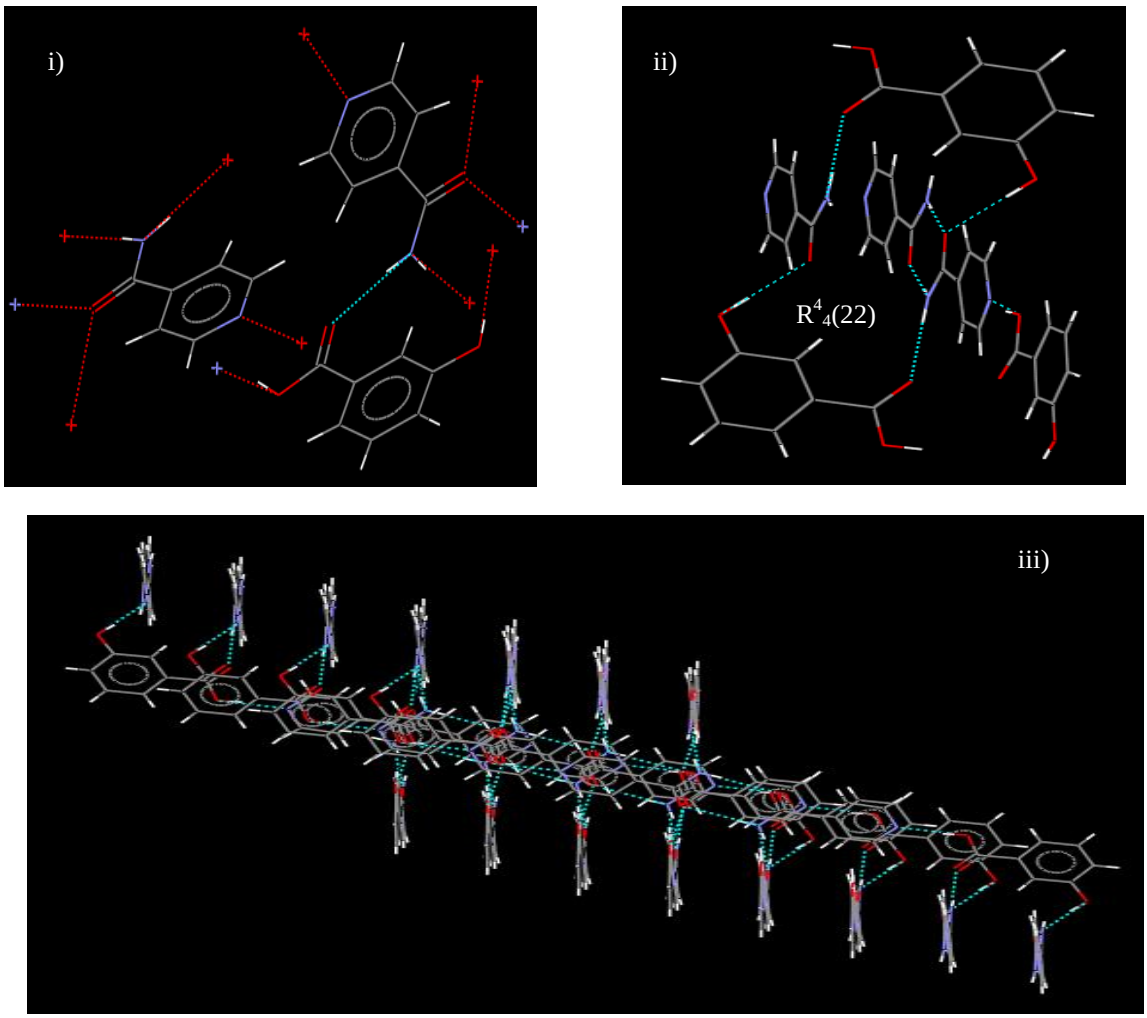

Within this ladder conformation a secondary ring is formed via this N-H···O and O-H···O hydrogen bond interaction, giving $R^4_4(22)$ ring.

4.4.4 Succinic Acid: Isonicotinamide Co-crystal

Succinic acid is a di-carboxylic acid that has been reported to co-crystallise with Isonicotinamide, (Aakeroy, 2006). The CSD shows that there are two structures reported, LUNNUD and LUNNUD01. In our investigation using dSNAP both structures were included. As a result, Group Fc clusters substructures LUNNUD_03 and LUNNUD01_03, Group Fe clusters fragments LUNNUD_02 and LUNNUD01_01 and Group Hd clusters LUNNUD_01 and LUNNUD01_02.

Group Fc shows that the corresponding fragments have the acid group positioned near the pyridine, above/below plane

Both LUNNUD_03 and LUNNUD01_03 have the same interaction with no deviation being picked up by dSNAP. The fragment viewer shows that the acid group is positioned in the opposite direction to the amide, it is located above/below amide of the Isonicotinamide molecule.

Figure 4.37: Fragment viewer showing LUNNUD_03 and LUNNUD01_03 from Group Fc.

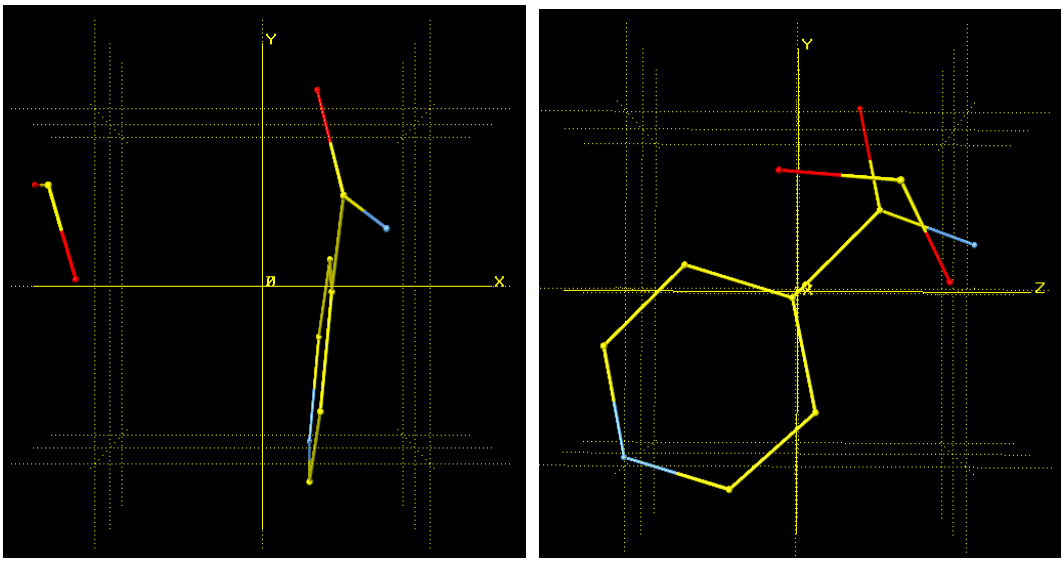

4.4.4.1 Mercury analysis for LUNNUD from Group Fc:

The contact from the cluster analysis does not become obvious when opening the selected fragments in Mercury. dSNAP has clustered the two fragments to have a O-C···C (3.392) and O-C···O (3.219), this is only highlighted when the 'short contacts' option is selected from Mercury.

Figure 4.38: Interaction of LUNNUD_03 in Mercury

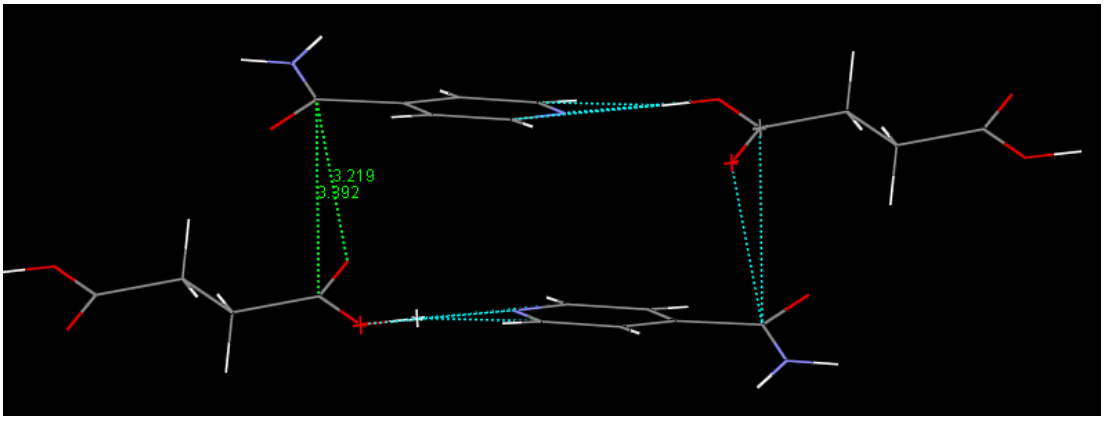

Figure 4.39: Interactions highlighted in Mercury of fragment LUNNUD01_03

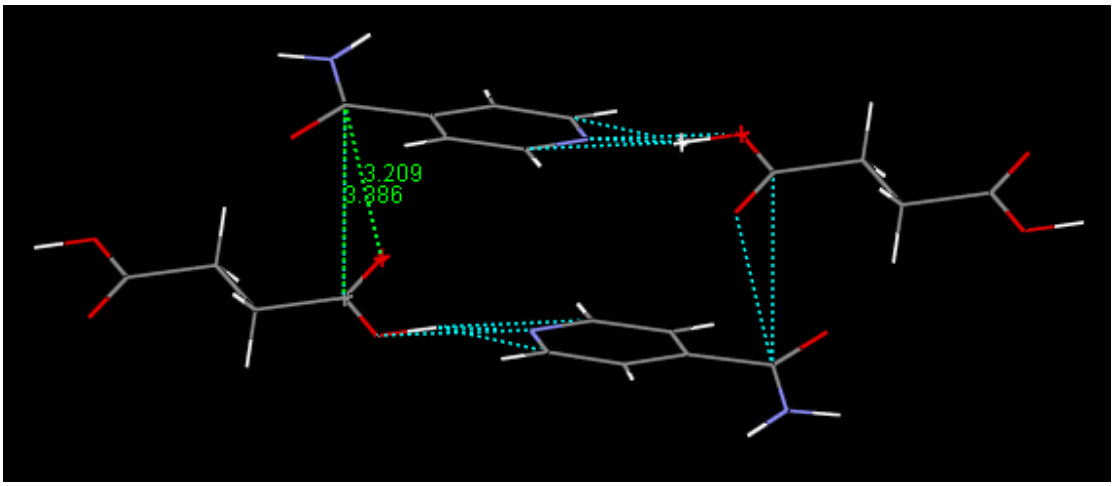

The fragments look exactly the same and so do the contacts with very little deviation. Extension of the primary contacts and the short contacts, we see that the fragment extends to layer as infinite sheets.

Group Fe clusters the LUNNUD_02 and LUNNUD01_03 fragments to have acid group's located next to amide this suggests that there is some acid-amide interaction, Figure 4.40.

Figure 4.40: dSNAP Viewer showing the LUNNUD_02 and LUNNUD01_03 fragments

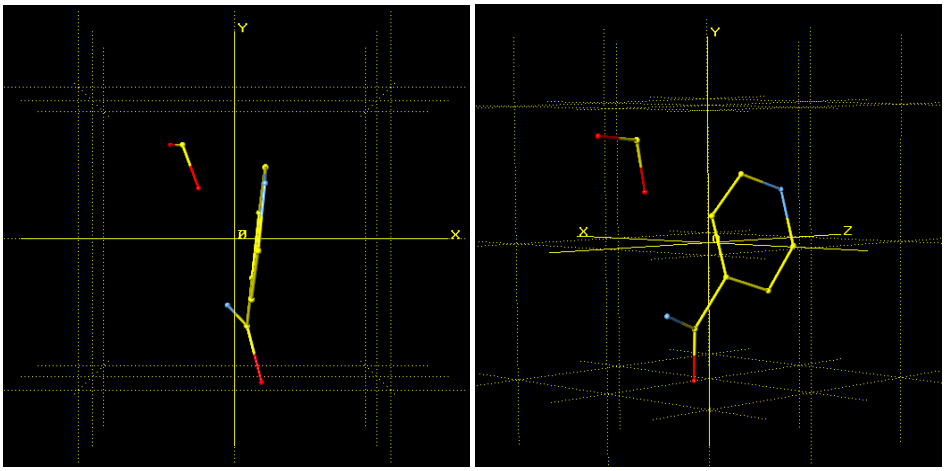

4.4.4.2 Mercury analysis of LUNNUD_02 and LUNNUD01_03

Mercury shows that the dSNAP observation is true; there is an interaction between the amide of Isonicotinamide and the carbonyl of the acid, N-H···O.

Figure 4.41: Mercury analysis of Fragments LUNNUD_02 and LUNNUD01_03, interaction highlighted to show interaction between the amide of Isonicotinamide and the carbonyl of the acid, N-H···O and acid-pyridine interactions

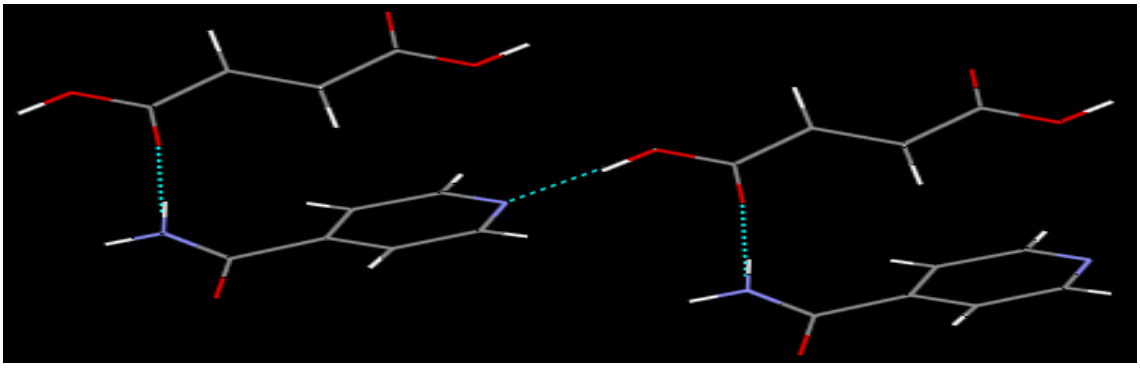

On extension of the N-H···O interactions we see an infinite 1-D chain, which holds a $R^4_4(28)$ and $R^6_6(26)$ ring. This is shown in Figure 4.42 and Figure 4.43.

Figure 4.42: Extended sheet of co-crystal Succinic Acid : Isonicotinamide LUNNUD.

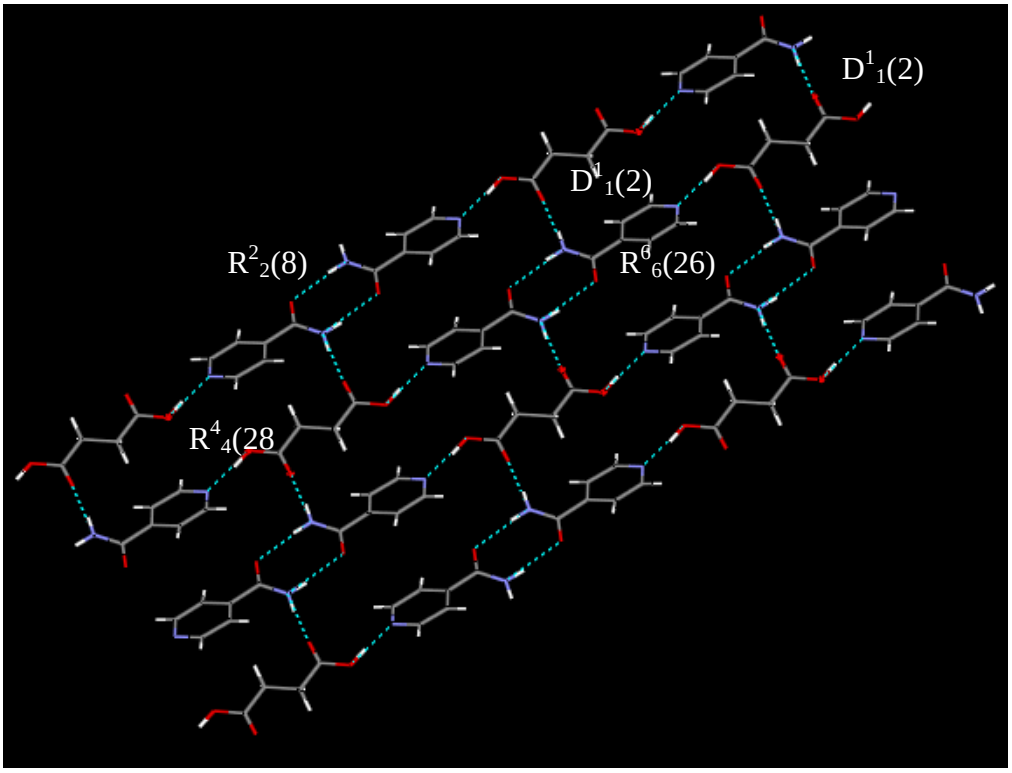

Figure 4.43: Extended sheet of co-crystal Succinic Acid : Isonicotinamide LUNNUD01

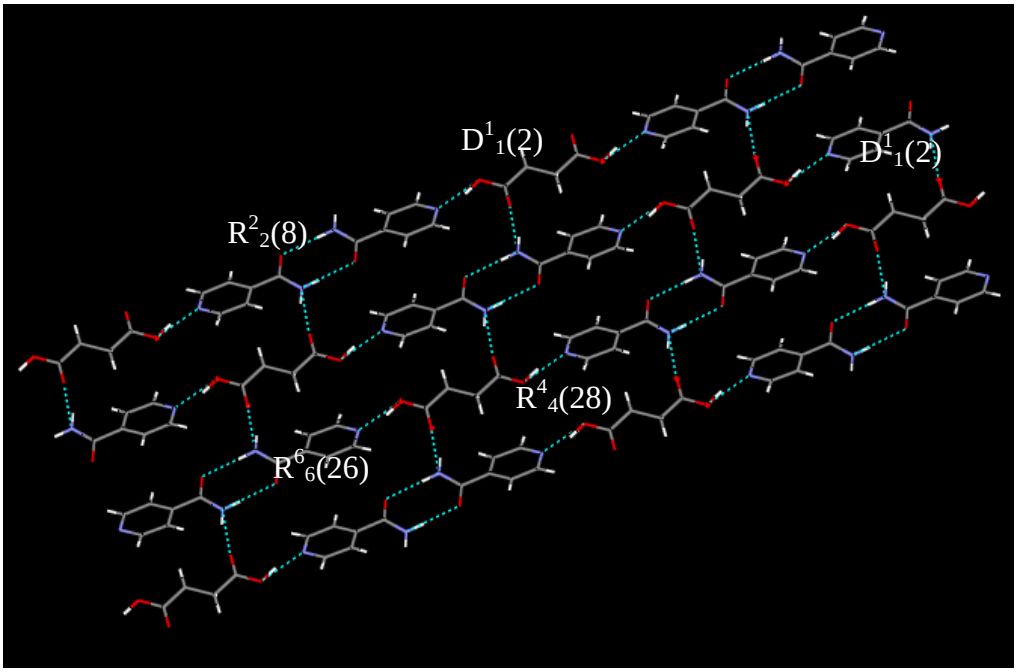

Group Hd clusters LUNNUD_01 and LUNNUD01_02 to have O3 of the acid group facing towards N1 of pyridine. This observation suggests that these fragments both exhibit the expected acid-pyridine interaction.

Figure 4.44: Fragment viewer showing the LUNNUD_01 and LUNNUD01_01 fragments Clustered by dSNAP in group Hd

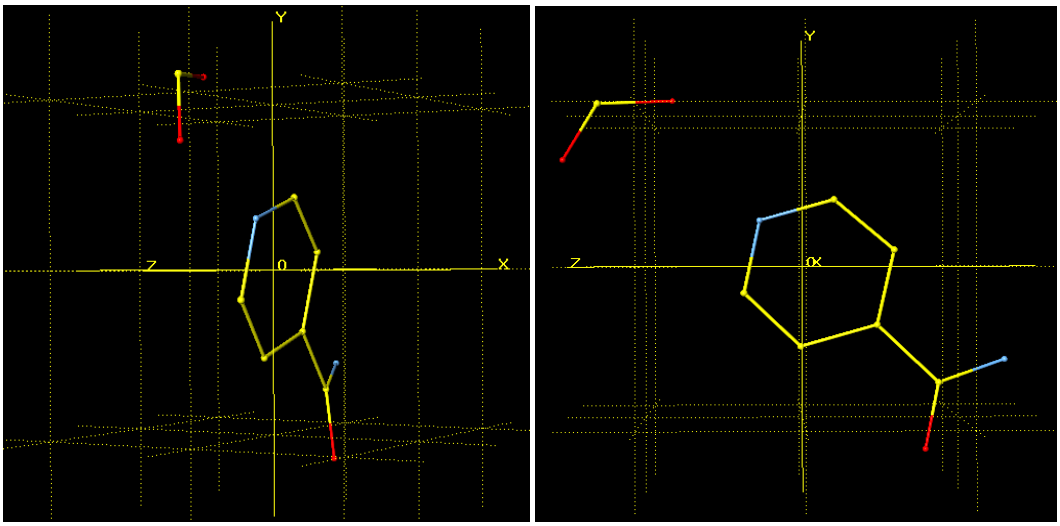

4.4.4.3 Mercury analysis of LUNNUD_01 and LUNNUD01_02

This example of Succinic Acid with Isonicotinamide, forms the expected acid-Pyridine hydrogen bonds, $D^1_1(2)$, additionally upon expansion of the chain a homomeric self complementary amide-amide interaction $R^2_2(8)$ is also observed (Figure 4.42-43).

Another observation is the conformation of the molecules which make the supermolcule of di-carboxylic acid-amide. This example differs from the monocarboxylic acid-amide and the benzoic acid derivative co-crystal structures presented in this section. The conformation we observe is of a cis-trans cis conformation, Figure 4.45

Figure 4.45: Cis-Trans-Cis conformation exhibited in the Succinic Acid-Benzamide co-crystal

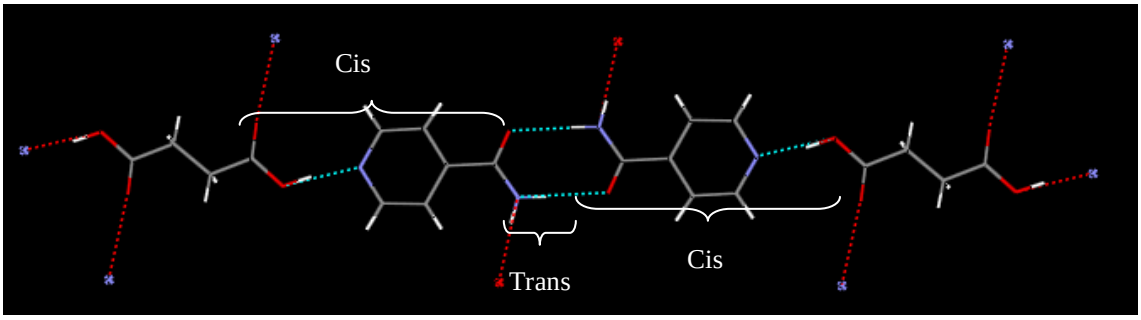

4.4 Summary

The dSNAP analysis has been identified as a way forward, even with the code having issues with the symmetry of dimer pairs and the low number of Isonicotinamide co-crystal in the database (N = 20). The analysis by this means did highlight the subtleties, which were present in the packing motifs of the Isonicotinamide co-crystals. In particular, the presence of chains with differing conformational orientation as these chain assemblies pack together to form the overall structure. In particular the cis and trans orientation of the amide and acid carbonyl to each other and the planar and off planar layer assemblies. All of which are required to maximise the hydrogen bond usage of the components comprising the co-crystals. To further understand this behaviour of the model component comparison, attempts to maximise and grow single crystals have further been identified with the use of a high through-put screen coupled with further collaboration with the University of Glasgow to beta test the polySNAP software on screening co-crystals.

Chapter Five: Investigating and comparing co-crystallisation of 1° amides with carboxylic acids. High through-put approach

5.1 Introduction

A critical but potential rate-limiting step in co-crystal studies is the effort and turnaround of the initial screening for new entities. To date low through-put and conventional approaches have been employed. In order to potentially expand the data set required to address the focus of the project; which was to develop an understanding of the success rate profile noted for certain coformers with a Benzamide and Isonicotinamide. The low through-put of conventional approaches was ported to a high throughput platform, with the assigned combinatorial set of condition set to search and fine tune crystallisation conditions pertaining to cooling rates, solution loading and solvent.

This chapter describes the attempt to apply a high through-put to screening techniques to explore further the combinatorial crystallisation conditions associated with screening for co-crystals. One allied outcome of this high through-put work was to enable the industrial partners to develop an in house protocol for co-crystal screening, and to assess how efforts of the partner companies and academic collaborators involved in diffraction setup (Pharmorphix), diffraction outputs (Syngenta, and Bradford) and diffraction analysis (polySNAP Glasgow) would integrate overall.

The work presented was undertaken using the facilities at Syngenta Ltd Huddersfield site, where a High-through-put robot, Crissy® -Automation Platform by Zinsser Analytical, was made available to screen for co-crystals at various compositions. For this work the laboratory screen initially used in previous chapters was further extended using the synthon approach, where compounds which hold desirable and most favourable donor/acceptor sites have been selected as the coformers for this screen. All

the compounds to act as co-formers were selected from Sigma-Aldrich and ordered by Syngenta, these were further reduced from the hundreds available to 16 co-formers. The active ingredients were as before, Benzamide and Isonicotinamide with the addition of Nicotinamide. The co-formers selection was based upon functional groups configuration by expanding co-former set to iso structural mono-carboxylic acid, di-carboxylic acid and benzoic acid derivatives, and varying solvent polarity by including the following four solvents, *o*-xylene, isohexane, ethyl acetate and methanol all of which meet health and safety according to Syngenta laboratory policy. All materials were approved and bought by Syngenta.

Analysis of the data from the screen was sent to Pharmorphix for characterisation using a General Area Detector Diffraction System, better known as GADDS. The issue with using reflectance GADDS diffraction data is peak width, and resolution and background noise is prevalent in such diffraction patterns, and as such present a challenge with regards to data analysis. Currently PolySNAP offers a platform to address this and the diffraction type would be a challenge to the algorithms, and for this reason, this was undertaken in collaboration with Prof Gilmore's group and Dr Parkin (Glasgow).

5.2 Experimental

The screening grids were designed with the assistance of Dr James Forrest at Syngenta, the grids were set out to accommodate 1:2 , 2:1 and 1:1 ratios of the 3 active ingredients (AI), (Benzamide, Isonicotinamide, Nicotinamide), with the 16 conformers, and the four solvents. Evaporation plates with 96 wells were used; this allowed plates to be split into 2 accommodating 16 coformers at a time and two solvents per active ingredient. Please refer to Appendix F for full plate format used for high through-put screen.

Co-crystallisation was attempted from supersaturated stock solutions of active ingredients and coformers, all weights and measurements of solvents used are given in the table below. The stock solutions are placed in a rack along with the solvents which are to be used, all the data in table 5.1 and the plate format from Appendices c was input into a spreadsheet which programs the Zinsser of how much sample to inject into each well and at which ratios.

Table 5.1: Summary of the quantities used in the dispensing process for High through-put experiment with Zinsser Robot

		RMM (g)	Solubility (%)	Solvent	Mass (g)	Solvent Volume (ml)	Concentration (M/l)
	Benzamide	121.14	10	Methanol	4.00	40	0.825
	Isonicotinamide	122.12	10	Methanol	4.00	40	0.819
Coformer no.	Nicotinamide	122.12	10	Methanol	4.00	40	0.819
1	1, 4 Benzene dimethanol	138.16	5	Propanol	1.75	35	0.362
2	2 Nitrobenzoic acid	167.12	10	Methanol	1.75	17.5	0.598
3	3 Aminobenzoic acid	137.14	3	Methanol	0.88	35	0.183
4	3 Nitrobenzoic acid	167.12	10	Acetone	1.75	17.5	0.598
5	4 Aminobenzoic acid	137.14	10	Methanol	1.75	17.5	0.729
6	4 Nitrobenzoic acid	167.12	3	Acetone	0.88	35	0.150
7	Adipic acid	146.14	10	Methanol	1.75	17.5	0.684
8	Butanoic acid	88.1	10	Methanol	1.75	17.5	1.135

9	Fumaric acid	116.07	5	Methanol	1.75	35	0.431
10	Maleic acid	116.1	10	Methanol	1.75	17.5	0.861
11	Malic acid	134.09	10	Methanol	1.75	17.5	0.746
12	Phthalic acid	166.14	5	Ethanol	1.75	35	0.301
13	Pimelic acid	160.17	10	Methanol	1.75	17.5	0.624
14	Succinic acid	118.09	10	Methanol	1.75	17.5	0.847
15	Tartaric acid	150.09	10	Methanol	1.75	17.5	0.666
16	Trans β hydromuconic acid	144.13	3	Methanol	0.88	35	0.174

A total of 6 plates containing 96 wells were ran on the Zinsser, after the evaporation process the plates were dispatched to Pharmorphix Ltd who obtained the PXRD for each well, using a reflectance D8 Bruker GADDS diffractometer. The PXRD patterns obtained were then analysed using PolySNAP.

5.3 Results and Discussion

The GADSS diffraction data generated was analysed using the program PolySNAP courtesy of Prof Chris Gilmore and Dr Gordon Barr of the University of Glasgow. This collaboration was motivated by the need for users to further test the types of diffraction data the PolySNAP approach would be capable of processing, in this case, GADSS data with high noise and of low resolution with non uniform base line.

5.3.1 PolySNAP

In previous chapters we have discussed dSNAP and how this program clusters discrete interaction in a large dataset. Another program also developed by the Gilmore research group at University of Glasgow is PolySNAP.

Previous papers by Barr (2005, 2006) have shown how pattern matching coupled with cluster analysis and multivariate statistical methods can be used to classify large numbers of powder patterns (PolySNAP) (Krzanowski, 2000).

5.3.1.1 What is PolySNAP?

PolySNAP is a software package that is designed to match and analyse full profile spectral, powder patterns and other numerical data. The use of full profile allows for more flexible and accurate identification of samples, even when data quality is low or when preferred orientation effects are significant.

The software provides a user-friendly interface and several powerful and novel statistical methods to rank samples in order of their similarity to any other selected sample, allowing unknowns to be quickly identified. In quantitative mode, patterns of mixtures and potential pure phases can be identified.

The matching procedure can be automated for computer-controlled high-throughput analysis. An unlimited number of patterns can be prescreened, and PolySNAP allows for datasets of up to 1, 500 patterns with four different data types to then be analysed in a single run, and provides highly flexible graphical output to summarise and visualise the results. This highlights any unusual data, and means that time is not wasted looking at the many patterns that behave exactly as expected. It can work with or without the provision of reference patterns, and includes additional features such as an automated report writer and a logfile to assist with audit trail procedures.

The key component of the program is the visualisation tools based on Dendrogram and pie charts, as well as principal-component analysis (PCA) and metric multidimensional scaling as a basis of three-dimensional score plots. Below, Figure 5.1, displays a flow chart representation of the main processes, further details of the methods are explained in previous papers by Barr et al (Barr, 2005, 2006, Parkin, 2006).

Figure 5.1: Flow chart representing the main processes and methods involved in the polySNAP program

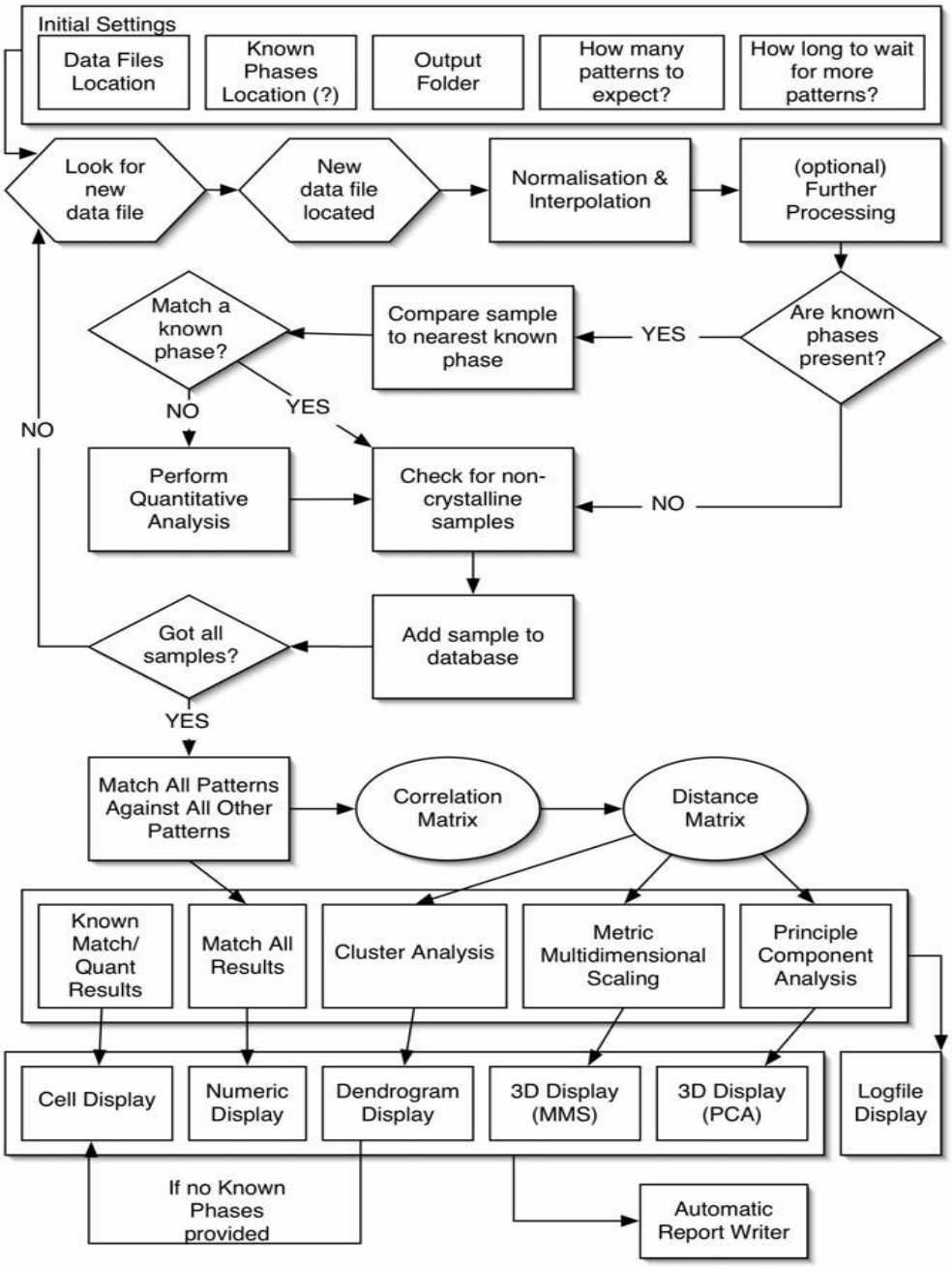

In this research, PolySNAP has been used to cluster powder pattern profiles generated from the high through-put screen approved and initiated in site at Syngenta Huddersfield.

The screening set consists of 6 plates, full analysis and examination of the results of plate BD001 is detailed in the next section and a brief discussion of the remaining plates, BD002-6. Tabulated results of plates 2-6 can be found in Appendix (F)

5.3.2 Analysis of Plate BD001

Plate one of the screen was of Benzamide with the 16 coformers in ratios 2:1, 1:1, 1:2 and two solvents *o*-xylene, and isohexane. The raw files from Pharmorphix were input into polySNAP and the cluster analysis was run. The output seen in the cell display and Dendrogram is presented in Figure 5.2 and 5.3.

Figure 5.2: Plate BD001 output of the PolySNAP analysis viewed in the Cell Display. The different colours highlight clusters of groups with similarity.

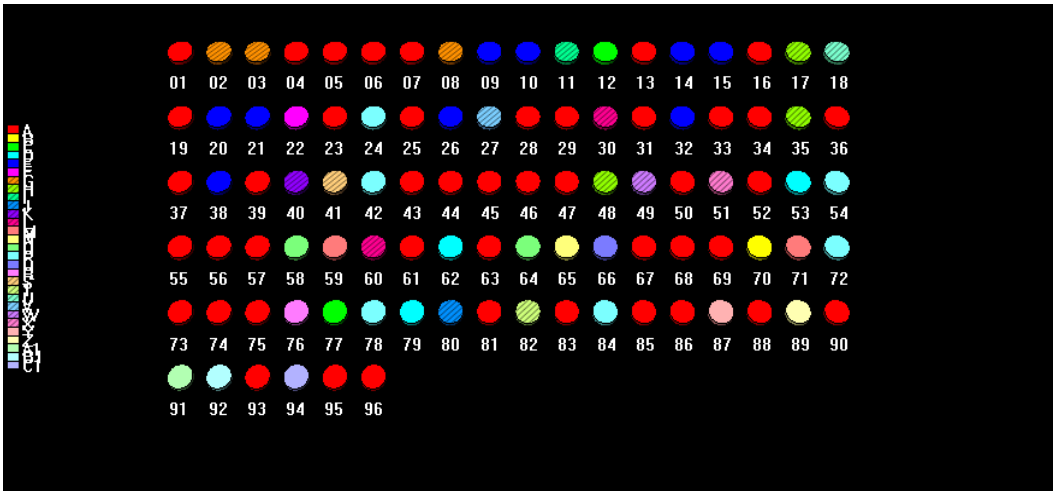

Figure 5.3: Output from Dendrogram Display, this shows the clustering in a tree diagram form.

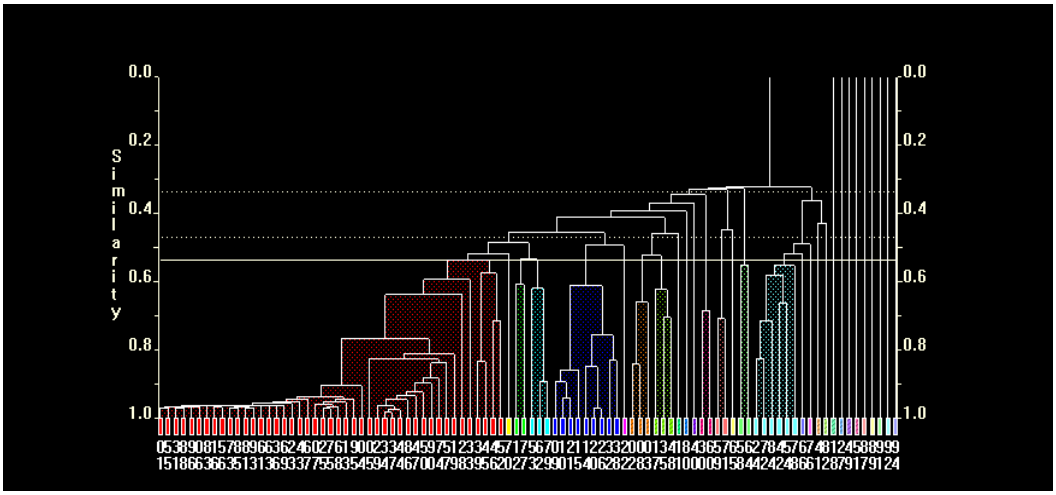

Here, we see that polySNAP has successfully read the data files and clustered into 27 groups, each sample has been denoted with a number, 1-96, which is in accordance to the PXRD raw files generated by Phamorphix.

PolySNAP also produces a logfile, from which the amorphous samples have been highlighted as shown below

\par Sample OS_BD001_01_18.raw has only 1 marked peaks, and an amorphous indicator of 95.2 - Probably amorphous.
\par Sample OS_BD001_01_27.raw has only 1 marked peaks, and an amorphous indicator of 95.6 - Probably amorphous.
\par Sample OS_BD001_01_49.raw has only 1 marked peaks, and an amorphous indicator of 95.7 - Probably amorphous.
\par Sample OS_BD001_01_51.raw has only 1 marked peaks, and an amorphous indicator of 95.8 - Probably amorphous.
\par Sample OS_BD001_01_87.raw has only 0 marked peaks, and an amorphous indicator of 96.1 - Probably amorphous.
\par Sample OS_BD001_01_89.raw has only 0 marked peaks, and an amorphous indicator of 96.0 - Probably amorphous.
\par Sample OS_BD001_01_91.raw has only 1 marked peaks, and an amorphous indicator of 96.1 - Probably amorphous.
\par Sample OS_BD001_01_92.raw has only 0 marked peaks, and an amorphous indicator of 95.5 - Probably amorphous.
\par Sample OS_BD001_01_94.raw has only 1 marked peaks, and an amorphous indicator of 95.1 - Probably amorphous.
\par 9 samples were flagged as possibly non-crystalline.

These files were extracted out of the data set as were other files that gave poor spectra.

The remaining samples from the high through-put were re-run into polySNAP along with the raw files of pure components using the quantitative mode; this element of the program allows patterns of mixtures and potential pure phases to be identified.

Once matching analysis finished the users can view the ‘cell display’ tab. Here, users are able identify samples which are new phases, amorphous and mixtures, however in this case and for each plate this was not possible to achieve as the expected cell display was not visible, just a black background. This error/bug in the program has been communicated to Professor Gilmore’s research group at The University of Glasgow.

The Dendrogram display was visible and clustering is shown below. Upon looking at the logfile and further communication with Dr Gordon Barr of the University of Glasgow, the quantitative results from the logfile are meaningless due to the huge background noise in the data and the poor correlation in the clusters.

The dataset was run again with the following advanced options tick boxed in order to subtract the background noise:

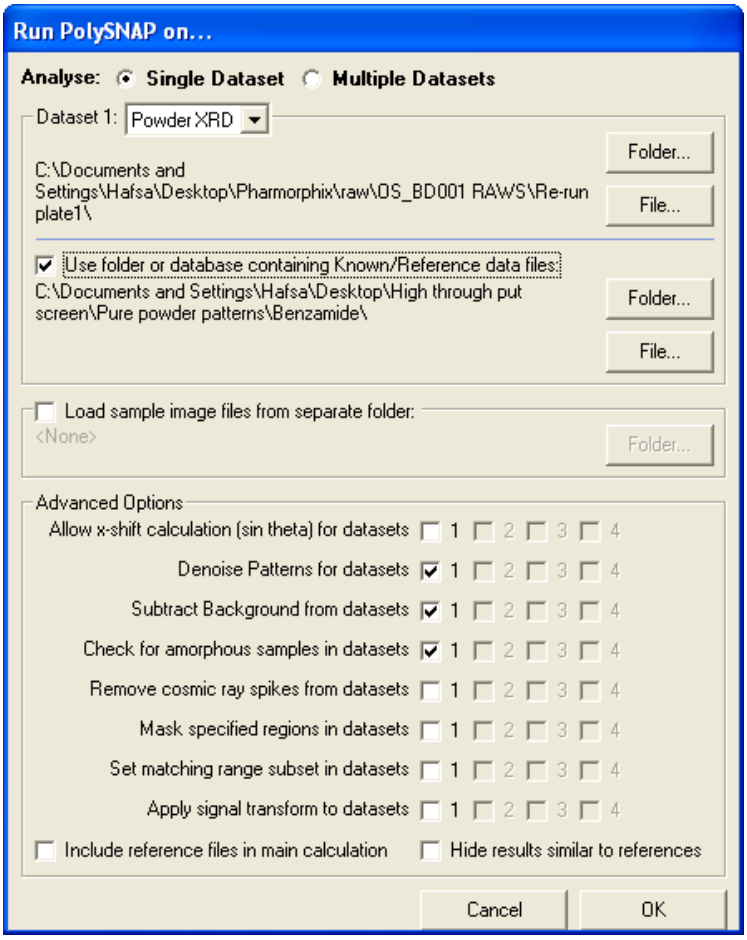

The cell display was visible and is shown below Figure 5.4. The remaining samples after eliminating amorphous and poorly diffracted sample and eliminating background noise have all been highlighted as 'Other' as suggest from the key on the left hand side

this suggests that these may possibly be co-crystals as neither of the pure components powder patterns have been identified by this clustering analysis.

Figure 5.4: Output from Cell Display, highlighting samples from the plate which have been coloured in a stripy brown manner, from the key on the left this suggest that these samples are 'Other' and not any of the pure components

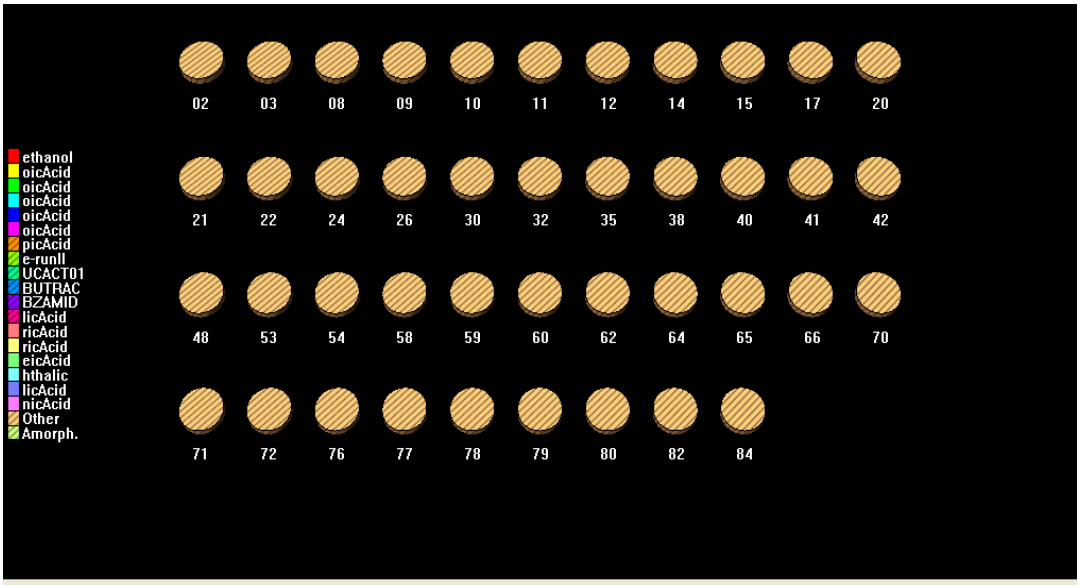

The Dendrogram below had a cut point of 0.4, however this was adjusted to 0.61 which is below the upper confidence level, this results in a cluster analysis giving 31 groups in their individual colors, Figure 5.5

Figure 5.5: Output from Dendrogram Display with a cut level adjusted to 0.61, this shows the clustering in a tree diagram form. The clusters are different colours according to samples which hold similar pattern profiles.

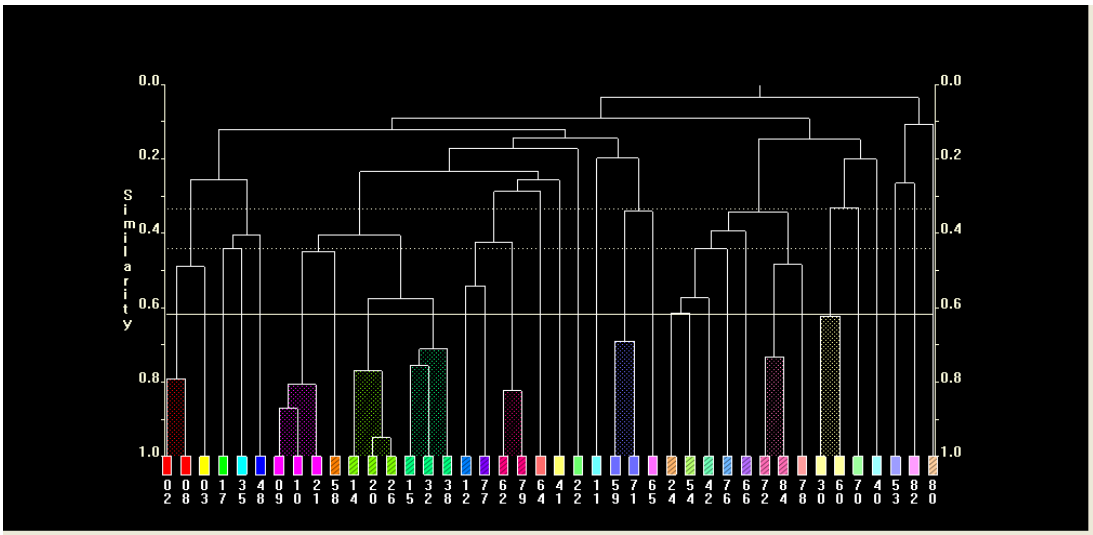

It is possible to examine these clusters and compare powder patterns using the PXRD pane, which is located below the dendrogram window in the polySNAP program. Hopefully by cross-referencing with the plate format in Appendix F the groups should consist of samples with same components. Below are the results of plate 1 tabulated, which have clustered as explained.

Table 5.2: Summary of the clustering viewed from Dendrogram, these have been cross referenced with the plate format as shown in Appendix F * respectively to sample number column

Group	Sample Number	Coformer, (Composition ratios *)
Red	02, 08	3 (1:2, 1:2)
Yellow	03	6 (1:1)
Green	17	12 (2:1)
Light Blue	35	12 (1:1)
Blue	48	15 (1:1)
Pink	09, 21 10	6 (1:1, 1:2) 9 (2:1)
Stripy Brown	58	
Stripy Green	14, 20, 26	4, (2:1), (2:1), (1:1)
Stripy Greeny Blue	15, 32, 38	6 (1:2) 4 (1:1), (1:2)
Stripy Light Blue	12	14 (1:1)
Stripy Purple	77	13 (1:2)
Stripy Pink	62, 79	5 (1:1) 3 (2:1)
Salmon Pink	64	10 (1:2)
Pastel Yellow	41	12 (1:2)

Pastel Green	22	9 (1:1)
Pastel Light Blue	11	11 (1:2)
Pastel Sky Blue	59, 71	13 (2:1) (1:1)
Pastel Pink	65	13 (1:1)
Stripy Brown	24	14 (1:2)
Stripy Green	54	15 (1:2)
Stripy Greeny Blue	42	15 (1:1)
Stripy Blue	76	11 (2:1)
Stripy Purple	66	16 (2:1)
Stripy Pink	72, 84	16 (2:1) (1:1)
Pale Orange	78	16 (1:1)
Pale Yellow	30, 60	15 (2:1) (1:2)
Pale Green	70	10 (1:2)
Pale Blue	40	10 (2:1)
Pale Sky Blue	53	13 (2:1)
Pale Pink	82	11 (2:1)
Stripy Light Brown	80	5 (1:2)

From table 5.2 it shows there are some clusters which included samples with differing components, but many clusters include two or more samples clustered with same samples in their respective ratios and solvents.

The results of plate one show that there are many samples that have clustered with sample with similar components and composition which are available in different solvents, however, there are still many samples within the dataset with poor powder patterns.

The 3D MMDS presents these results in 3D space, samples that are similar will be clustered close to each other whereas unlike samples are far apart. For plate BD001 the resulting MMDS plot is given below in various view points to appreciate the spread of the data.

Figure 5.6: Various views of the 3D MMDS plots for plate 1

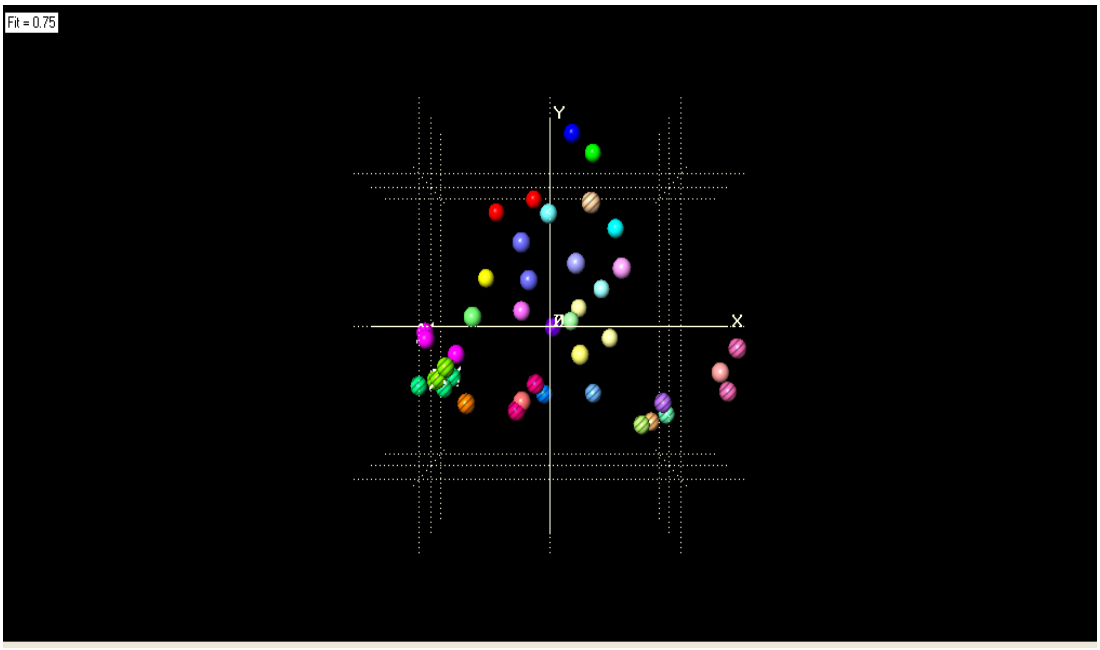

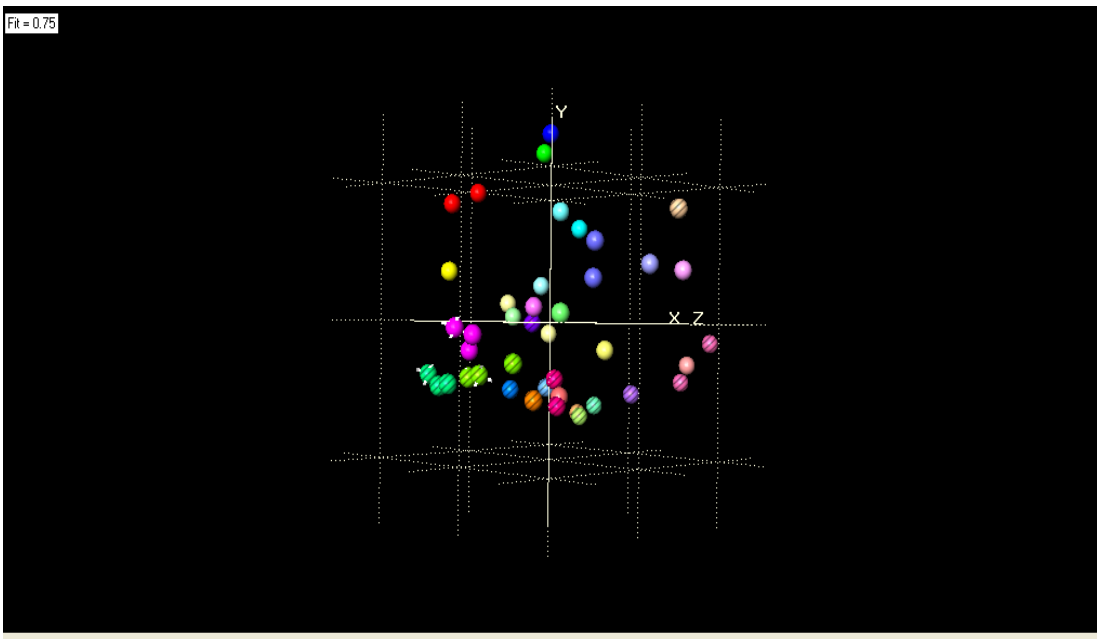

It is clear to see that the MMDS plot data set highlights a spread of the data with only samples 20 and 26 clustered close together and have the highest similarity in their respective powder pattern.

Figure 5.7: A zoomed in view of the MMDS plot of plate 1 showing samples 20 and 26, which cluster close together as compared to the other samples

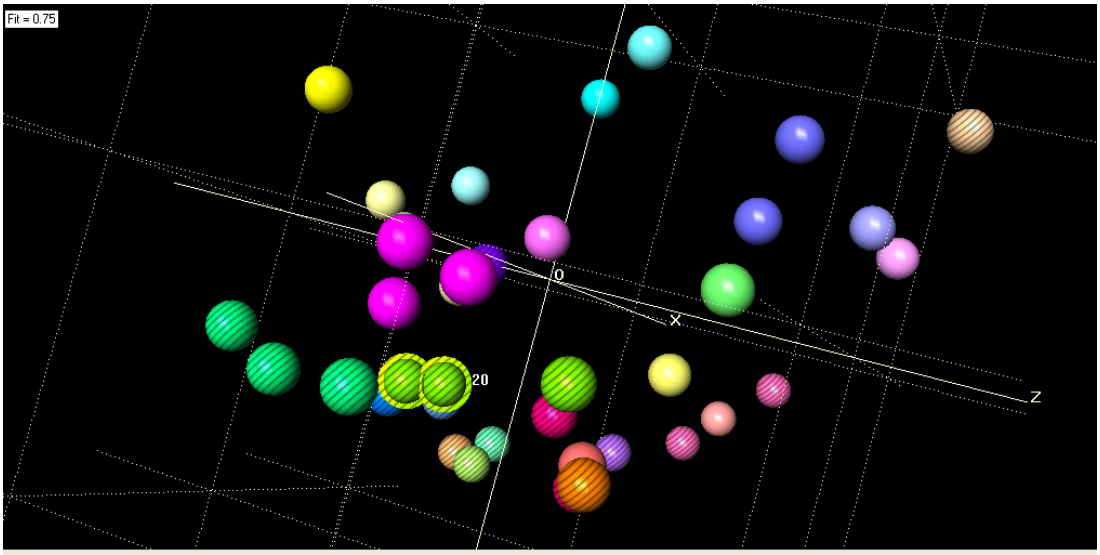

Below we see patterns 20 and 26 overlaid in pattern viewer. PolySNAP gives these patterns a similarity rank of 0.949. We can see that there is similarity in the patterns and these two samples would be the exact same crystalline material produced from the co-crystal screen.

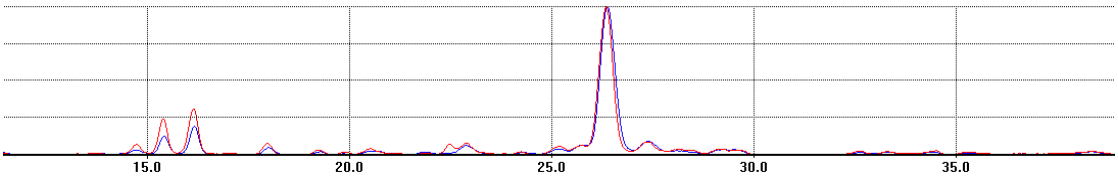

Form the table and the dendrogram analysis above we know that these sample consist of Benzamide with coformer 4 which is 3-nitrobenzoic acid at ratios 2:1 for sample 20 and 1:1 for sample 26.

A comparison with the AI, Benzamide and the carboxylic acid co-former, 3-nitrobenzoic Acid, it is possible to identify characteristic peaks from the starting components in the final product and highlight new peaks which suggest a new phase has been formed. Figure 5.8 depicts the sample 20 and 26, and overlays them with the pure components which enables us to view whether a new phase peak is present.

Figure 5.8: Powder patterns display of the sample 20 and 26 overlaid with the pure components to identify peaks that suggest new phases

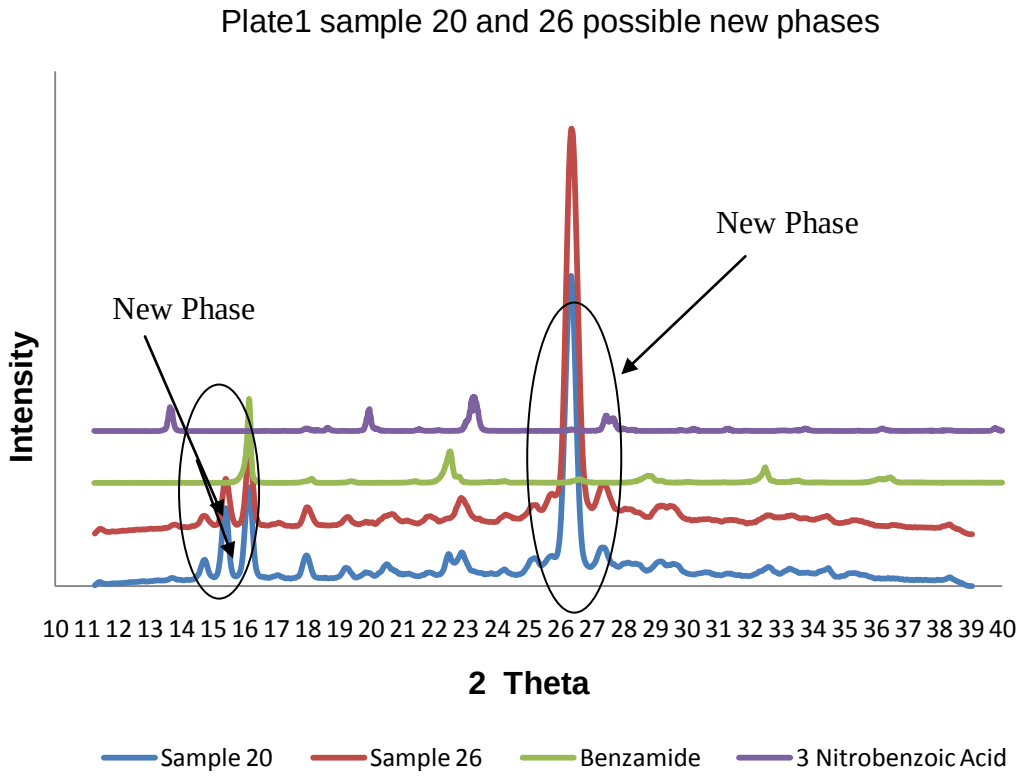

The characteristic peaks according to the pure components can be identified between 2θ angles of 22-24˚, which could be from both Benzamide, and 3-nitrobenzoic acid. A Benzamide peak at 16˚ 2θ is also present in both sample 20 and 26. Peaks between 14-16˚ 2θ and at 26.2˚ 2θ suggest a new phase is present as neither of these peaks are present in the starting components.

5.3.3 Summary of the Analysis of Plate BD002

Plate two of the screen was of Benzamide with the 16 coformers in ratios 2:1 1:1 1:2 and two solvents ethyl acetate, and methanol. The raw files from Pharmorphix were input into polySNAP and the cluster analysis was run as highlighted above. Appendix F shows the cell display and Dendrogram of plates 2-6

Again polySNAP has clustered samples with similar ratios and same components together as well as samples with different coformers such as the light blue, stripy greeny blue and stripy light blue groups. (Appendix F a shows the clustering in the Dendrogram BD002)

Observing the MMDS plot, Figure Fa1 (appendix F) the data is spread with only a close cluster present in the light blue group and a clustering with the salmon pink and pastel yellow group. Further examination as presented in appendix c shows that although the software has clustered a well defined groups, to maximize and fully understand the findings, data correlation with the design of the plates and the components highlights a shift in peaks of some of the powder patterns, example highlighted in samples belonging to the salmon pink group and yellow group demonstrate this, (please refer to powder patterns in appendix F Figure Fa4). We see that there are new peaks are present in these samples, suggesting potential new phases, however to fully validate this, DSC and possibly Raman spectroscopy may need to be established and exercised through polySNAP.

5.3.4 Summary of the Analysis of Plate BD003

Plate three of the screen was of Isonicotinamide with the 16 coformers in ratios 2:1 1:1 1:2 and two solvents *o*-xylene, and isohexane. The raw files from Pharmorphix were input into polySNAP and the cluster analysis was run. This gave the output found in appendix F b.

The cell display and Dendrogram of plate 3 clusters the samples nicely into 25 groups, closer examination via 3D MMDS plot, Figure Fb1.-3, shows only a few groups closely clustered. By cross referencing with the plate format, some groups have been found to consist mixed components which can only possibly be explained by cross contamination when transporting and preparing plates for diffraction experiments.

5.3.5 Summary of the Analysis of Plate BD004

Plate four of the screen was of Isonicotinamide with the 16 coformers in ratios 2:1, 1:1, 1:2 and two solvents ethyl acetate, and methanol. The raw files from Pharmorphix were input into polySNAP and the cluster analysis was ran as highlighted above this gave the output tables in appendix F c.

The polySNAP clustering shows that there are many clustering groups which consist of multiple co-formers, closer examination via 3D MMDS plots shows the samples in the groups have a high similarity rank, however cross referencing with the plate format shows that the co-former components do not match up. A closer view of the diffraction patterns from this plate can be found in appendix F Figure Fc2.

5.3.6 Summary of the Analysis of Plate BD005

Plate five of the screen was of Nicotinamide with the 16 coformers in ratios 2:1 1:1 1:2 and two solvents *o*-xylene, and isohexane. The raw files from Pharmorphix were input into polySNAP and the cluster analysis was run. This gave the output in the cell display and Dendrogram shown in appendix F d.

The Dendrogram displayed in appendix F, Figure Fd1-2 shows the clustering of 10 groups, the 3D MMDS plot show the data is much more spread in space with nothing being clustered close together, Again, the output shows the same miss match of sample as discussed in the above plates.

5.3.7 Summary of the Analysis of Plate BD006

Plate six of the screen was of Nicotinamide with the 16 coformers in ratios 2:1 1:1 1:2 and two solvents ethyl acetate, and methanol. The raw files from Pharmorphix were input into polySNAP and the cluster analysis was run as highlighted above this gave the output shown in Appendix F e.

The cell display shown for plate BD006 presents data of 30 samples labelled as ‘other’ (light pinky purple colour), suggesting new phases, and two samples which could be possible mixtures of several components. Ideally a mixture of the two components is desirable but here we see that polySNAP has highlighted sample 51 to consist of a mixture of 7 possible components, and sample 89 of 5 components. It could be speculated that this is due to cross contamination when handling/ preparing the plate for PXRD analysis.

Closer examination of the data using the 3D MMDS , Figure Fe2, feature highlights the clustering of the red and blue group to be quiet close, cross referencing with the plate format highlights that the groups consist of mixed co-formers as previously seen in plates 1-5. The two groups where re-clustered individually to take a closer look, the findings are given in appendix F Figures Fe3-Fe11.

5.4 Summary

This chapter discusses the high through-put method used to maximise co-crystal output using a coformer set which is an extension of the one used in chapter 3, for the component model active ingredients, Isonicotinamide and Benzamide. Extending the components and coformers used for the low through-put screen has also been the subject of the work presented. This included the addition of Nicotinamide and a contribution of a further 16 acid co-formers selected using the acid – amide synthon approach. Implementing, the high through-put method has been a challenge with regards set up and organisation layout of the well plates, along with format and method development. However, experiments have been established with the use of an automated robotic high through-put device. Analysis of this sample generated from the screen has been addressed with the use of reflectance GADDS, a diffraction device which is able to cater for such high through-put data. The resulting diffraction patterns have further been analysed by collaborating with University of Glasgow, and using the polySNAP program. The screen has tested the software as a protocol to identify new phases from the co-crystal screen, as a result, the data shows that there are issues with background noise which results in poor correlation in the clustering. This has repeatedly been viewed for each of the plates, after further analysis, the plates show that

data has been classed as other, which is expected since the aim was to grow co-crystals, however, after cross referencing with the plate format to pin point and highlight which components should be present there seems to be a disagreement, which could be due to cross contamination when handling the plates and shipping to Pharmorphix for GADDS analysis. Additionally, since the plates have been split into two sections, accommodating for experiments in two solvents per plate, it is expected that a sample with ratio or 1:1 in solvent 1 should be same in solvent 2. This is not the case, results show that sample with same stoichiometric ratio in each solvent are clustered individually, or with sample which consist of a different coformer. For these reasons, solvent selection and solubility may need to be further refined, and a screening protocol fine tuned to identify the clustering problems faced. Due to the discrepancies from this method, Hotstage microscopy has been developed for the AI and the 16 acid coformers studied.

Chapter Six: Screening with Hotstage Microscope and validating with complementary thermal methods

6.1 Introduction

Previously in chapter 3 the implementation and outcomes of a solvent evaporation route to co-crystal screening was presented. Within this low throughput screen thermal microscopy was used to verify the components which gave rise to new co-crystal presented by eutectic profiles consistent with co-crystal formation. In this chapter the thermal microscopy was used as a pre-screening tool for an extended set of co-formers. The opportunity and implementation of the Hotstage microscopy technique in highlighting co-crystal phase in multi component systems was previously outlined in chapter 2. As the thermal microscopy techniques provide visual confirmation and eutectic information on new crystal phase formation between two components, when a new phase formation or a phase separation is likely to occur during the heating process and in this chapter we extended the application of this technique to a larger set of co-formers. To date the successful co-crystal phases formed during the low through-put solution screen in chapter 3 and the results in appendix B show this trend for the components of this screen, the emergence of these eutectic points are also reflected and confirmed by DSC traces as discussed in chapter 3.

In this chapter we discuss the outcomes of thermal microscopy on a pre-screen for the systems screened in the high through-put method. The high through-put screening included the three active ingredients, Benzamide, Isonicotinamide and Nicotinamide, and a host of acid coformers consisting of families of di-carboxylic acids and benzoic acid derivatives (chapter 2 Figures 2.4 - 2.5). As mentioned earlier these acid coformers have been carefully selected and used to fit the health and safety guidelines at Syngenta Ltd. All the samples used for this work and the high through-put work were initiated on

site at Syngenta Huddersfield. Sample slides for the Hotstage work were prepared at Syngenta as chemicals were not permitted to be taken off site, with permission, slides were transported to University of Bradford, Institute of Pharmaceutical Innovation building, so that samples could be ran on the Zeiss microscope, equipped with Linkam controlled heated stage and axioplan imaging software. The screen is an expansion of the initial screen discussed on chapter 3,

6.2 Experiment

The preparation of the slides uses the Kofler contact method, (Kofler, 1941), which is a means to identifying the eutectic profile consistent with that required of co-recrystallisation of two compounds from their hot molten state. The details of the method have been previously presented, in chapter 1 and 2 sections 1.10.1.3 and 2.6. However, to summarise the approach, on a glass microscope slide, under a cover slip at one end contains pure acid and the other pure amide. The region in between the pure phases, also referred to as the mixing zone, holds the presence of a new phase upon heating, this can be observed under a polarised light microscope. A detailed account of the preparation of the slides has been described in chapter 1 and 2.

Again to summarise, and as mentioned in chapter 3, the heating stage (Hotstage) was purchased from Linkam, a Zeiss microscope was used which has the axioplan imaging software. A heating profile from room temperature to 280° C at a rate of 1° C per minute was used. Images were captured at 5x's magnification at 60 seconds intervals. Maximum temperature may vary with respect the melting points of the component being discussed in this chapter. We have used the Kofler contact method to detect the

possibility of physical interactions of the two phases and evaluated using the method by differential scanning calorimeter (DSC) as a primary thermal analysis method.

For the DSC experiments, physical mixtures were made of the Isonicotinamide and carboxylic acids, and Benzamide with carboxylic acids, these were accurately weighed using the quantities summarised in Table 3.1 chapter 3. Samples were heated in crimped and sealed hermetic aluminium pans. Similarly, an empty pan was used as a reference. Sample were heated over the relevant temperature range for each material (up to a maximum range of 25-260° C) under a stream of nitrogen gas at a heating rate of 10° C/min.

6.3 Results and discussion

6.3.1 Hotstage Microscopy

The first screen consists of the components previously studied in the solution screen in chapter 3. The outcomes are given in Table 6.1, which represents the samples which hold new phases and the respective temperatures at which starting material melts and at which the new phases emerge and melt away. Table 6.2, is a summary of the components involved in the low through-put screen. From these tables (6.1 and 6.2) we note that this method of screening proves that there are more potential phases visible with the Benzamide matrix. However, with the exception of Fumaric and Tartaric acid which sublime upon heating during the preparation of the microscope slide and the exception of 3-hydroxybenzoic acid which did not show any new phases, all the other phases found in the solution screen have been identified as well as new phases for the unsuccessful Glutaric, Adipic, 2-hydroxybenzoic, 4-hydroxybenzoic acid and Benzoic

acid. These have all been discussed in chapter 3 and results are displayed in appendix B. Additionally to this, it has been possible to suggest the composition ratios as component phases melt away. For example, the Benzamide with 2-hydroxybenzoic acid has two potential phases. The first phase has been suggested to be a 1:1 phase which appears at 110.5° C and melts at 112.3° C (Figure 6.1 images 1 and 2). At the same time there seems to be another phase present that begins to melt once the first phase melts away, with the emergence of a phase growing at 115.6 ° C melting at 121.5 ° C (Figure 6.1 images 3-9), it can be suggested that this is the 2:1 co-crystal phase of this system.

Table 6.1: A summary of Hotstage microscopy results from low through-put screen and high through-put screen of Isonicotinamide, Benzamide and Nicotinamide. The results show the number of new phases and the respective temperatures.

		Isonicotinamide Mp 155-157° C		Benzamide Mp 127-130° C		Nicotinamide Mp 128-131° C	
	Mp °c	New Phases	New Phase Melt (°C)	New Phases	New Phase Melt (°C)	New Phases	New Phase Melt (°C)
1, 4 Benzene dimethanol	116-119	no	n/a	1	92.2	1	105.1
2-Hydroxybenzoic Acid	158	2	135.8, 137.8	2	112.3, 120.3	1	140.7
3-Hydroxybenzoic Acid	201	1	196.3	no	n/a	1	123.3
4-Hydroxybenzoic Acid	214	1	182.6	1	88.1	2	95, 183.1
2-Nitrobenzoic Acid	146-148	1	129	1	117	1	81.5
3-Nitrobenzoic Acid	139-141	no	n/a	2	140.2, 164.2	3	134.1, 143, 154
4-Nitrobenzoic Acid	237	1	221	1	180 - 185.6	1	183.7
3-Aminobenzoic acid	178-180	2	137.3, 149.3	no	n/a	no	n/a
4-Aminobenzoic	187-189	1	149	no	n/a	1	113

acid							
Adipic Acid	152	1	169.3	1	101.1	1	132.4
Benzoic Acid	121	1	153.5	1	82.5	2	89.2, 95.2
Cinnamic Acid	133	2	136.3, 159.3	no	n/a	2	99.3, 121.3
Fumaric Acid	287	decompose/sublime	n/a	decompose/sublime	n/a	decompose/sublime	n/a
Glutaric Acid	95	1	151.2	1	88.9	1	138.6
Maleic acid	130-131	decompose/sublime	n/a	decompose/sublime	n/a	decompose/sublime	
Malic acid	131-133	1	230	no	n/a	1	125.5
Mandelic Acid	119	1	113.9	1	76	no	n/a
Phthalic acid	200	1	134.1	no	n/a	no	n/a
Pimelic acid	103-105	1	135	1	94.4	1	110.2
Succinic Acid	185	1	203	1	117	1	148.5
Tartaric acid	170	decompose/sublime	n/a	decompose/sublime	n/a	decompose/sublime	n/a
Trans β hydromuconic acid	195-196	1	181.7	no	n/a	2	131.2, 134.2

Table 6.2: A summary of the Hotstage microscopy results of Isonicotinamide and Benzamide with components used for the low through-put screen. The results show the number of new phases and the respective temperatures and ratios

		Isonicotinamide Mp 155-157° C		Benzamide Mp 127-130° C	
	Acid Mp °C	New Phases	New Phase Melt ° C	New Phases	New Phase Melt ° C
Fumaric Acid	287	Sublimes	n/a	Sublimes	n/a
Succinic Acid	185	1 (1:1)	203	1 (1:1)	117
Tartaric acid	170	Sublimes	n/a	Sublimes	n/a
Glutaric Acid	95	1 (1:1)	151.2	1 (1:1)	88.9
Adipic Acid	152	1 (1:1)	169.3	1 (1:1)	101.1
Benzoic Acid	121	1 (1:1)	153.5	1 (1:1)	82.5
2-Hydroxybenzoic Acid	159	2 (1:1, 2:1)	135.8, 137.8	2 (1:1, 2:1)	112.3, 121.5
3-Hydroxybenzoic Acid	201	1 (1:1)	196.3	no	n/a
4-Hydroxybenzoic Acid	214	1 (1:1)	182.6	1 (1:1)	88.1
Mandelic Acid	119	1 (1:1)	113.9	1 (1:1)	76
Cinnamic Acid	133	2 (1:1, 2:1)	136.3, 159.3	no	n/a
4-Nitrobenzoic Acid	237	1 (1:1)	221	1 (1:1)	180 - 185.6

Figure 6.1: Images highlighting the emergence of new phases of the Benzamide 2-hydroxybenzoic acid system, using Hotstage microscopy method with Linkam controlled heating stage mounted on a Zeiss Microscope using cross polarised light and axiocam camera at times 5 magnification lens.

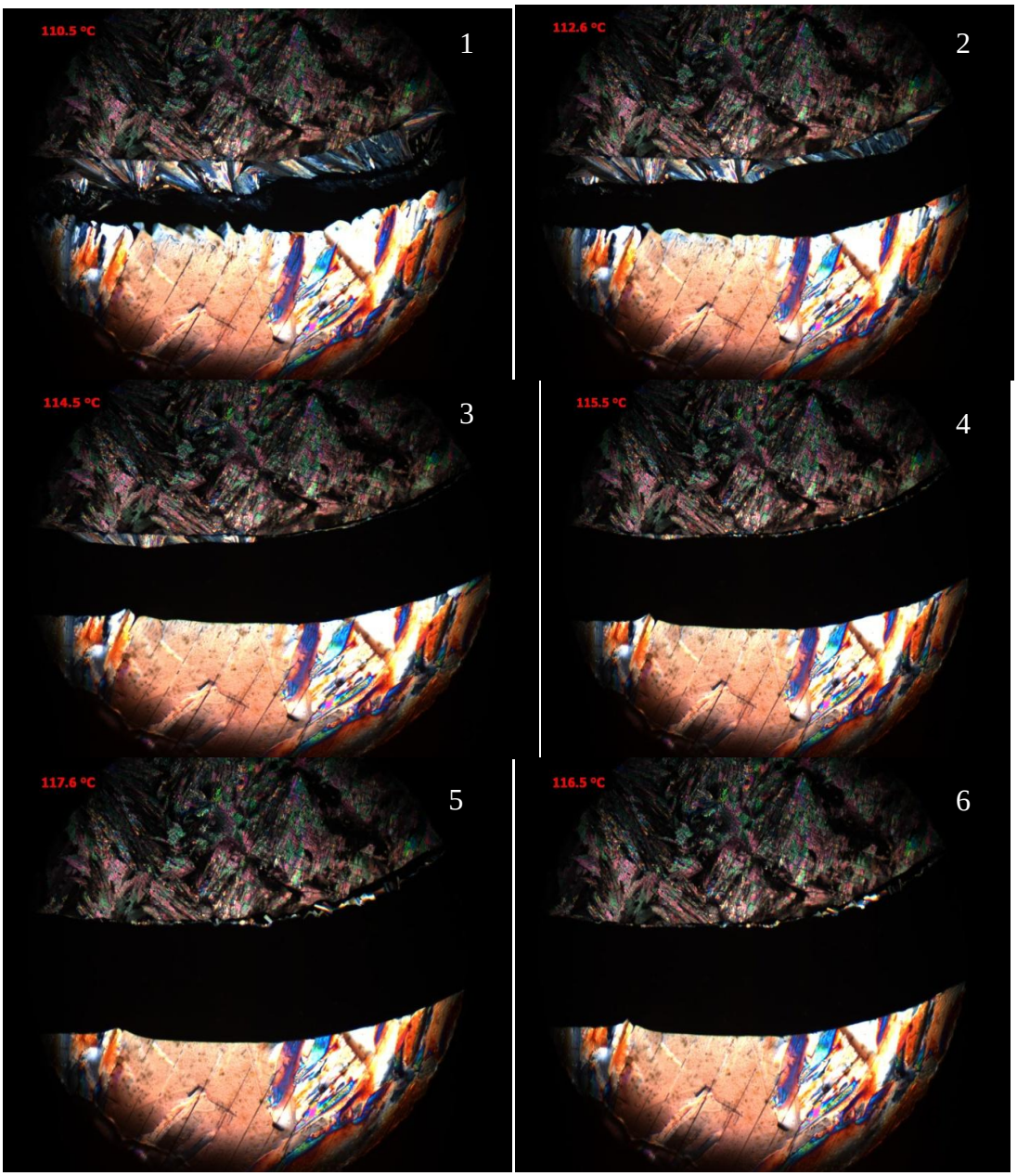

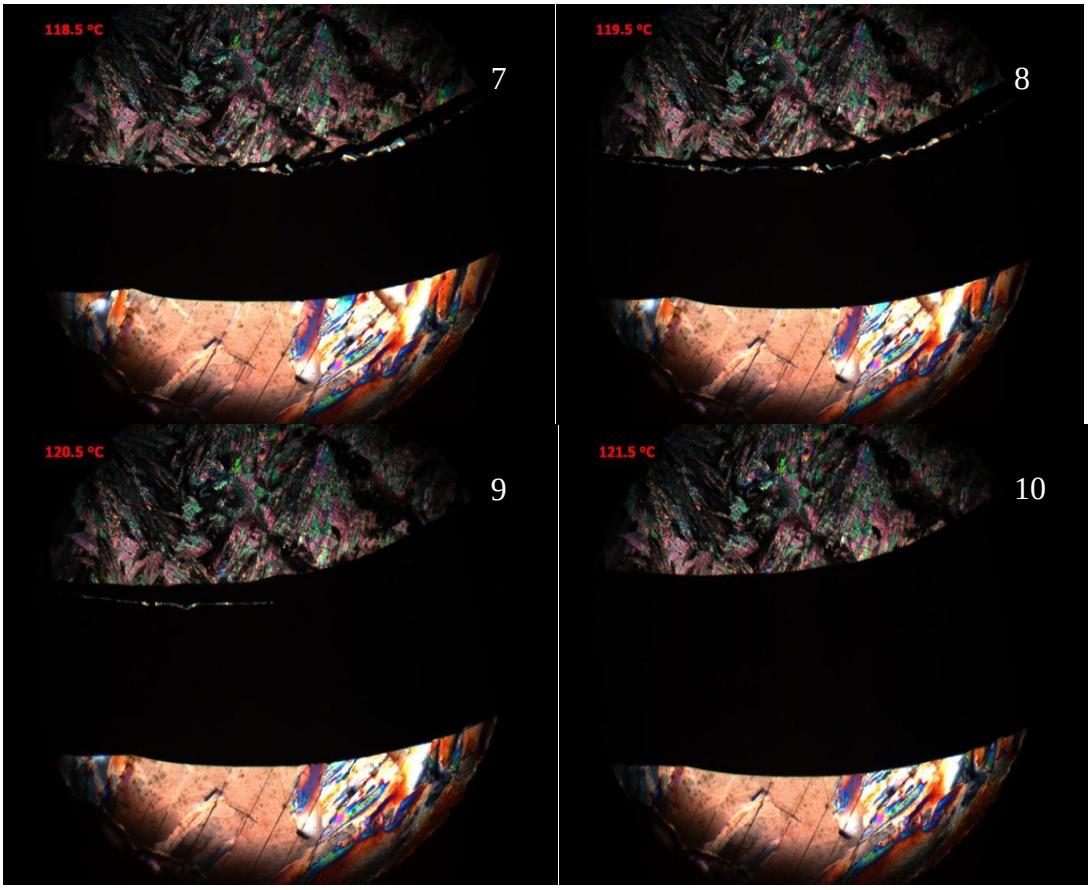

A similar picture is portrayed for the Isonicotinamide with 2-hydroxybenzoic acid Kofler melt. Similarly to Benzamide, there are two phases present upon melting, 1:1 at 135.8° C and 2:1 at 137.8° C. The co-crystal structure has been solved and presented in McMahon et al 2004 who have reported that the melting temperature of the co-crystal is between 119-121° C. However for the Hotstage this does not coincide with the reported work, Figure 6.2 shows the Hotstage images for Isonicotinamide with 2-hydroxybenzoic acid.

Figure 6.2: Hotstage images highlighting the phases viewed for Isonicotinamide with 2-hydroxybenzoic acid

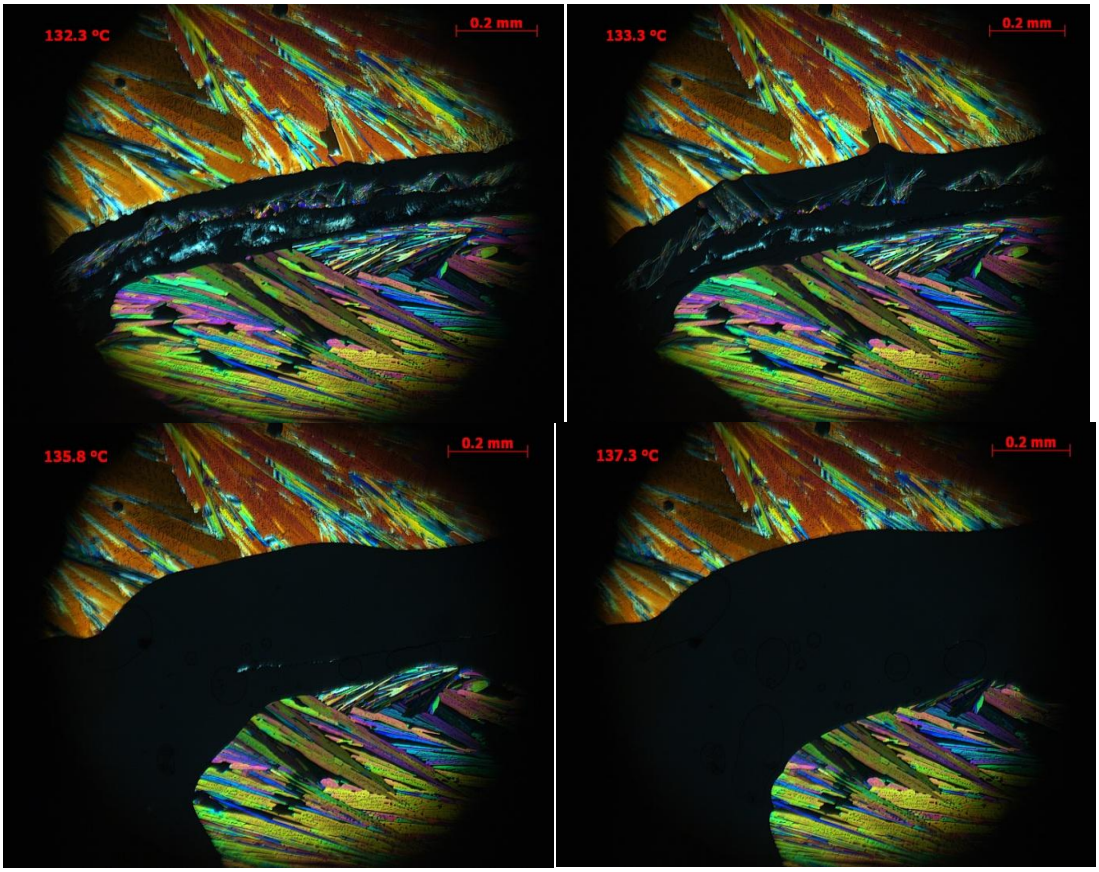

The procedure was repeated on Hotstage, and the same results were achieved, to ensure that this was not the only thermal method employed; DSC has been exploited as a means to validate the Hotstage results. This is discussed in the section below. Additionally, it was decided by all parties involved in the project to introduce Nicotinamide as an active ingredient for the high through-put screen since it is a well studied Pharmaceutical which holds to be a robust acceptor/donor. Therefore, Hotstage analysis was executed for all of the coformer acids used in this study with Nicotinamide. These have all been summarised in Table 6.1. The table shows that there are 17 out of the 22 coformers with Isonicotinamide which successfully melt and show a new phase. Only 2 of these failed to show new phases upon melting where the remaining 3 decomposed/sublimed upon preparation of the slide. Nicotinamide has

successfully shown phases with 16 of the coformers examples, with only the 3-Aminobenzoic acid, Phthalic and Mandelic failing to show new phases in the mixing zone upon melting. The test example, which literature has shown to be least studied and least successful to co-crystallise has from the Kofler contact method screen, shown new phases with 12 of the 22 coformer acid examples used in the project discussed here. One of these has been reported, Succinic acid with Benzamide, in the Cambridge structural database. There are 7 coformers which have failed to show that a co-crystal phase is present, along with 3 which decompose/sublime upon heating.

The images of the Hotstage analysis for the components can be found on the compact disc provided in Appendix I.

The components used for the high through-put screen have only been analysed using Hotstage microscopy; it was unfortunate not to have been able to carry out DSC to verify the result due to Syngenta migrating to their new site in Berkshire. The Hotstage analysis however does show that there are many new phases present and the technique is invaluable as a screening tool.

6.3.2 Results and Discussion of DSC

The DSC analysis of the samples from the low through-put screen are summarised in Table 6.3. The melting temperatures found during the Hotstage compared with the endothermic peaks identified during the DSC analysis are displayed.

We see that in some cases for both the Isonicotinamide systems and Benzamide systems, there is correlation where during Hotstage analysis a phase that melts at a temperature higher or lower than the starting components, is also identified by an endothermic peak during the DSC analysis. These peaks can be seen in the examples displayed in Figure 6.3. This Figure shows the Isonicotinamide DSC trace and the Benzamide trace with 2-hydroxybenzoic acid. All remaining DSC traces can be viewed in Appendix G.

These results do suggest that there should be a number of Benzamide co-crystals in existence, and the co-former profile would be comparable in usage with those seen for the other principal components Nicotinamide and Isonicotinamide. The current outcomes from melt need to be contrasted with those from solution growth and ternary phase behaviour in order to rationalise the historical lack of reported co-crystal using Benzamide over the other amides.

Table 6.3: Summary of the endothermic peak detected from DSC analysis of the primary screen viewed in low through-put analysis compared with the results achieved form Hotstage analysis

		Isonicotinamide	Mp 155-157° C	Benzamide	Mp 127-130° C
	Mp °c	DSC endothermic (°C) Average peak	New Phase Melt (°C)	DSC endothermic (°C) Average peak	New Phase Melt (°C)
Fumaric Acid	287	156.13, 207.71	sublime/decomposed	119.77, 134.49	sublime/decomposed
Succinic Acid	185	155.92, 165.95	203	118.46, *128.34*	117
Tartaric acid	170	128.53, *153.76*, 174.94	sublime/decomposed	119.47, 139.93	sublime/decomposed
Glutaric Acid	95	*91.48*, 133.12, 145.60	151.2	79.75, 86.40, 90.27	88.9
Adipic Acid	152	141.99, 151.82, 156.53	169.3	93.48, 96.84	101.1
Benzoic Acid	121	*120.15,* 141.27, 161.26	153.5	84.83	82.5
2-Hydroxybenzoic Acid	158	121.84, 124.24, 131.50	135.8, 137.8	111.17, 118.00	112.3, 120.3
3-Hydroxybenzoic Acid	201	148.15, 192.12	196.3	93.29	none
4-Hydroxybenzoic Acid	214	145.23, 184.34	182.6	93.00, 130.06, 169.15	88.1
Mandelic Acid	119	81.57, 107.50	113.9	74.93	76
Cinnamic Acid	133	127.38, 139.01, 144.79, *156.18*	136.3, 159.3	85.93	none

4-Nitrobenzoic Acid	237	155.05, 223.28	221	124.81, 180.60	180 - 185.6

* All Figures in italic and highlighted blue have been identified as starting components

Figure 6.3: Summary of the endothermic peaks for A) Isonicotinamide with 2-hydroxybenzoic acid and B) Benzamide with 2-hydroxybenzoic acid

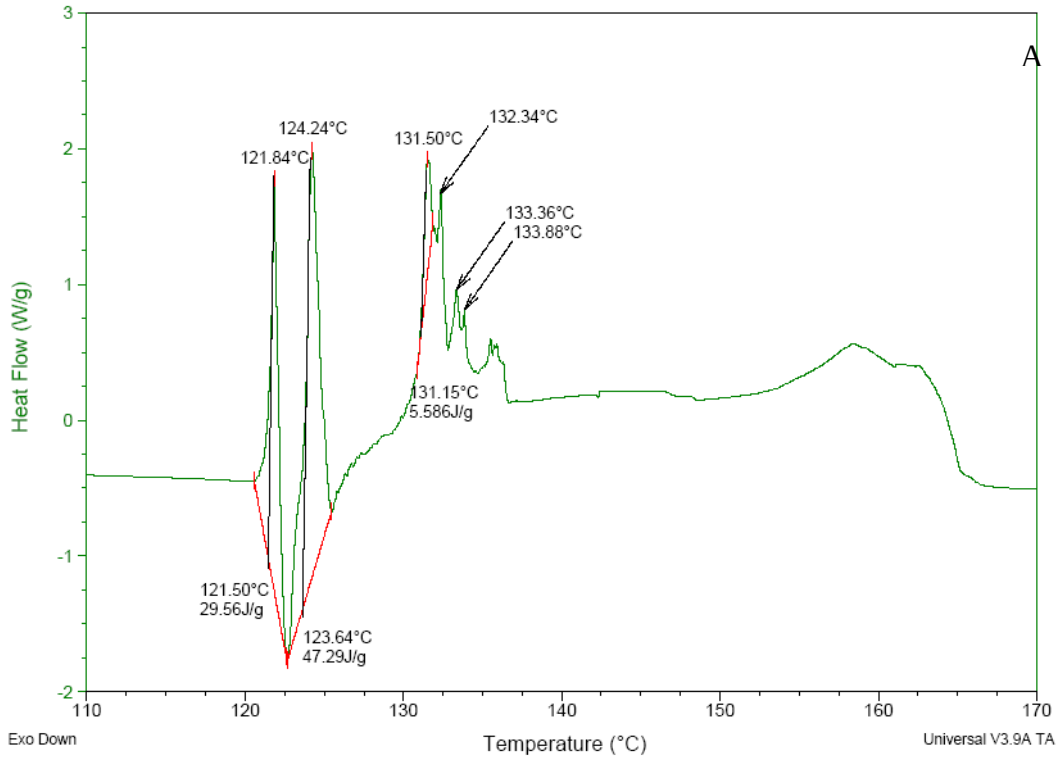

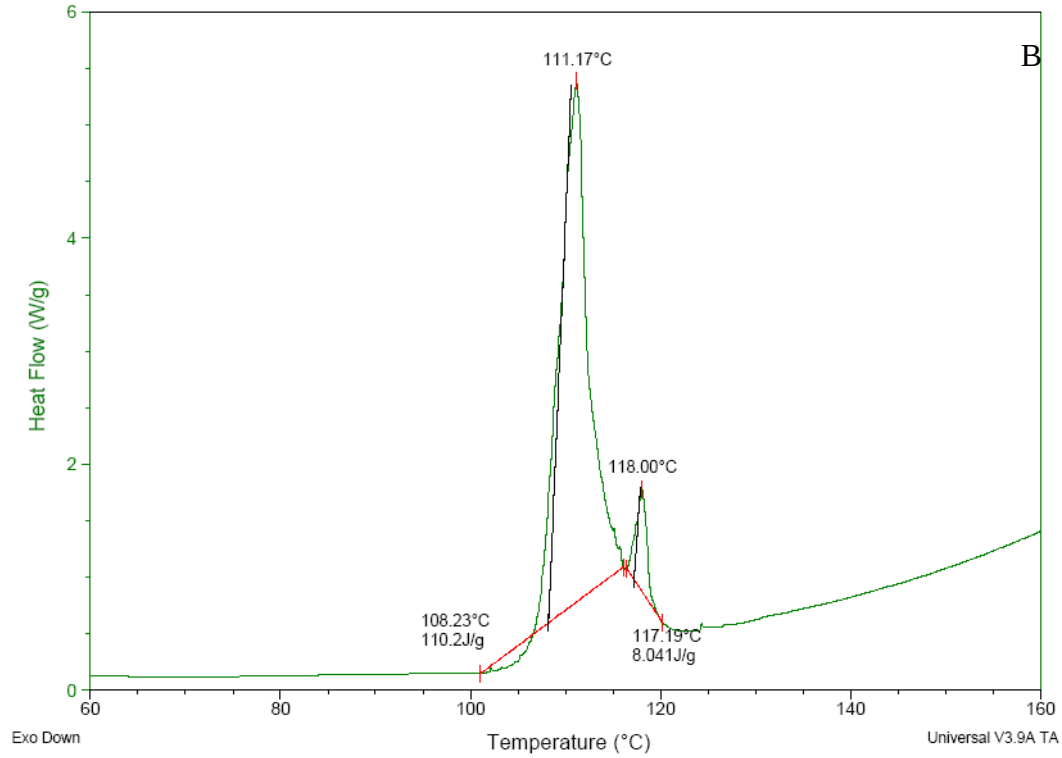

6.4 Summary

The work presented in this chapter demonstrates the simplicity of the Hotstage microscopy technique as a tool of screening for co-crystal formation. As described previously, upon melting of two phases, upon separation a new phase should emerge if the two starting components are capable of forming a co-crystal. This can be observed under polarised microscope when heating.

The results presented here are in two parts:

a) Low through-put screen viewed in chapter 3 coupled with DSC analysis to confirm the melting phases and possible new phases

b) Components which have previously been subjected to the high through-put analysis in the previous chapter.

The aim of this study is a comparison of the success rate of Benzamide with the model amide, Isonicotinamide. The previous low through-put screen resulted in the co-crystallisation characterisation via PXRD of 5 of the model coformers, chapter 3, here we find that a thermal technique, using the Kofler contact method produces identification of 8 potential new phases, the remaining two coformers, sublime when preparing the slide. To verify the results of hot melt, DSC has been used, it has been found that this technique complements the results from the thermal microscopy screen.

To increase the success rate, the components involved in the high through-put screen have undergone this method of Hotstage microscopy technique, in total resulting in 17 hits of co-crystals with the model amide, Isonicotinamide, and 12 for the Benzamide which has not been thought to co-crystallise as well according to literature review. Additionally, Nicotinamide has been introduced, which has a hit of 16 new phases. Unfortunately, DSC has only been implemented for the low through-put screen, this is due to restrictions of taking chemicals off site from Syngenta and because of the relocation of the Syngenta site to southern England.

Chapter Seven: Phase Diagram determination

7.1 Introduction

In previous chapters, we have explored and identified screening methods ranging from simple bench evaporation method to a high through-put screen and complementary screening with thermal microscopy. Additionally, a feature of the project was to undertake a comparison of the primary amide Benzamide, and Nicotinamide success rate with a library of co-formers with an amide which has been reported to co-crystallise with a healthy success rate (Isonicotinamide) with the same library of co-formers. An important factor was the understanding the deviation between a successful co-crystal through host stage studies and poor performance and lack of propensity towards crystallisation or failure in large number of solvents when attempted from solution. Within this work the low through-put method was employed as the route to achieve the growth of single crystals, as identified from the Hotstage microscopy of the minor matrix screen (chapter 3) as well as a high through-put method of an extended screen carried out at Syngenta Ltd. The resulting crystallisation outcomes employed in the project have established a further understanding of the impact of the solvent choice made upon crystallisation outcomes. To further this understanding from the screening results, a series of complementary pairs of co-crystal using the amides and co-former Succinic acid ternary phase diagrams were measured.

As previously mentioned in chapter 1, the preferred manufacture route to co-crystal growth is solvent crystallisation. In order to achieve this and also gain a further appreciation of why melt co-crystal formation transferred to solution fails the following ternary phase diagram studies were undertaken. The choice of approach through the construction of a phase diagram of a two-component system was undertaken as these phase diagrams can give a practical insight for preparing co-crystals. Previously it has

been discussed how similar solubility determines the straight forward phase diagram of a 1:1 mixture where all the regions are well defined, however, components with a less comparable solubility tend to map a phase diagram skewed like the one shown in the study by Chiarella et al, 2007, thus narrowing the region where co-crystal growth is possible.

Within this chapter, we view phase diagrams of Isonicotinamide with Succinic Acid, Benzamide with Succinic Acid and Nicotinamide with Succinic Acid in water and methanol. The crystal structures of the former two systems have been published and deposited in the CSD, in this study, we have successfully grown single crystal of the Nicotinamide and Succinic acid co-crystal and this will also be presented here.

7.2 Experiment

The methods for determining ternary phase diagrams have been reported widely, consequently a brief over view of the approach routinely adopted will be given. In the first instance for mapping a phase diagram a measurement of the solubility of the starting components and co-crystals is undertaken. The literature was reviewed for solubility, and where this was not reported the simplest gravimetric method was established to evaluate solubility. Typically, 0.1g of each starting material has been weighed out and solvents, methanol and water were added gradually until samples complete dissolved at room temperature. All results have been tabulated below.

Table 7.1: Solubility of all the starting components and co-crystal in water and methanol

Solubility	Water (0.1g)	Methanol (0.1g)
Isonicotinamide	2 ml	1 ml
Benzamide	Slightly Soluble * 10 ml	1 ml
Nicotinamide	Easily Soluble * 1.1 ml	1.2 ml
Succinic Acid	1.3 ml	1.3 ml
Co-crystal Solubility	Water (0.1g)	Methanol (0.1g)
Isonicotinamide: Succinic Acid	17 ml	23 ml
Benzamide: Succinic Acid	16 ml	2.5 ml
Nicotinamide: Succinic Acid	2.5 ml	2 ml

From these solubilities, we are able to note an expected level skew in the phase diagrams. For the following: Benzamide and Succinic acid system in water with a significant skew and a slight skew in the Isonicotinamide: Succinic acid in methanol system.

After determining the solubility of the starting components, the next step is to locate the co-crystal regions. For this, mixtures of the amide and acid at various molar ratios but fixed molar content were weighed out. A fixed amount of solvent was added to each vial containing the sample mixture weighed and allowed to slurry for an hour at 50°C for each water and methanol system, after slurrying, samples were allowed to cool. These samples were then capped and incubated at 20 °C for at least 7 days. The solid from each was collected by Buchner filtration and examined by powder diffraction for new crystal phases. This weighing procedure was repeated, as the amount of solvent

varied, this allowed crystal samples to be prepared in a cross section manner across the phase diagram, eventually identifying the regions where co-crystal phases begin to grow. The quantities used for this study are given in the table below. Experiments were delayed 3^{+} months due to breakdown of the RUMED incubator unit with-in the laboratory, once fixed, experiments were set up simultaneously for all systems in the two solvents mentioned, Methanol and Water.

Table 7.2: Summary of the quantities used to map phase diagram. * Isonicotinamide and Nicotinamide have same molecular weight, therefore the same weights have been used

% Mole Acid	Succinic Acid	Benzamide	Isonicotinamide/Nicotinamide *	% Mole Amide
100	2.362	0	0	0
90	2.213	0.248	0.244	10
80	1.889	0.498	0.489	20
70	1.653	0.746	0.733	30
60	1.417	0.995	0.977	40
50	1.181	1.244	1.221	50
40	0.945	1.493	1.466	60
30	0.709	1.742	1.710	70
20	0.472	1.990	1.954	80
10	0.024	2.239	2.198	90
0	0	2.488	2.443	100

7.3 Results and Discussion

The phase diagrams obtained from the solution slurries after incubation are displayed below, characterisation of the sample after filtration was with PXRD. A freely available and user-friendly software, ProSim, (www.prosim.net) has been used to map the co-ordinates for the sample onto a ternary phase diagram plot. Figure 7.1shows that the data when plotted are concentrated into the top 90% of the ternary phase diagram, this makes it difficult to view the phase behaviour of the samples collected. ProSim has a zoom in and zoom out function, allowing users to view the top 90% region and further view the outlined regions from experimental data Figure 7.2.

Figure 7.1: Ternary Phase diagram of Isonicotinamide, Succinic Acid in water

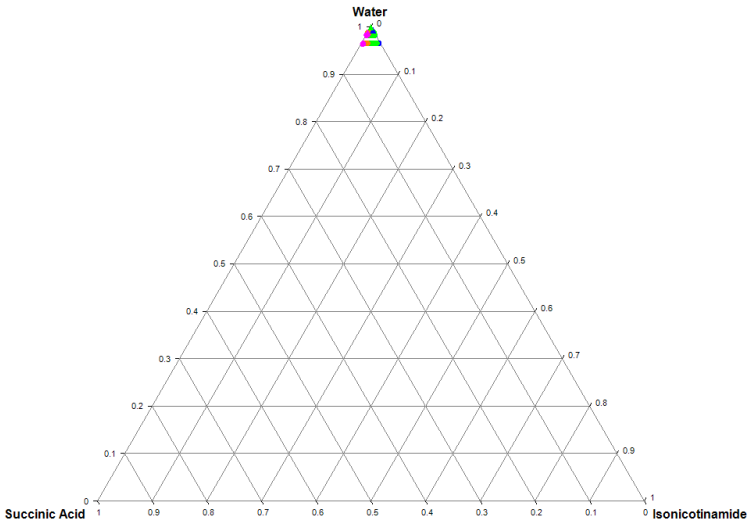

Figure 7.2: Ternary Phase diagram of Isonicotinamide, Succinic Acid in water Zoomed into the top 90%

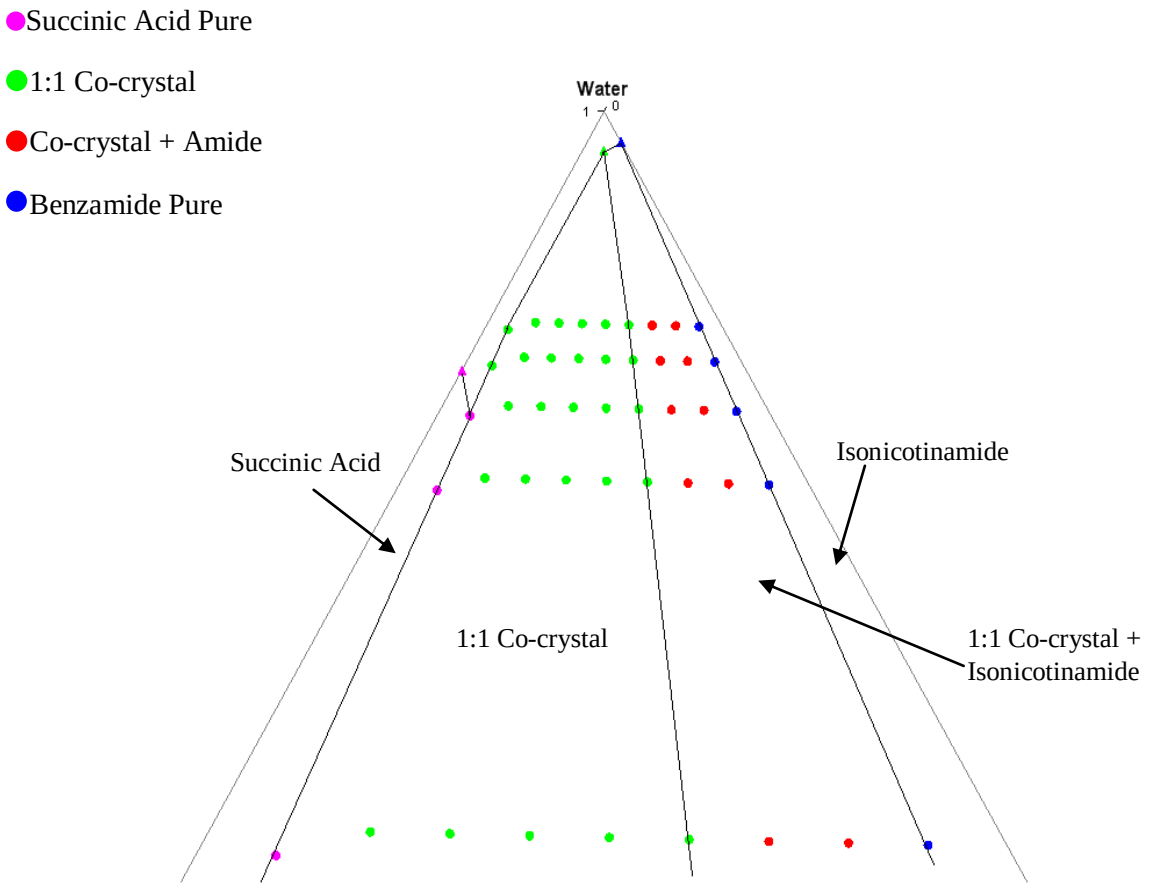

Figure 7.2 and Table 7.1 show that there is a significant difference in the solubility between Succinic acid and Isonicotinamide in the water system (0.1g in 1.2ml vs. 0.1g in 2ml) leading to a strongly skewed phase diagram. The 1:1 co-crystal region from the slurry samples have been identified, as have the pure phases and a region which seems to be a mixture of co-crystal and the amide pure phase. The methanol system (Figure 7.3, 7.4) paints a picture similar to the expected model shown in chapter 1, Figure 1.11a, this is due to the solubilities of the components involved differing only very slightly from each other. We see that the 1:1 complex in this methanol system is much lower in solubility compared to the water system. The data also has highlighted a mixture of co-crystal complex with the Isonicotinamide in 10 ml of methanol. This could be an

anomaly therefore further sampling is required to map the regions with solvent less than 10 ml.

A similar example given in the work contributed by Seaton, 2008, uses Isonicotinamide and benzoic acid in water and methanol. The work, displays a heavily skewed phase diagram in the water system, and a better behaved plot in the methanol system.

Figure 7.3: Ternary Phase diagram of Isonicotinamide, Succinic Acid in methanol

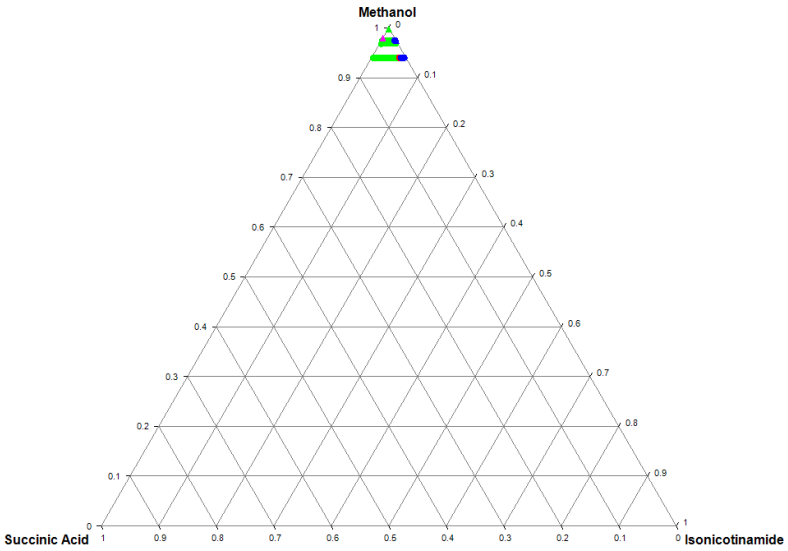

The Benzamide with Succinic acid in water system also maps a skewed organisation of the phases, Figure 7.5, 7.6, this is expected, as Benzamide is slightly soluble in water. The emergence of the 1:1 phase has been established, as has the mixture of the co-crystal with Benzamide.

Figure 7.4: Ternary Phase diagram of Isonicotinamide, Succinic Acid in methanol Zoomed into the top 90%

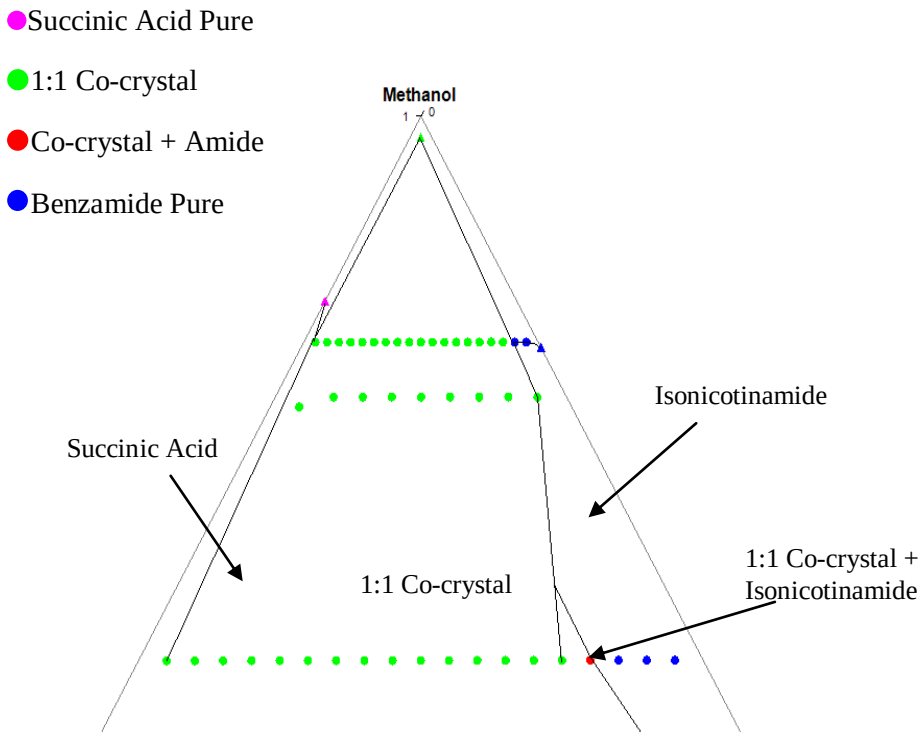

Figure 7.5: Ternary Phase diagram of Benzamide, Succinic Acid in Water

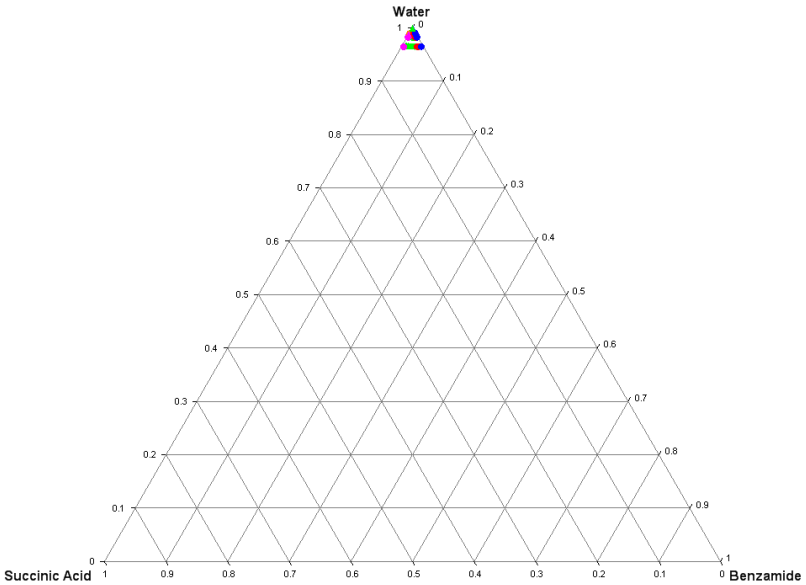

Figure 7.6: Ternary Phase diagram of Benzamide, Succinic Acid in methanol Zoomed into the top 90%

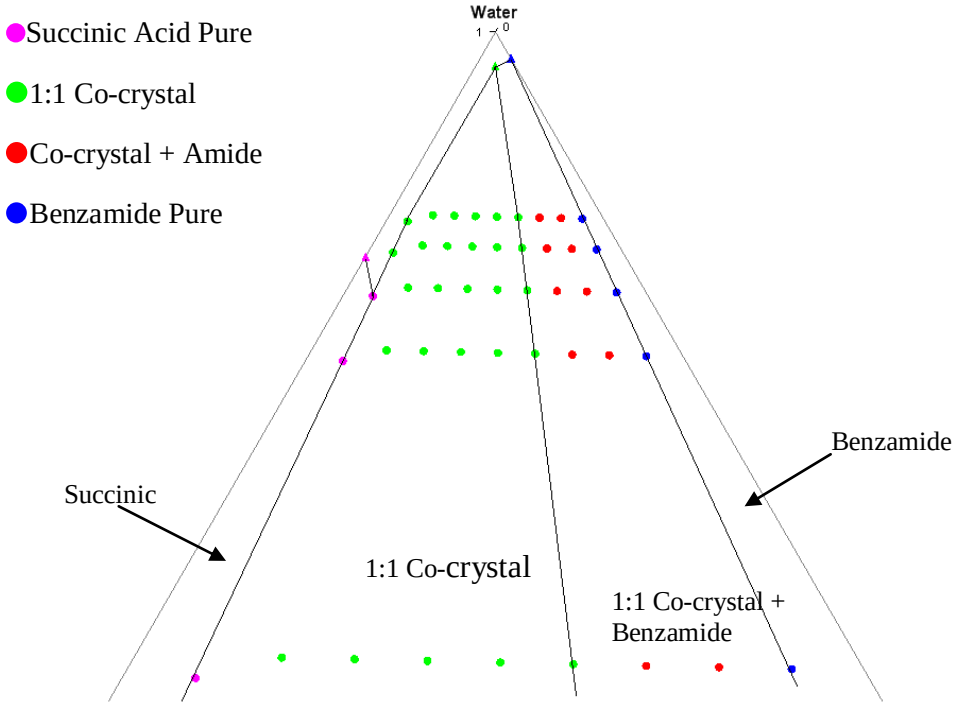

However, the Benzamide system in methanol produces a phase diagram, Figure 7.7, 7.8, with a well defined eutectic which seems more normalised and expected given the solubilities of the starting components are similar. In methanol, it is possible to see that the co-crystal undergoes congruent dissolution, therefore suggesting that it is possible to crystallise the co-crystal by evaporating an under-saturated solution containing the 1:1 stoichiometric amounts of Benzamide and Succinic acid in solution. However, this requires further experimental work to generate a better defined eutectic curve.

Figure 7.7: Ternary Phase diagram of Benzamide, Succinic Acid in Methanol

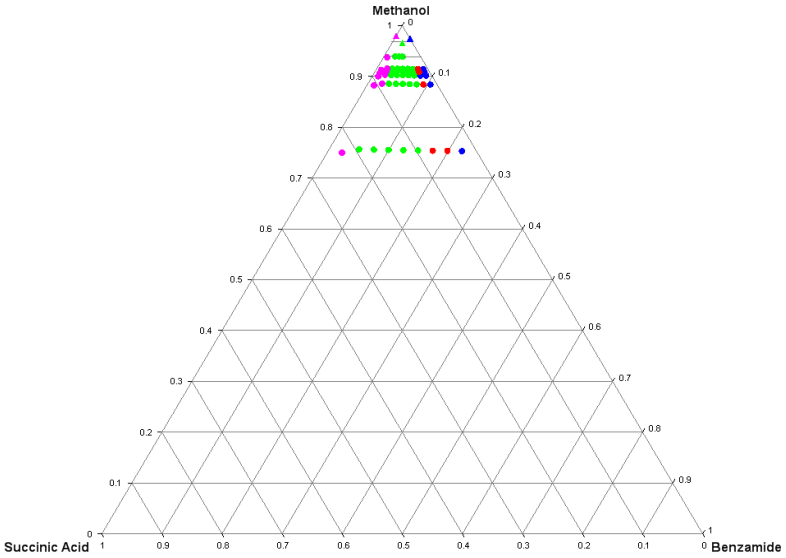

Figure 7.8: Ternary Phase diagram of Benzamide, Succinic Acid in Zoomed

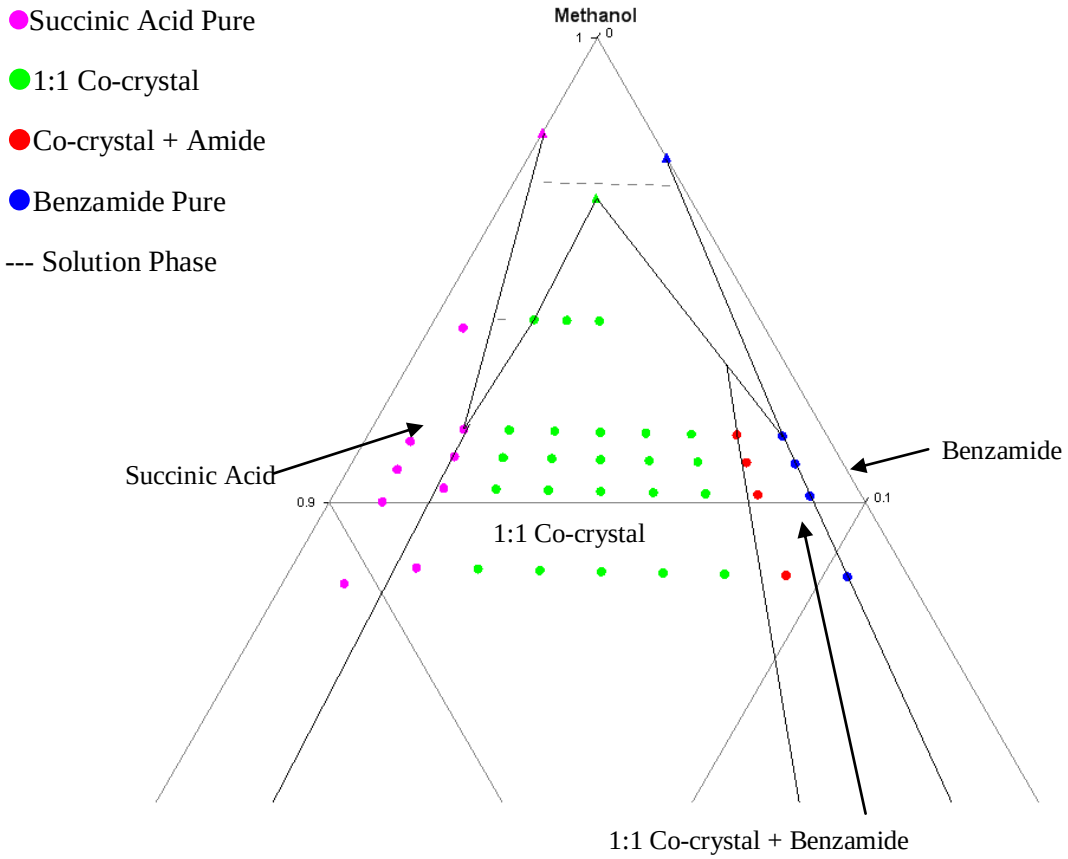

The Nicotinamide system in water produces an experimental representation of the ideal phase diagram theorised in chapter 1, Figure 7.9, 7.10. Again we see that Nicotinamide and Succinic acid have similar solubility, leading to a diagram from which we can see that the co-crystal undergoes congruent dissolution as the solubility curve of the co-crystal crosses the co-crystal component stoichiometric ratio line (*dotted line a*) of 1:1 co-crystal component. This means that the co-crystal can grow in an unsaturated solution as well as a saturated solution of 1:1 stoichiometric amounts of acid and amide.

In methanol, the phase diagram of Nicotinamide and Succinic acid, Figure 7.11, 7.12, also shows three phases, co-crystal, pure Nicotinamide and pure Succinic acid phase regions. Although the solubility curve is not as well defined as the water system, it is still possible to say that the same observation of co-crystal growth can be envisaged as seen for the water system.

Figure 7.9: Ternary Phase diagram of Nicotinamide, Succinic Acid in Water

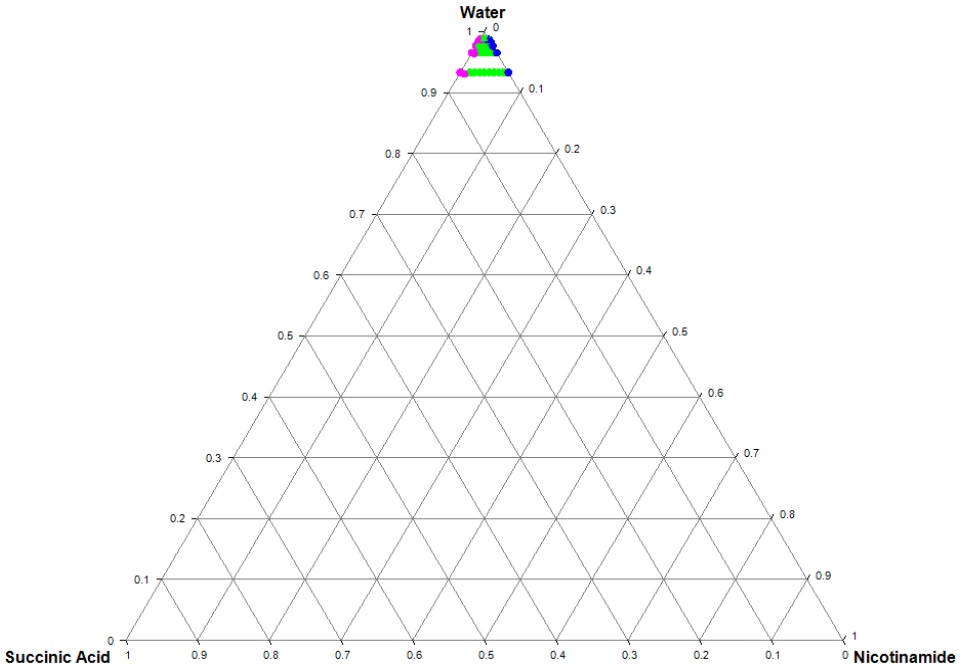

Figure 7.10: Ternary Phase diagram of Nicotinamide, Succinic Acid in Zoomed

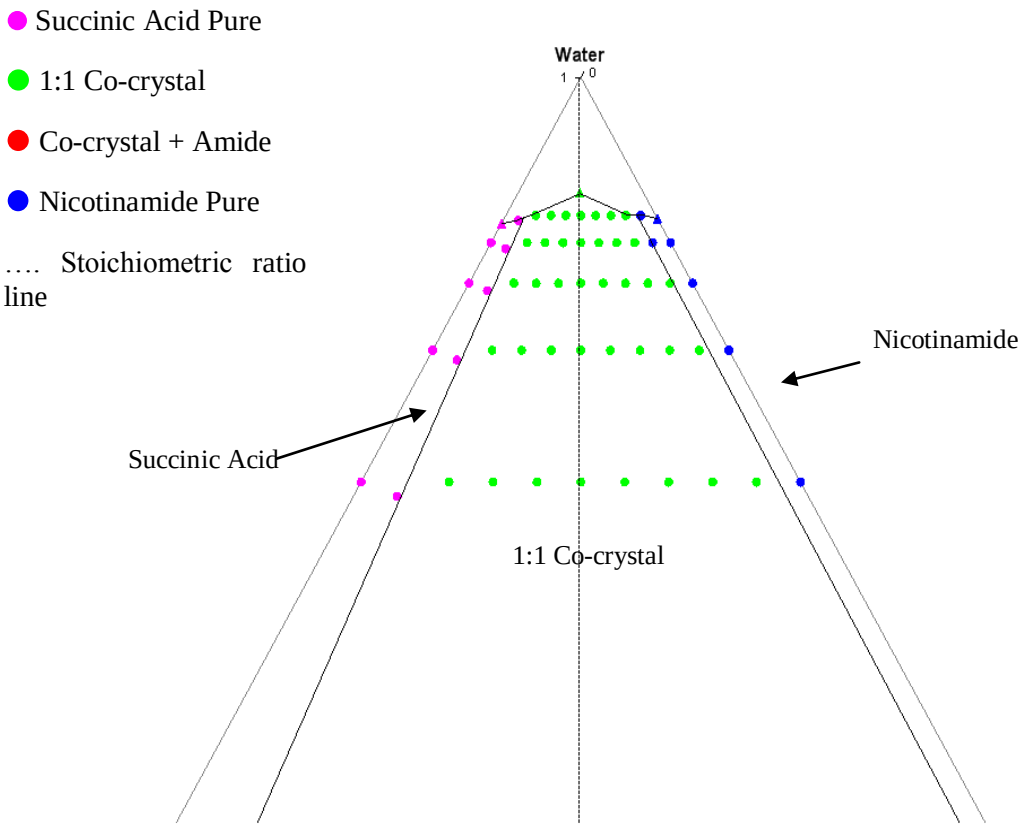

Figure 7.11: Ternary Phase diagram of Nicotinamide, Succinic Acid in Methanol

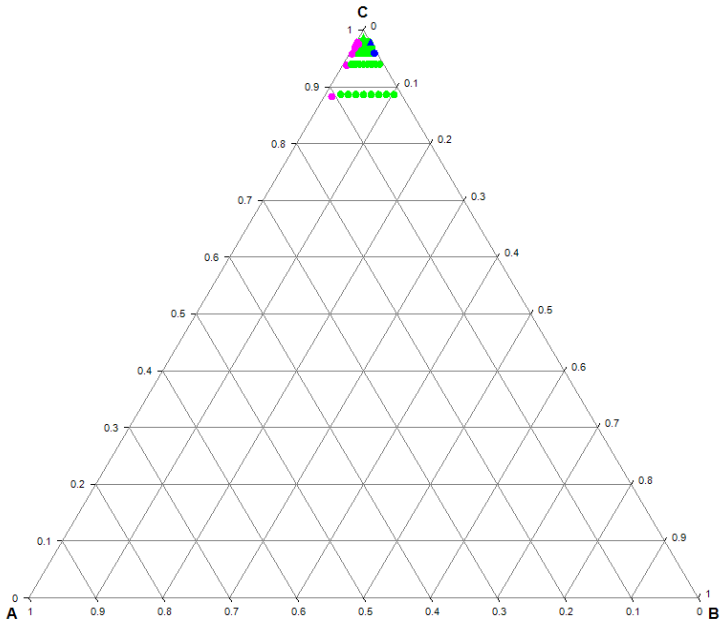

Figure 7.12: Ternary Phase diagram of Nicotinamide, Succinic Acid in Zoomed

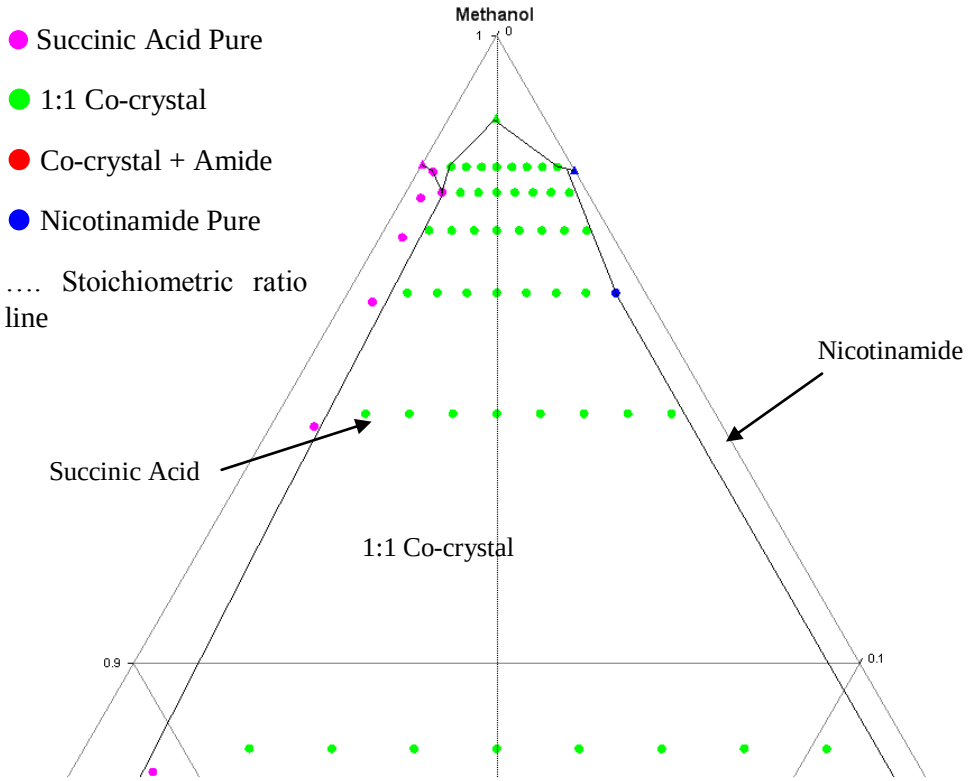

7.3.1 Single crystal analysis

During this study, sample containing the single crystal of the Nicotinamide and Succinic acid system has been grown and analysed using single crystal, courtesy of University of Bradford's in-house crystallographer, Dr Ian Scowen. The analysis is given below.

From the X-ray powder diffraction new phases have been identified, Figure 7.13**.** Suitable material for single crystal structure determination has been grown for water and methanol system, the experimental details for structures are given below in Table 7.3.

Figure 7.13: Powder diffraction data comparison of the Nicotinamide with Succinic Acid grown from water and methanol compared to pure starting components to identify potential new peaks.

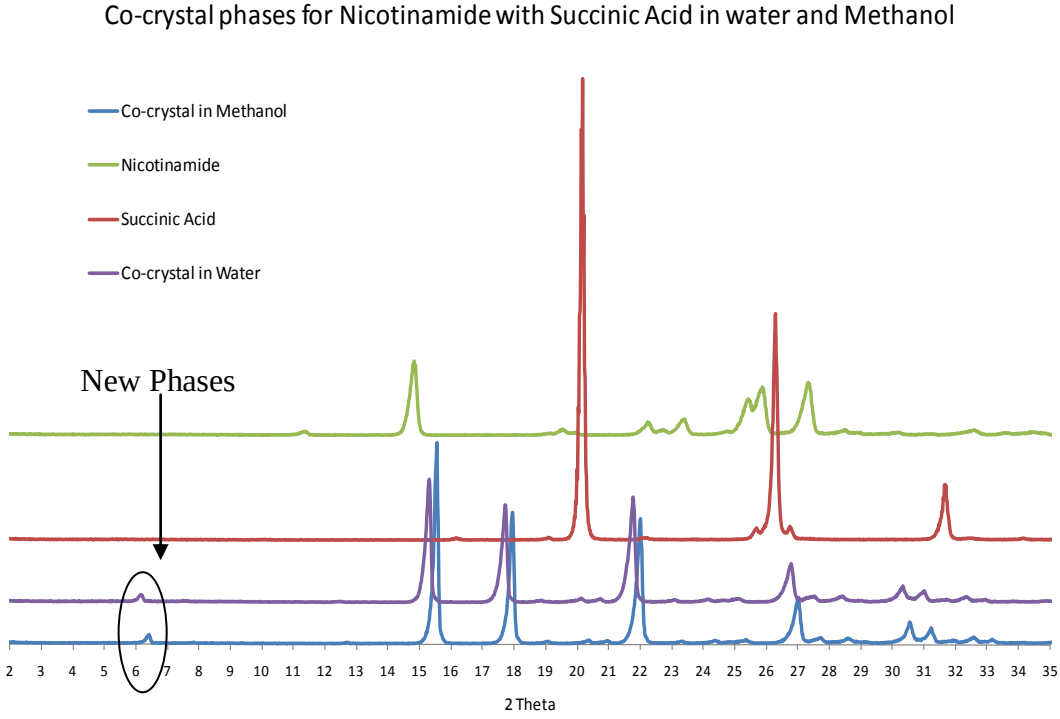

From the powder pattern a new peak is identified between 6-7˚ 2θ for both the water and methanol derived co-crystals. The single crystal data is presented in the table 7.3. A full detail of refinement, atomic coordinates, isotropic displacement parameters ($Å^2$), atomic displacement parameters ($Å^2$), geometric parameters (Å), and hydrogen-bond geometry (Å) is given in appendix D.

Table 7.3: Crystallographic Data for Nicotinamide with Succinic Acid in water and Methanol

Compound	Nicotinamide: Succinic Acid (H_2O)	Compound	Nicotinamide: Succinic Acid (MeOH)
Formula	$C_{10}H_{12}N_2O_5$	Formula	$C_{10}H_{12}N_2O_5$
Mass, M_r	240.11	Mass, M_r	240.11
Temp (K)	173 (2) K	Temp (K)	173 (2) K
Cryst Syst	Triclinic	Cryst Syst	Triclinic
Space Group	P-1	Space Group	P-1
Z	4	Z	4
a (Å)	5.0946 (10) Å	*a* (Å)	5.0864 (5) Å
b (Å)	11.601 (3) Å	*b* (Å)	11.5807 (15) Å
c (Å)	14.324 (3) Å	*c* (Å)	14.2811 (15) Å
α (deg)	77.633 (12)°	α (deg)	77.655 (4)°
β (deg)	86.608 (11)°	β (deg)	86.734 (6)°
γ (deg)	89.369 (11)°	γ (deg)	89.337 (6)°
V (Å)	825.5 (3) $Å^3$	*V* (Å)	637.72 (8) $Å^3$
R-Factor %	4.85	R-Factor %	7.07

Both crystals derived from water and methanol belong to the triclinic crystal system as the angles between axes $\alpha \neq \beta \neq \gamma \neq 90°$, similarly, the length of the axes $a \neq b \neq c$, suggest the P-1space group.

The expected packing of a Nicotinamide with a carboxylic acid should contain a hetero/homo dimer consisting of the amide···acid or an amide···amide interaction as well as an acid pyridine interaction. These have proven to be robust intermolecular interactions leading to multicomponent complex formation, Aakeroy, 2006. This next

section will investigate the packing of the Nicotinamide co-crystal grown from water and methanol.

7.3.2 Packing Analysis of Nicotinamide: Succinic Acid co-crystal

7.3.2.1 Packing arrangement for Co-crystal in water:

A Mercury analysis of this system shows that the structure has a Z value of 4. The Figure below depicts the hydrogen bonding between the components as a homo amide···amide dimer synthon (bong length 2.944 Å) and an acid···pyridine (bond length 2.688 Å) interaction with the neighbouring Succinic acid, Figure 7.14. Expanding the contacts further, we can see the stacking is of a zigzag conformation which upon further expansion stacks to form layers of sheets, Figure 7.15. ***(All the relevant CIF files are contained in a CD within Appendix H)***

Figure 7.14: Mercury analysis of Nicotinamide: Succinic Acid crystal structure showing the hetero dimer and acid-amide interaction.

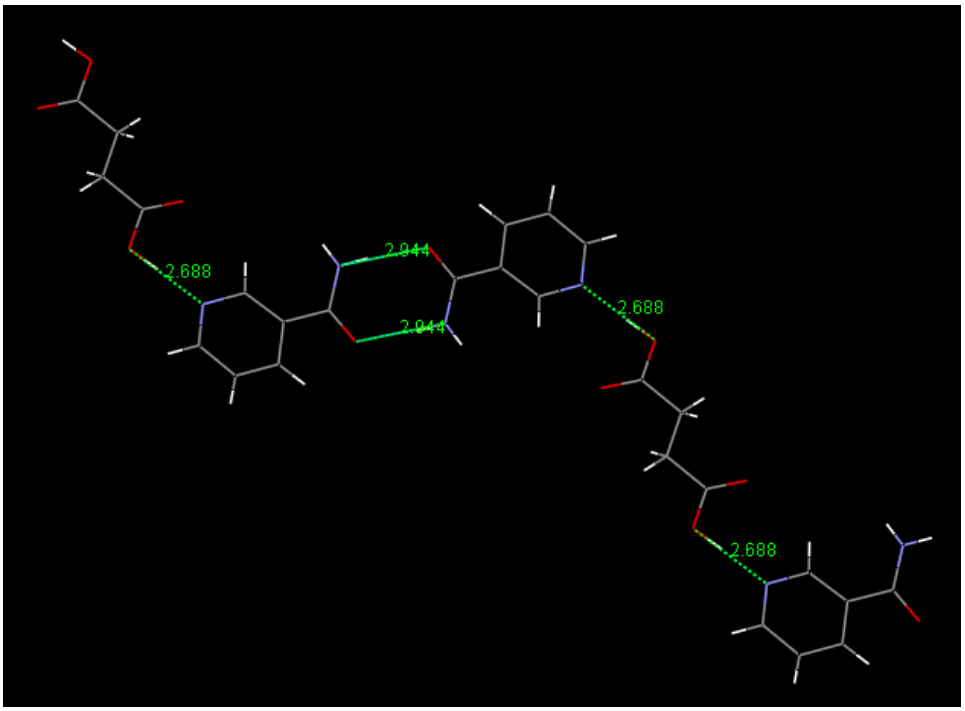

Figure 7.15: Stacking conformation with the unit cell of Nicotinamide: Succinic Acid i) Axis a, zigzag conformation, ii) offset of a direction of the unit cell showing formation of sheets

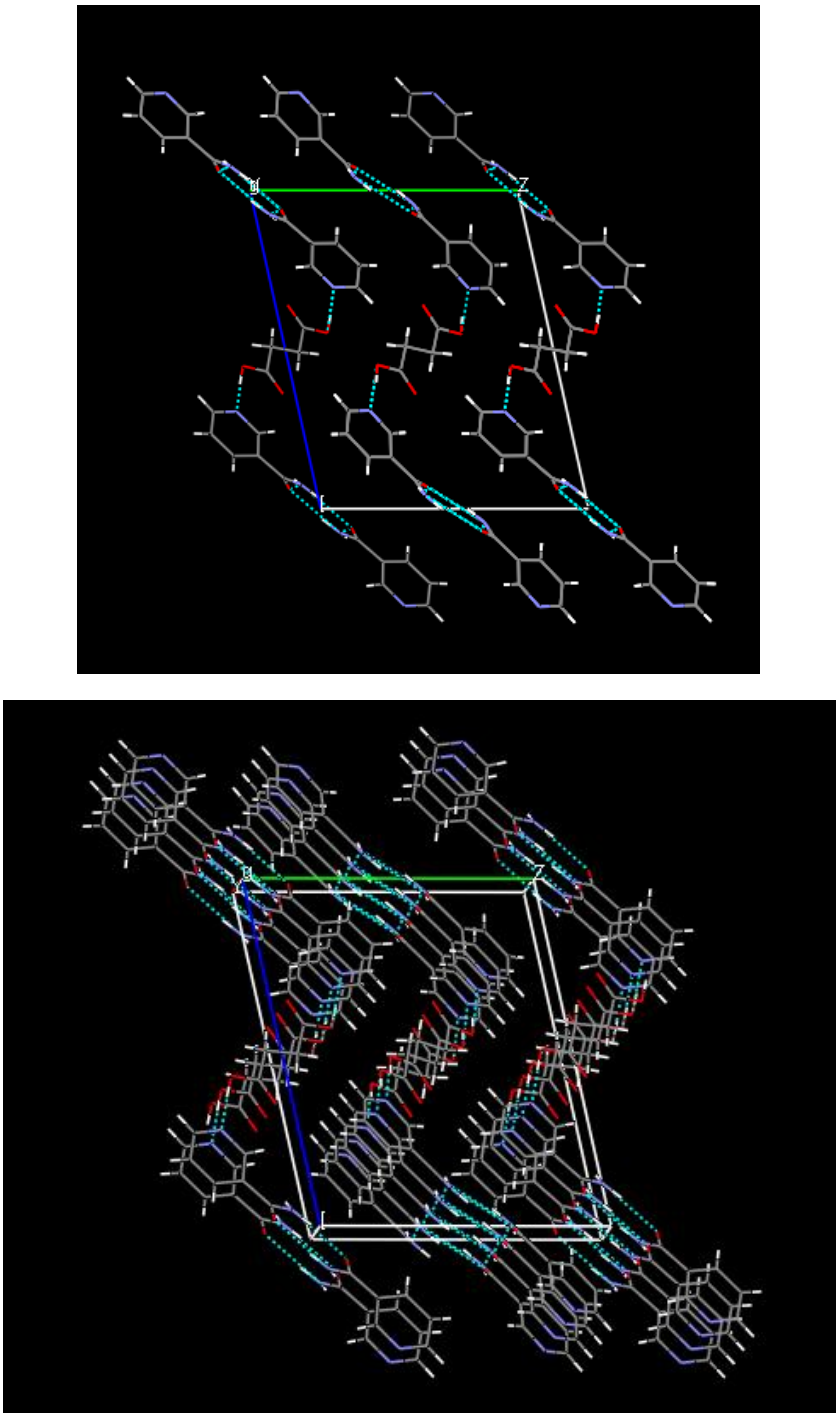

The hydrogen bonding angles and distances for the dimer interaction and acid pyridine interaction are shown in the table 7.4.

Table 7.4: Hydrogen-bond geometry (Å, °) of the amide – amide and acid – pyridine interactions

D—H···*A*	*D*—H	H···*A*	*D*···*A*	*D*—H···*A*
N2—H3···O1	1.65 (3)	1.96 (3)	2.944 (3)	174 (4)
O2—H1···N1	1.04 (3)	1.65 (3)	2.688 (2)	175 (3)

7.3.2.2 Packing arrangement for co-crystal in Methanol

Similarly, as observed with the water system, the Z value for this structure is 4. The complex grown from methanol has a unit cell dimension very close to the one observed for the system grown from water (see table 7.3). From Figure 7.16, we see that after Mercury analysis the hydrogen bonding is the expected hetero dimer and acid···pyridine interaction. Further expansion along these interactions shows packing similar to the previous crystal structure, a zigzag conformation which stacks in an offset manner and further extends to develop into a rippled sheet layers Figure 7.17 i-ii. Table 7.5, represents the hydrogen bonding angles and distance involved in this crystal structure.

Figure 7.16: Mercury analysis highlighting the hydrogen bonding of the hetero dimer and acid-pyridine interaction in the Nicotinamide: Succinic Acid crystal structure grown from methanol.

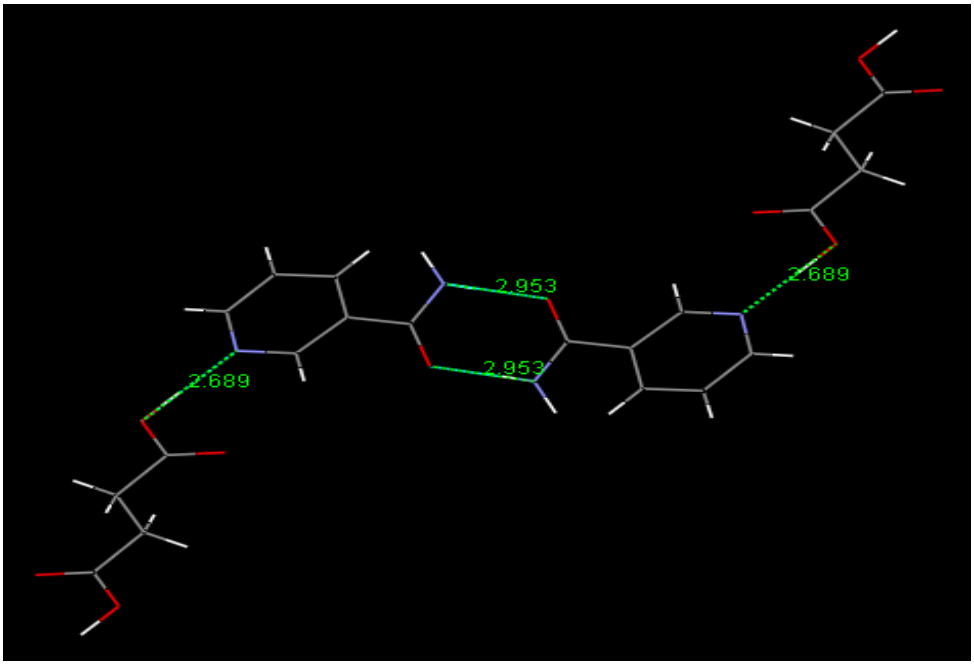

Figure 7.17: Stacking conformation with the unit cell of Nicotinamide : Succinic Acid i) Axis a, b) showing the zigzag conformation, ii) offset of axis a direction of the unit cell showing formation of sheets comprising of molecules stacking via the hetero dimer and acid-pyridine hydrogen bonding

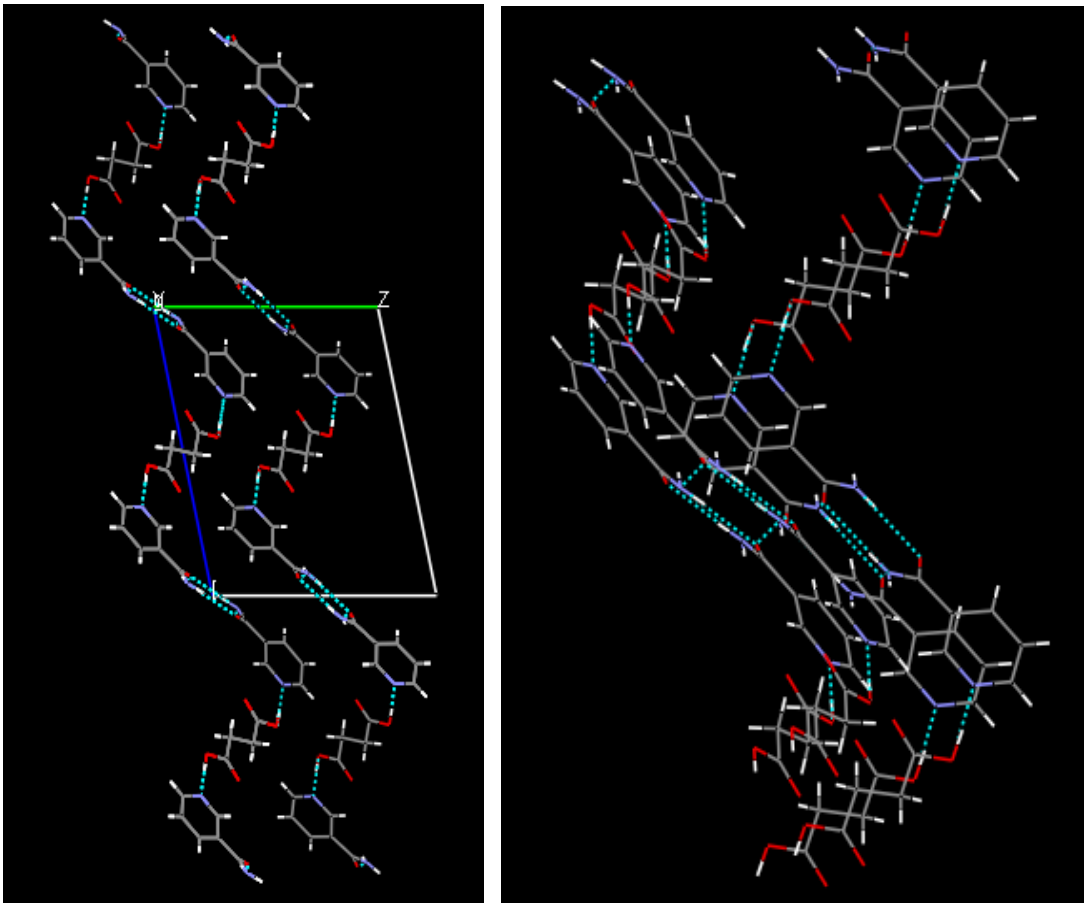

Table 7.5: Hydrogen-bond geometry (Å, °) of the amide – amide and acid – pyridine interactions

D—H···*A*	*D*—H	H···*A*	*D*···*A*	*D*—H···*A*
N2—H3···O1	0.99 (5)	2.01 (5)	2.953 (6)	177 (4)
O2—H1···N1	1.61 (5)	1.08 (5)	2.689 (5)	179 (5)

7.4 Summary

Chapter 7 presented the phase diagrams as a tool to further understand phase behaviour of three model co-crystal systems: Isonicotinamide with Succinic acid, Benzamide with Succinic acid and Nicotinamide with Succinic acid. The former two have crystal structures reported in the literature, so it was thought to be a nice comparison to map the behaviour in water and methanol. Nicotinamide has been introduced, since this system has not been published, and from the thermal analysis, a new phase has been highlighted in the Kofler contact melt described in previous chapters.

The Isonicotinamide system and Benzamide system show a co-crystal zone which is skewed towards the Succinic acid side of the ternary plot. This skewness is a result of solubility differences of the starting components. For the Nicotinamide system, well behaved phase diagrams have been derived for the water and methanol systems. Additionally, single crystals have been grown during this investigation of the Nicotinamide with Succinc acid.

Chapter Eight: Conclusion

8.1 Conclusion

The overall aim of this study was to develop an appreciation and generate a protocol which would enable a comparison to be made between model components which result in a co-crystal compared to a structurally similar compound, which emerged as problematic or unsuccessful at forming co-crystals, even though a viable pairing from a crystal engineering perspective exists. Progressing this understanding required gaining an appreciation of the hydrogen bonding interaction exhibited by this class of co-formers, and the overall behaviour of the surrounding peripheral functional groups of a co-former within a co-crystal to build an understanding of system design that have been established from the literature.

Overall a critical feature of the project was to understand the inter relationships and defining parameters which could lead to designing co-crystal complexes of benefit to the pharmaceutical or fine chemicals industry.

An initial screening matrix was established using Isonicotinamide and its reported co-crystals from the CSD, and as a comparative model, Benzamide was used to screen with the same set of co-formers. We find that from a simple bench evaporation method, only five out of the systems studied showed new phases from PXRD patterns. However, yielding a suitable crystal for single crystal determination has been a further challenge when adopting a low through-put approach, in particular when using a ReactArray Microvate device. Consequently, only two single crystals have successfully been grown and characterised in the study. This situation highlights the issue that crystallisation propensity may hinder the overall successful single crystal structures obtained. This then subsequently hinders the attempts of understanding the behaviour and nature of why one compound is more robust over another from the perspective of potential sites

for intermolecular interaction through envisaged design and the observed packing obtained from crystal structure determination. We note that powder diffraction data may be used to determine the crystal structure, however, this was not pursued due to quality of powder diffraction obtained from the sample generated. This would be a future direction to take with regards the project in light of the number of potential new systems this current work has generated.

Even though, from this initial hurdle, it has not been possible to maximise and grow enough material to further study the crystal structure for a comparative study within the systems studied. Collaboration with University of Glasgow has led to a project using dSNAP to enable the small number of structures we have to be classified with regards the molecular packing against the amide co-crystals in the CSD data base.

The outputs from the dSNAP study, consist of the structures extracted from CSD which contain our specimen amides, profiled for packing features and trends, these outcomes were subsequently employed in decoding in the crystal structures of the systems for which we obtained single crystal structures. This was a productive collaboration with the dSNAP developers. Despite the problems encountered with the code of the algorithm, the subtleties which are present in the packing motifs of the model amide, Isonicotinamide, were identified, this structural aspect of the work highlighted an interesting conformational situation within the co-former packing of the co-crystal. Where a key feature was found to be the cis and trans orientation of the amide and acid carbonyl to each other and the planar and off planar assemblies; all of which contribute to hydrogen bonding of the components that are the building blocks of a co-crystal.

This identification of these subtle orientations of the acid components formed the basis for the design and development of a sophisticated high through-put screen with

Syngenta. The screen design concept was to beta test, the notion of using this approach to deconvolute packing and use the outcomes to inform design strategy through maximising the co-crystal information contained in the output of the CSD.

This high throughput screening contribution was to show that results obtained indicate that the technique shows great potential and is viable route for screening for co-crystal as demonstrated from the polySNAP output. However, as a beta test of the technique utilising the polySNAP program, has brought a number of faults to light in the code to the developers of polySNAP. For this project a specific contribution, was the inclusion in the studies of a screening protocol developed specifically to this project to explore the impact of crystallisation condition and co-former functionality with polySNAP being used to verify similar crystalline forms within the screen. This was in self a significant contribution from the point of being an end user of the code and implementing the application of the code in such a high throughput screen.

Specifically, the challenge was implementing a successful analysis of the samples generated from the screen and this has been addressed with the use of reflectance GADDS diffraction data as the input to polySNAP. The screen has tested the software as a protocol to identify new phases from the co-crystal screen, as a result, the data shows that there are issues with background noise which results in poor correlation in the clustering. This has repeatedly been viewed for each of the plates, after further analysis, the plates show that data has been classed as “Other”, which is expected since the aim was to grow co-crystals, however, after cross referencing with the plate format to pin point and highlight which components should be present there seems to be a disagreement, which could be due to cross contamination when handling the plates and shipping to Pharmorphix for GADDS analysis. Additionally, since the plates have been split into two sections, accommodating for experiments in two solvents per plate, it is

expected that a sample with ratio or 1:1 in solvent 1 should be same in solvent 2. This is not the case, results show that sample with same stoichiometric ratio in each solvent are clustered individually, or with sample which consist of a different coformer. For these reasons, solvent selection and solubility may need to be further refined, and a screening protocol fine tuned to identify the clustering problems faced.

Due to the discrepancies from solution co-crystal screening method, the Hotstage microscopy (a melt crystallization approach) has been developed for the active ingredients and the all acid coformers studied here, and the outcomes on this aspect of the project are summarised here are in two parts:

- Low through-put screen viewed in chapter 3 coupled with DSC analysis to confirm the melting phases and possible new phases
- Components which have previously been subject to the high through-put analysis in the previous chapter.

The aim of these DSC and thermal microscopy studies was a comparison of the success rate of Benzamide with the model amide, Isonicotinamide without any solvent present, as this is a melt crystallisation approach. The previous low through-put screen with solvent present resulted in the co-crystallisation characterisation via PXRD of 5 of the model coformers, with a thermal technique, without solvent present using the Kofler contact method produces identification of 8 potential new phases, the remaining two coformers, sublime when preparing the slide. To verify the results of hot melt, DSC has also been used, and it was found that this technique complements the results from the thermal microscopy screen.

To increase the success rate of possible co-crystals, all the components involved in the high through-put screen have also undergone this Hotstage microscopy screening technique. In total this resulted in 17 hits of co-crystals with the model amide,

Isonicotinamide, and 12 hits for the Benzamide which has not been thought to co-crystallise as well according to literature review. Additionally, Nicotinamide has been introduced, which has a hit of 16 new phases. Unfortunately, DSC has only been implemented for the low through-put screen, this is due to restrictions of taking chemicals off site from Syngenta and because of the relocation of the Syngenta site to southern England.

In the examples presented for Hotstage microscopy, where samples have sublimed upon heating, it might be possible to use a 'cold contact' method over the Kofler contact method. This method would involve the components dissolved in a supersaturated solution where a drop of which is left to crystallise under the cover slip and create a mixing zone with the second component, upon heating under the microscope a new phase can be identified. This method would further maximise the output of thermal microscopy screening technique

To further understand phase behaviour of the three models discussed in this work, the mapping of a ternary phase diagram has also been a focus of this work.

The trends obtained were as follows: Isonicotinamide system and Benzamide system show a co-crystal zone that is skewed towards the Succinic acid side of the ternary plot. This skewness is a result of solubility differences of the starting components. In contrast the Nicotinamide system, exhibited as well behaved phase diagrams in both water and methanol. Additionally, single crystals have been grown during this investigation of the Nicotinamide with Succinic acid.

Significantly for the ternary phase work, there are a limited number of experimentally derived phase diagrams which have been report, and these show similar trends linked to solvent component solubility. Here we find that solubility of the components is

important, as the difference alters the location and size of the phase space regions of where the co-crystal is thermodynamically stable. This was then found to significantly influence the accessible solution composition available to maximise the formation of co-crystal over the crystallisation of mixtures or components. All of which was found to be solvent choice sensitive, in particular the critical impact of component solubility on the skewness of the overall phase diagram and the impact this has on the viable co-crystal region. A future approach to developing this further would be to map solution speciation over composition as defined by the ternary phase diagrams in a systematic way. This would enhance the perspective on solution chemistry and pre nucleation on co-crystal formation. This latter area is of immense debate in the overall understanding of crystal engineering in the context of nucleation control.

8.2 Future work

A number of crystallisation routes have been explored here to maximise the number of co-crystals available in order to fully understand co-crystal formation. The key model has been of small acid – amide. Many flaws have come to light with the protocols employed in this study. The lead for this work is the link between the pair wise design strategies to further study the objectives set out, the homo systems also need to be explored, such as acid – acid and amide – amide combinations allowing full appreciation of the hierarchical approach and design of and component suitability of co-crystallising compound. Coupling this work with the mathematical model discussed in chapter two section 2.8 could be the beginning of developing a predictive computational led mode/tool for co-crystal design using MOPAC,

References

References

A

Aakeroy, C. B. Acta Crystallographica Section B-Structural Science **1997**, 53, 569-586.

Aakeroy, C. B.; Beatty, A. M. *Australian Journal of Chemistry* **2001**, *54*, 409-+.

Aakeroy, C. B.; Beatty, A. M.; Helfrich, B. A. *Angewandte Chemie, International Edition* **2001**, *40*, 3240-3242.

Aakeroy, C. B.; Beatty, A. M.; Helfrich, B. A. *J. Am. Chem. Soc.* **2002**, *124*, 14425-14432.

Aakeroy, C. B.; Beatty, A. M.; Helfrich, B. A.; Nieuwenhuyzen, M. *Crystal Growth & Design* **2003**, *3*, 159-165.

Aakeroy, C. B.; Beatty, A. M.; Zou, M. *Materials Research Bulletin* **1998**, 225-241.

Aakeroy, C. B.; Borovik, A. S. *Coordination Chemistry Reviews* **1999**, *183*, 1-1.

Aakeroy, C. B.; Desper, J.; Helfrich, B. A. *Crystengcomm* **2004**, *6*, 19-24.

Aakeroy, C. B.; Hitchcock, P. B. *Journal of Materials Chemistry* **1993**, *3*, 1129-35.

Aakeroy, C. B.; Nieuwenhuyzen, M. *J. Am. Chem. Soc.* **1994**, *116*, 10983-10991.

Aakeroy, C. B.; Salmon, D. J. *CrystEngComm* **2005**, *7*, 439-448.

Aakeroy, C. B.; Salmon, D. J.; Smith, M. M.; Desper, J. *Crystal Growth & Design* **2006**, *6*, 1033-1042.

Aakeroy, C. B.; Seddon, K. R. *Chemical Society Reviews* **1993**, *22*, 397-407.

Allen, F. Acta Crystallographica Section B **2002**, 58, 380-388.

Allen, F. H.; Motherwell, W. D. S. *Acta Crystallographica Section B* **2002**, *58*, 407-422.

Almarsson, O.; Zaworotko, M. J. *Chemical Communications* **2004**, *2004*, 1889-1896.

B

Barr, G.; Collins, A.; Parkin, A.; Dong, W.; Gilmore, C. J.; Wilson, C. C. *CrystEngComm* **2006**, *9*, 245-253.

Barr, G.; Dong, W.; Gilmore, C.; Faber, J. *Journal of Applied Crystallography* **2004**, *37*, 635-642.

Barr, G.; Dong, W.; Gilmore, C.; Kern, A.; Parkin, A.; Wilson, C. *Zeitschrift für Kristallographie Supplements* **2007**, *2007*, 209-214.

Barr, G.; Dong, W.; Gilmore, C. J. *Journal of Applied Crystallography* **2004**, *37*, 874-882.

Barr, G.; Dong, W.; Gilmore, C. J. *Journal of Applied Crystallography* **2004**, *37*, 658-664.

Barr, G.; Dong, W.; Gilmore, C. J.; Parkin, A.; Wilson, C. C. *Journal of Applied Crystallography* **2005**, *38*, 833-841.

Barr, G.; Gilmore, C. J.; Paisley, J. *Journal of Applied Crystallography* **2004**, *37*, 665-668.

Bernstein, J. *Polymorphism in molecular crystals*; Oxford University Press, USA, 2002.

Bernstein, J. *Chemical Communications* **2005**, 5007-5012.
Bernstein, J.; Davey, R. J.; Henck, J.-O. *Angewandte Chemie, International Edition* **1999**, *38*, 3441-3461.
Bernstein, J.; Davis, R. E.; Shimoni, L.; Chang, N. L. *Angewandte Chemie International Edition in English* **1995**, *34*, 1555-1573.
Berry, D. J.; Seaton, C. C.; Clegg, W.; Harrington, R. W.; Coles, S. J.; Horton, P. N.; Hursthouse, M. B.; Storey, R.; Jones, W.; Fris?c?i, T. *Cryst. Growth Des* **2008**, *8*, 1697-1712.
Blagden, N.; Davey, R.; Dent, G.; Song, M.; David, W. I. F.; Pulham, C. R.; Shankland, K. *Crystal Growth & Design* **2005**, *5*, 2218-2224.
Blagden, N.; Davey, R. J. *Crystal Growth & Design* **2003**, *3*, 873-885.
Blagden, N.; de Matas, M.; Gavan, P. T.; York, P. *Advanced Drug Delivery Reviews* **2007**, *59*, 617-630.
Blagden, N.; Song, M.; Davey, R. J.; Seton, L.; Seaton, C. C. *Crystal Growth & Design* **2005**, *5*, 467-471.
Bond, A. D.; Royal Society of Chemistry, 2007; Vol. 9.
Braga, D. *Chemical Communications* **2003**, 2751-2754.
Braga, D.; Brammer, L.; Champness, N. R. *CrystEngComm* **2005**, *7*, 1-19.
Braga, D.; D'Addario, D.; Maini, L.; Polito, M.; Giaffreda, S.; Rubini, K.; Grepioni, F. Applications of Crystal Engineering Strategies in Solvent-free Reactions: Toward a Supramolecular Green Chemistry, 2006.
Braga, D.; Desiraju, G. R.; Miller, J. S.; Orpen, A. G.; Price, S. L. *Crystengcomm* **2002**, *4*, 500-509.
Braga, D.; Grepioni, F. *Chemical Communications* **2005**, 3635-3645.
Brittain, H. G. *Polymorphism in Pharmaceutical Solids*; Informa Healthcare, 1999.
Burrows, A. D. In Supramolecular Assembly Via Hydrogen Bonds I, 2004; Vol. 108.
Byrn, S.; Pfeiffer, R.; Stowell, J. **2001**.

C

Chiarella, R. A.; Davey, R. J.; Peterson, M. L. *Crystal Growth & Design* **2007**, *7*, 1223-1226.
Childs, S. L.; Chyall, L. J.; Dunlap, J. T.; Smolenskaya, V. N.; Stahly, B. C.; Stahly, G. P. *JOURNAL-AMERICAN CHEMICAL SOCIETY* **2004**, *126*, 13335-13342.
Clegg, W. *Crystal structure determination*; Oxford University Press, 1998.
Collins, A.; Parkin, A.; Barr, G.; Dong, W.; Gilmore, C. J.; Wilson, C. C. *Crystengcomm* **2007**, *9*, 245-253.
Corey, E. J. *Pure and Applied Chemistry* **1967**, *14*, 19-37.

D

Dale, S. H.; Elsegood, M. R. J.; Hemmings, M.; Wilkinson, A. L. *Crystengcomm* **2004**, *6*, 207-214.

Datta, S.; Grant, D. J. W. *Nature Reviews Drug Discovery* **2004**, *3*, 42-57.
Davey, R. J.; Allen, K.; Blagden, N.; Cross, W. I.; Lieberman, H. F.; Quayle, M. J.; Righini, S.; Seton, L.; Tiddy, G. J. T. *Crystengcomm* **2002**, *4*, 257-264.
Davis, R.; Lorimer, K.; Wilkowski, M.; Rivers, J.; Wheeler, K.; Bowers, J. *Crystals in Supramolecular Chemistry* **2004**, 6141.
Desiraju, G.; Gavezzotti, A. Journal of the Chemical Society, Chemical Communications **1989**, 1989, 621-623.
Desiraju, G.; PARSHALL, G. *Materials science monographs* **1989**, *54*.
Desiraju, G. R. Angewandte Chemie-International Edition in English **1995**, 34, 2311-2327.
Desiraju, G. R. *Chemical Communications* **1997**, 1475-1482.
Desiraju, G. R. *CURRENT SCIENCE* **2001**, *81*, 1038-1042.
Desiraju, G. R. *Nature* **2001**, *412*, 397-400.
Desiraju, G. R. *Accounts of Chemical Research* **2002**, *35*, 565-573.
Desiraju, G. R. *Crystengcomm* **2003**, *5*, 466-467.
Desiraju, G. R. Journal of Molecular Structure **2003**, 656, 5-15.
Desiraju, G. R. Nature (London, United Kingdom) **2003**, 423, 485.
Dunitz, J. D. *Chemistry-a European Journal* **1998**, *4*, 745-746.
Dunitz, J. D. *Crystengcomm* **2003**, *5*, 506-506.

E

Etter, M. C. Accounts of Chemical Research **1990**, 23, 120-126.
Etter, M.C.; Panunto, *Journal of the American society,* **1988**. 110 (17): p. 5896-5897.
Etter, M.C., Hydrogen bonds as design elements in organic chemistry. *Journal of Physical Chemistry*, **1991**. 95(12): p. 4601-10.

F

Friscic, T.; Jones, W. *Faraday Discussions* **2007**, *136*, 167-178.

G

Giron, D. *Thermochimica Acta* **1995**, *248*, 1-59.
Giron-Forest, D.; Goldbronn, C. H.; Piechon, P. *Journal of Pharmaceutical and Biomedical Analysis* **1989**, *7*, 1421-1433.
Grant, G.; Richards, W. *Computational chemistry*; Oxford university press, 1995.

H

Haines, P. J. *Principals of thermal analysis and calorimetry*; Royal society of chemistry, 2002.
Hatakeyama, T.; Zhenhai, L. *Handbook of Thermal Analysis*; John Wiley & Sons, 1998.
Hickey, M. B.; Peterson, M. L.; Scoppettuolo, L. A.; Morrisette, S. L.; Vetter, A.; Guzmán, H.; Remenar, J. F.; Zhang, Z.; Tawa, M. D.; Haley, S. *European journal of pharmaceutics and biopharmaceutics* **2007**, *67*, 112-119.
Hino, T.; Ford, J. L. International Journal of Pharmaceutics **2001**, 219, 39-49.
Hino, T.; Ford, J. L.; Powell, M. W. *Thermochimica Acta* **2001**, *374*, 85-92.
Hino, T.; Ford, J. L.; Powell, M. W. *Thermochimica Acta* **2001**, *374*, 85-92.
Horsewill, A. J.; Aibout, A. *Journal of Physics-Condensed Matter* **1989**, *1*, 9609-9622.
Huang, C.-M.; Leiserowitz, L.; Schmidt, G. M. J. Journal of the Chemical Society, Perkin Transactions 2: Physical Organic Chemistry (1972-1999) **1973**, 503-8.
Huang, L. F.; Tong, W. Q. *Advanced Drug Delivery Reviews* **2004**, *56*, 321-334.

I

Infantes, L.; Motherwell, W. D. S. *Zeitschrift fuer Kristallographie* **2005**, *220*, 333-339.

I

Jeffrey, G. *An introduction to hydrogen bonding*; Oxford University Press, USA, 1997.

J

John, V. B. *Understanding phase diagrams* Macmillan: London, 1974.
Jones, D. W.; Rychlewska, U. *Journal of Molecular Structure* **1999**, *474*, 3-7.

K

Kane, J. J.; Nguyen, T.; Xiao, J.; Fowler, F. W.; Lauher, J. W. *Molecular Crystals and Liquid Crystals* **2001**, *356*, 449-458.
Kofler, A. *Naturwissenschaften* **1943**, *31*, 553-557.
Kofler, L.; Kofler, A. Berichte der deutschen chemischen Gesellschaft (A and B

Series) **1943**, 76, 246-248.
Kofler, A. (1941), *Z.Phys. Chem. Abteilung A.*, **187**, 202-210.
Krzanowski, W. Principals of multivariate analysis: a user's perspective; Oxford University Press, USA, 2000.

L

Lau, E.; Satinder, A.; Stephen, S. In *Separation Science and Technology*; Academic Press, 2001; Vol. Volume 3.
Le Fèvre, R. Dipole moments: their measurement and application in chemistry; Methuen & Co. ltd., 1938.
Lehn, J. Journal of Chemical Sciences **1994**, 106, 915-922.
Leiserowitz, L. Acta Crystallographica, Section B: Structural Crystallography and Crystal Chemistry **1976**, B32, 775-802.
Leiserowitz, L.; Schmidt, G. M. J. Journal of the Chemical Society [Section] A: Inorganic, Physical, Theoretical **1969**, 2372-82.
Lynch, D. E.; SINGH, M.; Parsons, S. *Crystal Engineering* **2000**, *3*, 71-79.
Lynch, D. E.; Smith, G.; Freney, D.; Byriel, K. A.; Kennard, C. H. L. *Australian Journal of Chemistry* **1994**, *47*, 1097-1115.

M

McCrone, W. *Microchimica Acta* **1951**, *38*, 476-486.
McCrone, W. C. *Fusion Methods in Chemical Microscopy*; Interscience Publishers New York, 1957.
McMahon, J. A.; Bis, J. A.; Vishweshwar, P.; Shattock, T. R.; McLaughlin, O. L.; Zaworotko, M. J. *Zeitschrift Fur Kristallographie* **2005**, *220*, 340-350.
Mighell, A. D.; Karen, V. L. Journal of Research of the National Institute of Standards and Technology **1996**, 101, 273-280.
Morales, L. A., University of South Florida, 2003.
Morissette, S. L.; Almarsson, Ö.; Peterson, M. L.; Remenar, J. F.; Read, M. J.; Lemmo, A. V.; Ellis, S.; Cima, M. J.; Gardner, C. R. *Advanced Drug Delivery Reviews* **2004**, *56*, 275-300.

N

Nangia, A. *Crystengcomm* **2002**, *4*, 93-101.
Nangia, A.; Desiraju, G. R. *Chemical Communications* **1999**, 605-606.

O

Orpen, A. Acta Crystallographica Section B **2002**, 58, 398-406.
Oswald, I. D. H.; Motherwell, W. D. S.; Parsons, S. *Acta Crystallographica Section E-Structure Reports Online* **2004**, *60*, O2380-O2383.
Oswald, I. D. H.; Motherwell, W. D. S.; Parsons, S. *Acta Crystallographica Section E-Structure Reports Online* **2005**, *61*, O3161-O3163.
Oswald, I. D. H.; Motherwell, W. D. S.; Parsons, S. *Acta Crystallographica Section B-Structural Science* **2005**, *61*, 46-57.

P

Padrela, L.; Rodrigues, M. A.; Velaga, S. P.; Fernandes, A. C.; Matos, H. A.; de Azevedo, E. G. *The Journal of Supercritical Fluids* **2006**, *In Press, Corrected Proof*.
Parkin, A.; Barr, G.; Dong, W.; Gilmore, C. J.; Wilson, C. C. *Crystengcomm* **2006**, *8*, 257-264.
Pauling, L. The nature of the chemical bond and the structure of molecules and crystals: an introduction to modern structural chemistry; Cornell Univ Pr, 1960.
Penfold, B. R.; White, J. C. B. *Acta Cryst.* **1959**, *12*, 130-5.
Pope, M. I. Differential Thermal Analysis--A Guide to Technique and its Applications; Heyden and Son, Inc., 1977.

Q

R

Remenar, J. F.; Morissette, S. L.; Peterson, M. L.; Moulton, B.; MacPhee, J. M.; Guzman, H. R.; Almarsson, O. *JOURNAL-AMERICAN CHEMICAL SOCIETY* **2003**, *125*, 8456-8457.
Reynolds, J. E. F.; Parfitt, K.; Parsons, A. V.; Sweetman, S. C. *Martindale The Extra Pharmacopoeia*, 1993.
Rodríguez-Spong, B.; Price, C. P.; Jayasankar, A.; Matzger, A. J.; Rodríguez-Hornedo, N. *Advanced Drug Delivery Reviews* **2004**, *56*, 241-274.
Rodríguez-Spong, B.; Price, C. P.; Jayasankar, A.; Matzger, A. J.; Rodríguez-Hornedo, N. *Advanced Drug Delivery Reviews* **2004**, *56*, 241-274.

S

Schartman, R. R. International Journal of Pharmaceutics **2009**, 365, 77-80.
Schmidt, J.; Snipes, W. International Journal of Radiation Biology **1968**, 13, 101-109.

Seaton, C. C.; Parkin, A.; Wilson, C. C.; Blagden, N. *Cryst. Growth Des* **2008**, *8*, 363-368.
Seaton, C. C.; Parkin, A.; Wilson, C. C.; Blagden, N. **2008**.
Shan, N.; Batchelor, E.; Jones, W. *Tetrahedron Letters* **2002**, *43*, 8721-8725.
Shan, N.; Bond, A. D.; Jones, W. *Crystal Engineering* **2002**, *5*, 9-24.
Shan, N.; Bond, A. D.; Jones, W. *Tetrahedron Letters* **2002**, *43*, 3101-3104.
Shan, N.; Zaworotko, M. J. *Drug Discovery Today* **2008**, *13*, 440-446.
Shan, N.; Zaworotko, M. J. *Drug Discovery Today* **2008**, *13*, 440-446.
Shan, N.; Zaworotko, M. J. *Drug Discovery Today* **2008**, *13*, 440-446.
Sharma, B. L.; Bassi, P. S. Indian Journal of Chemistry, Section A: Inorganic, Physical, Theoretical & Analytical **1984**, 23A, 303-7.
Sharma, B. L.; Sharma, N. K.; Bassi, P. S. *Journal of Crystal Growth* **1984**, *67*, 633-8.
Sharma, C.; Desiraju, G. **1989**.
Sharma, C. V. K. *Crystal Growth & Design* **2002**, *2*, 465-474.
Steed, J. W.; Atwood, J. L. *Supramolecular chemistry*; 1st ed.; John Wiley & Sons, 2000.
Steiner, T. Angewandte Chemie International Edition **2002**, 41, 48-76.
Steiner, T.; Desiraju, G. R. *Chemical Communications* **1998**, 891-892.
Subramanian, S.; Zaworotko, M. J. *Coordination Chemistry Reviews* **1994**, *137*, 357-401.

T

Trask, A. V.; Jones, W. In *Organic Solid State Reactions*, 2005; Vol. 254.
Trask, A. V.; Motherwell, W. D. S.; Jones, W. *Chemical Communications* **2004**, *2004*, 890-891.
Trask, A. V.; van de Streek, J.; Motherwell, W. D. S.; Jones, W. *Crystal Growth & Design* **2005**, *5*, 2233-2241.

V

van de Streek, J.; Motherwell, S. Acta Crystallographica, Section B: Structural Science **2005**, B61, 504-510.
Vishweshwar, P.; McMahon, J. A.; Bis, J. A.; Zaworotko, M. J. *J Pharm Sci* **2006**, *95*, 499-516.
Vishweshwar, P.; McMahon, J. A.; Peterson, M. L.; Hickey, M. B.; Shattock, T. R.; Zaworotko, M. J. *Chemical Communications* **2005**, 4601-4603.
Vishweshwar, P.; Nangia, A.; Lynch, V. M. *Crystengcomm* **2003**, *5*, 164-168.
Vishweshwar, P.; Nangia, A.; Lynch, V. M. *Crystal Growth & Design* **2003**, *3*, 783-790.

W

Walsh, R. D. B.; Bradner, M. W.; Fleischman, S.; Morales, L. A.; Moulton, B.; Rodriguez-Hornedo, N.; Zaworotko, M. J. *Chemical Communications* **2003**, *2003*, 186-187.

Watson, D. G. Journal of Research of the National Institute of Standards and Technology **1996**, 101, 227-229.

Whitesides, G. M.; Simanek, E. E.; Mathias, J. P.; Seto, C. T.; Chin, D. N.; Mammen, M.; Gordon, D. M. *Accounts of Chemical Research* **1995**, *28*, 37-44.

Wilson, R. J.; Haines, P. J.; Royal Society of Chemistry, Cambridge, UK, 2002.

Z

Zaworotko, M. J.; Moulton, B.; McMahon, J.; Kuduva, S.; Rodriguez-Hornedo, N. *Abstracts of Papers of the American Chemical Society* **2003**, *225*, U959-U959.

Zhang, J.; Wu, L. X.; Fan, Y. G. *Journal of Molecular Structure* **2003**, *660*, 119-129.

Zhang, J.; Ye, L.; Wu, L. X. Acta Crystallographica Section C-Crystal Structure Communications **2005**, 61, O38-O40.

Zukerman-Schpector, J.; Tiekink, E. R. T. *Zeitschrift fur Kristallographie* **2008**, *223*, 233-234.

Appendices

Appendices

Appendix A: Packing of previously reported Co-crystals

AJAKEB

Isonicotinamide with 4-Nitrobenzoic Acid supermolecule is formed with 4 components that form amide-amide homosynthons, this leads to a ring, $R^2_2(8)$, and acid-pyridine interactions which leads to $D^1_1(2)$. These interactions extend to give 2-D cross linked laddered networks.

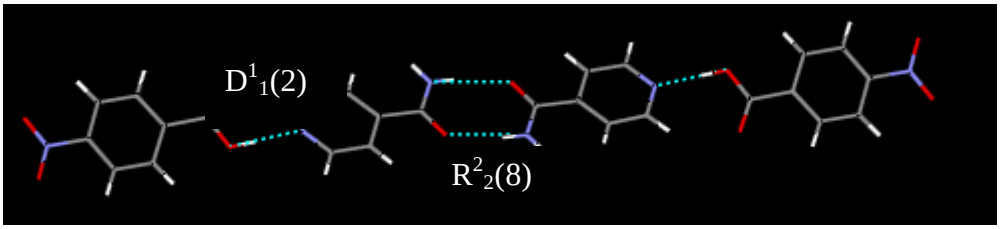

BUDWEC

Four component supermolecule are formed by amide-amide homosynthon, forming a $R^2_2(8)$ ring and an acid-pyridine interactions leading to a $D^1_1(2)$, these are extended to give cross linked ladder networks.

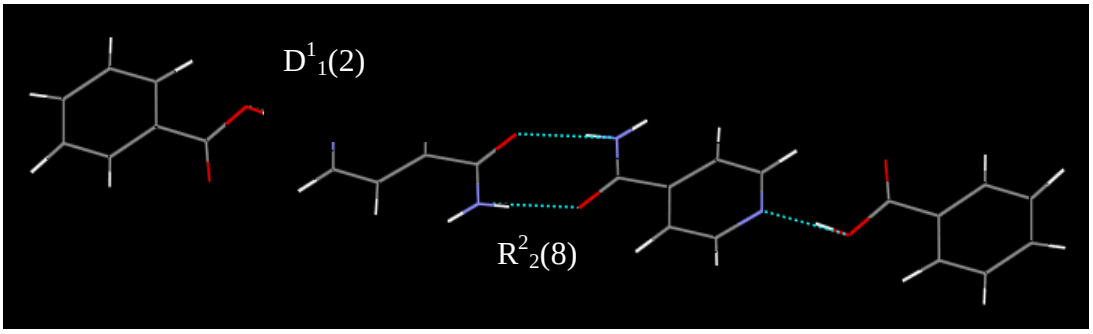

BZASUC

Here the Benzamide: Succinic acid components are assembled via acid-amide heterosynthons, forming a dimer with a $R^2_2(8)$ ring. Once extended via the N-H···O interactions a tape configuration is formed and we observe a secondary ring formation of $R^4_6(22)$.

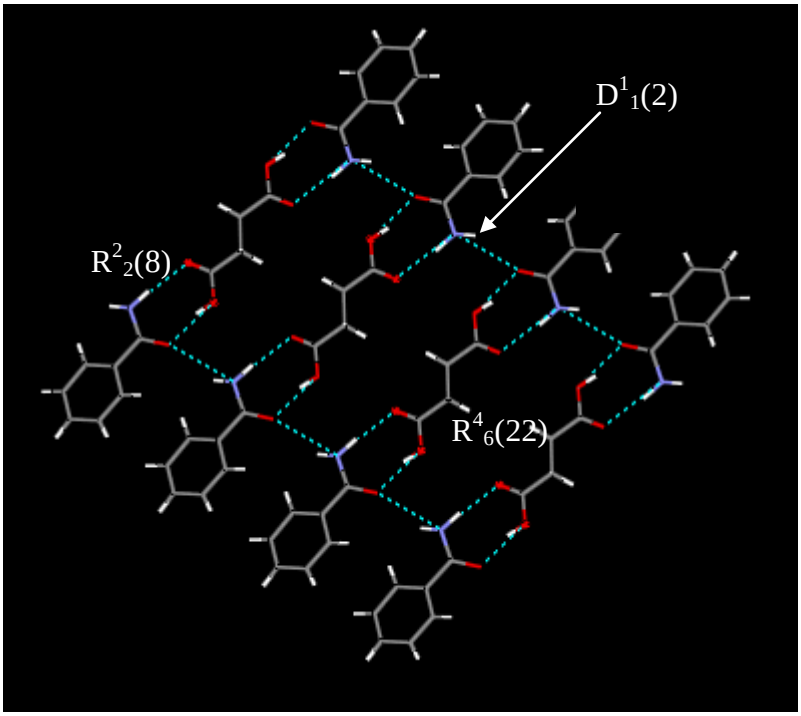

JAWWAG

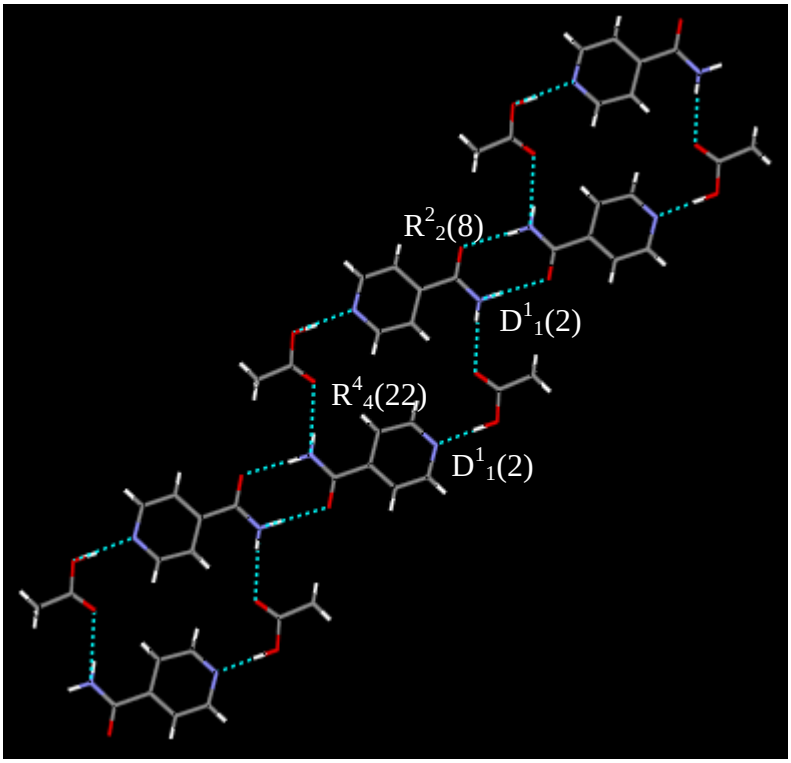

The structure of the Acetic Acid : Isonicotinamide co-crystal is formed with four components, where two of the Acetic Acid and two Isonicotinamide molecules are assembled via acid-pyridine synthon $D^1_1(2)$ and complementary amide-amide hydrogen interactions, forming a $R^2_2(8)$ ring. This co-crystal is extended to a 2D sheet formed via N-H···O and O-H···O hydrogen bonds between the supermolecules, this secondary ring can be denoted to have a graph set of $R^4_4(22)$.

LUNMAI

Isonicotinamide with Cinnamic Acid supermolecule is formed with 4 components that form amide-amide homosynthons, $R^2_2(8)$, and acid-pyridine interactions, when extended an infinite tape is formed, and a secondary ring, $R^4_4(22)$, via N-H···O and O-H···N hydrogen bonds between the supermolecules.

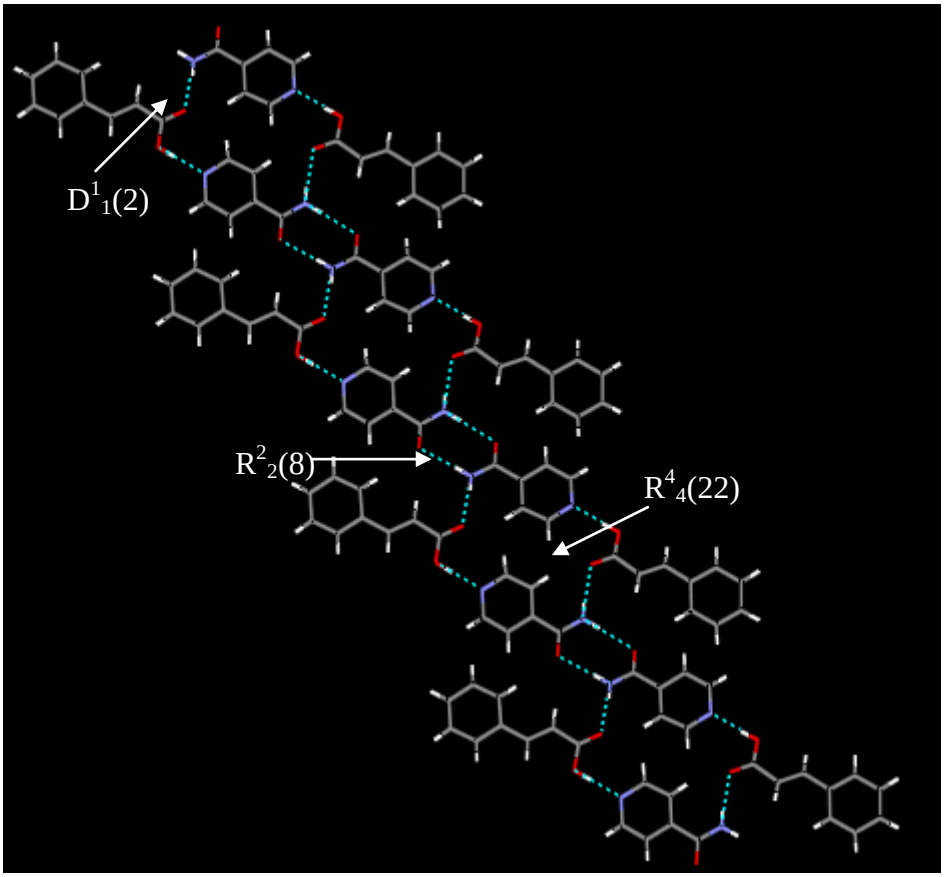

LUNMEM

Isonicotinamide forms amide-amide homosynthon, $R^2_2(8)$ with another Isonicotinamide, the primary aromatic nitrogen forms acid-amide interactions $D^1_1(2)$, once this is extended we see a 2-D cross linked laddered network.

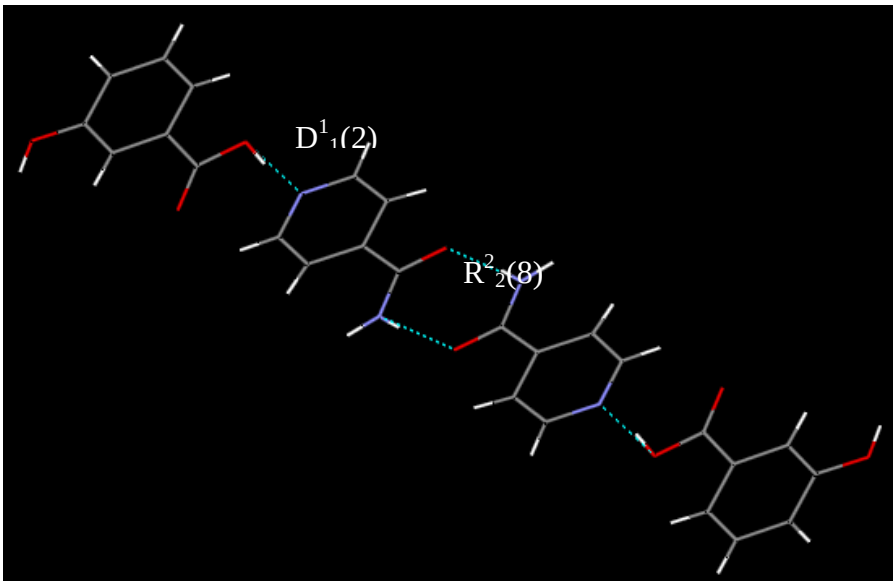

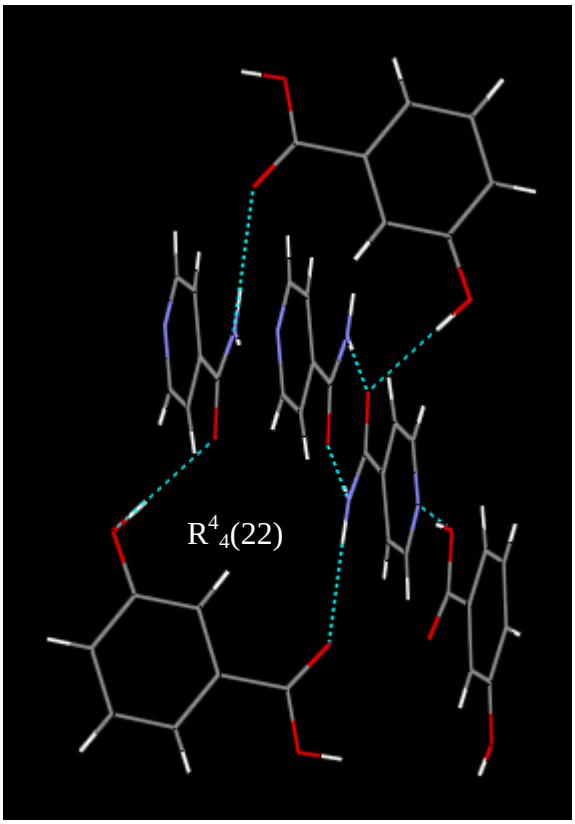

Within the ladder conformation, a secondary ring is formed via N-H···O and O-H···O hydrogen bonds, giving $R^4_4(22)$

LUNNOX

A 4 component supermolcule via acid-pyridine hydrogen bond interactions and self complementary amide-amide, $R^2_2(8)$ dimer, is observed. This extends to form a 1-D chain. Extension on N-H···O interaction between these chains give rise a 2-D sheet, within which a $R^6_6(26)$ ring is formed.

.

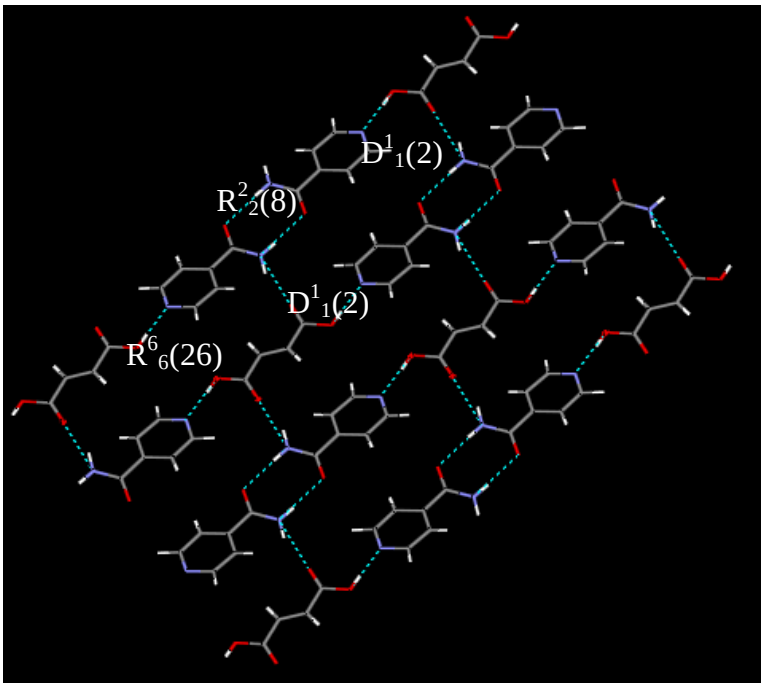

LUNNUD

This example of Succinic Acid with Isonicotinamide, forms the expected acid-Pyridine hydrogen bonds, $D^1_1(2)$, and homomeric self complementary amide-amide interaction $R^2_2(8)$. Further expansion of these structures via N-H···O interactions we see an infinite 1-D chain, which holds a $R^4_4(28)$ and $R^6_6(26)$ ring.

LUNNUD and LUNNUD01 are both the same crystal structures.

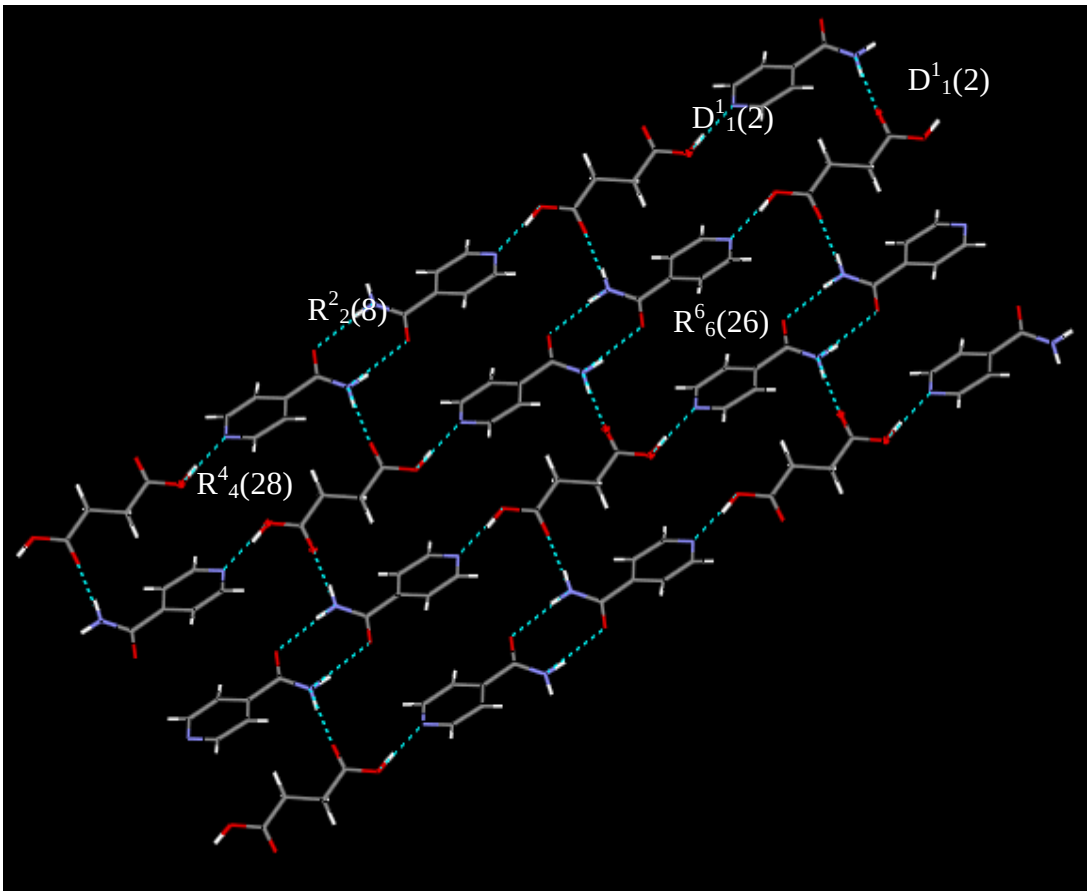

LUNNUD01

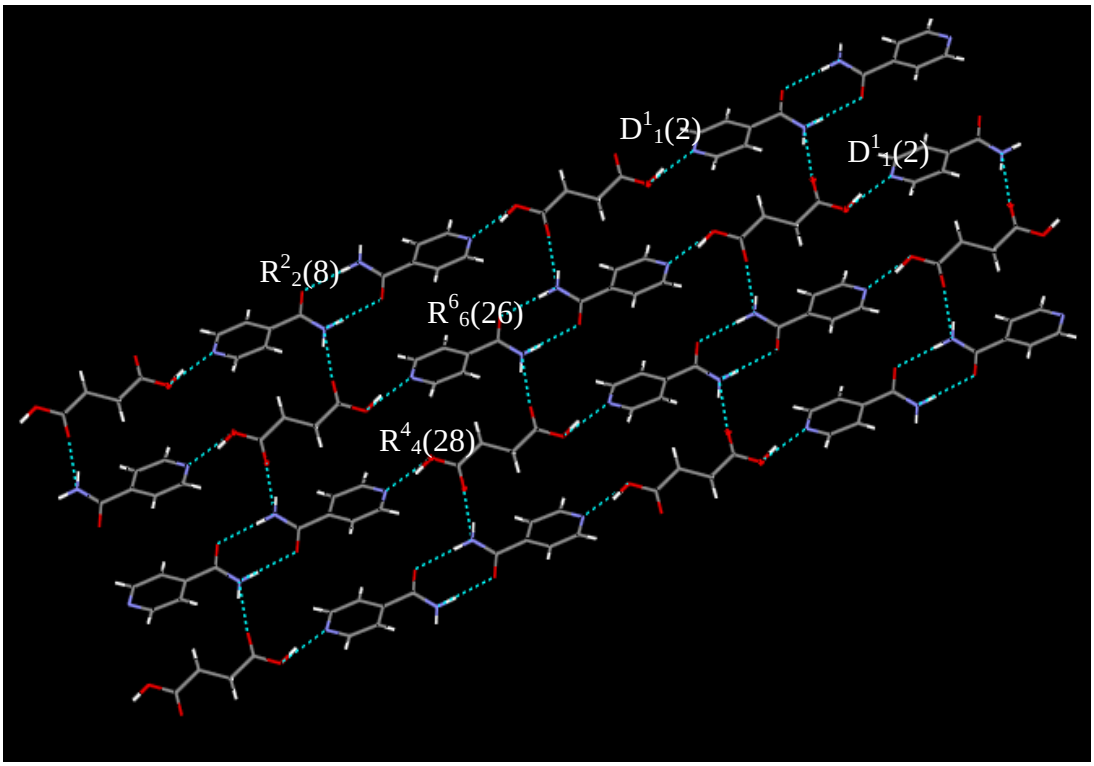

LUNPAL

The supermolcule is formed with 4 components, (2 Isonicotinamide and 2 Mandelic acid), these are assembled via acid-pyridine, $D^1_1(2)$, and complementary amide-amide hydrogen interactions, $R^2_2(8)$. When extended, this gives 2-D cross linked laddered network which consists of two secondary rings, $R^2_3(9)$ and $R^4_4(22)$.

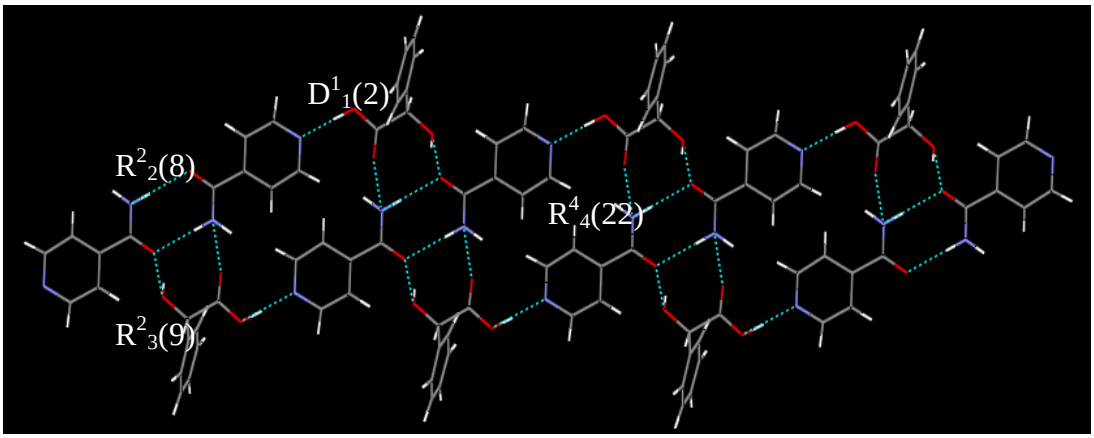

ULAWOT

A tape is formed with interaction between Glutaric acid group and the Pyridine of the Isonicotinamide. A sheet is formed via N-H···O and C-H···O interactions between the tapes resulting in the formation of $R^6_6(26)$.

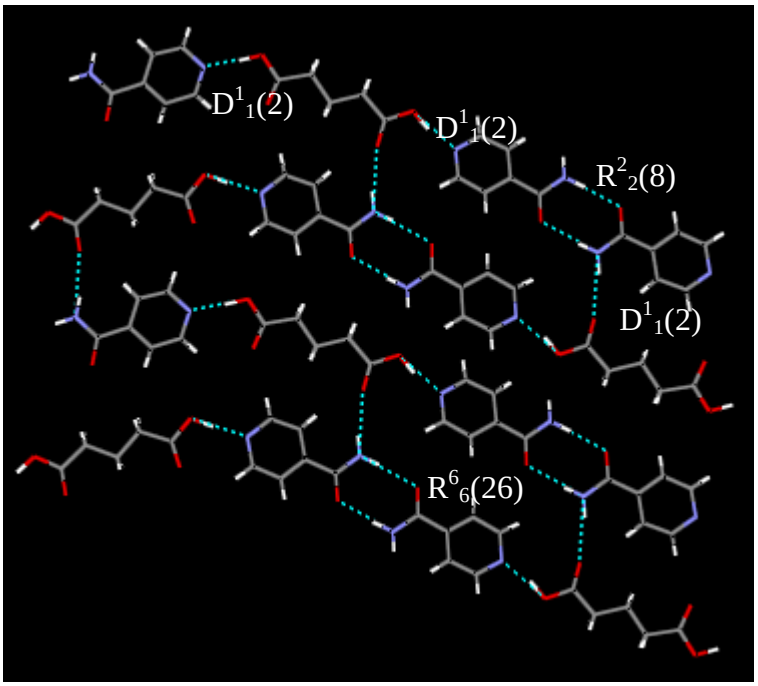

ULAWUZ

A tape is formed with interaction between Adipic acid group and the Pyridine of the Isonicotinamide. A sheet is formed via N-H···O interactions between the tapes as a result we see two secondary rings $R^4_4(22)$ and $R^6_6(36)$.

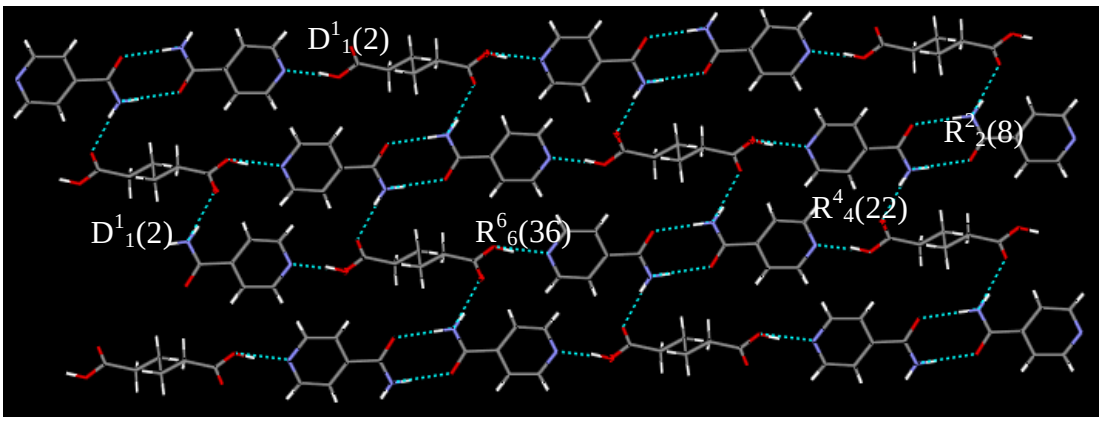

ULAXAG

Here we see that the COOH group of the Glutaric Acid is identical, however they hydrogen bond via different synthons, acid-pyridine giving a discrete interaction $D^1_1(2)$ and acid-amide interaction forming a dimer, $R^2_2(8)$. The molecule interacts to form tapes which are then connected via N-H···O hydrogen bonds between the tapes. From here a secondary ring of $R^4_4(22)$ is formed.

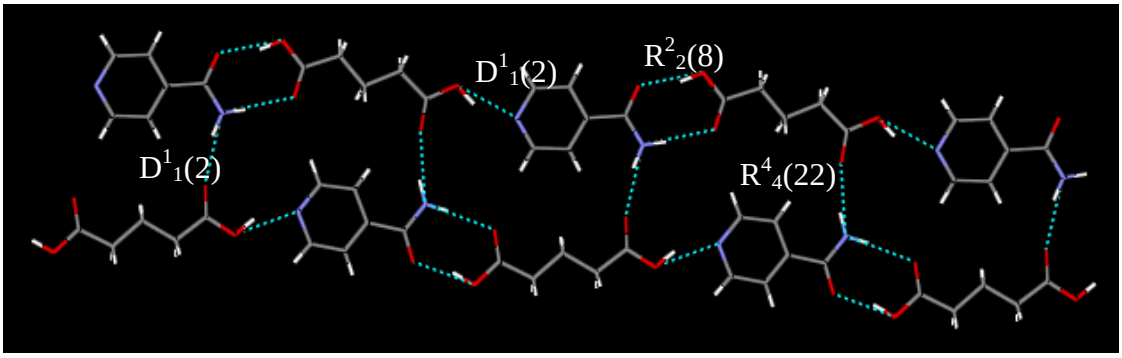

ULAXEK

A tape is formed via dimer interactions of the acid-amide interactions, $R^2_2(8)$, and acid-pyridine $D^1_1(2)$. A sheet is formed via N-H···O interactions between the tapes, this gives and extended ring of $R^6_6(38)$.

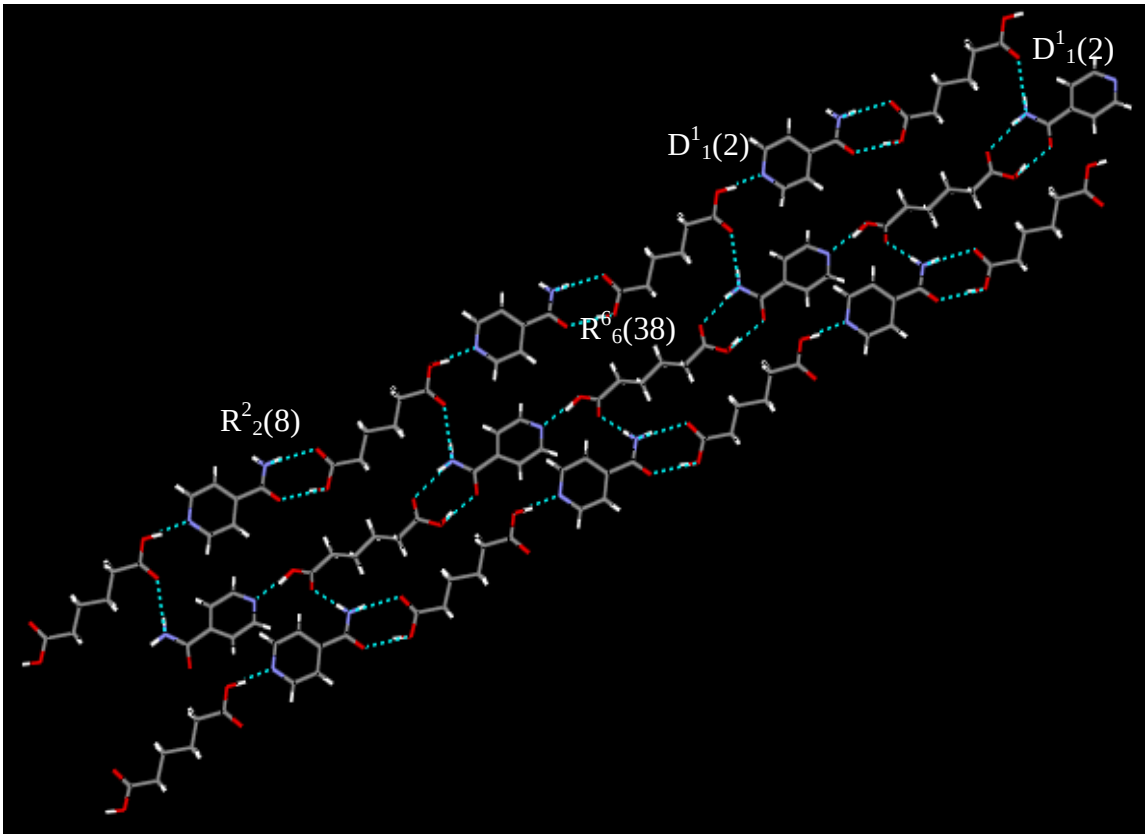

VAKTOR

Supermolecules are formed with 4 components, in the case of 4-Hydroxybenzoic Acid and Isonicotinamide a zigzag tape is formed, hydrogen interactions consist of phenol-pyridine, $D^1_1(2)$, and acid-amide heterodimer $R^2_2(8)$.

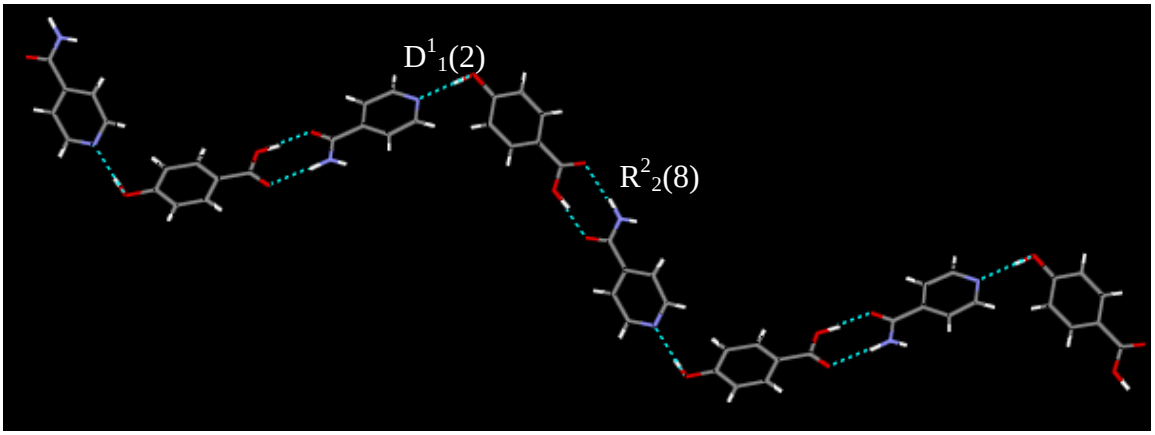

XAQQEM

The 2-Hydroxybenzoic Acid : Isonicotinamide co-crystal is an aggregate of four components these are assembled via acid-pyridine heterosynthons, $D^1_1(2)$, and homosynthon formed by amide-amide interactions, $R^2_2(8)$, from two Isonicotinamide molecules. There is also an intramolecular 6-membered hydrogen bond ring, $R^1_1(6)$, with the carbonyl group of the carboxylic acid. The four component units are extended into 2-D sheets via N-H···O that generate an infinite tape. This tape consists of a $R^2_4(8)$ ring.

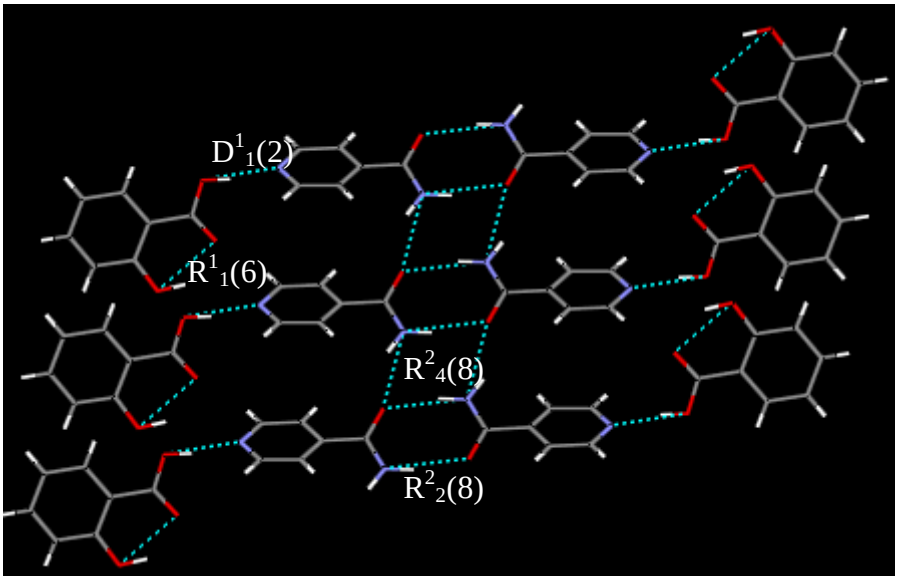

Appendix B: Critical peaks of New Benzamide co-crystal phases

Critical Peaks present in powder patterns of Benzamide co-crystal phases

Table Ba: Benzamide: Fumaric Acid Powder Pattern

Benzamide	Fumaric Acid	Co-crystal
8.027	18.520	6.02
15.796	22.859	10.052
18.016	24.574	11.906
	28.812	15.311
	29.417	

Table Bb: Benzamide: Tartaric Acid Powder Pattern

Benzamide	Tartaric Acid	Co-crystal
8.027	11.65	5.424
15.796	16.906	10.557
18.016	18.823	
	20.740	

Table Bc: Benzamide:3-Hydroxybenzoic Acid Powder Pattern

Benzamide	3-Hydroxybenzoic Acid	Co-crystal
8.027	7.724	9.297
15.796	16.401	14.015
18.016	16.704	
	19.428	

Table Bd: Benzamide: Mandelic Acid Powder Pattern

Benzamide	Mandelic Acid	Co-crystal
8.027	11.054	7.284
15.796	13.980	9.10
18.016	16.906	
	18.419	

Table Be: Benzamide:4-Nitrobenzoic Acid Powder Pattern

Benzamide	4-Nitrobenzoic Acid	Co-crystal
8.027	8.330	5.799
15.796	17.007	11.544
18.016	24.776	

Appendix C: Materials

Compound, suppliers, purity and batch identification number are given for all the materials used during experimental work at University of Bradford.

Active Ingredients

- Benzamide (batch number 521355-484) Purity 99%, Sigma-Aldrich Co. Ltd, Gillingham, Dorset
- Isonicotinamide (batch number 14725DE) Purity 99%, Sigma-Aldrich Co. Ltd, Gillingham, Dorset
- Nicotinamide (Lot & filling code number 1347071/22507P08) Purity 99%, Fluka, Riedel –de Haën®, Sigma-Aldrich Labrochemikalien GmbH

Coformer Acids

- Adipic Acid (Lot number A016837701) Purity 99%, Acros Organics, New Jersey, USA
- Benzoic Acid(batch number 10505AE) Purity 99%, Sigma-Aldrich Co. Ltd, Gillingham, Dorset
- 2-hydroxybenzoic Acid(batch number 066K3666) Purity 99%, Sigma-Aldrich Co. Ltd, Gillingham, Dorset
- 3-hydroxybenzoic Acid(batch number S15664-434) Purity 99%, Sigma-Aldrich Co. Ltd, Gillingham, Dorset
- 4-hydroxybenzoic Acid(batch number S17122-465) Purity 99%, Sigma-Aldrich Co. Ltd, Gillingham, Dorset
- Succinic acid(batch number 058K0706) Purity ≥99%, Sigma-Aldrich Co. Ltd, Gillingham, Dorset
- Fumaric Acid(Lot number A016609001) Purity 99%, Acros Organics, New Jersey, USA
- Tartaric Acid(batch number 504823-227) Purity 99%, Sigma-Aldrich Co. Ltd, Gillingham, Dorset
- Glutaric Acid(Lot number A009716901) Purity 99%, Acros Organics, New Jersey, USA
- Mandelic Acid(batch number U11516) Purity 99%, Sigma-Aldrich Co. Ltd, Gillingham, Dorset
- 4-nitrobenzoic Acid(batch number 521355-484) Purity 99%, Sigma-Aldrich Co. Ltd, Gillingham, Dorset
- Cinnamic Acid(batch number S23228-065) Purity 99%, Sigma-Aldrich Co. Ltd, Gillingham, Dorset

Solvents

- Methanol (batch number 0768457, 0919133, 0950855, 0958514) Purity 99.99% (HPLC grade), Fisher-Scientific UK Ltd, Bishop Meadow Road, Loughborough, Leics. Sigma-Aldrich Co. Ltd, Gillingham, Dorset

- Ethanol (batch number 0892401, 0892401) Purity 99.99% (HPLC grade), Fisher-Scientific UK Ltd, Bishop Meadow Road, Loughborough, Leics. Sigma-Aldrich Co. Ltd, Gillingham, Dorset
- Tetrahydrofuran(Lot number K29133125) 99.99% , BDH, Laboratory supplies, Poole, UK
- Ethyl Acetate (batch number 80015) Purity 99.99% (HPLC grade), Sigma-Aldrich Co. Ltd, Gillingham, Dorset

Water used was double distilled, Milli-RO®15 Water Purification System and Milli-Q® Reagent Grade Water System

Appendix D: Single crystal Data

Detailed crystal structure data from CIF files of Benzamide Fumaric and 4-nitrobenzoic acid Co-crystals.

Title Benzamide:Fumaric Acid

Hafsa Shamim Javed

Department of Pharmacy, University of Bradford, IPI Building, Richmond Road, Bradford, West Yorkshire, BD7 1DP, UK

Correspondence e-mail: h.s.javed@bradford.ac.uk

(BZAMD_FA)

Crystal data

$C_9H_9N_1O_3$	D_x = 1.419 Mg m^{-3}
M_r = 179.18	Melting point:? K
Monoclinic, $P2_1/n$	Mo $K\alpha$ radiation λ = 0.71073 Å
Hall symbol: ?	Cell parameters from 2331 reflections
a = 5.318 (6) Å	θ = 4–28°
b = 5.351 (6) Å	μ = 0.11 mm^{-1}
c = 29.64 (4) Å	T = 150 K
β = 96.03 (5)°	Cell measurement pressure: ? kPa
V = 838.8 (18) Å^3	Block, colourless
Z = 4	0.40 × 0.30 × 0.25 mm
F_{000} = 376	

Data collection

Rigaku R-AXIS RAPID Image Plate diffractometer	3322 measured reflections
Radiation source: ?	1296 independent reflections
Monochromator: graphite	969 reflections with $I > 2.0\sigma(I)$
Detector resolution: ? pixels mm^{-1}	R_{int} = 0.048
T = 150 K	θ_{max} = 27.5°
P = ? kPa	θ_{min} = 3.8°
ω scans	h = −6→6
Absorption correction: multi-scan FSPROCESS	k = −6→6
T_{min} = 0.90, T_{max} = 0.97	l = −38→38

Refinement

Refinement on F^2	Secondary atom site location: ?
Least-squares matrix: full	Hydrogen site location: inferred from neighbouring sites
$R[F^2 > 2\sigma(F^2)]$ = 0.057	H atoms treated by a mixture of independent and constrained refinement
$wR(F^2)$ = 0.192	Method = Modified Sheldrick $w = 1/[\sigma^2(F^2) + (0.13P)^2 + 0.02P]$, where $P = (\max(F_o^2, 0) + 2F_c^2)/3$
S = 1.04	$(\Delta/\sigma)_{max}$ = 0.0002
1291 reflections	$\Delta\rho_{max}$ = 0.31 e $Å^{-3}$
128 parameters	$\Delta\rho_{min}$ = −0.26 e $Å^{-3}$
? constraints	Extinction correction: Larson (1970), Equation 22
Primary atom site location: structure-invariant direct methods	Extinction coefficient: 150 (60)

Fractional atomic coordinates and isotropic or equivalent isotropic displacement parameters (Å^2)

	x	y	z	U_{iso}*/U_{eq}
C1	0.8791 (5)	−0.9717 (5)	0.49571 (8)	0.0224
C2	0.7848 (6)	−0.7569 (5)	0.46707 (8)	0.0217
O3	0.9586 (4)	−0.6423 (4)	0.44584 (6)	0.0320
O4	0.5658 (4)	−0.6942 (4)	0.46395 (7)	0.0362
C5	0.5092 (5)	0.0164 (5)	0.35356 (8)	0.0210
C6	0.5736 (5)	−0.1817 (5)	0.38860 (8)	0.0198
O7	0.7915 (4)	−0.2663 (4)	0.39453 (6)	0.0287
N8	0.3883 (5)	−0.2589 (5)	0.41218 (7)	0.0265
C9	0.3064 (5)	0.1788 (6)	0.35469 (9)	0.0265
C10	0.2602 (6)	0.3617 (6)	0.32154 (9)	0.0302
C11	0.4133 (6)	0.3790 (5)	0.28698 (9)	0.0289
C12	0.6141 (6)	0.2187 (5)	0.28545 (8)	0.0290
C13	0.6656 (6)	0.0392 (5)	0.31881 (8)	0.0243
H11	0.7527	−1.0792	0.5092	0.0273*
H91	0.1932	0.1646	0.3795	0.0324*
H101	0.1160	0.4805	0.3228	0.0364*
H111	0.3780	0.5087	0.2629	0.0344*
H121	0.7235	0.2318	0.2601	0.0350*

H131	0.8152	−0.0734	0.3180	0.0299*
H81	0.427 (6)	−0.400 (7)	0.4311 (10)	0.0324*
H82	0.217 (7)	−0.215 (6)	0.4032 (10)	0.0324*
H31	0.884 (6)	−0.504 (7)	0.4288 (11)	0.0389*

Atomic displacement parameters (Å^2)

	U^{11}	U^{22}	U^{33}	U^{12}	U^{13}	U^{23}
C1	0.0193 (16)	0.0231 (17)	0.0257 (13)	−0.0052 (12)	0.0067 (9)	0.0040 (10)
C2	0.0215 (18)	0.0205 (17)	0.0239 (13)	−0.0029 (13)	0.0065 (9)	0.0020 (9)
O3	0.0209 (13)	0.0351 (15)	0.0417 (12)	0.0024 (9)	0.0120 (8)	0.0225 (9)
O4	0.0216 (14)	0.0358 (15)	0.0524 (13)	0.0020 (10)	0.0096 (8)	0.0221 (9)
C5	0.0229 (18)	0.0171 (16)	0.0228 (12)	−0.0057 (13)	0.0011 (9)	−0.0011 (9)
C6	0.0172 (17)	0.0186 (15)	0.0240 (12)	−0.0017 (13)	0.0044 (9)	−0.0026 (9)
O7	0.0239 (14)	0.0306 (14)	0.0323 (11)	0.0027 (10)	0.0056 (7)	0.0110 (8)
N8	0.0220 (15)	0.0274 (16)	0.0315 (13)	0.0061 (12)	0.0094 (9)	0.0080 (10)
C9	0.0252 (17)	0.0240 (18)	0.0311 (14)	0.0055 (13)	0.0061 (10)	0.0011 (10)
C10	0.0272 (19)	0.0212 (18)	0.0412 (16)	−0.0001 (14)	−0.0008 (11)	0.0029 (11)
C11	0.034 (2)	0.0187 (17)	0.0322 (14)	−0.0044 (14)	−0.0052 (11)	0.0061 (10)
C12	0.034 (2)	0.0267 (18)	0.0272 (14)	−0.0001 (15)	0.0064 (10)	0.0061 (10)

C13	0.0226 (18)	0.0221 (17)	0.0290 (14)	0.0005 (13)	0.0058 (9)	0.0009 (10)

Geometric parameters (Å, °)

C1—C1^{i}	1.319 (6)	N8—H81	0.95 (3)
C1—C2	1.484 (4)	N8—H82	0.95 (4)
C1—H11	1.000	C9—C10	1.390 (4)
C2—O3	1.322 (3)	C9—H91	1.000
C2—O4	1.206 (4)	C10—C11	1.377 (5)
O3—H31	0.96 (4)	C10—H101	1.000
C5—C6	1.498 (4)	C11—C12	1.374 (4)
C5—C9	1.388 (4)	C11—H111	1.000
C5—C13	1.396 (4)	C12—C13	1.385 (4)
C6—O7	1.240 (3)	C12—H121	1.000
C6—N8	1.332 (4)	C13—H131	1.000

C1^{i}—C1—C2	123.5 (3)	C5—C9—C10	120.3 (3)
C1^{i}—C1—H11	118.2	C5—C9—H91	120.0
C2—C1—H11	118.2	C10—C9—H91	119.8
C1—C2—O3	114.8 (3)	C9—C10—C11	119.9 (3)
C1—C2—O4	121.7 (2)	C9—C10—H101	120.1
O3—C2—O4	123.5 (3)	C11—C10—H101	120.0
C2—O3—H31	110 (2)	C10—C11—C12	120.3 (3)
C6—C5—C9	123.2 (2)	C10—C11—H111	119.8
C6—C5—C13	117.6 (2)	C12—C11—H111	119.8
C9—C5—C13	119.2 (2)	C11—C12—C13	120.4 (3)
C5—C6—O7	119.9 (2)	C11—C12—H121	119.8
C5—C6—N8	117.1 (3)	C13—C12—H121	119.8
O7—C6—N8	123.0 (3)	C5—C13—C12	119.9 (3)

C6—N8—H81	115.4 (18)	C5—C13—H131	120.1
C6—N8—H82	121.0 (18)	C12—C13—H131	120.0
H81—N8—H82	120 (3)		

Symmetry codes: (i) −*x*+2, −*y*−2, −*z*+1.

Hydrogen-bond geometry (Å, °)

D—H···*A*	*D*—H	H···*A*	*D*···*A*	*D*—H···*A*
N8—H81···O4	0.95	1.95	2.893 (2)	169
O3—H31···O7	0.96	1.67	2.620 (2)	171

Refinement

Hydrogen atoms were located in geometrically defined positions and refined as riding groups, except for those involved in hydrogen bonds. The three hydrogen bonded protons were studied using 2 dimensional difference Fourier maps to check for potential site disorder; none was observed. The protons were placed geometrically and their positions refined.

Computing details

Data collection: d*trek/*CrystalClear*; cell refinement: FSProcess/*CrystalClear*; data reduction: FSProcess/*CrystalClear*; program(s) used to solve structure: *SIR92* (Altomare *et al.*, 1994); program(s) used to refine structure: *CRYSTALS* (Betteridge *et al.*, 2003); molecular graphics: Mercury; software used to prepare material for publication: *CRYSTALS* (Betteridge *et al.*, 2003).

Benzamide: 4-Nitrobenzoic Acid

Crystal data

$C_{14}H_{12}N_2O_4$	F_{000} = 284
M_r = 272.26	D_x = 1.418 Mg m^{-3}
?, ?	Melting point: ? K
Hall symbol: ?	Mo $K\alpha$ radiation λ = 0.71073 Å
a = 6.3184 (4) Å	Cell parameters from ? reflections
b = 6.8802 (5) Å	θ = ?–?°
c = 15.6401 (11) Å	μ = 0.11 mm^{-1}
α = 95.749 (5)°	T = 296 (2) K
β = 98.806 (4)°	Cell measurement pressure: ? kPa
γ = 106.239 (4)°	?, ?
V = 637.72 (8) Å^3	0.31 × 0.14 × 0.06 mm
Z = 2	

Data collection

? diffractometer	1849 reflections with $I > 2\sigma(I)$
Radiation source: fine-focus sealed tube	R_{int} = 0.077

Monochromator: graphite	θ_{max} = 27.3°
T = 296(2) K	θ_{min} = 1.3°
P = ? kPa	h = −8→8
Absorption correction: ?	k = −8→8
27857 measured reflections	l = −19→20
2815 independent reflections	Standard reflections: ?

Refinement

Refinement on F^2	Hydrogen site location: inferred from neighbouring sites
Least-squares matrix: full	H atoms treated by a mixture of independent and constrained refinement
$R[F^2 > 2\sigma(F^2)]$ = 0.120	$w = 1/[\sigma^2(F_o^2) + (0.1P)^2]$ where $P = (F_o^2 + 2F_c^2)/3$
$wR(F^2)$ = 0.317	$(\Delta/\sigma)_{max}$ = 0.032
S = 1.93	$\Delta\rho_{max}$ = 1.20 e Å^{-3}
2815 reflections	$\Delta\rho_{min}$ = −0.38 e Å^{-3}
190 parameters	Extinction correction: none
? constraints	Absolute structure: ?
Primary atom site location: structure-invariant direct methods	Flack parameter: ?
Secondary atom site location: difference Fourier map	Rogers parameter: ?

Refinement of F^2 against ALL reflections. The weighted *R*-factor *wR* and goodness of fit S are based on F^2, conventional *R*-factors *R* are based on F, with F set to zero for negative F^2. The threshold expression of $F^2 > 2\text{sigma}(F^2)$ is used only for calculating *R*-factors(gt) *etc*. and is not relevant to the choice of reflections for refinement. *R*-factors based on F^2 are statistically about twice as large as those based on F, and R–factors based on ALL data will be even larger.

Fractional atomic coordinates and isotropic or equivalent isotropic displacement parameters ($Å^2$)

	x	y	z	U_{iso}*/U_{eq}
C5A	0.0776 (7)	0.1798 (7)	0.1871 (3)	0.0192 (10)
H5A	−0.0158	0.1409	0.1323	0.023*
C1A	0.1319 ( )	0.2382 (6)	0.3446 (3)	0.0175 (10)
C3A	0.4519 (7)	0.3079 (7)	0.2747 (3)	0.0229 (10)
H3A	0.6066	0.3508	0.2781	0.027*
C4A	0.3082 (7)	0.2453 (7)	0.1954 (3)	0.0205 (10)
C6A	−0.0091 (7)	0.1740 (7)	0.2622 (3)	0.0235 (11)
H6A	−0.1637	0.1268	0.2584	0.0 8*
C7A	0.0238 (7)	0.2271 (7)	0.4232 (3)	0.0224 (10)
C2A	0.3591 (7)	0.3055 (7)	0.3504 (3)	0.0228 (11)
H2A	0.4527	0.3502	0.4050	0.027*
O2A	−0.1759 (5)	0.1519 (6)	0.4192 (2)	0.0361 (10)
O1A	0.1657 (5)	0.3133 (6)	0.49628 (19)	0.0338 (10)

O3A	0.610 (6)	0.2948 (6)	0.1246 (2)	0.0400 (10)
O4A	0.2803 (6)	0.2012 (6)	0.0456 (2)	0.0362 (9)
N1A	0.4050 (7)	0.2472 (6)	0.1158 (3)	0.0280 (10)
C1B	0.7689 (7)	0.2642 (6)	0.7393 (3)	0.0213 (10)
C6B	0.5527 (7)	0.2172 (7)	0.7576 (3)	0.0260 (11)
H6B	0.4276	0.1831	0.7128	0.031*
C5B	0.5291 (8)	0.2227 (7)	0.8452 (3)	0.0267 (11)
H5B	0.3857	0.1871	0.8583	0.032*
C3B	0.9251 (8)	0.3298 (8)	0.8925 (3)	0.0291 (12)
H3B	1.0498	0.3709	0.9377	0.035*
C7B	0.8142 (7)	0.2548 (7)	0.6470 (3)	0.0211 (10)
C4B	0.7078 (8)	0.2779 (7)	0.9111 (3)	0.0285 (11)
H4B	0.6874	0.2817	0.9688	0.034*
C2B	0.9521 (7)	0.3192 (7)	0.8062 (3)	0.0198 (10)
H2B	1.0957	0.3497	0.7935	0.024*
O1B	1.0070 (5)	0.3173 (6)	0.6354 (2)	0.0361 (10)
N1B	0.6385 (7)	0.1820 (6)	0.5814 (2)	0.0300 (10)

Atomic displacement parameters (Å^2)

	U^{11}	U^{22}	U^{33}	U^{12}	U^{13}	U^{23}

C5A	0.018 (2)	0.023 (2)	0.014 (2)	0.0025 (18)	0.0002 (17)	0.0015 (18)
C1A	0.025 (2)	0.017 (2)	0.016 (2)	0.0117 (18)	0.0056 (17)	0.0059 (17)
C3A	0.017 (2)	0.023 (2)	0.033 (3)	0.0085 (18)	0.0085 (19)	0.007 (2)
C4A	0.028 (3)	0.017 (2)	0.020 (2)	0.0073 (19)	0.0118 (19)	0.0017 (18)
C6A	0.016 (2)	0.028 (3)	0.026 (2)	0.0054 (19)	0.0062 (19)	0.002 (2)
C7A	0.020 (2)	0.020 (2)	0.029 (3)	0.0079 (19)	0.0065 (19)	0.005 (2)
C2A	0.023 (2)	0.029 (3)	0.015 (2)	0.006 (2)	0.0039 (18)	0.0014 (19)
O2A	0.029 (2)	0.053 (2)	0.0205 (18)	0.0013 (17)	0.0103 (14)	−0.0003 (16)
O1A	0.0238 (18)	0.057 (2)	0.0154 (17)	0.0056 (16)	0.0060 (14)	−0.0008 (16)
O3A	0.029 (2)	0.063 (3)	0.0274 (19)	0.0107 (17)	0.0119 15)	0.0033 (17)
O4A	0.033 (2)	0.059 (3)	0.0179 (18)	0.0163 (17)	0.0033 (15)	0.0063 (16)
N1A	0.035 (3)	0.025 (2)	0.032 (2)	0.0112 (18)	0.023 (2)	0.0115 (18)
C1B	0.031 (3)	0.016 (2)	0.018 (2)	0.0060 (19)	0.0085 (19)	0.0019 (18)
C6B	0.021 (2)	0.028 (3)	0.030 (3)	0.0077 (19)	0.0065 (19)	0.007 (2)
C5B	0.028 (3)	0.025	0.029 (3)	0.009 (2)	0.013 (2)	0.000 (2)

		(3)				
C3B	0.034 (3)	0.036 (3)	0.014 (2)	0.009 (2)	0.0004 (19)	0.000 (2)
C7B	0.031 (3)	0.018 (2)	0.014 (2)	0.0059 (19)	0.0055 (19)	0.0040 (18)
C4B	0.044 (3)	0.021 (3)	0.027 (3)	0.013 (2)	0.018 (2)	0.005 (2)
C2B	0.020 (2)	0.025 (3)	0.016 (2)	0.0086 (18)	0.0030 (17)	0.0014 (18)
O1B	0.0230 (19)	0.058 (3)	0.0224 (18)	0.0013 (16)	0.0099 (14)	0.0060 (16)
N1B	0.031 (2)	0.037 (2)	0.020 (2)	0.0082 (18)	0.0046 (17)	0.0020 (17)

Geometric parameters (Å, °)

C5A—C6A	1.369 (6)	O4A—N1A	1.206 (5)
C5A—C4A	1.380 (6)	C1B—C2B	1.373 (6)
C1A—C2A	1.365 (6)	C1B—C6B	1.394 (6)
C1A—C6A	1.402 (6)	C1B—C7B	1.511 (6)
C1A—C7A	1.493 (6)	C6B—C5B	1.400 (7)
C3A—C4A	1.370 (6)	C5B—C4B	1.344 (7)
C3A—C2A	1.399 (6)	C3B—C2B	1.383 (6)
C4A—N1A	1.469 (6)	C3B—C4B	1.402 (7)

C7A—O2A	1.212 (5)	C7B—O1B	1.222 (5)
C7A—O1A	1.310 (5)	C7B—N1B	1.332 (6)
O3A—N1A	1.231 (5)		

C6A—C5A—C4A	117.8 (4)	O4A—N1A—C4A	118.8 (4)
C2A—C1A—C6A	119.7 (4)	O3A—N1A—C4A	117.8 (4)
C2A—C1A—C7A	122.8 (4)	C2B—C1B—C6B	120.2 (4)
C6A—C1A—C7A	117.6 (4)	C2B—C1B—C7B	117.0 (4)
C4A—C3A—C2A	118.0 (4)	C6B—C1B—C7B	122.8 (4)
C3A—C4A—C5A	123.1 (4)	C1B—C6B—C5B	118.2 (4)
C3A—C4A—N1A	118.2 (4)	C4B—C5B—C6B	121.8 (4)
C5A—C4A—N1A	118.7 (4)	C2B—C3B—C4B	119.2 (4)
C5A—C6A—C1A	121.0 (4)	O1B—C7B—N1B	122.7 (4)
O2A—C7A—O1A	123.6 (4)	O1B—C7B—C1B	119.5 (4)
O2A—C7A—C1A	123.3 (4)	N1B—C7B—C1B	117.7 (4)
O1A—C7A—C1A	113.1 (4)	C5B—C4B—C3B	119.8 (4)
C1A—C2A—C3A	120.4 (4)	C1B—C2B—C3B	120.7 (4)
O4A—N1A—O3A	123.4 (4)		

All e.s.d.'s (except the e.s.d. in the dihedral angle between two l.s. planes) are estimated using the full covariance matrix. The cell e.s.d.'s are taken into account individually in the estimation of e.s.d.'s in distances, angles and torsion angles; correlations between e.s.d.'s in cell parameters are only used when they are defined by crystal symmetry. An approximate (isotropic) treatment of cell e.s.d.'s is used for estimating e.s.d.'s involving

l.s. planes.

Computing details

Data collection: ?; cell refinement: ?; data reduction: ?; program(s) used to solve structure: *SHELXS97* (Sheldrick, 1990); program(s) used to refine structure: *SHELXL97* (Sheldrick, 1997); molecular graphics: ?; software used to prepare material for publication: ?.

Appendix E: Re-clustering of dSNAP results

Re-clustering has taken place where groups varied in similarity. These re-clustering have been presented by a dendrogram and all observations of sub-clustering have been listed in the corresponding tables. Please note that for each reclustered group the table is listed according to each coloured sub group which can be seen in the dendrogram, for example Group Aa refers to re-clustering of group A from the initial search, and the small case 'a' refers to the red cluster observed in the re-cluster.

Cluster A

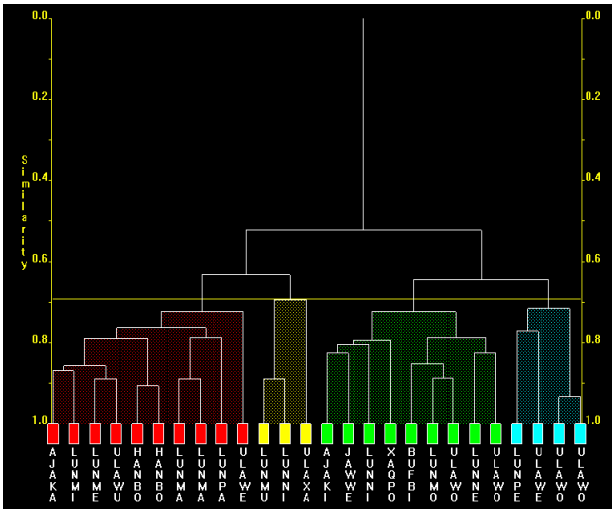

Group	
Aa	O2 is orientated towards N1
Ab	Similar to Aa slight offset
Ac	Similar to Aa slight offset
Ad	Similar to Aa slight offset

Cluster C

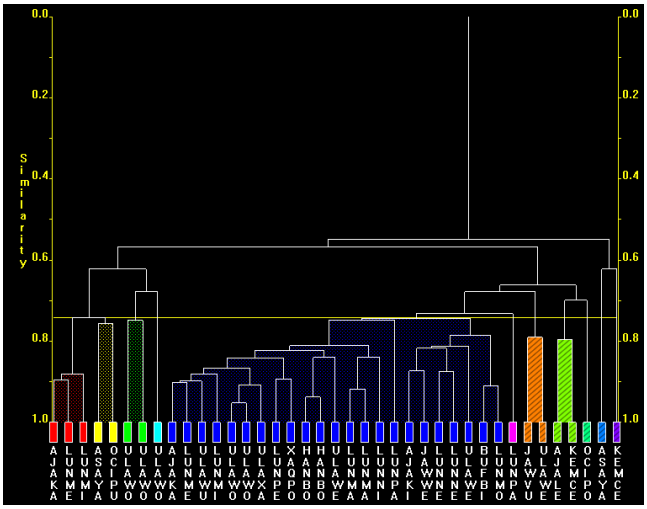

Group	
Ca	O2 positioned towards N1 of the Pyridine ring, slight offset in orientation to group A sub cluster
Cb	Acid group orientated above/below the ring group of primary amide
Cc (2 Fragments)	Frag 1, O2 orientated towards N1 of the pyridine ring on a slight offset Frag 2, O3 orientated towards the N1 of Pyridine ring, offset is in opposite direction of frag 1
Cd (1 fragment)	Orientated above/below the amide group, however not parallel to the amide group.
Ce	Orientation of acid group is next to the amide group, showing a lot of deviation, fur sub clustering required.
Cf	O3 is orientated towards the N1 of Pyridine, O3 is away from it
Cg	O2 orientated towards the N1 of Frag 1, Frag 2 is opposite, i.e. O3 both have offset positions in orientation
Ch	Acid groups orientated towards the amide group, both acids are facing in opposite directions
Ci	O3 orientated towards N1 of Pyridine
Cj	Acid positioned above/below amide, O2 orientated towards N2 or amide
Ck	Orientation is above/below the amide but facing the opposite way to the amide

Cluster E

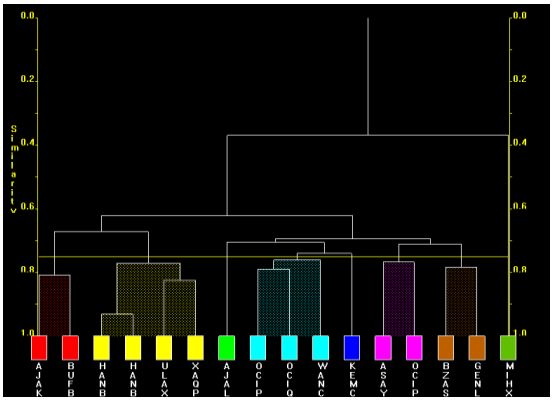

Group	
Ea	O3 and O2 facing the amide group forming a dimer
Eb	O3 and O2 facing the amide group forming a dimer
Ec	O3 and O2 facing the amide group forming a dimer
Ed	O3 and O2 facing the amide group forming a dimer
Ee	O3 and O2 facing the amide group forming a dimer
Ef	O3 and O2 facing the amide group forming a dimer
Eg	O3 and O2 facing the amide group forming a dimer
Eh	O3 and O2 facing the amide group forming a dimer

Cluster F

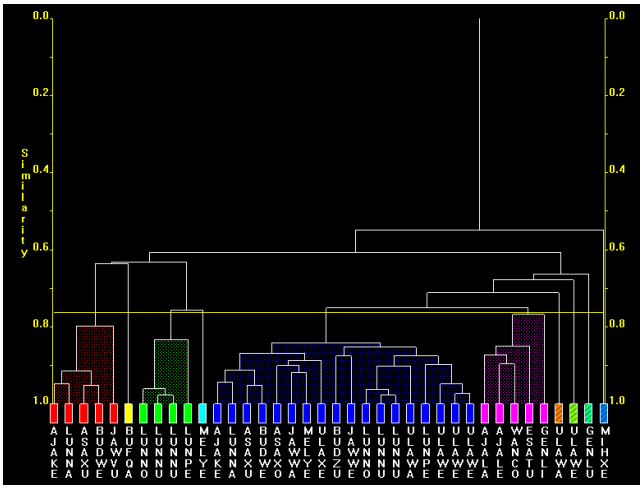

Group	
Fa	Acid group positioned near pyridine, above/below plane
Fb	Acid group positioned near pyridine, above/below plane
Fc	Acid group positioned opposite direction to amide above/below plane
Fd	Acid above/below plane, C7 of acid over N1, O3 away from amide, O2 facing O1 of amide but slightly offset.
Fe	Acid group next to amide, too much deviation needs to be reclustered
Ff	Further clustering required
Fg	Acid above/below plane, positioning is slightly offset of the amide
Fh	Position of acid is away from amide more near to pyridine where O3 is facing towards N2 of Pyridine
Fi	O3 positioned towards N1 of amide, O2 facing away from it
Fj	O3 positioned towards N1 of amide
Fk	O2 positioned towards N2 of amide, whereas O3 is away

Cluster G

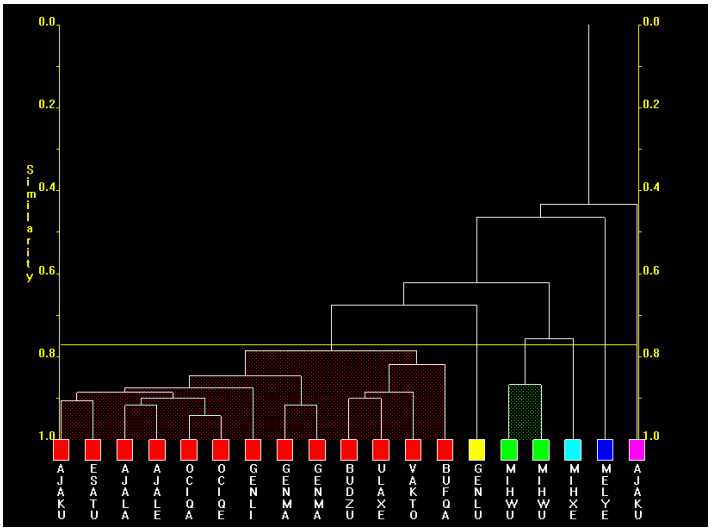

Group	
Ga	Ideal dimer is shown
Gb	Ideal dimer is shown
Gc	Ideal dimer is shown
Gd	Ideal dimer is shown
Ge	O2 facing N1 of amide, O3 is facing away
Gf	Acid group is above/below plane of amide, O2 directly above/below N1 as O3 is above/Below O1 of amide.

Cluster H

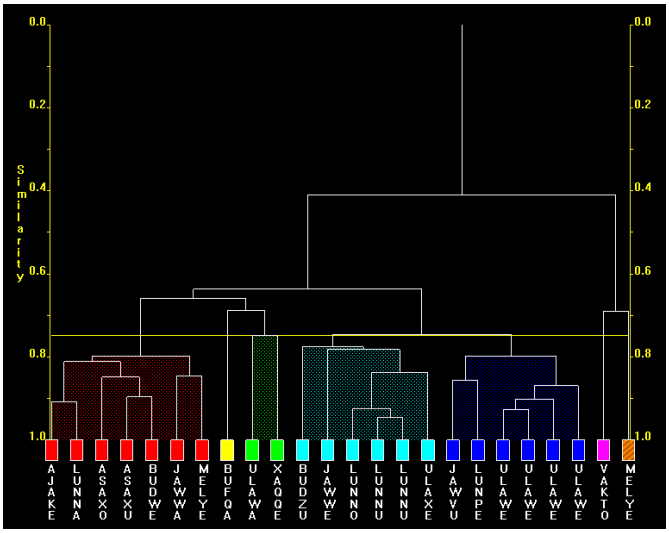

Group	
Ha	O2 facing N1 of pyridine, O3 pointing away
Hb	Both Oxygen's facing towards the Pyridine ring
Hc	Both Oxygen's facing towards the Pyridine ring but with a lot of deviation
Hd	O3 towards N1 of pyridine, O2 facing opposite direction
He	Acid is position to left/right of N1 of pyridine where O3 is towards N1
Hf	Acid is position to left/right of N1 of pyridine where O3 is towards N1
Hg	Acid group positioned left/right of pyridine, O3 is positioned near N1, O2 of acid is facing away.

Appendix F: High through put screen and polySNAP output

i) Plate format used for HTP

Active 1	Benzamide	Solvent 1	*o*-xylene
Active 2	Nicotinamide	Solvent 2	Isohexane
Active 3	Isonicotinamide	Solvent 3	Ethyl acetate
		Solvent 4	Methanol

Stoichiometric ratios per well

	1	2	3	4	5	6	7	8	9	10	11	12
A	2:1	1:2	1:1	2:1	1:2	1:1	2:1	1:2	1:1	2:1	1:2	1:1
B	1:1	2:1	1:2	1:1	2:1	1:2	1:1	2:1	1:2	1:1	2:1	1:2
C	1:2	1:1	2:1	1:2	1:1	2:1	1:2	1:1	2:1	1:2	1:1	2:1
D	2:1	1:2	1:1	2:1	1:2	1:1	2:1	1:2	1:1	2:1	1:2	1:1
E	1:1	2:1	1:2	1:1	2:1	1:2	1:1	2:1	1:2	1:1	2:1	1:2
F	1:2	1:1	2:1	1:2	1:1	2:1	1:2	1:1	2:1	1:2	1:1	2:1
G	2:1	1:2	1:1	2:1	1:2	1:1	2:1	1:2	1:1	2:1	1:2	1:1
H	1:1	2:1	1:2	1:1	2:1	1:2	1:1	2:1	1:2	1:1	2:1	1:2

Evaporation plate 1&3

	1	2	3	4	5	6	7	8	9	10	11	12
A	1	3	6	9	11	14	1	3	6	9	11	14
B	1	4	6	9	12	14	1	4	6	9	12	14
C	1	4	7	9	12	15	1	4	7	9	12	15
D	2	4	7	10	12	15	2	4	7	10	12	15
E	2	5	7	10	13	15	2	5	7	10	13	15
F	2	5	8	10	13	16	2	5	8	10	13	16
G	3	5	8	11	13	16	3	5	8	11	13	16
H	3	6	8	11	14	16	3	6	8	11	14	16
	Solvent 1						Solvent 2					

Evaporation plate 2&4

	1	2	3	4	5	6	7	8	9	10	11	12
A	1	3	6	9	11	14	1	3	6	9	11	14
B	1	4	6	9	12	14	1	4	6	9	12	14
C	1	4	7	9	12	15	1	4	7	9	12	15
D	2	4	7	10	12	15	2	4	7	10	12	15
E	2	5	7	10	13	15	2	5	7	10	13	15
F	2	5	8	10	13	16	2	5	8	10	13	16
G	3	5	8	11	13	16	3	5	8	11	13	16
H	3	6	8	11	14	16	3	6	8	11	14	16
	Solvent 3						Solvent 4					

ii) polySNAP analysis of plates BD002-6

a) Plate BD002

Cell Display

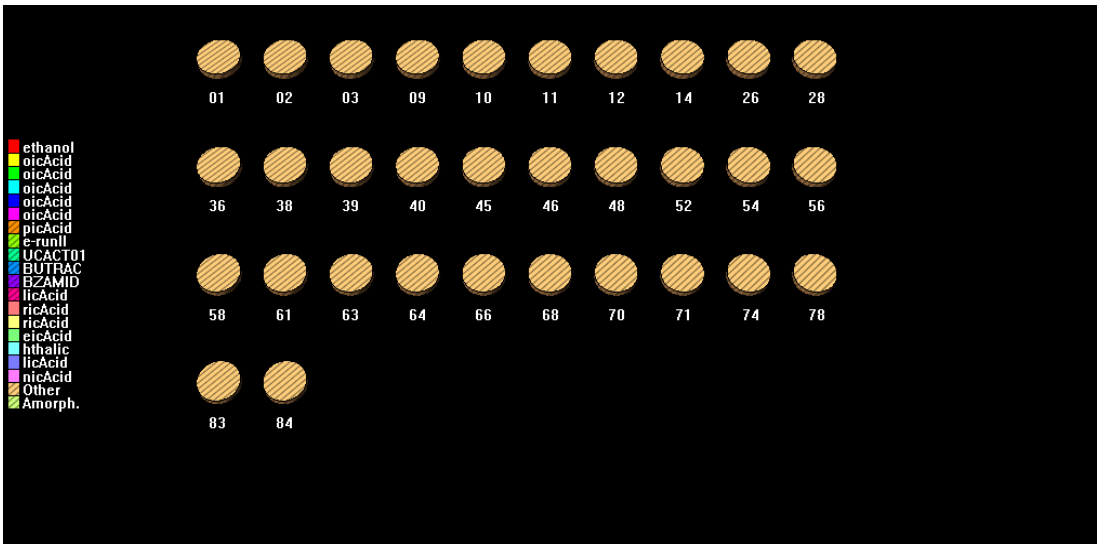

Dendrogram

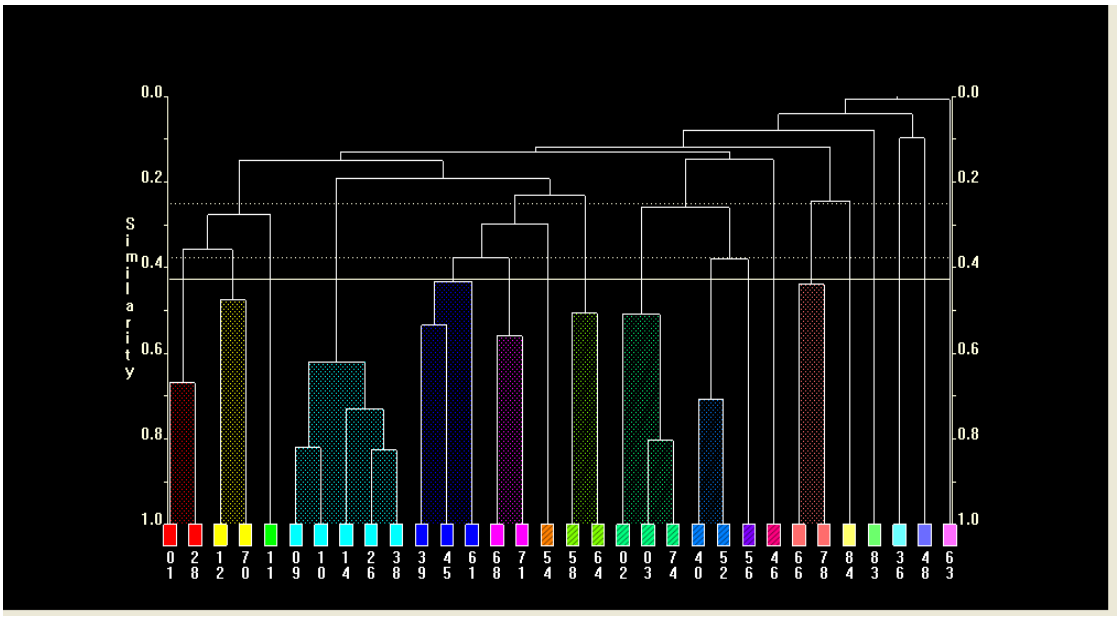

We exhibit a clustering from the dendrogram with 18 defined groups, these groups have been examined and highlighted in the table below.

Table Fa1: Summary of the clustering viewed from Dendrogram, these have been cross referenced with the plate format as shown in Appendix F * respectively to sample number column

Group	Sample Number	Coformer, (Composition ratios *)
Red	01, 28	1 (2:1) 9 (1:2)
Yellow	12, 70	12 (1:1) 10 (1:2)
Green	11	11, (1:2)
Light Blue	09, 10, 14, 26, 38	6 (1:1) 9 (2:1) 4 (2:1) (1:1) (1:2)
Blue	39, 45, 61,	7 (1:1) (1:1) 2 (1:2)
Pink	68, 71	5 (1:1) 13 (1:1)
Stripy Brown	54	15 (1:2)
Stripy Green	58, 64	10 (1:1) (1:2)
Stripy Greeny Blue	02, 03, 74	3 (1:2) 6 (1:1) 5 (1:2)
Stripy Light Blue	40, 52	10 (2:1) 15 (1:2)
Stripy Purple	56	5 (2:1)
Stripy Pink	46	10 (2:1)
Salmon Pink	66, 78	16 (2:1) (1:1)
Pastel Yellow	84	16 (1:1)
Pastel Green	83	13 (1:2)
Pastel Light Blue	36	15 (2:1)

Pastel Sky Blue	48	15 (1:1)
Pastel Pink	63	8 (2:1)

Figure Fa1: Various views of the 3D MMDS plots for plate 2

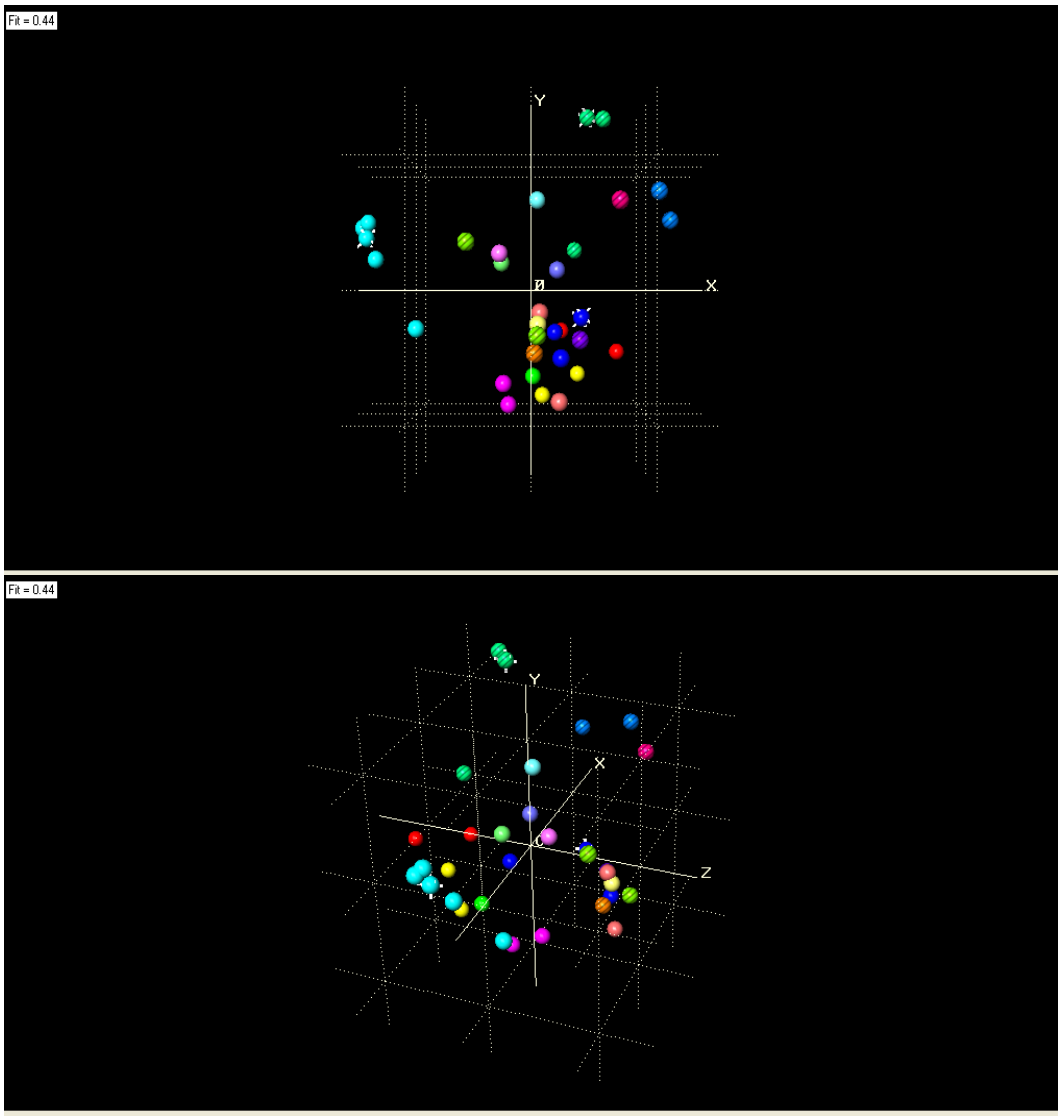

Figure Fa2: A zoomed in view of the MMDS plot of plate 2 showing samples 9 and 10, which cluster close together as compared to the other samples

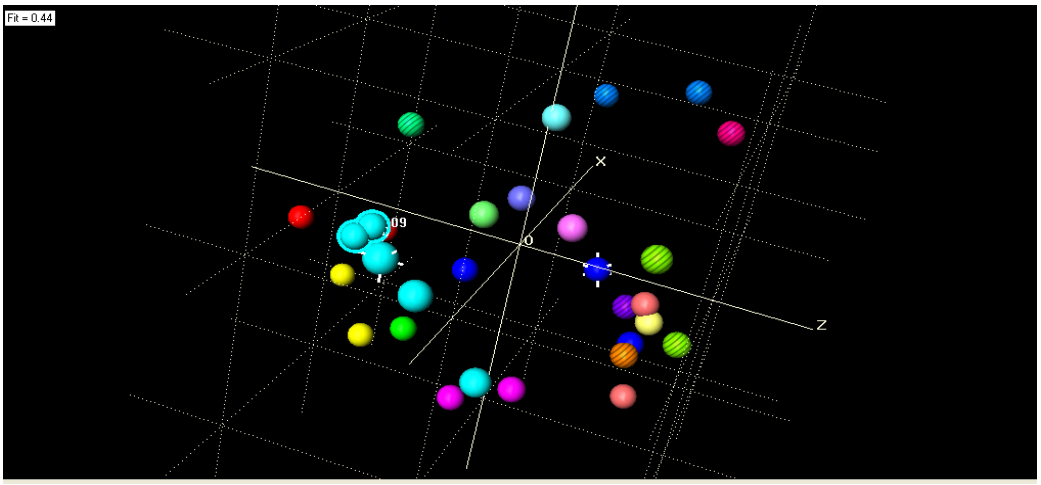

The MMDS plot has highlights that in the light blue cluster we samples 9 and 10 cluster together, Figure Fa2, cross reference of these samples with the dendrogram and the tabulated analysis above shows that these samples consist of component 6, (4-nitrobenzoic acid) with ratio of 1:1 and component 9 (Fumaric acid) with a ratio of 2:1. The samples have been overlaid in the pattern viewer and have been assigned a similarity rank of 0.821.

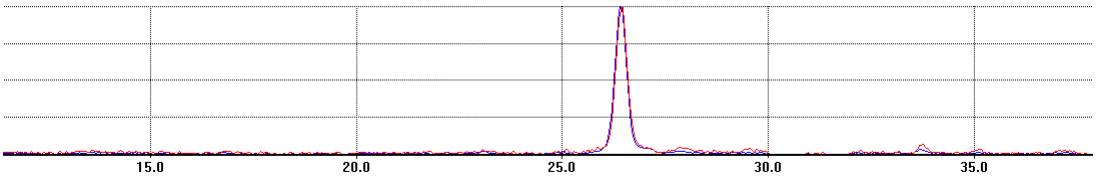

It is evident from this example that the quality of the pattern is poor with only one defined peak for these samples. It can only be suggested that there has been some contamination when handling the plate before the analysis.

Figure Fa3: MMDS plot of plate 2 showing samples 78 and 84, which cluster close together as compared to the other samples

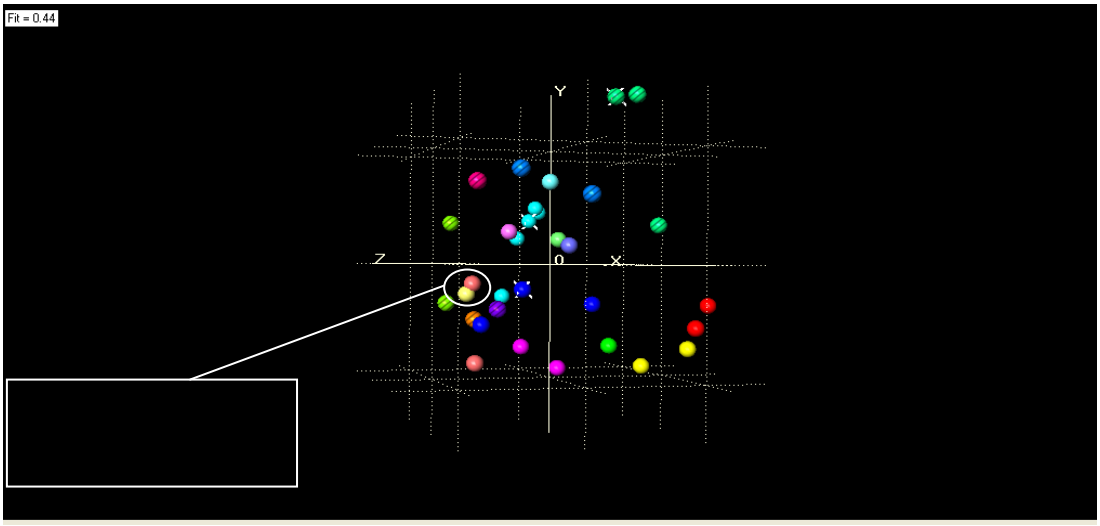

Rotating the 3D MMDS plot, Figure 5.11 we see that salmon pink (78) and pastel yellow (84) spheres are clustered close together. The PXRD pane shows the overlaid patterns of these samples.

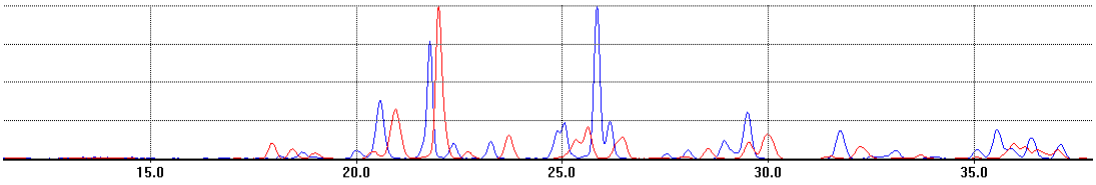

We see there is some similarity in the patterns with a slight shift, the quality of the pattern matching is poor for these samples. Using the dendrogram analysis, both the pastel yellow and salmon pink cluster sample consisting of Benzamide with conformer 16 which is Trans β hydromuconic acid. Although the salmon pink group has two samples clustered in the dendrogram, in the MMDS plot these are plotted with a significant distance between them. Below is the PXRD comparison of samples 78 and 84 with starting components Benzamide and Trans β hydromuconic acid, Figure Fa4.

Figure Fa4: Powder patterns display of the sample 78 and 86 overlaid with the pure components to identify peaks that suggest new phases

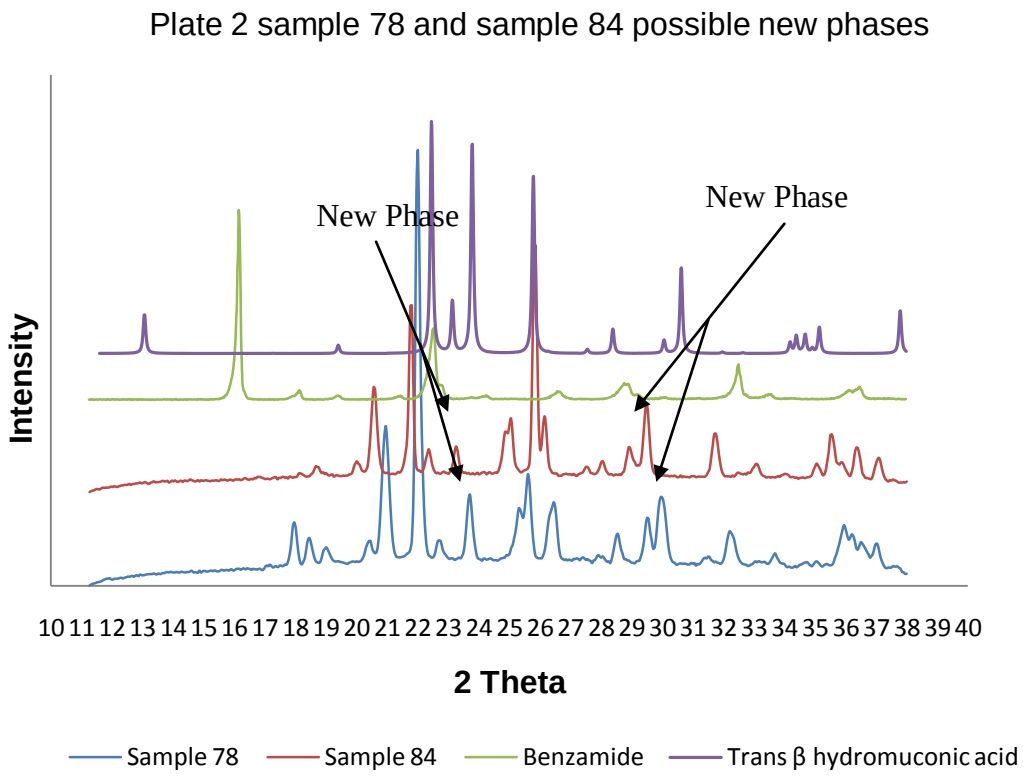

It seems to be evident that the samples from the screen are the same with a slight shift. A new peak has been highlighted between 20-22˚ 2θ and a peak between 24-26˚ 2θ which also seem to be new peaks not present in the starting components. However, further data from DSC and Raman maybe required and input into polySNAP to back up this sampling similarity.

b) Plate BD003

Cell display

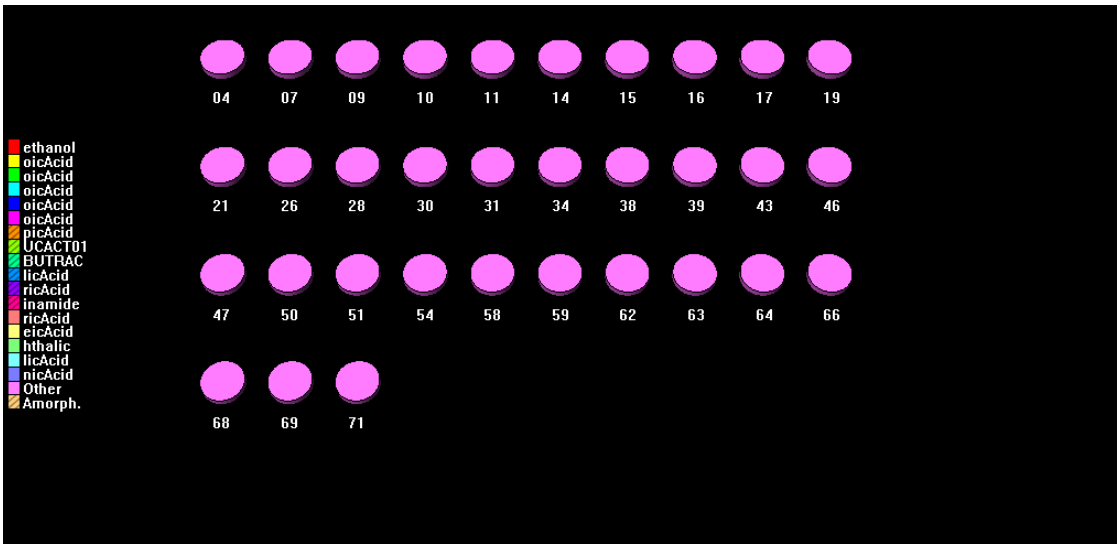

Dendrogram

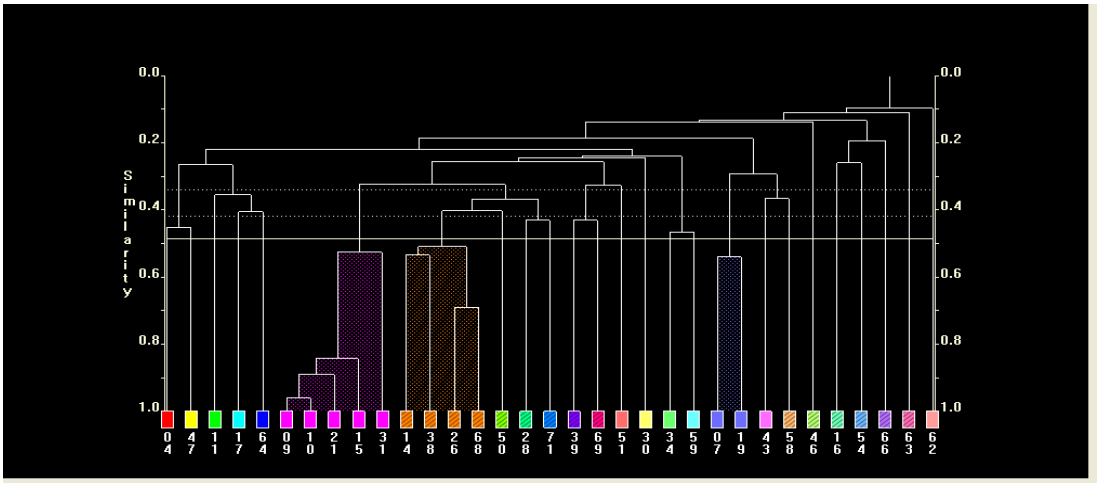

Table Fb1: Summary of the clustering viewed from Dendrogram, these have been cross referenced with the plate format as shown in Appendix F * respectively to sample number column

Group	Sample Number	Coformer, (Composition ratios *)
Red	04	9 (2:1)
Yellow	47	12 (1:2)
Green	11	11 (1:2)
Light Blue	17	12 (2:1)
Blue	64	10 (1:2)
Pink	09, 21, 15, 10, 31	6 (1:1), (1:2), 1:2) 9 (2:1) 1 (1:2)
Stripy Brown	14, 38, 26, 68	4 (2:1), (1:2), (1:1) 5 (1:1)
Stripy Green	50	5 (2:1)
Stripy Greeny Blue	28	9 (1:2)
Stripy Light Blue	71	13 (1:1)
Stripy Purple	39	7 (1:1)
Stripy Pink	69	8 (2:1)
Salmon Pink	51	7 (2:1)
Pastel Yellow	30	15 (2:1)
Pastel Green	34	9 (1:2)
Pastel Light Blue	59	13 (2:1)
Pastel Sky Blue	07, 19	1 (2:1) (1:1)
Pastel Pink	43	2 (2:1)
Stripy Brown	58	10 (1:1)
Stripy Green	46	10 (2:1)

Stripy Greeny Blue	16	9 (1:1)
Stripy Blue	54	15 (1:2)
Stripy Purple	66	16 (2:1)
Stripy Pink	63	8 (2:1)
Pale Orange	62	5 (1:1)

Figure Fb1: MMDS plot of plate 3

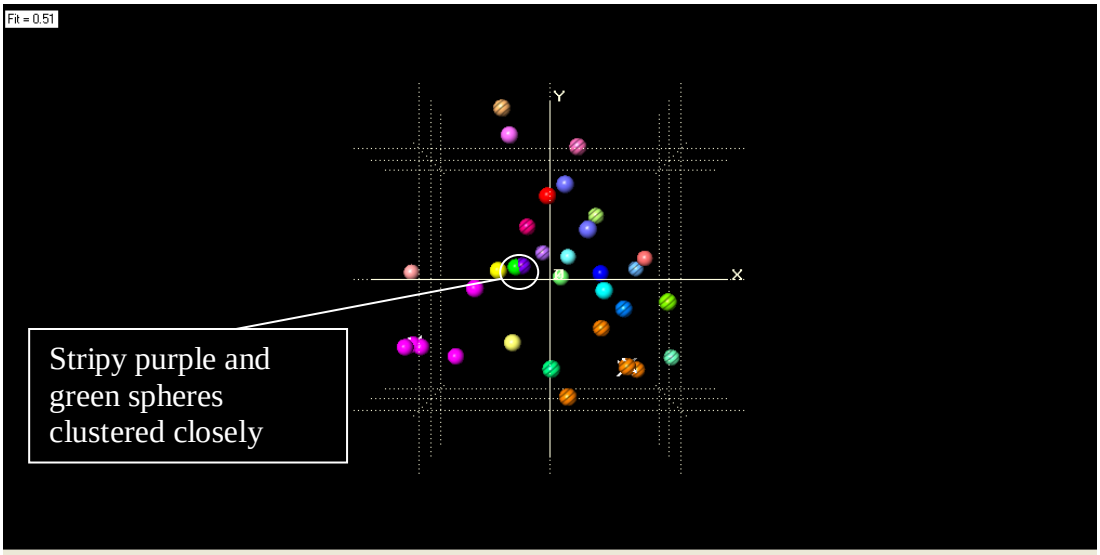

The purple stripy sphere and green sphere cluster very close together, Figure Fb1, however from overlaying the powder patterns, shown below Figure Fb2 we see the patterns are very different with a similarity rank of 0.190

Cross referencing these samples with the dendrogram analysis tabulated above, the stripy purple sample is sample 39, consisting of Isonicotinamide with co-former 7, Adipic acid, with a composition ratio of (1:1) and the sample clustered in the green group is Isonicotinamide with co-former 11 which is Malic acid with a composition ratio of (1:2).

Figure Fb2 Overlaid powder diffraction patterns as would be observed from the pattern viewing pane in polySNAP. Powder pattern red is the stripy purple sphere represented in the dendrogram, highlighted as sample 66 and blue is sample 11, which is the green sphere.

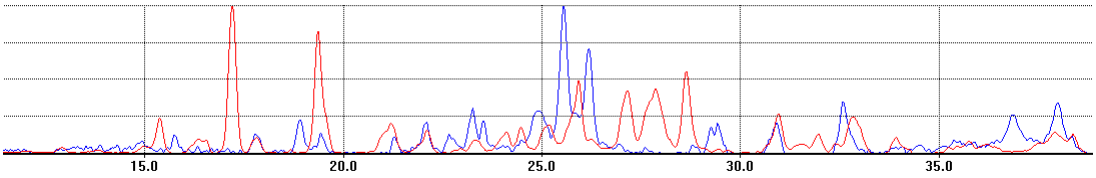

Further examination of the 3D MMDS plot shows a small cluster of the pink group. The close clustered spheres are samples 09 and 10, Figure Fb3.

Figure Fb3: MMDS plot of plate 3 showing samples 9 and 10, which cluster close together as compared to the other samples

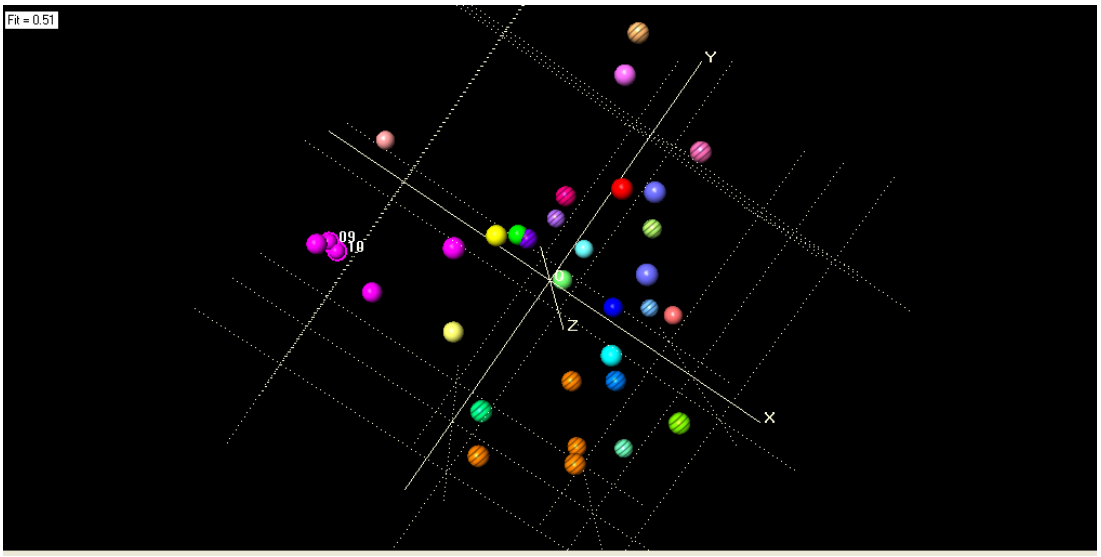

In the PXRD overlay pane below we see a strong similarity of the samples which polySNAP has ranked to have a similarity of 0.961. However, cross referencing this information with the dendrogram analysis shows that these two samples consist of Isonicotinamide with co-former 6 and 9, which are Adipic acid and Fumaric acid, respectively. This does not explain what the new phase is and how it is similar unless there has been some cross contamination during the screening process or when transporting to Pharmorphix for PXRD analysis.

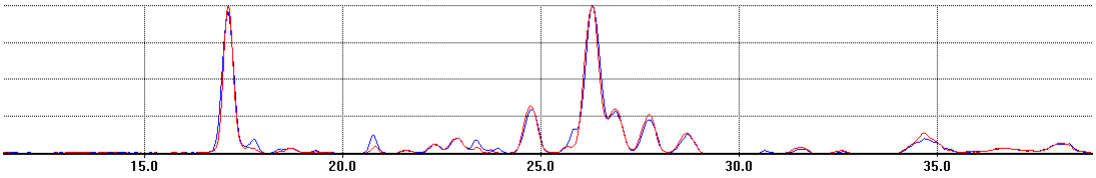

c) Plate BD004

Cell display

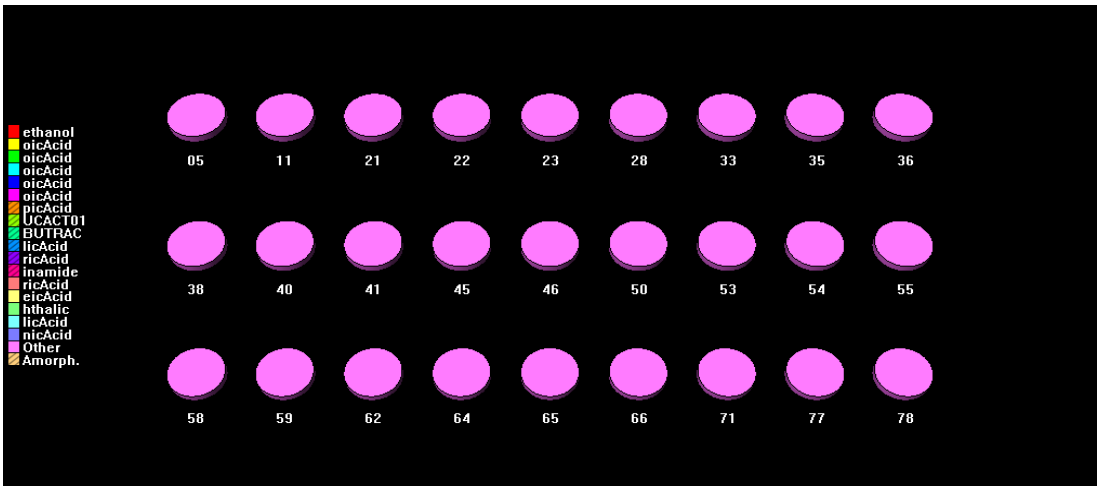

Dendrogram

The cut of level is 0.49 giving a clustering of 14 groups. These groups were further examined and cross referenced with the plated format. The details are given in the table below.

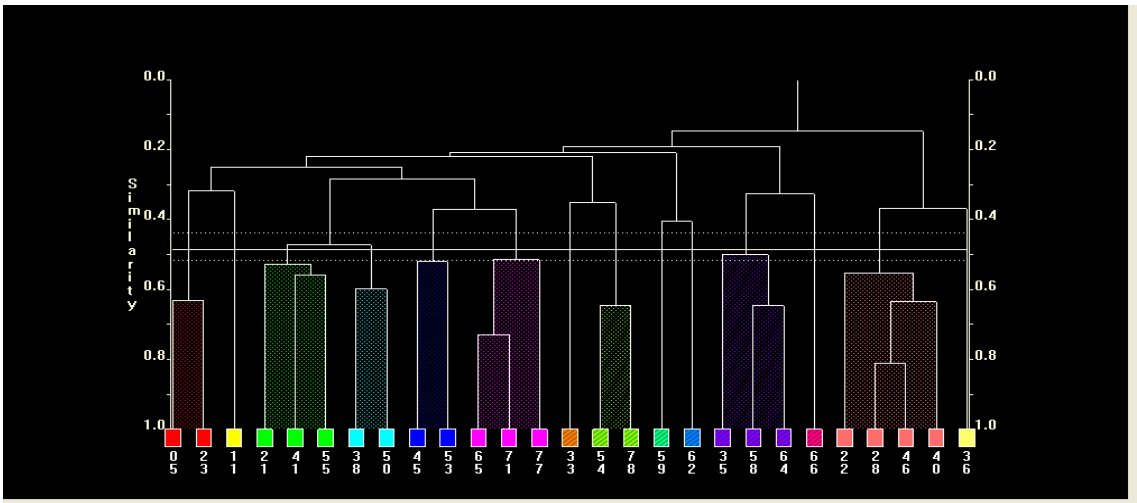

Table Fc1: Summary of the clustering viewed from Dendrogram, these have been cross referenced with the plate format as shown in Appendix F * respectively to sample number column

Group	Sample Number	Coformer, (Composition ratios *)
Red	05, 23	11(1:2) 12 (2:1)
Yellow	11	11 (1:2)
Green	21, 41, 55	6 (1:2) 12 (1:2) 2 (1:1)
Light Blue	38, 50	4 (1:2) 5 (2:1)
Blue	45, 53	7 (1:1) 13 (2:1)
Pink	65, 71, 77	13 (1:1) (1:1) (1:2)
Stripy Brown	33	7 (2:1)
Stripy Green	54, 78	15 (1:2) 16 (1:1)
Stripy Greeny Blue	59	13 (2:1)
Stripy Light Blue	62	5 (1:1)
Stripy Purple	35, 58, 64	12 (1:1) 10 (1:1), (1:2)
Stripy Pink	66	16 (2:1)
Salmon Pink	22, 28, 46, 40	9 (1:1), (1:2) 10 (2:1), (2:1)
Pastel Yellow	36	15 (2:1)

Again, the polySNAP clustering has shown that there are many groups clustering which consist of Isonicotinamide with different acid co-formers such as the red, green, light blue, blue group, stripy green, stripy purple and salmon pink groups. This shows the program lacks consistency in its clustering techniques as well as the data consisting of poor diffracted samples.

3D MMDS plot in Figure Fc1 shows clustering of pink group, samples 65 and 71.

Figure Fc1: Top image is MMDS plot of plate 4, Bottom, close up of the MMDS plot identifying close clustering of sample 65 and 71

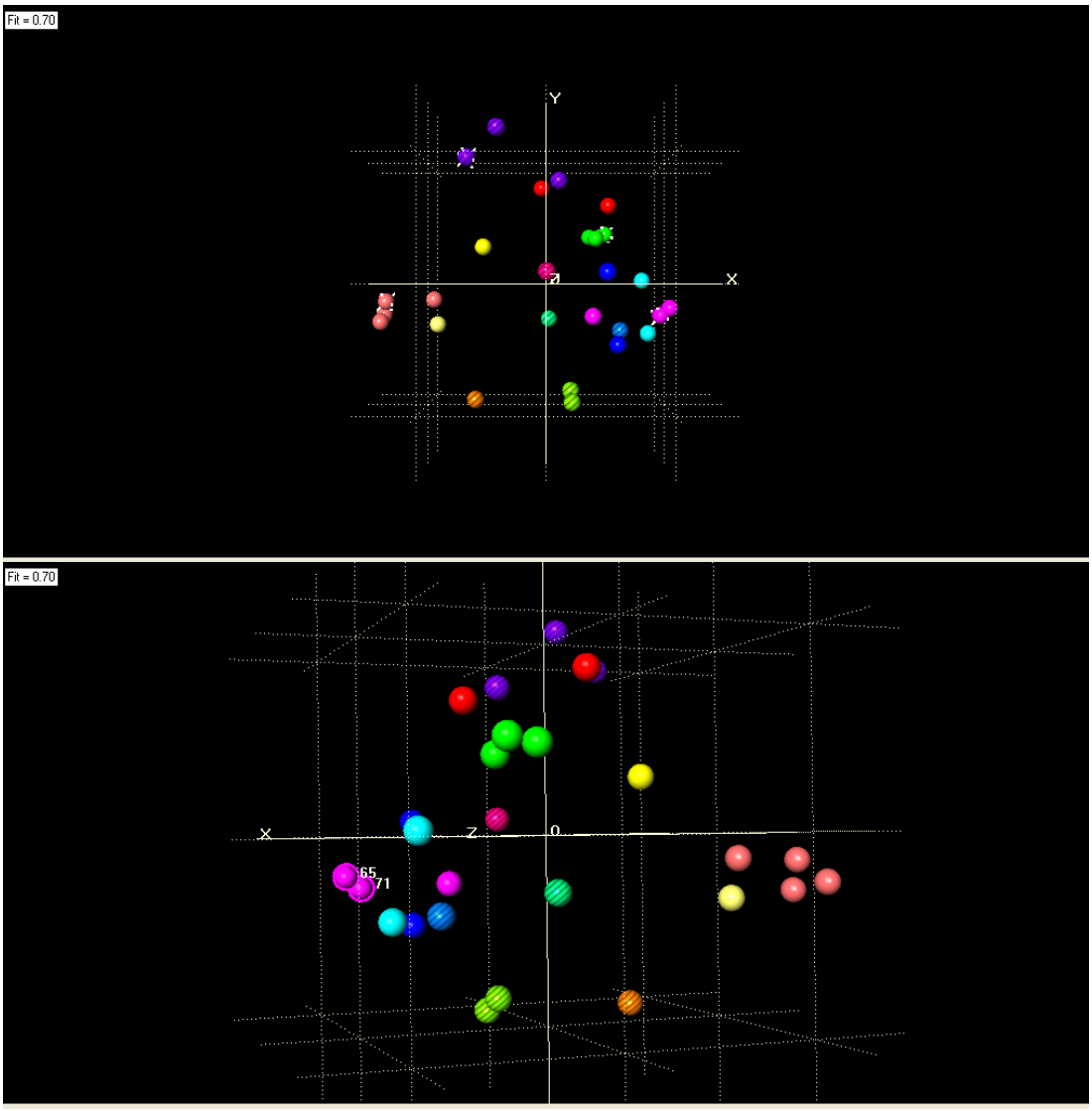

Overlaying the powder patterns of these samples given a similarity rank 0.730, below we can see that there are few distinct similarities in the peaks.

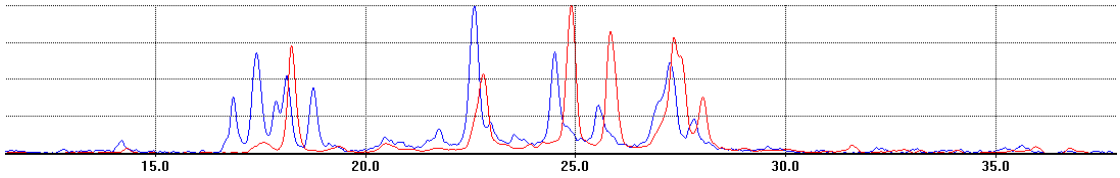

Cross referencing these samples with the dendrogram analysis highlights that sample 65 and 71 both have a composition ratio of 1:1, as experiments were carried out using two different solvents per plate. The conformer identified is conformer 13, which is Pimelic acid. These samples have been displayed below along with the starting components to identify new peaks and similarities in the powder patterns, Figure Fc2.

Figure Fc2: Powder patterns display of the sample 65 and 71 overlaid with the pure components to identify peaks that suggest new phases

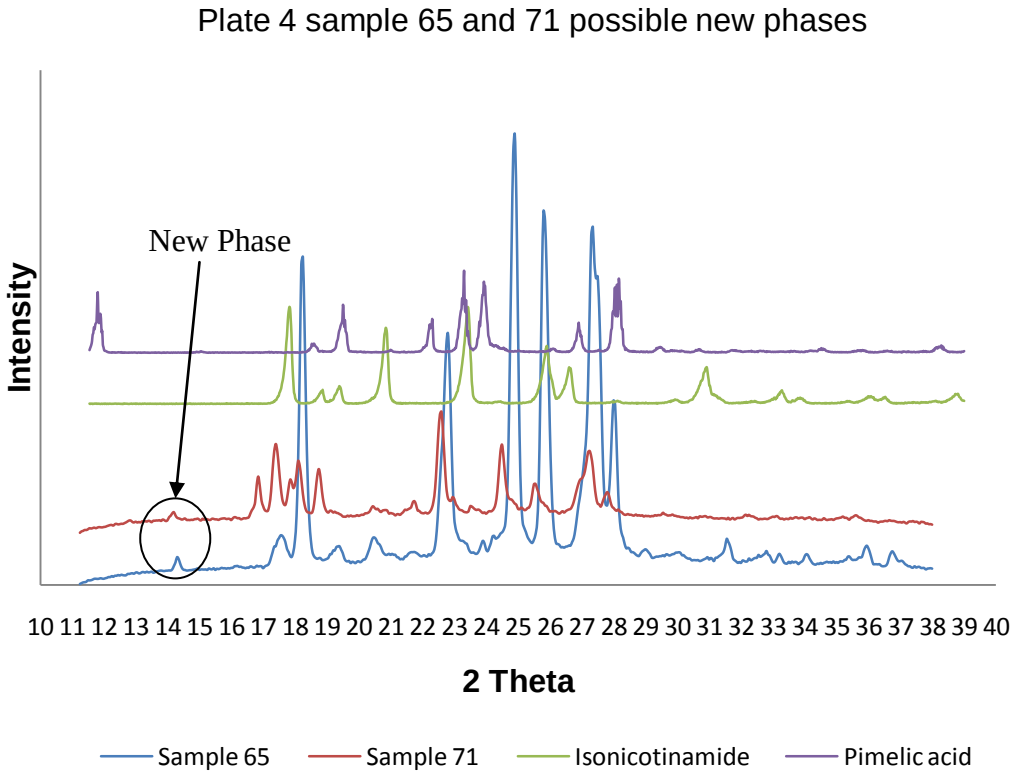

Upon analysis and comparison a small peak at 14.3˚ 2θ suggests a new phase peak. However it is difficult to highlight new phases and characteristic peaks from the starting components as the data collection is not a full profile collection. As we can see Pimelic

acid has the emergence of a peak at 12˚ 2θ, powder patterns of the starting components are from 2˚ 2θ to 50˚ 2θ, where as for high through-put screen sample, analysis is only from 11.25˚ 2θ, it also involves large amounts of background noise.

d) Plate BD005

Cell Display

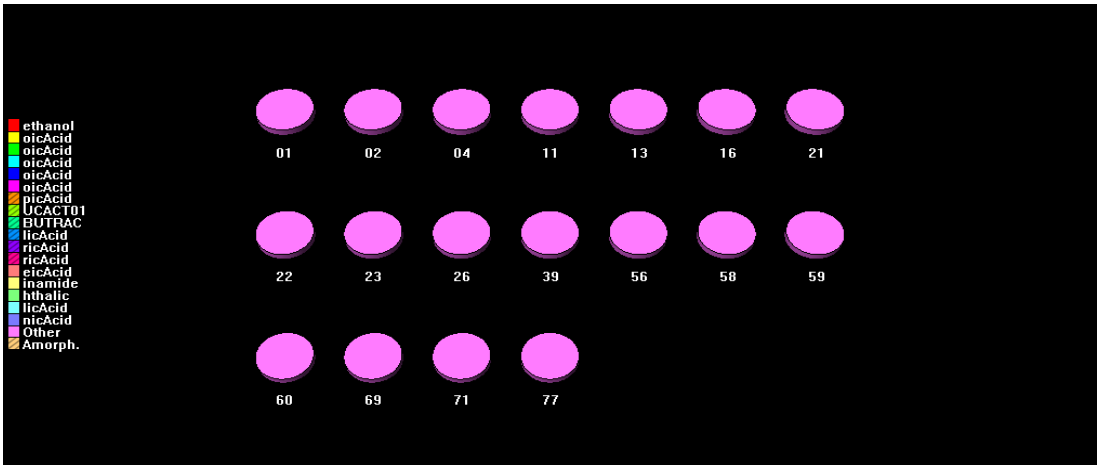

Dendrogram

The dendrogram has clustered to give a similarity level cut of 0.41, resulting in presents the dendrogram below, resulting in 10 groups. The table below presents the analysis of the groups by cross referencing with plate format in Appendix F(i).

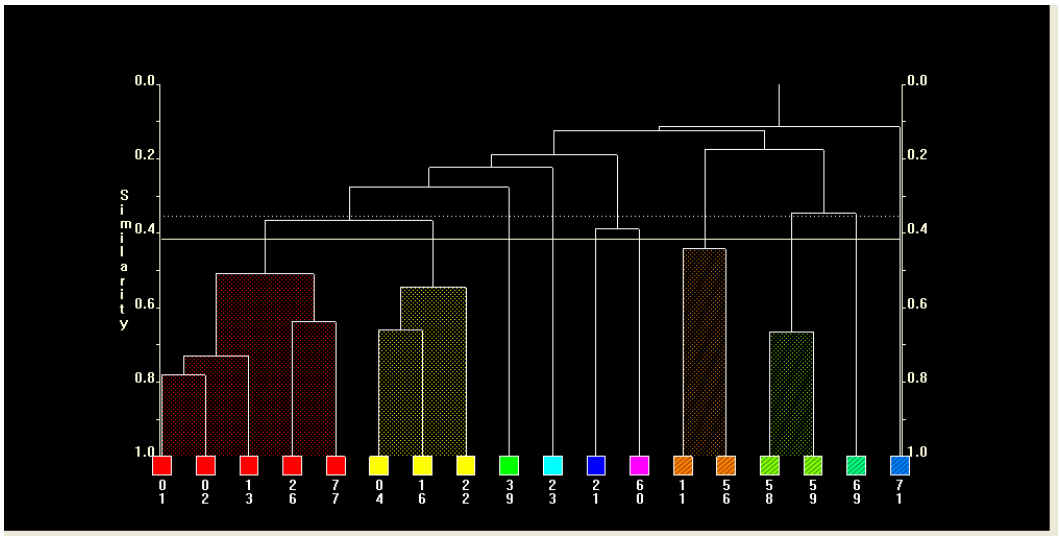

Table Fd1: Summary of the clustering viewed from Dendrogram, these have been cross referenced with the plate format as shown in Appendix F * respectively to sample number column

Group	Sample Number	Coformer, (Composition ratios *)
Red	01, 13, 02, 26, 77	1 (2:1), (1:1) 3 (1:2) 4 (1:1), 13 (1:2)
Yellow	04, 16, 22	9 (2:1) (1:1) (1:1)
Green	39	7 (1:1)
Light Blue	23	12 (2:1)
Blue	21	6 (1:2)
Pink	60	15 (1:2)
Stripy Brown	11, 56	11 (1:2) 5 (2:1)
Stripy Green	58, 59	10 (1:1) 13 (2:1)
Stripy Greeny Blue	69	8 (2:1)
Stripy Light Blue	71	13 (1:1)

From this analysis it is observed that polySNAP has clustered samples into groups with different co-formers. Looking at the 3D MMDS plot, the clustering is much more spread in space, Figure Fd1.

Figure Fd1: MMDS plot of plate 5

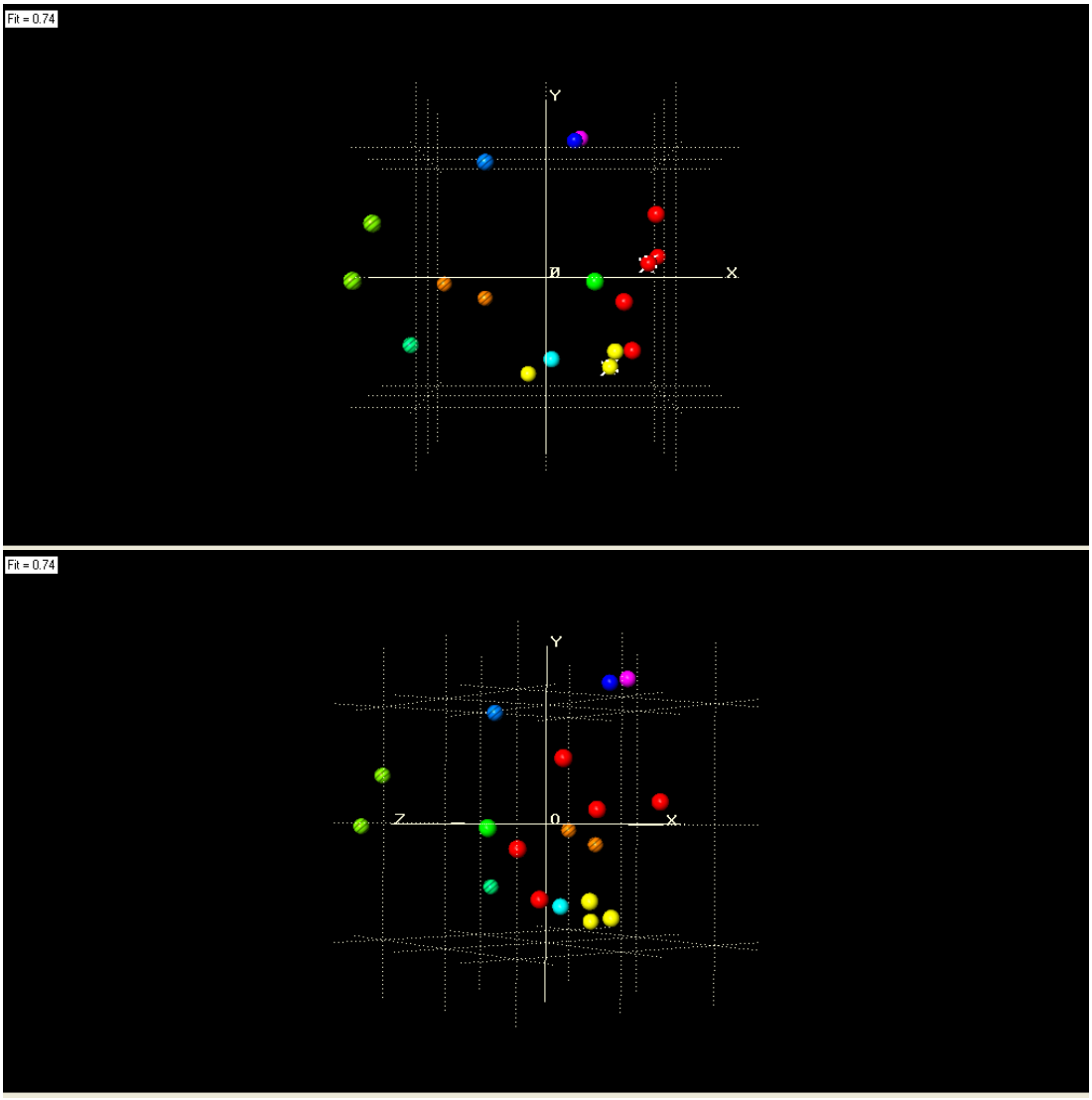

PolySNAP is showing that for this data set nothing is clustered close together in the MMDS plot.

Figure Fd2: Dendrogram of plate 5

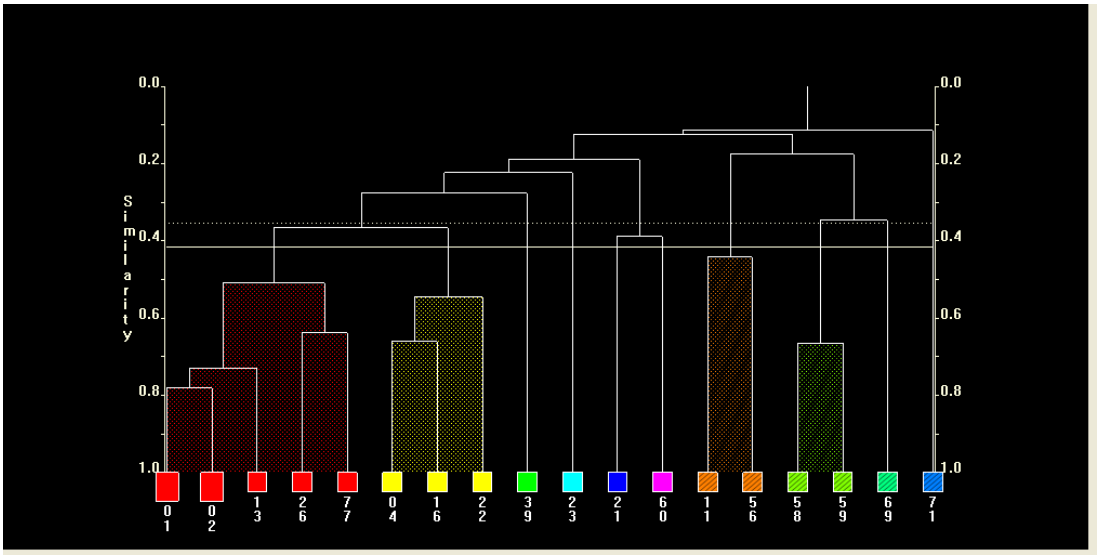

If we look back at the dendrogram we can see that sample 01 and 02, as highlighted above, Figure Fd2, cluster to have a similarity of 0.78. Over laying the PXRD spectra of these is shown below.

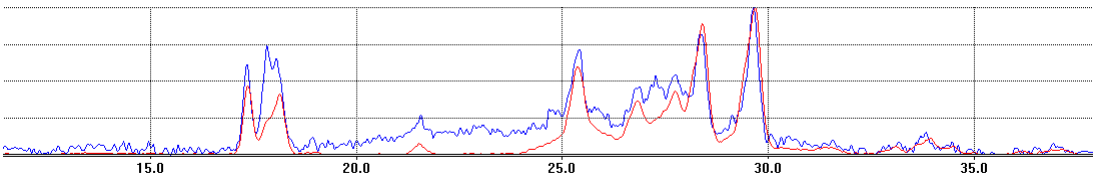

This looks like that these samples are the same, however from the table above sample 01 and 02 are co-formers 1, 1, 4 Benzene dimethanol, and coformer 3, 3 aminobenzoic acid respectively.

Therefore these powder patterns should be different to each other. It can be assumed that these powder patterns are the same because of cross contamination during experiment and/or during preparation for sample plates to be transported to Pharmorphix.

However, for this plate, polySNAP has clustered sample 4, 16 and 22 together in the dendrogram. These samples are of Nicotinamide with carboxylic acid co-former 9,

Fumaric acid, with the respective composition ratios of 2:1, 1:1, in solvent *o*-xylene, and 1:1 in isohexane. The powder patterns have been plotted in Excel and compared with the starting components to identify potential new phase peaks, Figure Fd3.

Figure Fd3: Powder patterns display of the sample 16 and 22 overlaid with the pure components to identify peaks that suggest new phases

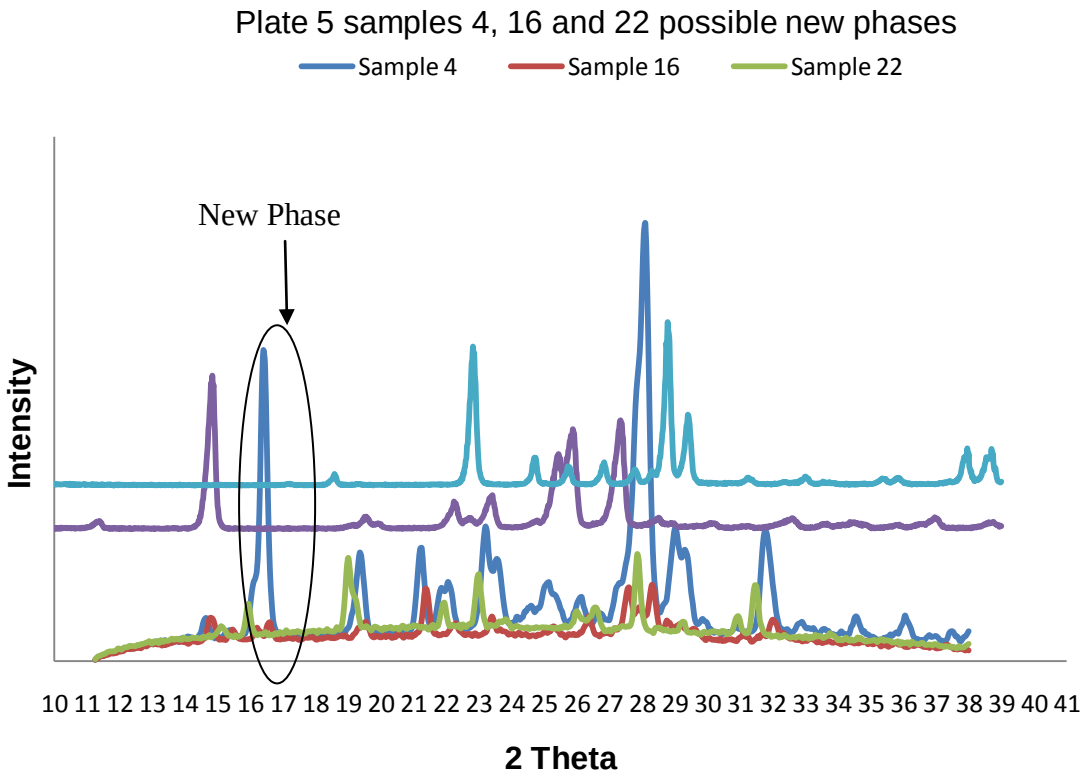

The powder patterns show various characteristic peaks from the two starting components, and new peaks which suggest a new phase between 16-17˚ 2θ. However, further analysis of the sample as mentioned earlier such as DSC and Raman analysis of this data could be employed to back up these findings.

e) Plate BD006

Cell display

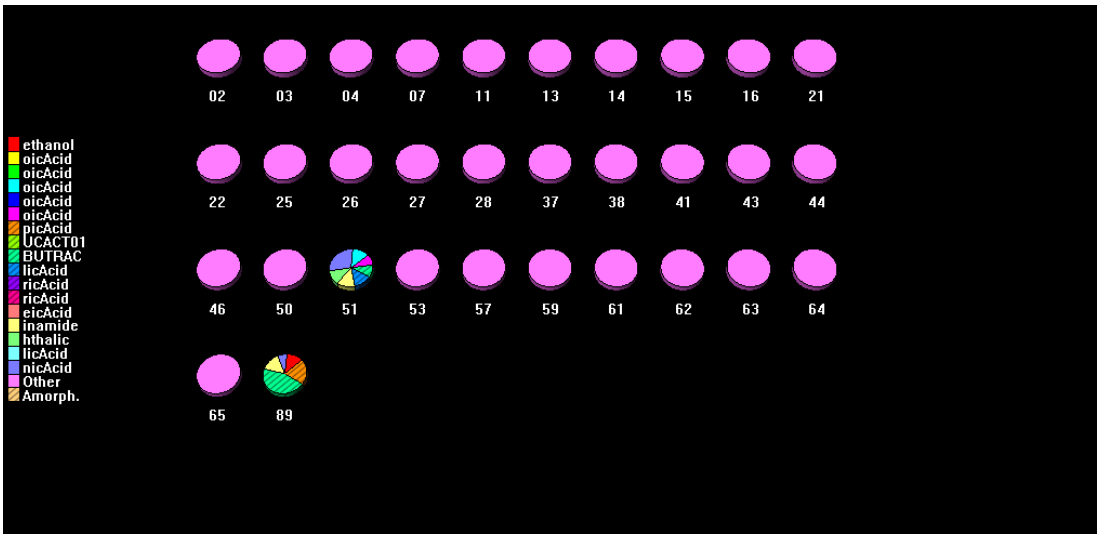

This display of plate 6 presents data of 30 samples labelled as 'other', suggesting new phases, and two samples which could be possible mixtures of several components. Ideally a mixture of the two components is desirable but here we see that polySNAP has highlighted sample 51 to consist of a mixture of 7 possible components, and sample 89 of 5 components. It could be speculated that this is due to cross contamination when handling/ preparing the plate for PXRD analysis.

It would be expected that these two samples, 51 and 89, would be clustered into individual groups. However, the dendrogram does that show this to be the case for sample 89, which has been clustered with the light blue group and sample 51 is clustered on its own as stripy purple group.

The cut level of the dendrogram is 0.65 that defines 15 groups.

Figure Fe1: Dendrogram of plate 6

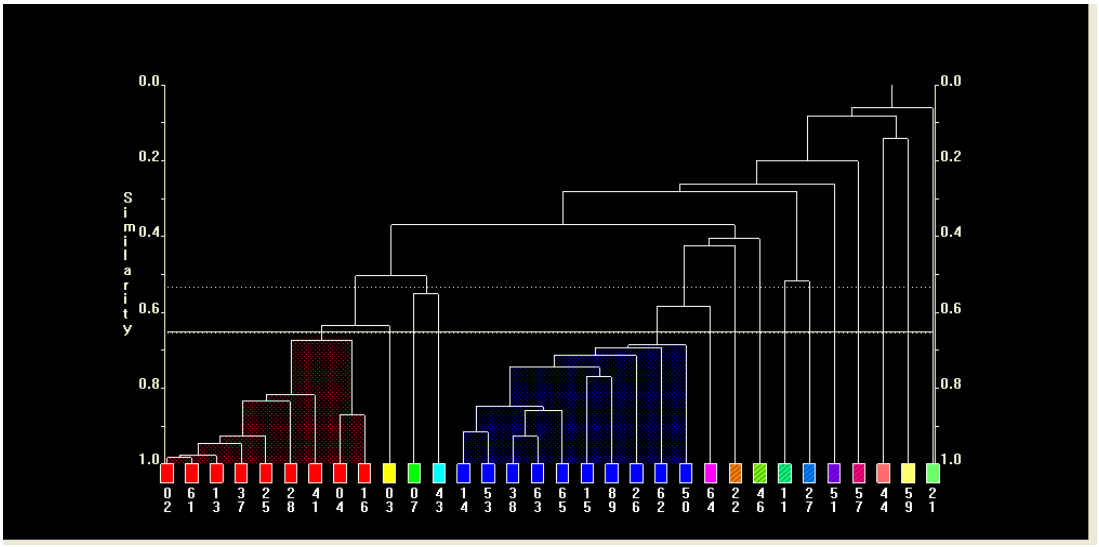

The table below shows the samples in the clustering groups and highlights the component compositions.

Table Fe1: Summary of the clustering viewed from Dendrogram, these have been cross referenced with the plate format as shown in Appendix F * respectively to sample number column

Group	Sample Number	Coformer, (Composition ratios *)
Red	02, 61, 37, 13, 25, 28, 04, 16 41,	3 (1:2) 2 (1:2) (2:1) 1 (1:1), (1:2) 9 (1:2), (2:1), (1:1) 12 (1:2)
Yellow	03	6 (1:1)
Green	07	1 (2:1)
Light Blue	43	2 (2:1)
Blue	14, 26 53, 38, 65, 63, 15,	4 (2:1), (1:1) 13 (2:1), (1:2), (1:1) 8 (2:1) 6 (1:2)

	89, 62, 50	14 (2:1) 5 (1:1), (2:1)
Pink	64	10 (1:2)
Stripy Brown	22	9 (1:1)
Stripy Green	46	10 (2:1)
Stripy Greeny Blue	11	11 (1:2)
Stripy Light Blue	27	7 (2:1)
Stripy Purple	51	7 (1:2)
Stripy Pink	57	7 (1:2)
Salmon Pink	44	4 (1:2)
Pastel Yellow	59	13 (2:1)
Pastel Green	21	6 (1:2)

For this plate, polySNAP has clustered many samples into individual groups, and two larger clustering groups which have samples with different starting components.

The 3D MMDS plot below, Figure Fe2, also shows the two groups, red and blue, to form close packed clustering, however, since these groups consist of sample with different starting components they have been re-clustered and analysed below, Figure Fe3.

Figure Fe2: MMDS plot of plate 6

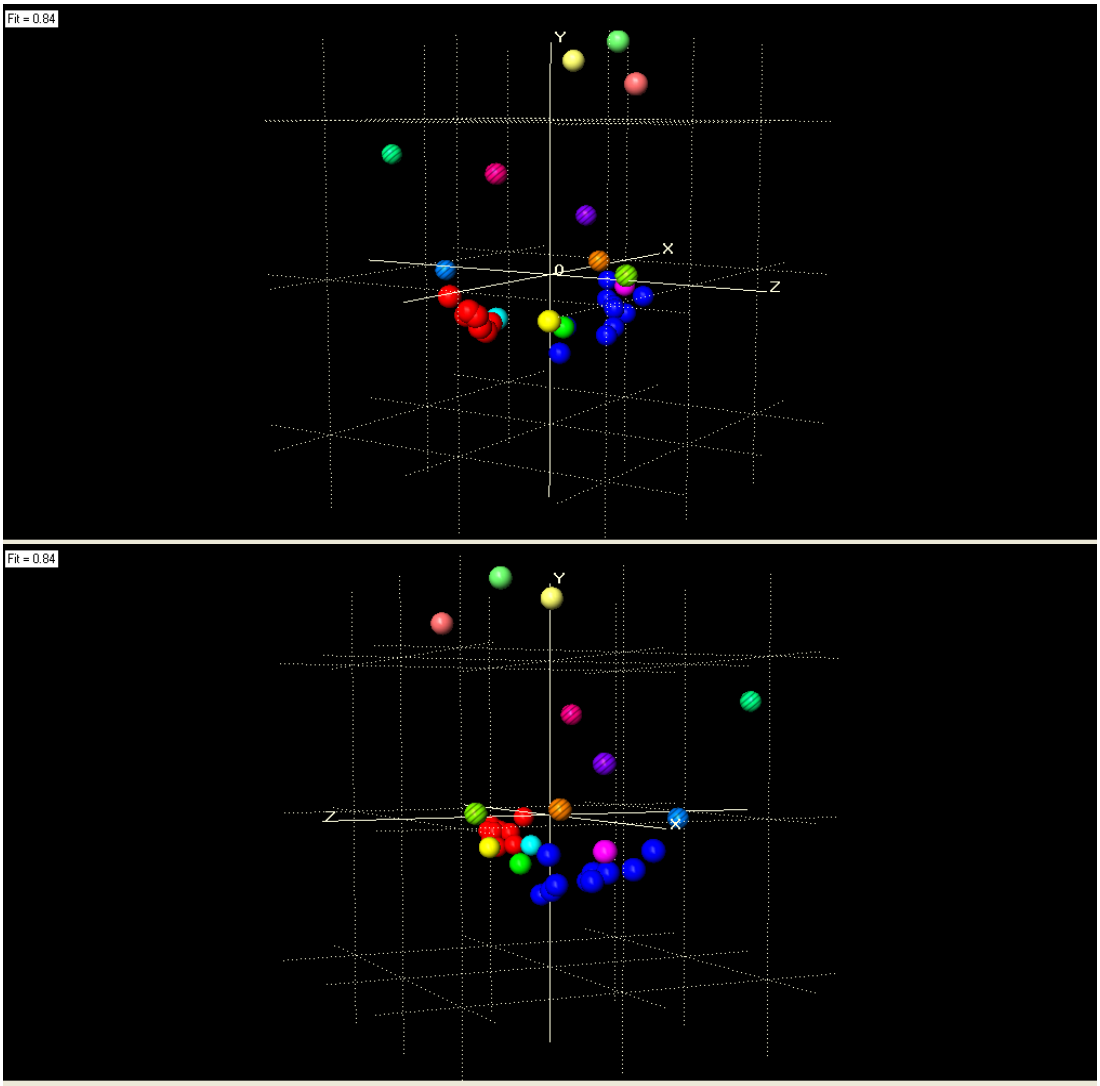

Figure Fe3: Dendrogram as shown in Figure Fe1, dendrogram is a representing the re-clustering of red group from plate 6

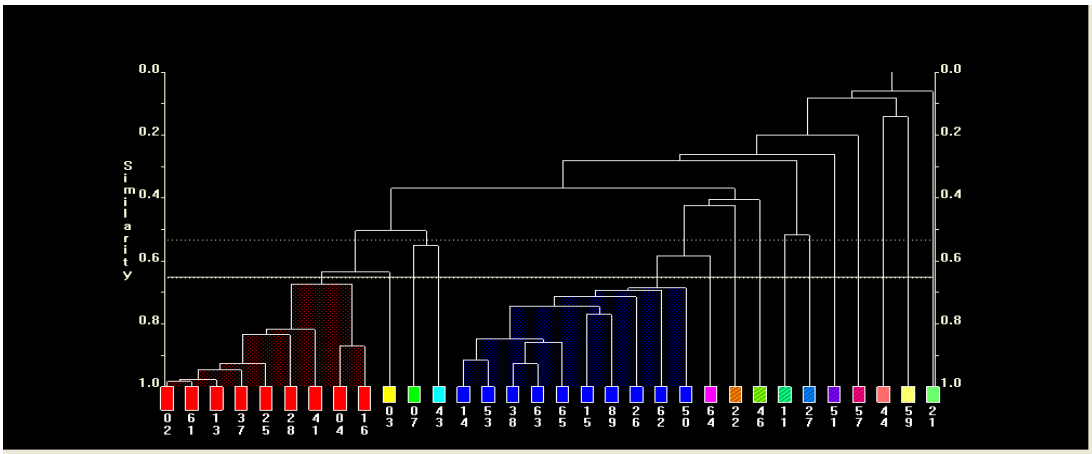

After re-clustering the cell display, Figure Fe4, and dendrogram highlight that there are 3 clustering groups, the table below details the samples per group and the component and composition ratios.

Figure Fe4: Cell display and dendrogram of re-clustering of red group from plate 6

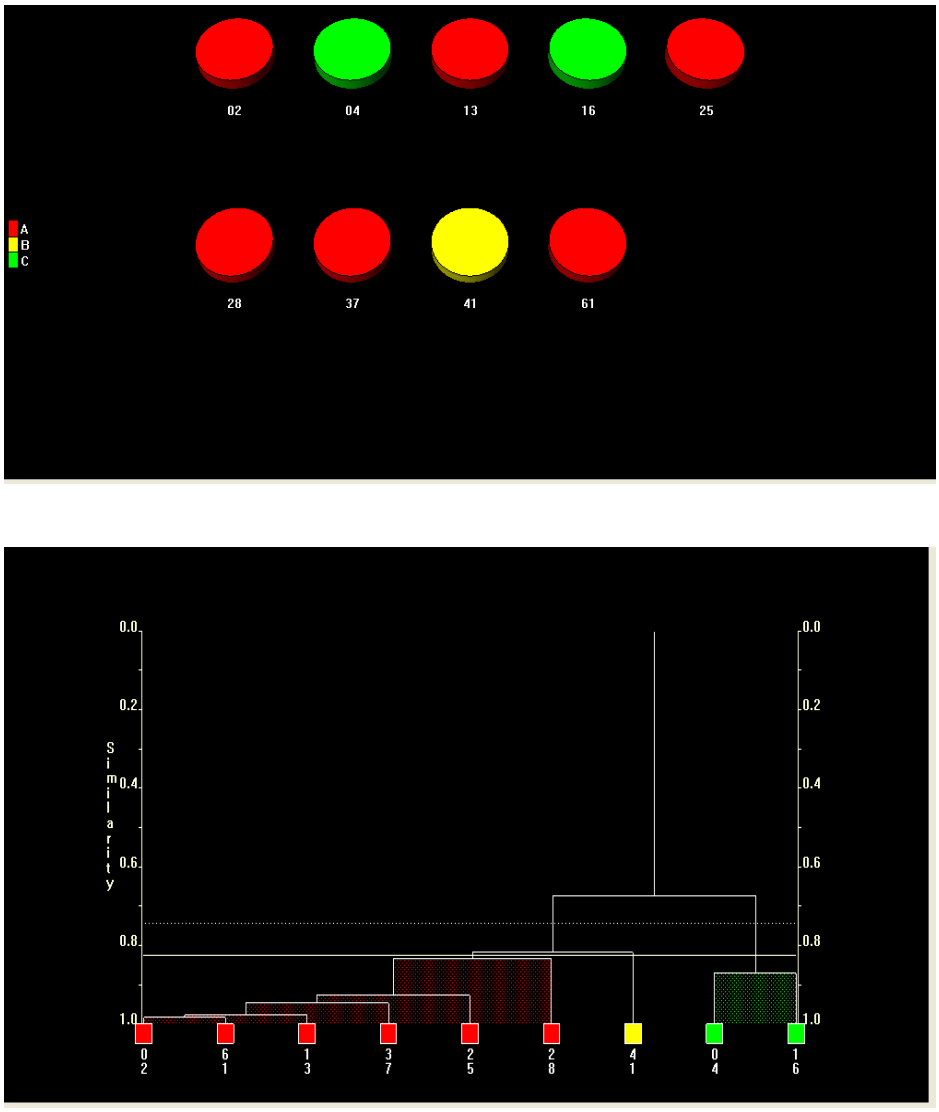

Table Fe2: Summary of the clustering viewed from Dendrogram, these have been cross referenced with the plate format as shown in Appendix F * respectively to sample number column

Group	Sample Number	Coformer, (Composition ratios *)
Red	02, 61, 37 13, 25 28	3 (1:2) 2 (1:2) (2:1) 1 (1:1), (1:2) 9 (1:2),
Yellow	41	12 (1:2)
Green	04, 16	9 (2:1), (1:1)

Again the samples here have been clustered as seen previously where one group consists of many carboxylic acids. The 3D MMDS plots, Figure Fe5, are slightly better looking with the red group clustering close together but having a heavily tight clustering of three spheres as highlighted below, Figure Fe6, Fe7

Figure Fe5: MMDS plot of re-cluster of red group from plate 6

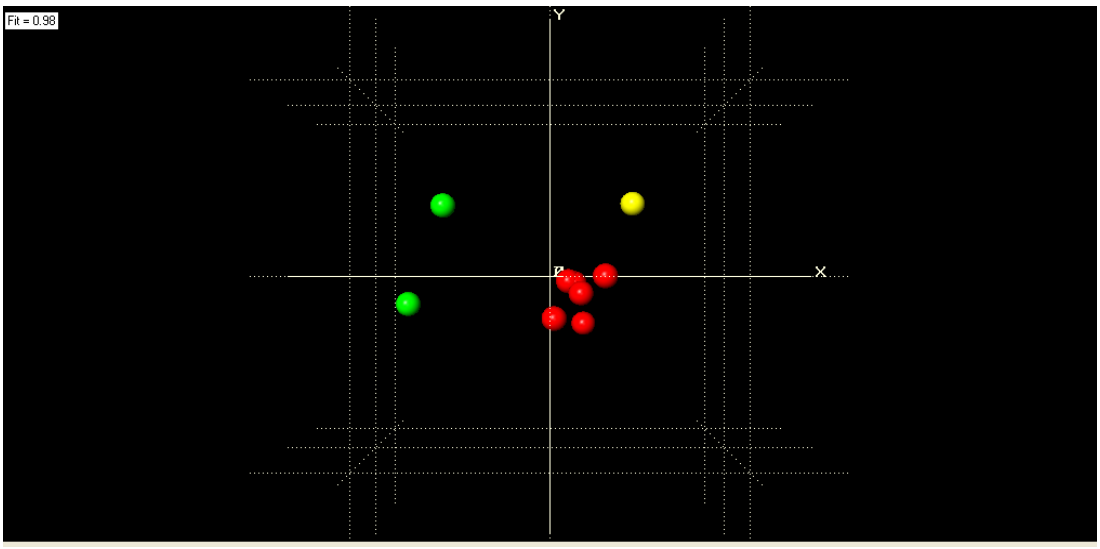

Figure Fe6: A zoomed in view of the MMDS plot of re-clustered red group from plate 6 showing samples 2, 3 and 61, which cluster close together as compared to the other samples

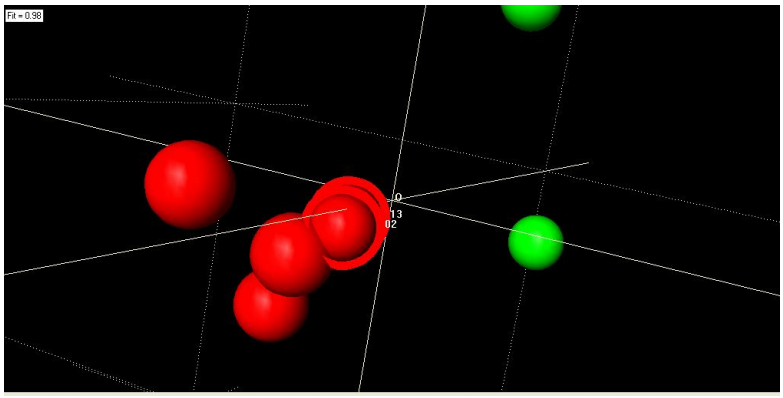

These have been highlighted to be sample 02, 13 and 61. Overlaying these samples 02, 13 shows that these patterns are very alike and have been assigned with a similarity rank of 0.977.

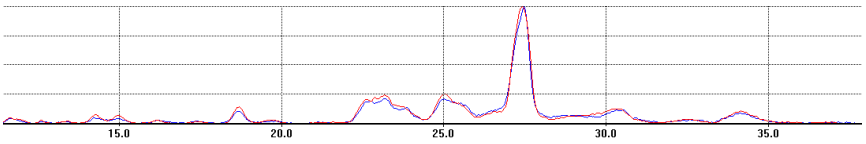

Figure Fe7: A zoomed in view of the MMDS plot of re-clustered red group from plate 6 showing samples 2, and 16

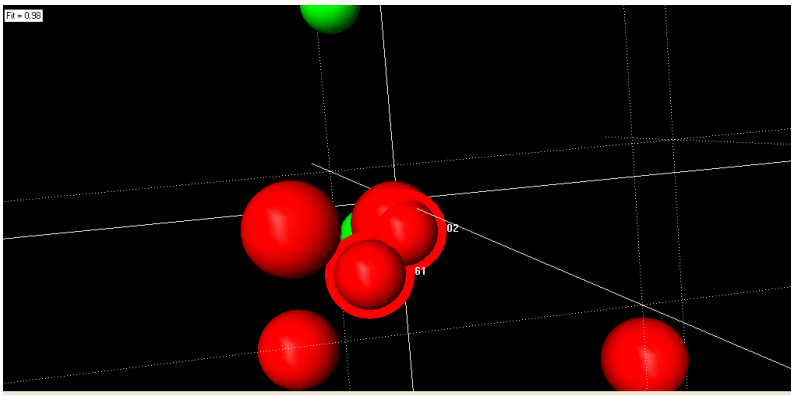

Overlaying samples 02 and 61 also presents patterns that are alike and have a similarity rank 0.984.

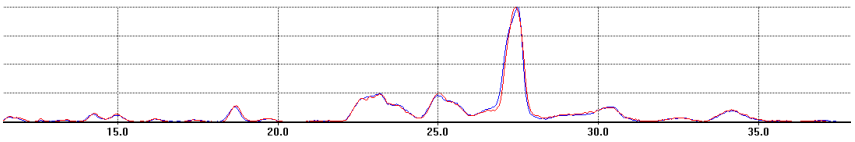

However, from the table above these samples consist of different co-formers. A similar story is observed after the re-clustering analysis of the blue group, Figure Fe8.

Figure Fe8: Re-clustering of blue group from plate 6

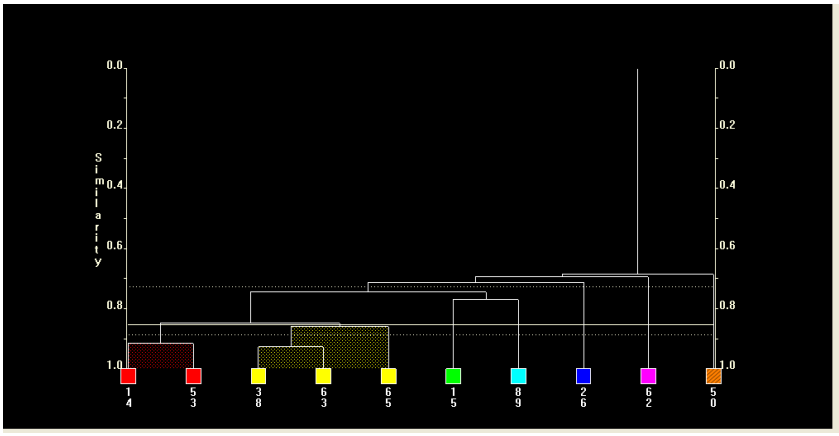

Figure Fe9: Cell display of re-clustering of blue group from plate 6

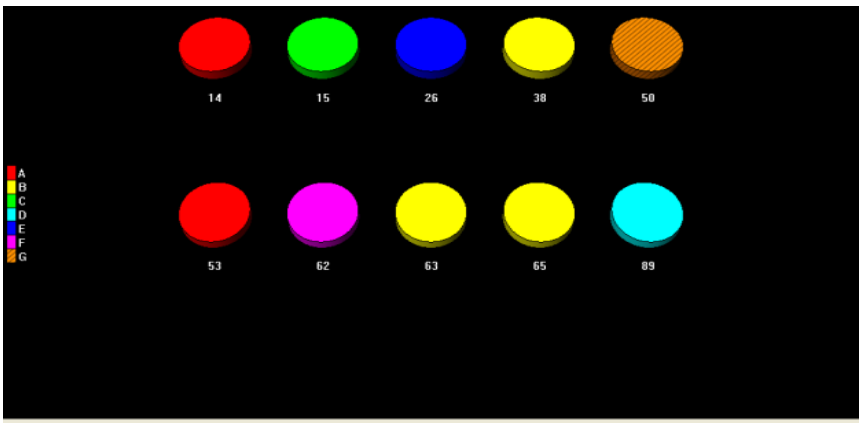

This data from the dendrogram was cross referenced with the plate format and is presented in the table below.

Table Fe3: Summary of the clustering viewed from Dendrogram, these have been cross referenced with the plate format as shown in Appendix F * respectively to sample number column

Group	Sample Number	Coformer, (Composition ratios *)
Red	14	4 (2:1)
	53	13 (2:1)
Yellow	38, 65	13 (1:2), (1:1)
	63	8 (2:1)
Green	15	6 (1:2)
Light Blue	89	14 (2:1)
Blue	26	4 (1:1)
Pink	62	5 (1:1)
Stripy Brown	50	5 (2:1)

The 3D MMDS plot shows that there is a strong cluster of two samples from the yellow group and a sample from the red group, Figure Fe10.

Figure Fe10: MMDS plot of re-cluster of blue group from plate 6, highlighted are two spheres which cluster close, samples 63 and 65

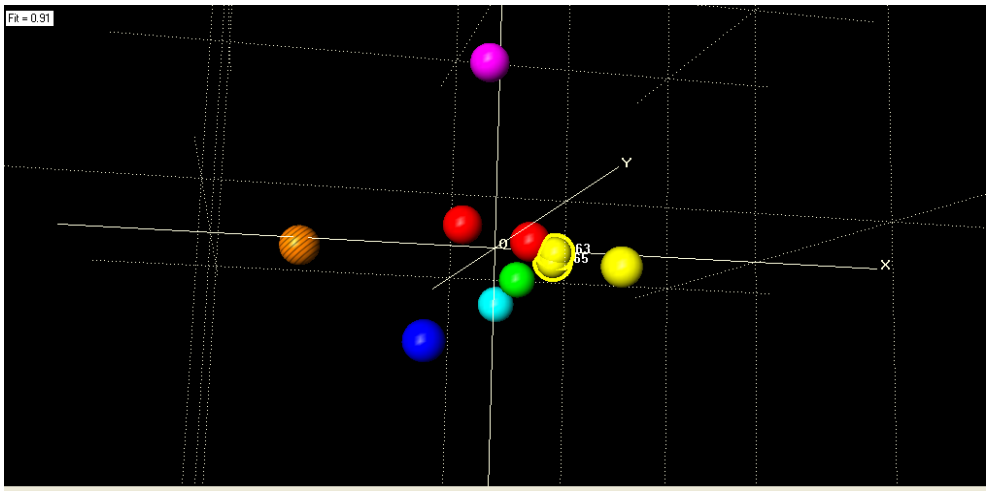

Sample 63 and 65 highlighted above in the MMDS has a rank 0.864 and the powder patterns of these samples are given below.

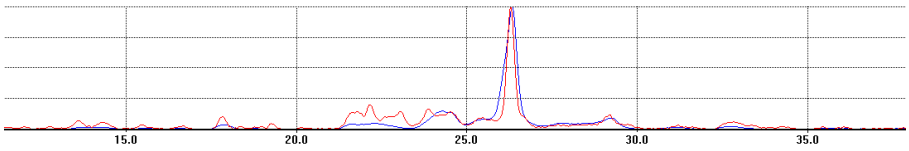

From this pattern we see that the notable peak could be the reason why these samples are clustered with such a high similarity level. Additionally, these samples consist of different staring co-formers. Sample 63 should have Nicotinamide with co-former 8, butanoic acid, with a composition ratio of 2:1 and sample 65 should consist of Nicotinamide with co-former 13, pimelic acid, in 1:1 composition ratio.

Figure Fe11: MMDS plot of re-cluster of blue group from plate 6, highlighted are two spheres which cluster close, samples 63 and 14

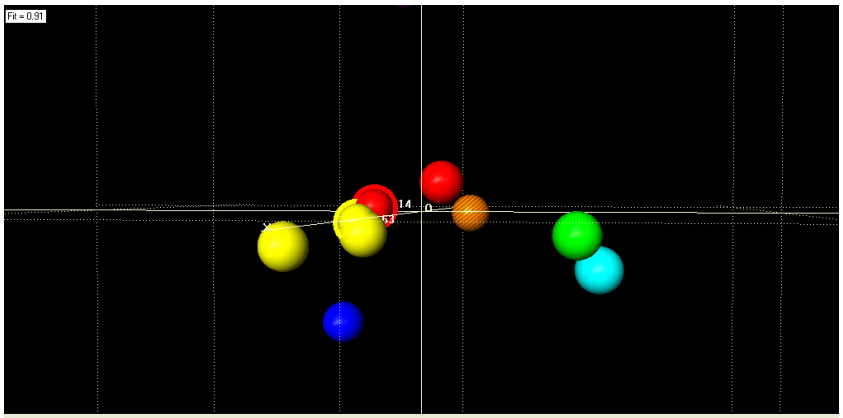

The red and yellow sample clustered together here, Figure Fe11, are samples 63 and 14 for which the powder pattern below has been displayed showing the same dominant peak, which could possibly be giving the similarity rank of 0.900.

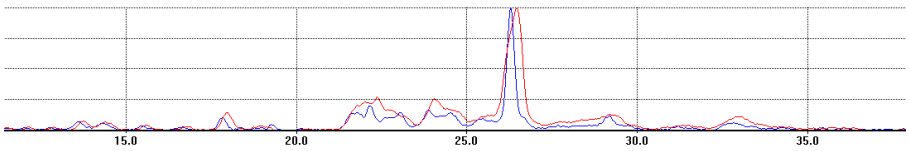

However these samples are of differing carboxylic acid co-formers. Sample 14 should consist of Nicotinamide with co-former 4, 3-nitrobenzoic acid, in a 2:1 composition ratio.

Appendix G: DSC traces from thermal study as discussed in chapter 6

Figure 6.4: Summary of the endothermic peaks for A) Isonicotinamide with 3-hydroxybenzoic acid and B) Benzamide with 3-hydroxybenzoic acid

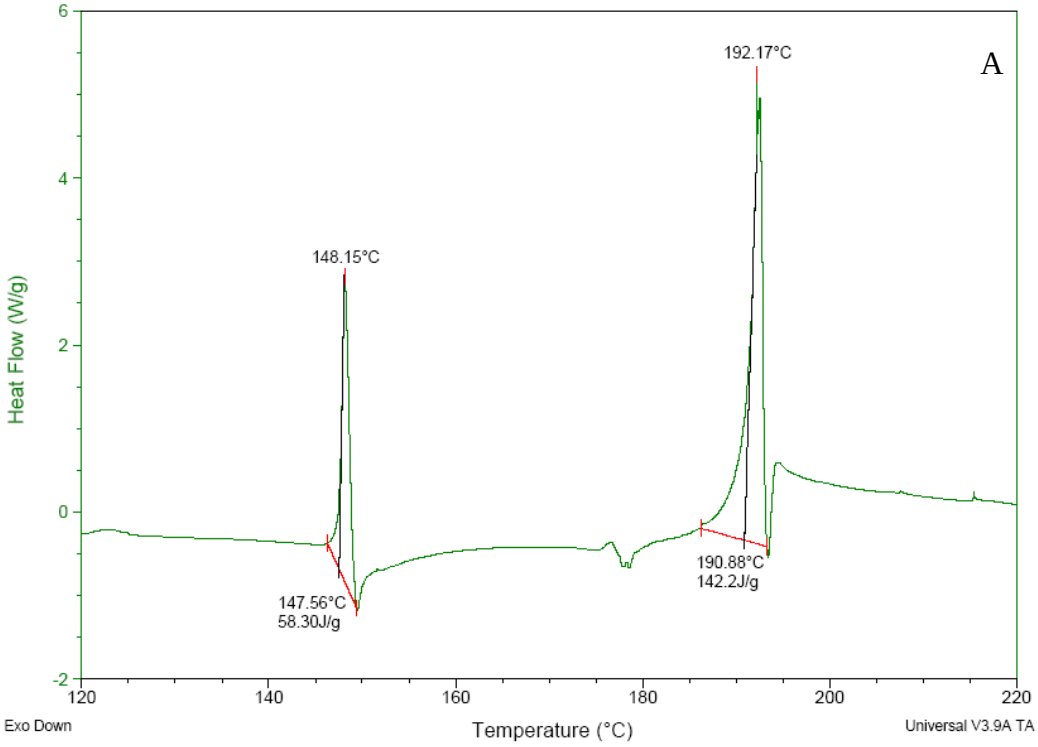

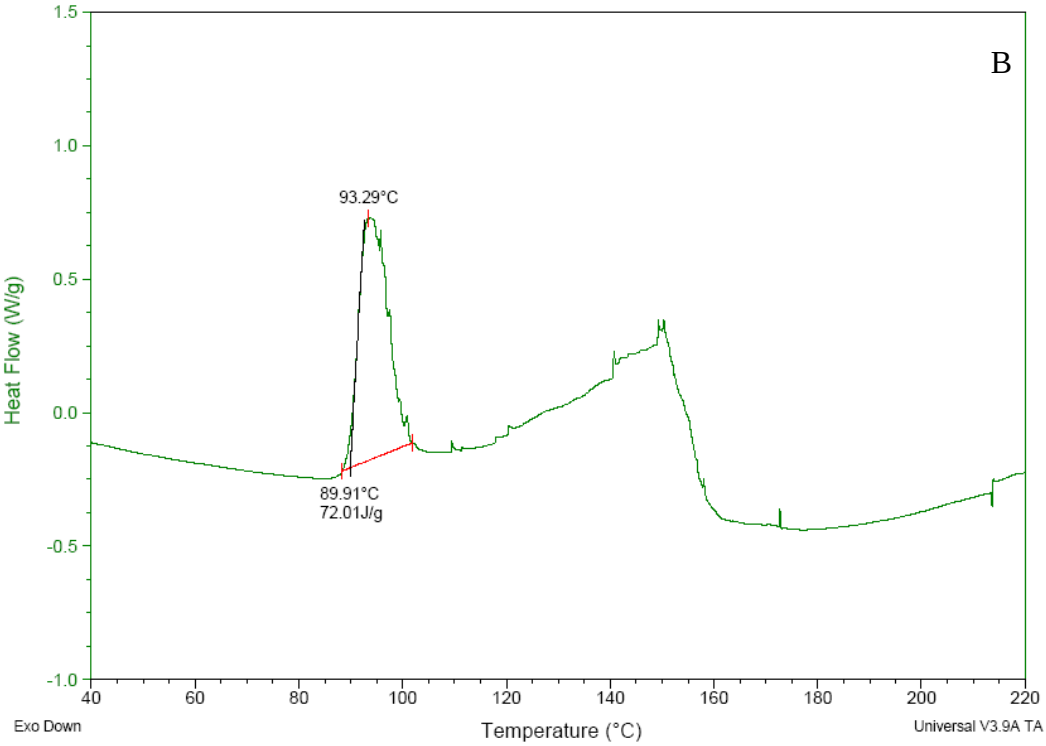

Figure 6.5: Summary of the endothermic peaks for A) Isonicotinamide with 4-hydroxybenzoic acid and B) Benzamide with 4-hydroxybenzoic acid

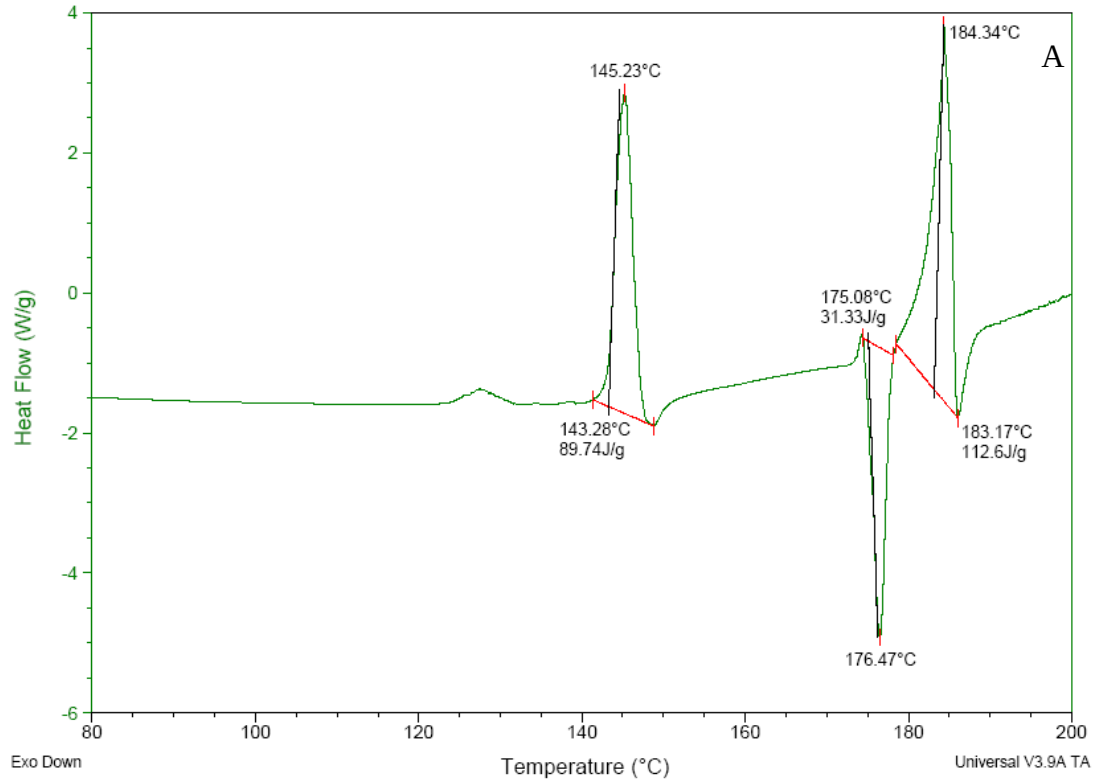

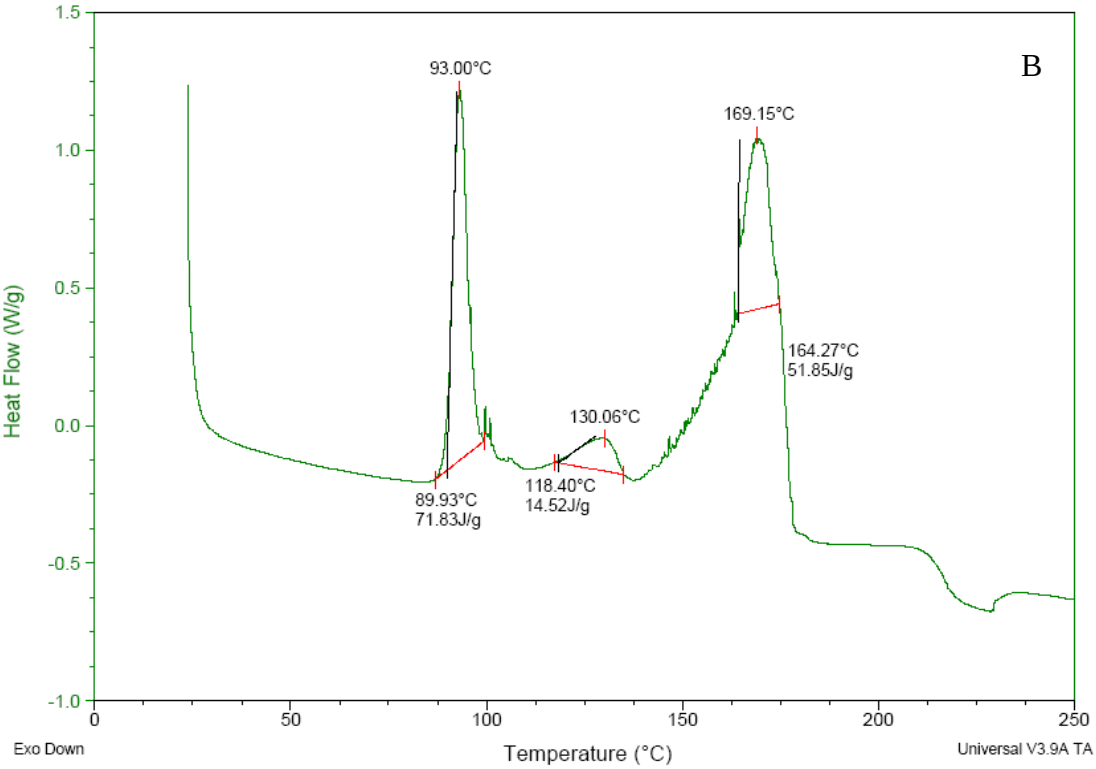

Figure 6.6: Summary of the endothermic peaks for A) Isonicotinamide with 4-nitrobenzoic acid and B) Benzamide with 4-nitrobenzoic acid

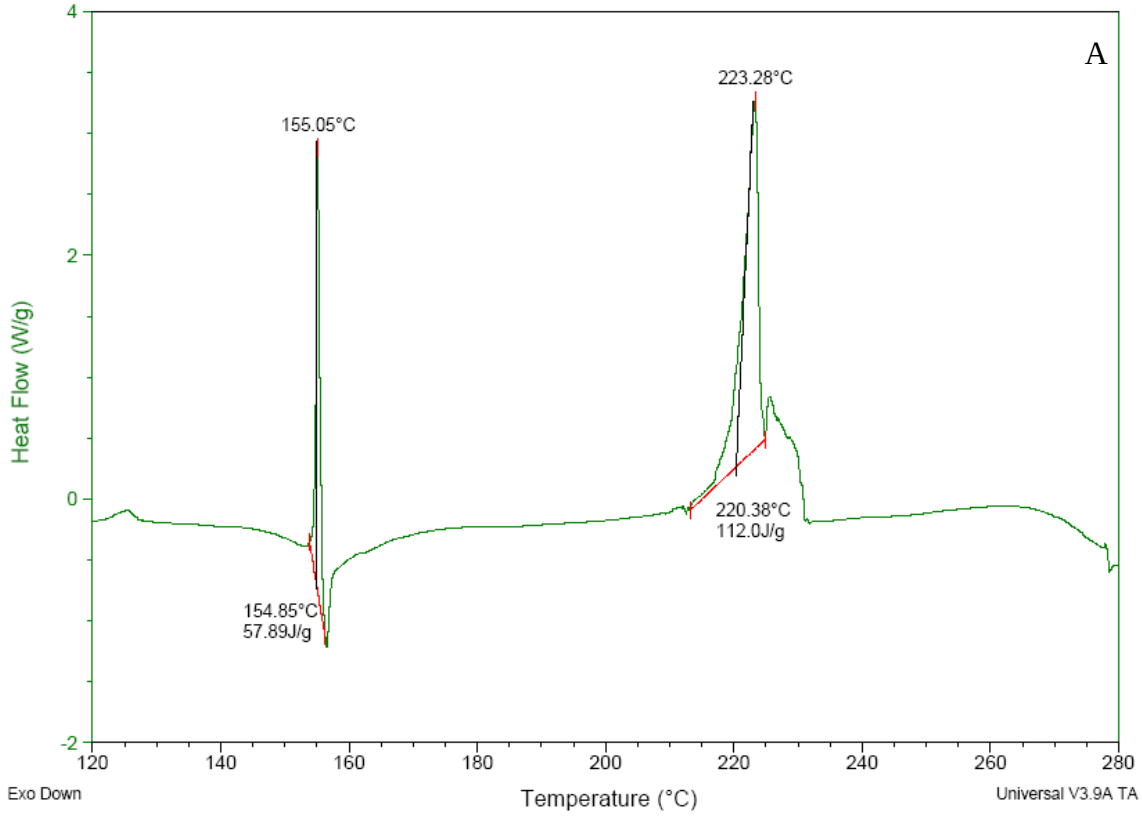

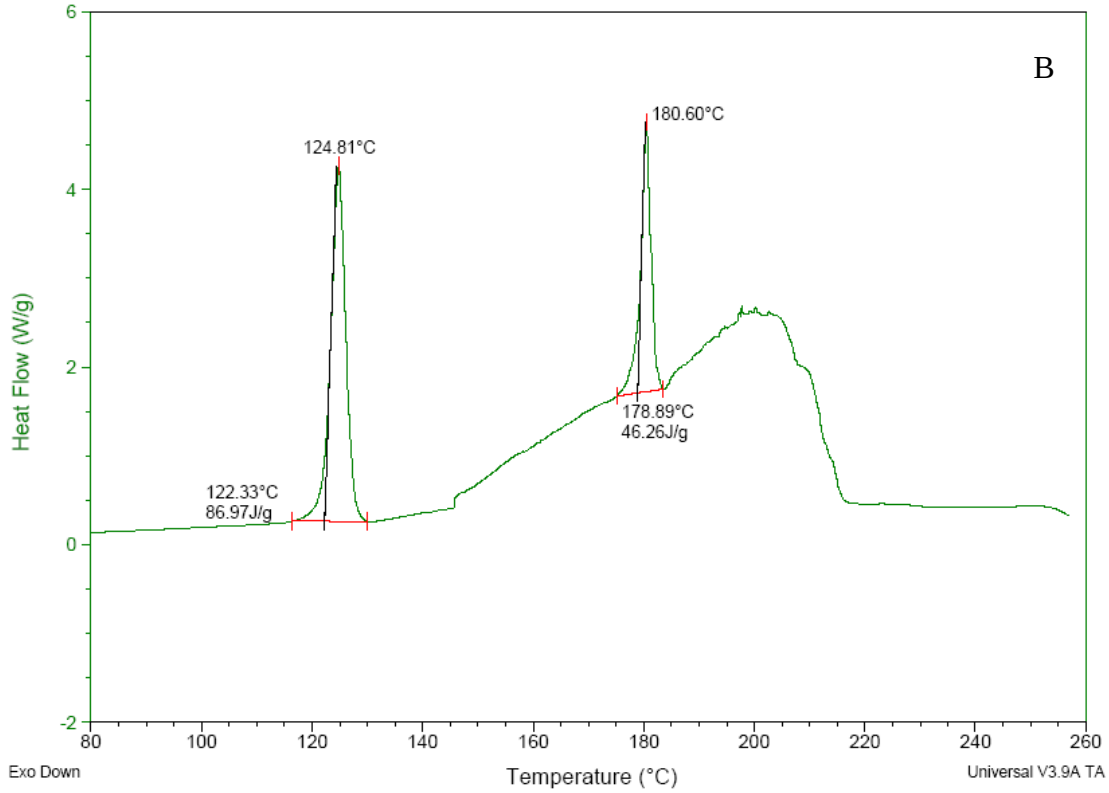

Figure 6.7: Summary of the endothermic peaks for A) Isonicotinamide with Adipic acid and B) Benzamide with Adipic acid

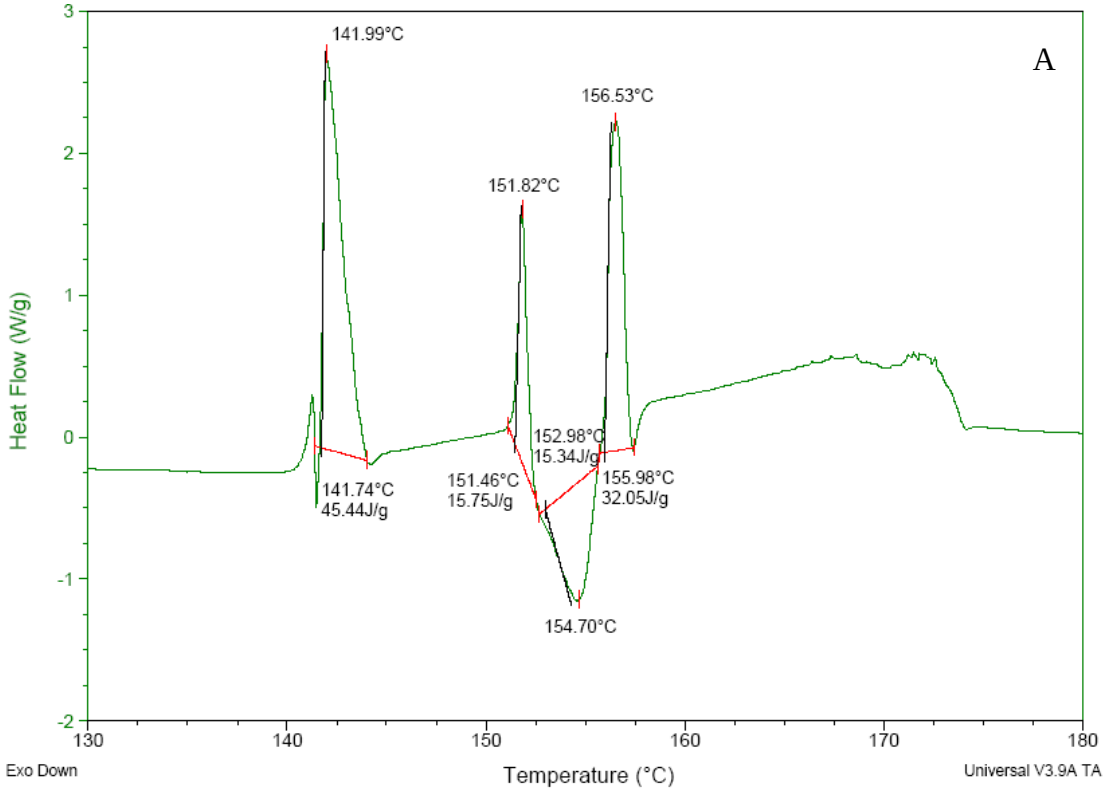

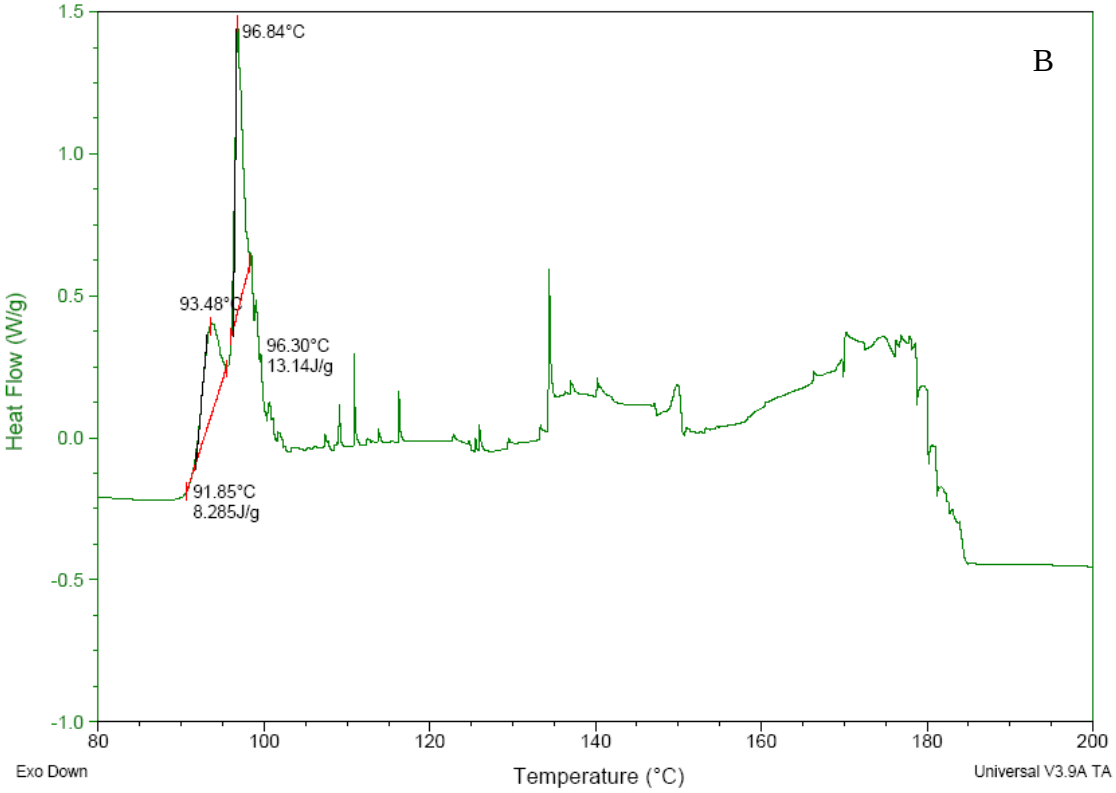

Figure 6.8: Summary of the endothermic peaks for A) Isonicotinamide with Benzoic acid and B) Benzamide with Benzoic

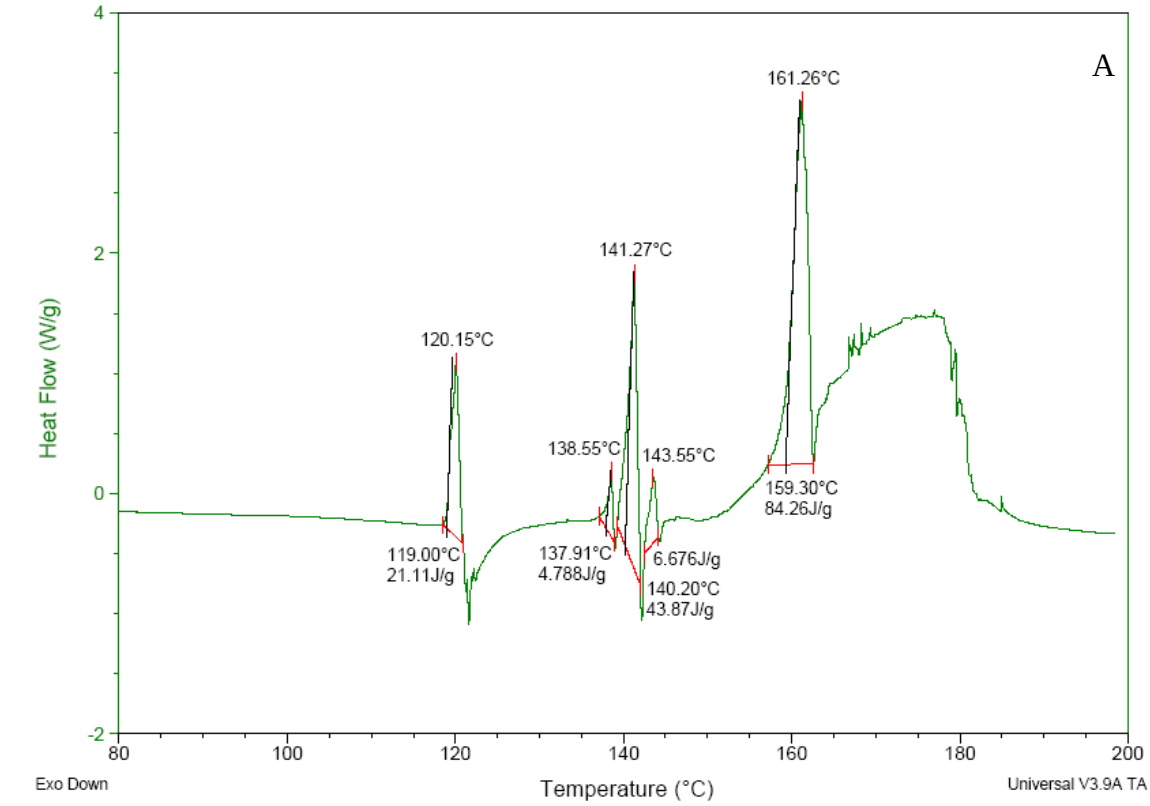

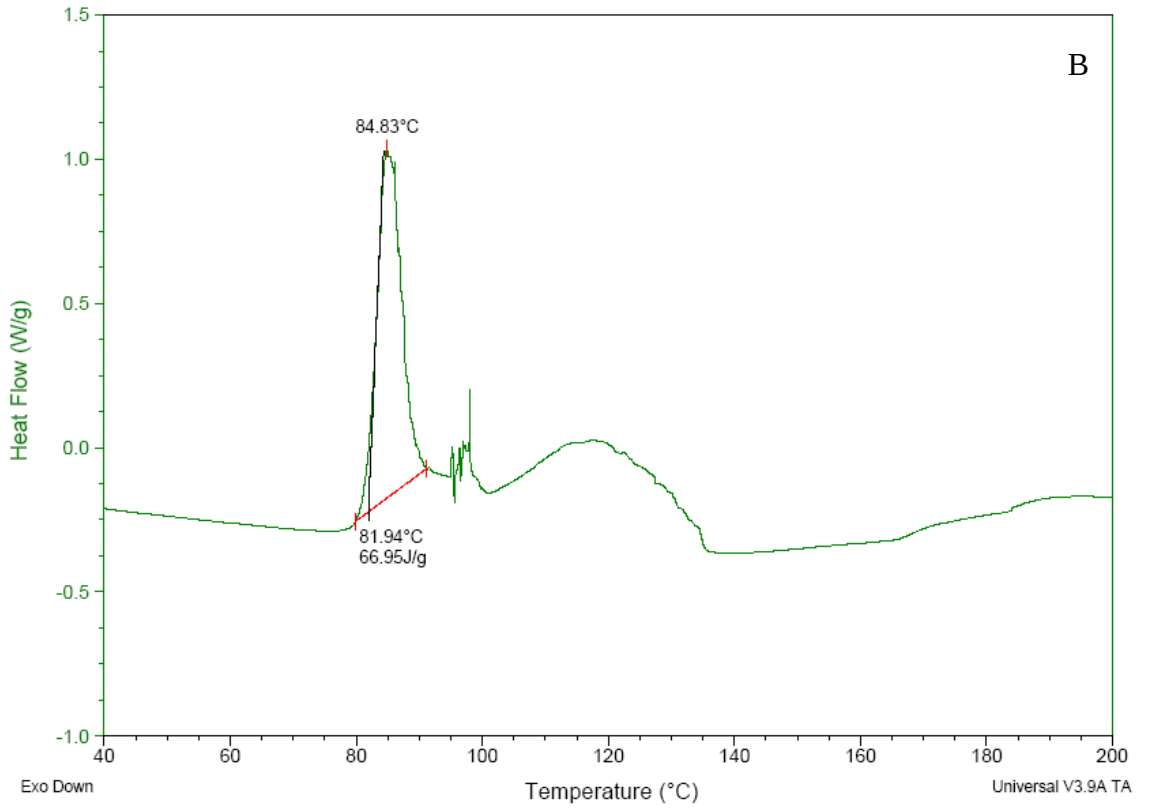

Figure 6.9: Summary of the endothermic peaks for A) Isonicotinamide with Cinnamic acid and B) Benzamide with Cinnamic acid

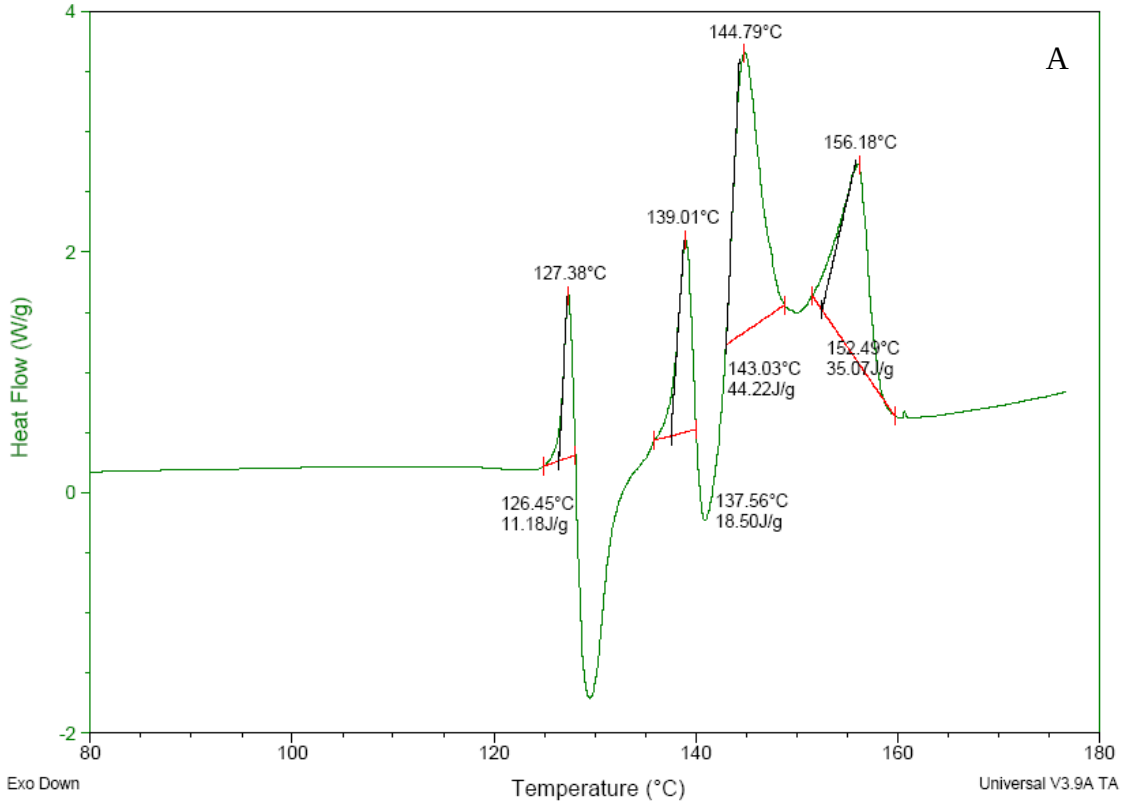

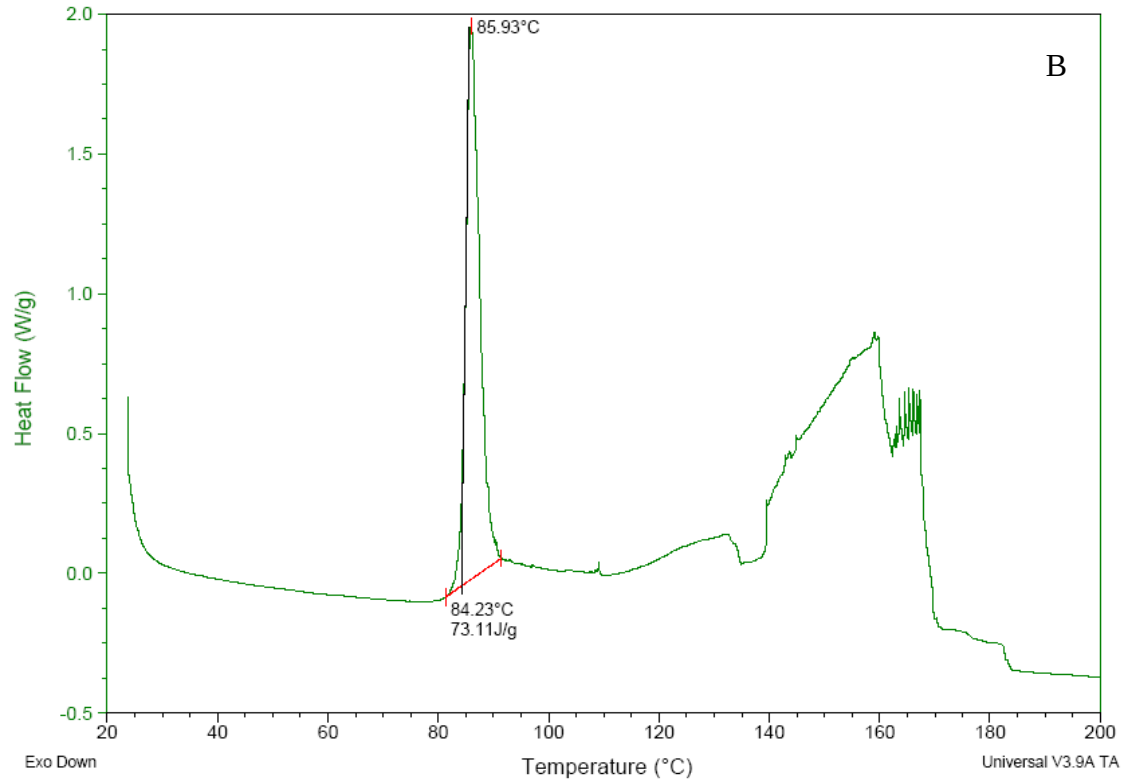

Figure 6.10: Summary of the endothermic peaks for A) Isonicotinamide with Mandelic acid and B) Benzamide with Mandelic Acid

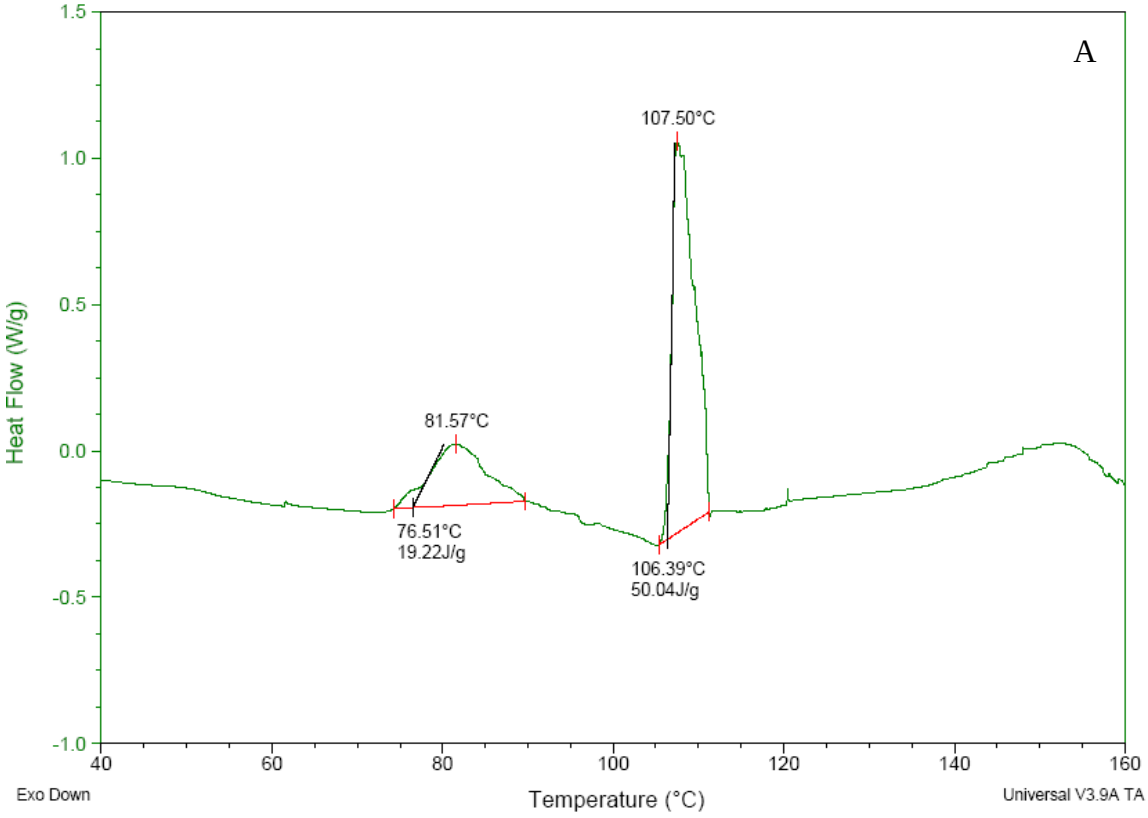

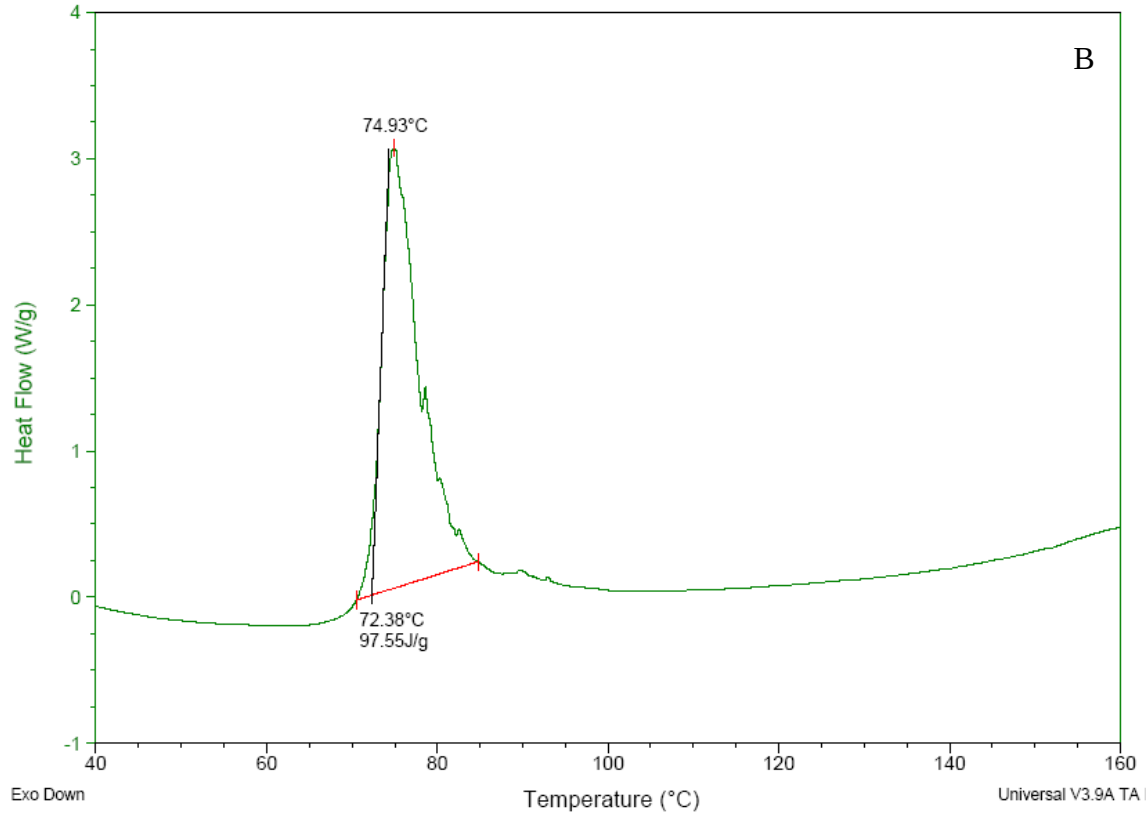

Figure 6.11: Summary of the endothermic peaks for A) Isonicotinamide with Fumaric acid and B) Benzamide with Fumaric Acid

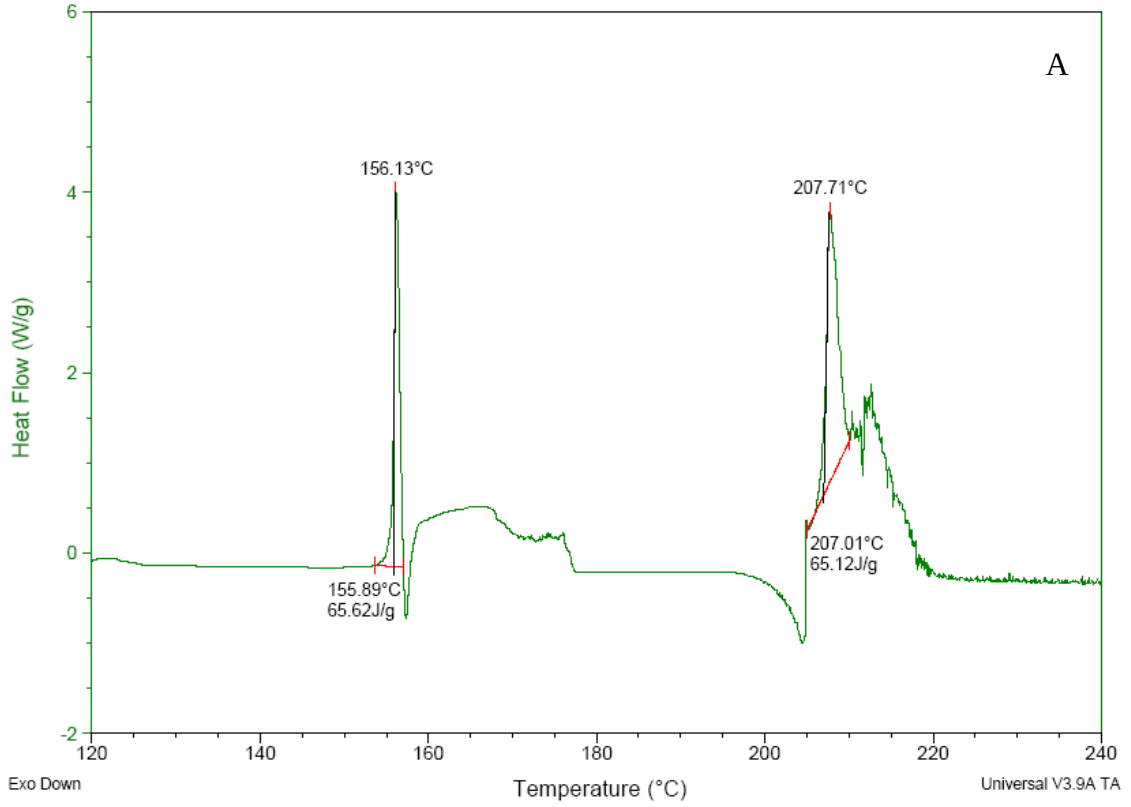

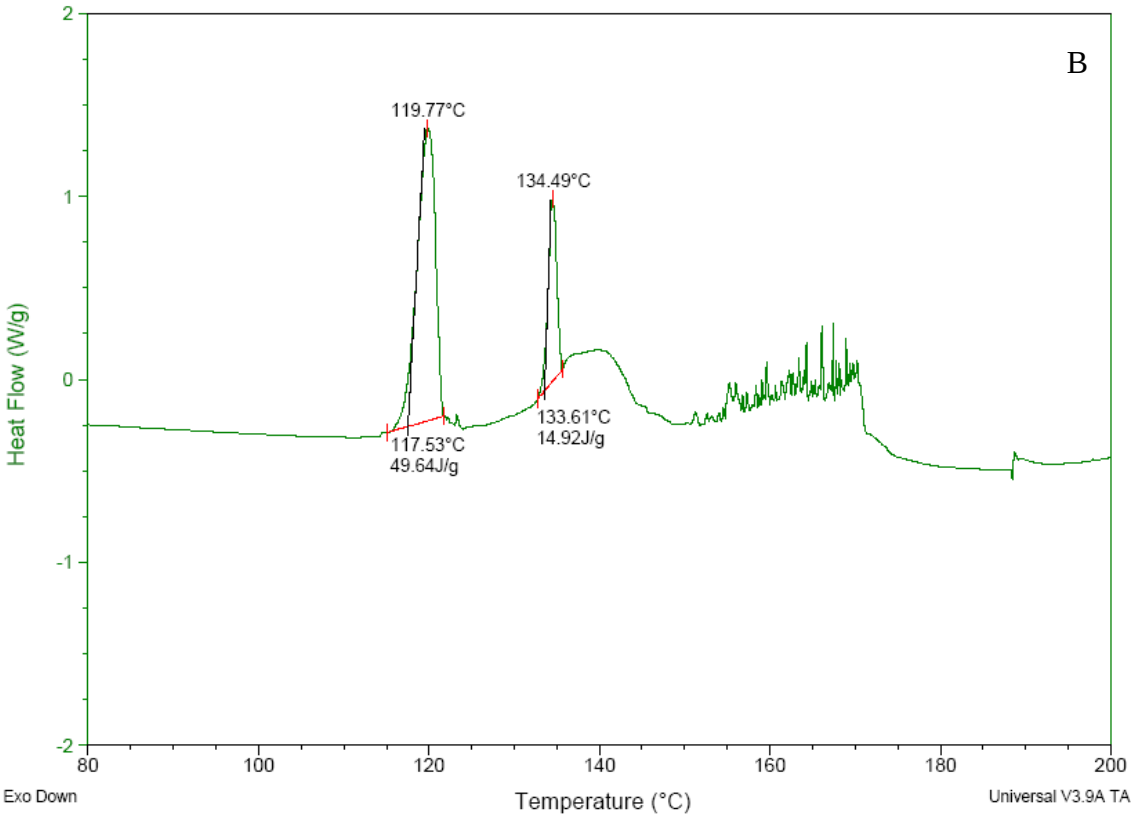

Figure 6.12: Summary of the endothermic peaks for A) Isonicotinamide with Glutaric acid and B) Benzamide with Glutaric acid

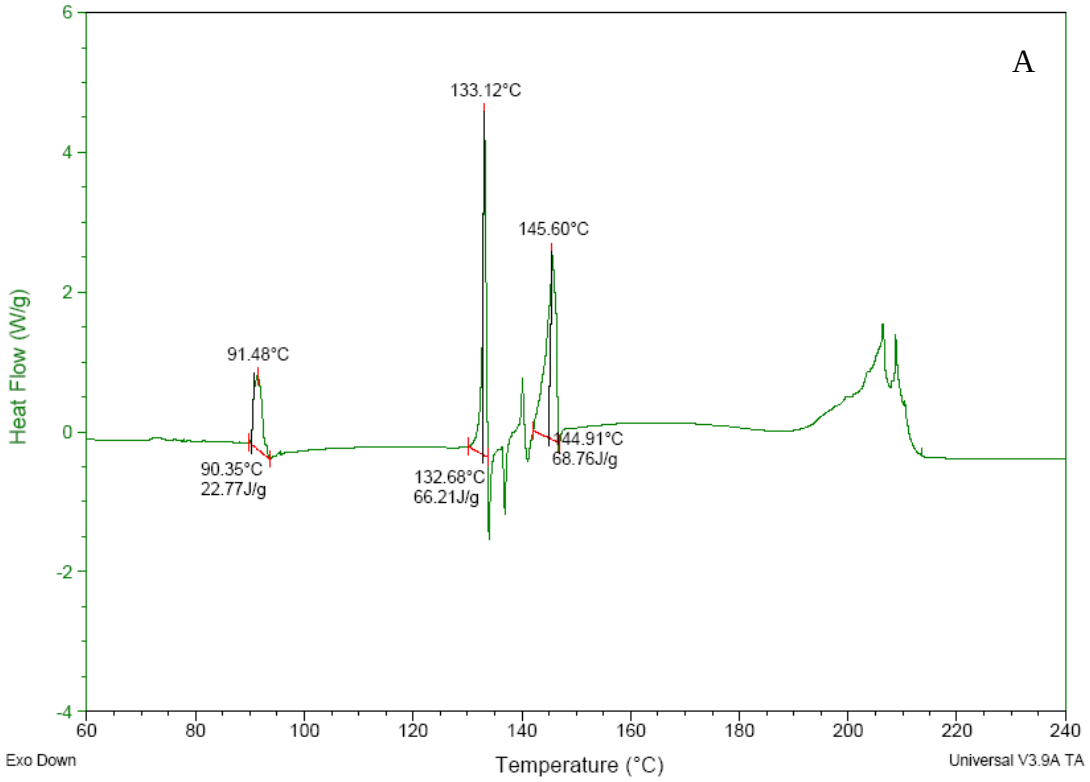

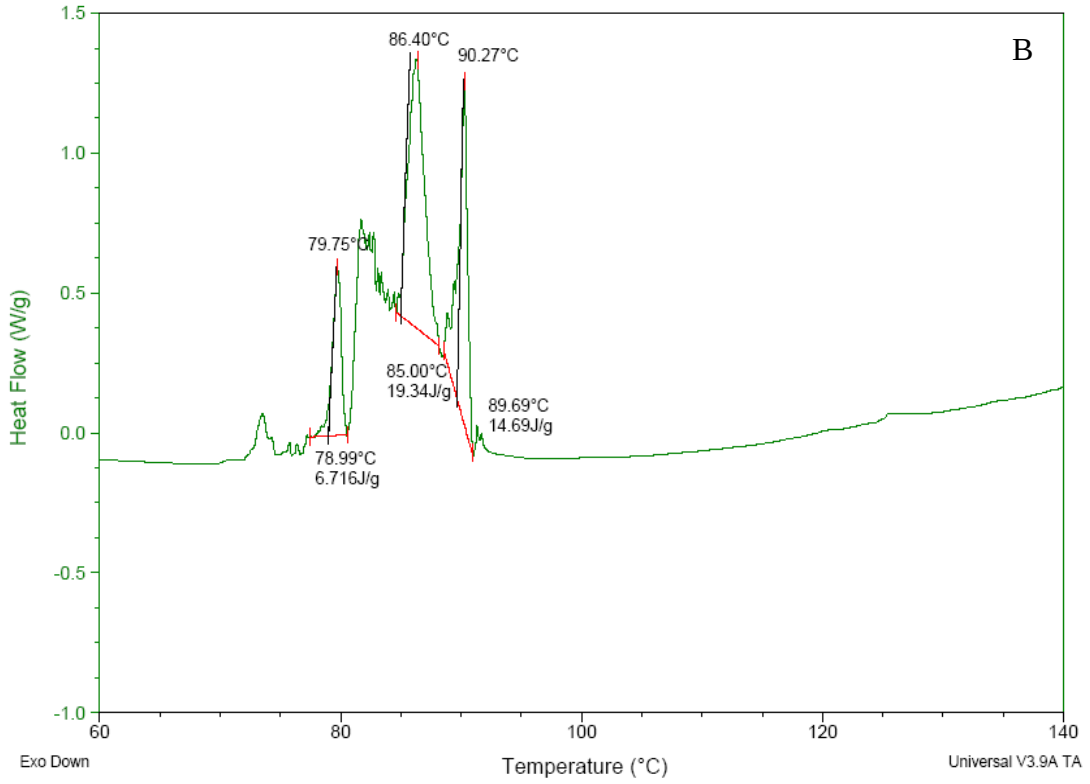

Figure 6.13: Summary of the endothermic peaks for A) Isonicotinamide with Succinic acid and B) Benzamide with Succinic Acid

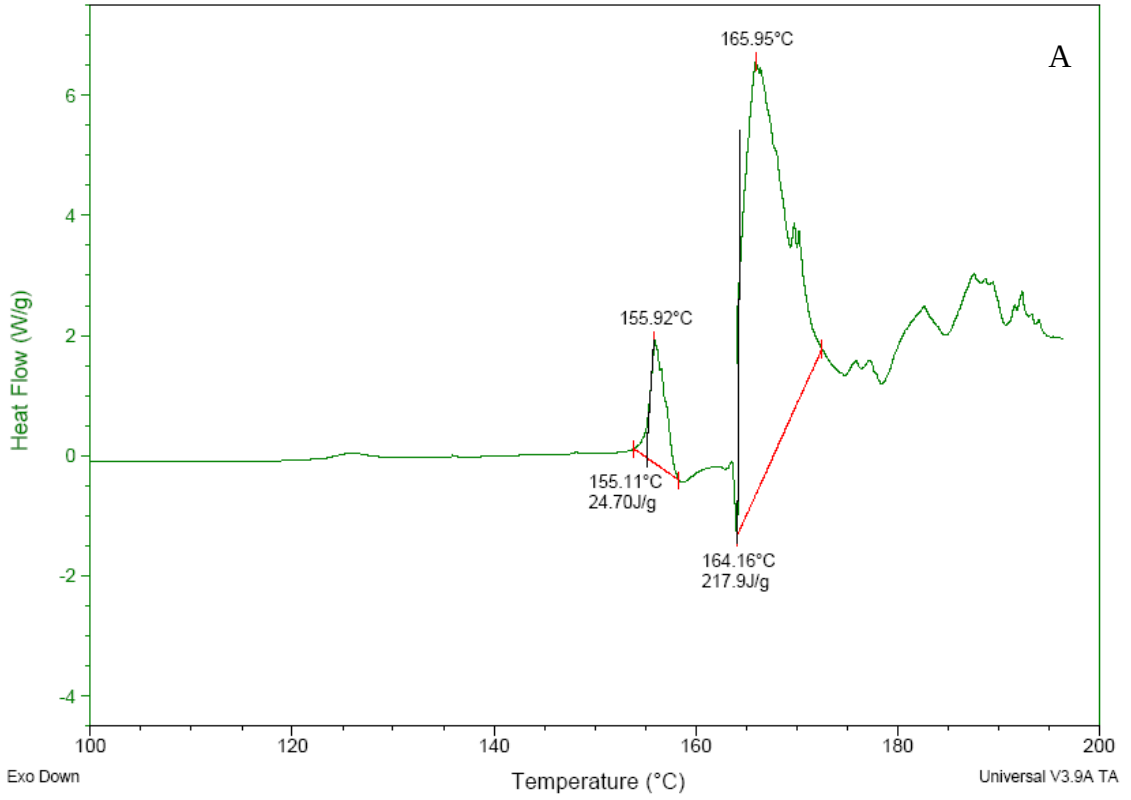

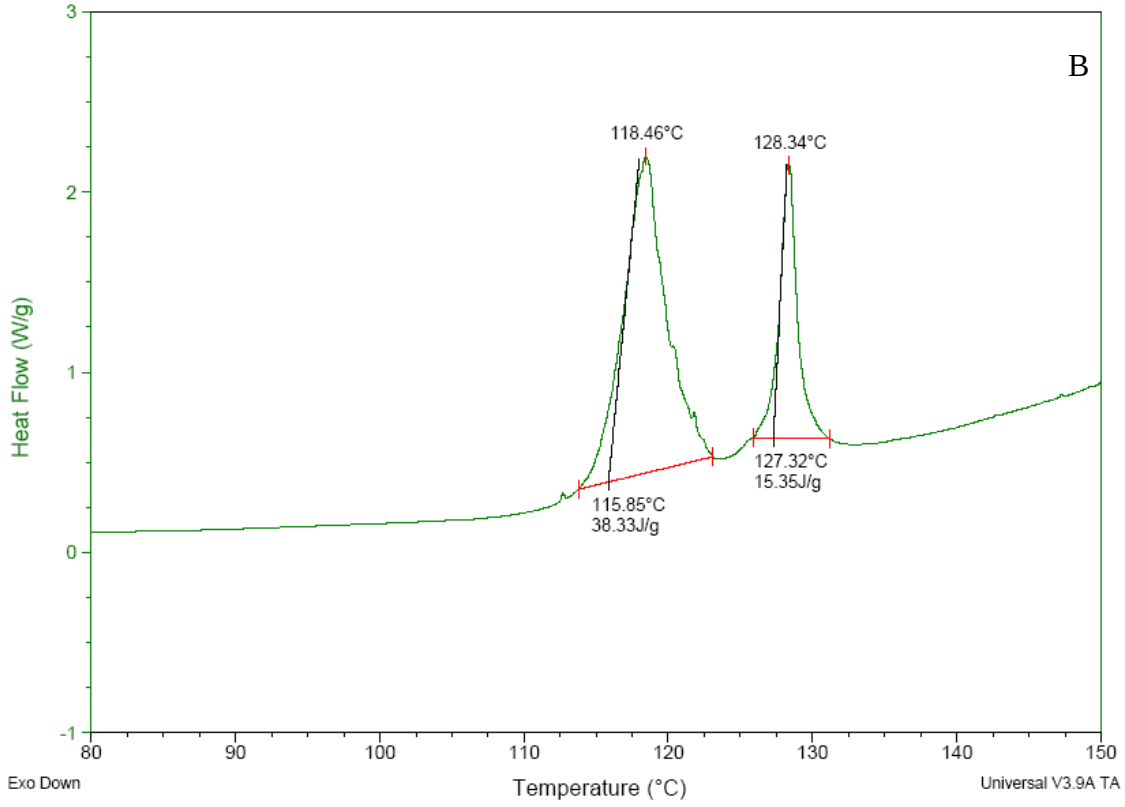

Figure 6.14: Summary of the endothermic peaks for A) Isonicotinamide with Tartaric acid and B) Benzamide with Tartaric acid